THE UNIVERSITY OF MICHIGAN

INDUSTRY PROGRAM OF THE COLLEGE OF ENGINEERING

THE INFLUENCE OF TRANSVERSE HARMONIC OSCILLATIONS
ON THE HEAT TRANSFER FROM FINITE AND
INFINITE VERTICAL PLATES IN FREE CONVECTION

A dissertation submitted in partial fulfillment
of the requirements for the degree of
Doctor of Philosophy in the
University of Michigan
Department of Mechanical Engineering
1962

October, 1962

IP-585

ACKNOWLEDGMENTS

TABLE OF CONTENTS

iii

TABLE OF CONTENTS CONT'D

LIST OF FIGURES

a   amplitude of wall vibration

C   length of 1/2 the plate, $C = L/2$

C_p the specific heat per unit mass of the fluid

div   the divergence of the vector $\vec{V}$, div $\vec{V} = \dfrac{\partial u}{\partial x} + \dfrac{\partial v}{\partial y}$

D/D_T^* the substantive derivative operator for the stationary coordinate system

D/D_T the substantive derivative operator for the moving coordinate system

e   base of the natural logarithm

$F(\eta)$ defines the free convection velocity distribution

Gr_L the Grashof number, $g\beta L^3 \Delta\Theta_0 / \nu^2$

Gr_X the Grashof number, $g\beta X^3 \Delta\Theta_0 / \nu^2$

g   body force per unit mass acting parallel to the wall

$H(\eta)$ defines the free dimensionless convection temperature distribution, T_0

i   the square root of -1

K   thermal conductivity of the fluid

K_0 dimensionless term $\dfrac{\beta\Delta\Theta_0}{\sqrt[4]{G_{RL}}}$

$K_1 \ldots K_4$ functions of Prandtl number

L   the length of the plate

n   the exponent in e^n

Nu_L the Nusselt number, h^L/K

Nu_X the local Nusselt number, h^X/K

Pr   the Prandtl number of the fluid

P   pressure

$\underline{P}$ pressure from potential flow, $\dfrac{2x-1}{2\sqrt{x(x-1)}}$

T dimensionless temperature, $\Theta - \Theta_\infty / \Theta_0 - \Theta_\infty$

T_0, T_{2S} the steady components of the temperature distribution $T \approx T_0 + \epsilon^2 T_{2s}$

T_1 $T_I = \text{Real}\,(T_1\, e^{i\omega t})$

t dimensionless time, $\dfrac{\nu\sqrt{G_{RL}}}{L^2}\,\tau$

U^* velocity parallel to the wall in the stationary coordinate system

u dimensionless velocity parallel to the wall in the moving coordinate system

u_I velocity parallel to the wall in the moving coordinate system

u_1 $u_I = \text{Real}\,(u_1\, e^{i\omega t})$

u_{2s} steady velocity normal to the wall in the moving coordinate system

U potential flow parallel to the wall in the moving coordinate system

$\bar{u}$ component of the complex velocity

V_0 velocity of the plate normal to the wall in the stationary coordinate system

V^* velocity normal to the wall in the stationary coordinate system

v dimensionless velocity normal to the wall in the moving coordinate system

v_I velocity normal to the wall in the moving coordinate system

v_1 $v_I = \text{Real}\,(v_1\, e^{i\omega t})$

v_{2s} steady velocity normal to the wall in the moving coordinate system

$\bar{V}$ component of the complex velocity

W complex potential, for potential flow

$\bar{X}$ distance parallel to the wall in the moving coordinate system

$\bar{X}^*$ distance parallel to the wall in the stationary coordinate system

X dimensionless parallel distance, $X = \bar{X}/L$

$\bar{Y}^*$ distance normal to the wall in the stationary coordinate system

$\bar{Y}$ distance normal to the wall in the moving coordinate system

Y dimensionless normal distance, $Y = \dfrac{\bar{Y}}{L} \sqrt[4]{G_{RL}}$

Z coordinate normal to the X-Y plane

∞ subscript indicating a condition far from the wall

GREEK LETTERS

α the thermal diffusivity of the fluid $K/\rho\, C_p$

β coefficient of thermal expansion, $\rho = \rho_\infty[1-\beta\Delta\Theta_o]$

$\Delta\Theta_o$ temperature difference, $\Delta\Theta_o = \Theta - \Theta_\infty$

∇^2 the Laplacian Operator in the moving coordinate system

∇^{*2} the Laplacian Operator in the stationary coordinate system

δ the boundary layer thickness

ξ dimensionless distance, $y\sqrt{\omega/2}$

χ the stream function for ψ_{2s}

v_{2s} steady velocity normal to the wall in the moving coordinate system

$\bar{V}$ component of the complex velocity

W complex potential, for potential flow

$\bar{x}$ distance parallel to the wall in the moving coordinate system

$\bar{x}^*$ distance parallel to the wall in the stationary coordinate system

X dimensionless parallel distance, $X = \bar{x}/L$

$\bar{y}^*$ distance normal to the wall in the stationary coordinate system

$\bar{y}$ distance normal to the wall in the moving coordinate system

Y dimensionless normal distance, $Y = \dfrac{\bar{y}}{L} \, \sqrt[4]{G_{RL}}$

Z coordinate normal to the X-Y plane

∞ subscript indicating a condition far from the wall

GREEK LETTERS

α the thermal diffusivity of the fluid $K/\rho \, C_p$

β coefficient of thermal expansion, $\rho = \rho_\infty [1-\beta \Delta\Theta_o]$

$\Delta\Theta_o$ temperature difference, $\Delta\Theta_o = \Theta - \Theta_\infty$

∇^2 the Laplacian Operator in the moving coordinate system

∇^{*2} the Laplacian Operator in the stationary coordinate system

δ the boundary layer thickness

ξ dimensionless distance, $y\sqrt{\omega}/2$

χ the stream function for ψ_{2s}

ϵ	$\epsilon = a\omega/L$ (Chapter II), $\epsilon = (a/L) \dfrac{\beta\Delta T_o}{\sqrt{G_{RL}}} \omega^2$ (Chapter III)
$\zeta(\eta)$	$\zeta(\eta) = \displaystyle\int_\infty^\eta \eta H'(\eta) d\eta$
η	the similarity variable, $\eta = y/(4x)^{1/4}$
ηd	the dimensional similarity variable
Θ	temperature
μ	the absolute viscosity of the fluid
ν	the kinematic viscosity of the fluid
ρ	the density of the fluid
τ	time
τ_s	shear stress
$\emptyset$	phase angle of velocisty and temperature oscillations defined by, for example

$$\text{Real } u_1 e^{i\omega t} = |u_1| \cos(\omega t + \emptyset)$$

ψ_o	the free convection stream function
ψ_{2s}	the secondary flow stream function
Ω	frequency of wall vibration
ω	dimensionless frequency, $\omega = \dfrac{L^2 \Omega}{\nu \sqrt{G_{RL}}}$
λ	acoustic wave length
γ	$\gamma = \omega(4X)^{1/2}$

NOMENCLATURE FOR CHAPTER IV

All discussion directly involving the analysis of Chapter II and III is done in terms of symbols used in those chapters. Additional symbols used elsewhere in Chapter IV are given below.

A   the total area of the heated section of the test plate

a   the amplitude of plate vibration

D   the diameter of stainless steel rods where they attach to the corners of the heated section. See Figure 4-15

h_c the free convection heat transfer coefficient under non-vibratory conditions at a particular value of $\Delta\Theta$.

h_{co} the free convection heat transfer coefficient under non-vibratory conditions at a particular energy input to the heated section corresponding to a temperature difference of $\Delta\Theta_o$.

h_k the conduction heat transfer coefficient

h_L the heat transfer coefficient for losses

h_{Lo} the heat transfer coefficient for losses at a particular energy input corresponding to a temperature difference of $\Delta\Theta_o$

h_r the radiation heat transfer coefficient defined by Equation (4-4)

h_s the convection heat transfer coefficient for the rods attached to the corners of the heated section. See Figure 4-15.

h_v the increase in the convection heat transfer coefficient due to vibration at a particular $\Delta\Theta$

k_R the thermal conductivity of the rods attached to the corners of the heated section. See Figure 4-15.

L   the distance between the thermocouples mounted on the rods attached to the corners of the heated section. See Figure 4-15

m_r see Equation (4-7). $m_r = 4\ h_s/Dkr$

NOMENCLATURE FOR CHAPTER IV

All discussion directly involving the analysis of Chapter II and III is done in terms of symbols used in those chapters. Additional symbols used elsewhere in Chapter IV are given below.

A   the total area of the heated section of the test plate

a   the amplitude of plate vibration

D   the diameter of stainless steel rods where they attach to the corners of the heated section. See Figure 4-15

h_c the free convection heat transfer coefficient under non-vibratory conditions at a particular value of $\Delta\theta$.

h_{co} the free convection heat transfer coefficient under non-vibratory conditions at a particular energy input to the heated section corresponding to a temperature difference of $\Delta\theta_o$

h_k the conduction heat transfer coefficient

h_L the heat transfer coefficient for losses

h_{Lo} the heat transfer coefficient for losses at a particular energy input corresponding to a temperature difference of $\Delta\theta_o$

h_r the radiation heat transfer coefficient defined by Equation (4-4)

h_s the convection heat transfer coefficient for the rods attached to the corners of the heated section. See Figure 4-15.

h_v the increase in the convection heat transfer coefficient due to vibration at a particular $\Delta\theta$

k_R the thermal conductivity of the rods attached to the corners of the heated section. See Figure 4-15.

L   the distance between the thermocouples mounted on the rods attached to the corners of the heated section. See Figure 4-15

m_r see Equation (4-7). $m_r = \sqrt{h_s / D_{k_r}}$

q   the total rate of energy input to the heated section

q_k heat transfer loss due to conduction through the rods attached to the corners of the heated section. See Figure 4-15

q_L the combined heat transfer lossed due to conduction and radiation. $q_L = (q_k + q_r)$

q_R heat transfer loss due to radiation

Rev   vibrational Reynolds number, $\dfrac{a\omega L}{\nu}$

Tp   absolute temperature of the heated section of the test plate

Ta   absolute temperature of the ambient

x_r distance along the rods attached to the four corners of the heated section.

GREEK LETTERS

ϵ the emissivity of the polished aluminum plates forming the heated section

θ temperature

θ_0 temperature of the heated section of the test plate

θ_∞ temperature of the ambient

θ_r temperature at a point on the rod shown in Figure 4-15

$\Delta\theta$ temperature difference between the heated section of the test plate and ambient. $\Delta\theta = (\theta_0 - \theta_\infty)$

$\Delta\theta_0$ temperature difference $\Delta\theta$ corresponding to steady state under nonvibratory conditions at a particular energy input to the heated section.

$\Delta\theta_r$ difference between the temperature at a point along the rod and ambient. $\Delta\theta_r = (\theta_r - \theta_\infty)$

σ the Stefan-Boltzman constant. $\sigma = .1713 \times 10^{-8} \dfrac{BTU}{hr\text{-}ft^2\text{-}(°R)^4}$

CHAPTER I

INTRODUCTION AND LITERATURE SURVEY

This thesis treats the influence of transverse harmonic oscillations on the heat transfer from finite and infinite, vertical plates in free convection. It attempts to resolve some of the questions pertaining to steady effects produced on free convection flows from purely periodic distrubances, mainly that of the time-independent modification of the heat transfer coefficient. Both analytical and experimental methods have been used to achieve this result.

The literature relating to this particular field is reviewed, owing to its diversification it was expedient to divide it into three groups designated as A, B, and C.

Group A includes papers o:
emphasis on oscillatory flows and t.
Group B includes references on unsteady motions resulting from sound waves, and the related heat transfer problems. Group C includes references and books concerned primarily with heat transfer which general nature was helpful for a theoretical solution to this problem.

Papers from the field of acoustics were investigated because they are related to oscillating boundary layers. When plane acoustic waves interact with a stationary object a steady, i.e., time-independent rotational flow occurs. Also, a steady rotational flow occurs in an oscillating fluid or is generated in a quiescent fluid where solid boundary oscillate. These phenomena are sometimes called acoustic streaming or secondary flow. Examples of these phenomena are flow in a Kundt's

tube, that near vibrating cylinders and spheres, the flow near vibrating plates and membranes, and that near orifices transversed by sound. Flow in the vicinity of vibrating gas bubbles, and that associated with standing waves in tubes and between walls also are examples in which secondary flows exist. For more details concerning these phenomena the work of early observers can be found in the bibliographies of Holtsmark, Johnsen, Sekkeland, and Skavlen (B-8), Nyborg (B-15,16), and Westervelt (B-24).

The fluid dynamic problem in the absence of heat transfer will be considered first.

Schlichting (A-32) used successive approximations to solve the non-linear momentum equation, and therefore, illustrated streaming mathematically. He showed that streaming is a consequence of the non-linear characteristics, i.e., the convective inertia terms, of the momentum equations for a viscous fluid. Absence of the inertia terms will result mathematically in no streaming. Therefore, streaming is believed to be the result of a physical interaction between inertia and viscous effects in a fluid.

Schlichting (A-32) considered the case of a plane wall executing harmonic oscillations in an otherwise quiescent fluid and applied his solution to a circular cylinder, using Prandtl's boundary layer simplifications of the Navier-Stokes equations. He also made experimental verifications of streaming. Holtsmark, et al., (B-8) considered the flow around a circular cylinder in two dimensions for an oscillating incompressible fluid with the axis of the cylinder normal to the direction of oscillation. They conducted both experimental and analytical studies. Using successive approximations they solved the complete set of Navier-Stokes

equations. Higher order approximations and discussions of these two papers are in Andres and Ingard (B-1, 2), Ramez, Corelli and Westervelt (B-17). In the case of a cylinder, two regions of streaming were predicted in each quadrant around a cylinder. Next to the cylinder an inner vortex system which has been called the DC boundary layer was found. The thickness of the DC boundary is defined as the distance from the surface to the streamline $\psi = 0$. Next to this inner system is an outer vortex system called the AC boundary layer. In limited space the core of the AC vortices is located at a finite distance. In unlimited space the outer vortex cores are an infinity. Schlichting took photographs of a cylinder oscillating in water with fine metallic particles in it to render the motion visible and found good agreement with the theoretical patterns of stream lines. Holtsmark, et al, (B-8) used a Kundt's tube arrangement and MgO smoke in air oscillating around a circular cylinder and took photographs. Their agreement between theory and experiment is excellent for periodic flow and very good for streaming. For limited space both Schlichting and Holtsmark found DC and AC systems which were similar in general nature, but Schlichting's case gives a much thinner DC system and the velocities in the outer system are higher. For unlimited space Schlichting's analysis predicts no DC system. Raney, et al, (B-17) pointed out that Schlichting's analysis is characterized by small values of vibration amplitude therefore is not necessarily valid for large values of vibration Reynolds number. They also present experimental curves showing the existence of a universal curve for the DC boundary-layer thickness.

Rott (A-30) and Glauert (A-11) both used the method of succes-
sive approximations to study cases of viscous incompressible stagnation
flow onto an infinite plate which is oscillating in its own plane where
the first approximation is Hiemenz flow. Glauert (A-11) used his re-
sults in applying them for a cylinder of arbitrary cross-section in the
following cases. 1) cylinder fixed, stream oscillates in magnitude;
2) cylinder fixed, stream oscillates in direction; 3) stream constant,
cylinder oscillates in the stream direction; 4) stream constant, cylin-
der oscillates in the transverse direction; and 5) stream constant, cylin-
der oscillates about its axis. Rosenblatt (A-24) using successive approxi-
mations considered torsional oscillations of a plane in a viscous fluid.
He found that a true representation of this flow can only be obtained
through inclusion of the convective inertia terms, which is important in
determining the character of the flow at large distances from the plate.
This is another example of this streaming or secondary flow phenomena.

Lighthill (A-20) has considered the cases of incompressible
steady flow on an arbitrary cylinder which is oscillating with small ampli-
tude. This can be said to be the case of low-frequency small perturbation
analysis of Blasius flow. Cheng and Elliot (A-4) considered arbitrary
and specific time-dependent motions of a semi-infinite plate. They com-
pared one of their cases, which corresponded physically, to that of
Lighthill. Lighthill used the momentum-integral technique and they used
a more rigorous mathematical procedure. It is significant that the
momentum-integral technique was checked because both solutions for the
case of wall shear stress were found to be in agreement in form and num-
erical constants. Lighthill (A-15) also discussed the temperature fluc-
tuations using successive approximations.

Lin (A-22) has devised a linearized method to study boundary-layers over a flat plate subjected to rapidly oscillating external flows. He has shown that high-frequency oscillations behave like shear waves of the Stokes type regardless of the mean flow. He reasoned that if the frequency of oscillation is very high, then local acceleration is much larger than the time-dependent part of the convection or momentum. Then the time-dependent part can be treated by linear theory which is then related to the problem first studied by Rayleigh and Stokes.

Karlsson (A-16) has considered an unsteady turbulent boundary layer by studying the non-linear effects of low speed parallel flow, harmonically oscillating in magnitude about a constant mean over a flat plate. It was found surprisingly enough, that the effect due to non-linear interaction was quite small for fluctuation amplitudes as large as 34% of the free stream velocity. Tennekes (A-38) used the results of Karlsson and suggested the possibility of constructing the response of the boundary layer to any input transient by a linear Fourier synthesis of the response. This theory compared favorably with Karlsson's experimental results.

Hill and Stenning (A-15) have made a study of the effects of free stream oscillations on laminar boundary layers of the Howarth type and made experimental measurements. They found that the existing solutions of Lighthill (A-20), Lin (A-22) and Nickerson (A-26) for low and high frequencies are adequate for describing the flow. For the intermediate frequency range they solved for a theoretical solution which accounted for the flow in that region.

The following papers include heat transfer effects along with the fluid dynamic problems.

Stuart (A-36) solved the Navier-Stokes equations exactly for incompressible flow for the case of a flat plate with constant suction and a fluctuating free stream velocity. By including viscous dissipation he obtained the exact solution of the energy equation for the case of zero heat transfer between the wall and fluid.

Ostrach (A-27) extended the Stokes solution by analyzing the temperature distribution in a fluid over an oscillating infinite surface with heat transfer by including compressibility and viscous dissipation. It was found that the heat transfer for the oscillating surface can be considerably different from that of conduction alone, and that oscillation can alter the fluid temperature appreciably.

Moore (A-25) analyzed the laminar compressible boundary layer over an insulated semi-infinite flat plate moving with time-dependent velocity. Ostrach (A-27) extended the results of Moore representing a more exact treatment and included the effects of heat transfer. For the particular case of a plate oscillating about a steady velocity the unsteady effects can alter the boundary-layer characteristics appreciably. This paper did not settle the question what effect oscillations have on mean skin-friction and heat transfer.

Kestin, Maeder, and Wang (A-17) have considered the case of a flat plate on which the free stream is a flow wherein a sinusoidal velocit disturbance is carried downstream with the mean velocity. They obtained a solution by expanding the velocities and temperatures in terms of series expansions in increasing powers of the small relative amplitudes (λ) of

the sinusoidal disturbance. This procedure will yield an equation to solve for expansions up to λ^n. The zero-order solution is the case of Blasius. By considering another series expansion for the first and second-order equations they were able to obtain the time-averaged skin friction and heat transfer coefficient. This second expansion limited their study to low frequencies and the first expansion to small amplitudes. Their analysis predicts a slight increase in the skin friction coefficient and a slight decrease in the heat transfer coefficient. It is significant to point out that the terms that contribute to the time-averaged coefficient in this analysis are part of an infinite series and that only the first term was used. The part that contributes is from the second order solution and is the steady part of that solution.

Nickerson (A-26) has considered a flat plate executing simple harmonic oscillations in a steadily moving fluid with zero pressure gradient. Using series expansions for stream and temperature functions he was able to obtain successive approximations and make experimental observations. He carried his analysis far enough to obtain steady second-order velocity and temperature solutions which are the result of oscillations. He theoretically obtained the result that there would be a slight steady increase in heat transfer and skin friction coefficients. The increase in heat transfer coefficient was within the range of experimental error and therefore could not be checked. Velocity profiles obtained using a hot-wire anemometer showed good agreement with theory.

Chung and Anderson (A-6) analyzed the laminar free-convection boundary layer on a vertical plate or a horizontal cylinder under unsteady conditions. For a Prandtl number of 0.72 they found that if the

wall temperature increases with time there is an increase in the heat transfer whereas the heat transfer is decreased when the acceleration of gravity field is increased with time.

Schoenhals and Clark (A-33) have considered the response of velocity and temperature of a laminar incompressible fluid to a vertical plate oscillating harmonically in a horizontal direction. They considered the harmonic oscillations of a semi-infinite plate with free convection and the fluid response of a finite adiabatic plate to harmonic oscillations. Using successive approximations streaming was found to exist for the case of the finite plate. They did not theoretically consider the time-averaged heat transfer coefficient, but studied the temperature and velocity response of a free convection boundary layer within the first two approximations. Experimentally they studied the effects of oscillation on free convection on a finite plate and presented results showing the increase in heat transfer coefficient.

In the case of an infinite vertical plate oscillating vertically, considered by Rott (A-30) and Glauert (A-11), should the oncoming stream be of sufficient strength to permit ignoring the buoyancy effect of the temperature field, then oscillations have no effect when the wall is maintained at a constant temperature.

Analytical results for the increases of heat transfer rates have not been as fruitful as the considerations of the fluid dynamics of adiabatic systems. This is confirmed by experimental observations.

Experimentally there has been confirmation that oscillation of a solid or oscillation of the flow over a solid increases the heat transfer rate. Also, it has been experimentally confirmed that various types

of sound fields increase the heat transfer rate. These facts have been
demonstrated by the papers (A-1,7,8,9,22,33,34,38,40,41) and (B-4,5,6,
18,19). For flow through tubes the increases have been demonstrated by
(A-12,18) and (B-10,20). Also the phenomena of transition from laminar
to turbulent flow and flow separation have been experimentally observed.

In the case of sound field effects on the free convection
boundary layer of a horizontal cylinder, flow visualizations and shadow-
graph pictures were studied by Fand and Kaye (B-4), Holman (B-5), Holman
and Mott-Smith (B-6), Soehngen and Holman (B-18), and Sprott, Holman and
Durand (B-19). A critical or threshold sound pressure level of 136 db
was found below in which no increase in the heat transfer coefficient
was found and above which it increased. The point was made that stream-
ing is the physical mechanism causing the increase and that its interac-
tion is evident at the critical sound pressure level at onset of the in-
crease of heat transfer coefficient. Soehngen, et al, (B-18) found that
the heat transfer coefficient could be increased three times that of no
sound for the same temperature difference. Sprott, et al, (B-19) and
Holman, et al, (B-6) found that the heat transfer coefficient could be
increased by 100%. Fand, et al, (B-4) found that the heat transfer co-
efficient could be increased by 300% by high intensity stationary and
progressive sound fields on the free convection boundary layer of a
horizontal cylinder.

Fand and Kaye (A-7) investigated the influence of vertical
mechanically induced simple harmonic vibrations upon the rate of heat
transfer by free convection from a heated horizontal cylinder to air.
For intensities of vibration less than 0.3 ft/sec they reported negligible

change in the heat transfer coefficient. Above this value the coeffi-
cient changes significantly. A flow-visualization method employing
smoke as the medium indicated that vibrationally induced turbulence is
the mechanism which caused the increase. They also reported that above
0.9 ft/sec and $\Delta T \geq 100°F$ there is a "fully developed turbulent flow."

Fand and Peebles (A-8) made an investigation of the comparison
of the influence of mechanical and acoustical vibration on free convec-
tion from a horizontal cylinder. They found that although there is a
ten-fold difference in frequency and a difference in amplitude, the heat
transfer correlation for horizontal acoustical vibrations is also valid
for horizontal mechanical vibrations and the character of the boundary
layer is the same. They found a critical intensity of 0.36 ft/sec.

Shine (A-35), Tsui (A-39) and Schoenhals, et al, (A-34) studied
experimentally the effects of a vertical plate oscillating horizontally
with free convection. Shine and Tsui both used Zehnder-Mach interferome-
ters in their studies. Tsui claimed that the flow seemed to be transi-
tional on the basis of his observations. In his experiment the maximum
percentage increase was found to be 24%. Shine defined a "critical in-
tensity" (amplitude times frequency) peculiar to his system, and showed
experimentally that above it heat transfer is increased and below it no
change was observed. He noted that coincident with the occurrence of
change in heat transfer coefficient there was an inception of waviness
in the fringes of the boundary layer, which was intensified by increases
in vibration intensity. He pointed out this waviness indicates a flow
transition from laminar flow and may represent the physical mechanism
causing the increases. Schoenhals, et al, (A-33) data do not show

evidence of a critical intensity value. They experimentally found an increase in the heat transfer coefficient of 46% due to horizontal oscillations of a finite vertical plate.

Martinelli and Boelter (A-17) have investigated the effect of vertical oscillation upon the rate of heat transfer from a horizontal tube immersed in otherwise quiescent water. They found increases up to 400%. It was found that the coefficient of heat transfer was unaffected for low values of vibration Reynolds number.

Teleki (A-38) has investigated a case physically similar to that of Martinelli, et al, (A-22) except the media was air. He found increases up to 200% and did experience a critical intensity in his heat transfer coefficients.

Lemlich (A-19) has investigated electrically heated wires subjected to both vertical and horizontal vibrations in air and observed an increase in heat transfer coefficient irrespective of the direction of vibration. He did not experience a critical intensity in his heat transfer coefficient. He found increases as high as 400%.

CHAPTER II

FIRST AND SECOND ORDER PERTURBATIONS OF A LAMINAR
FREE CONVECTION BOUNDARY LAYER DUE TO
TRANSVERSE HARMONIC OSCILLATIONS OF A
THIN PLATE OF FINITE LENGTH

Statement of the Problem

Figure 2-1 is a sketch of the physical system to be investigated.
Consider a heated thin plate of finite length L with the stationary co-
ordinate system fixed at the base of the plate. The plate is undergoing
transverse harmonic oscillations normal to the $X^* - Z^*$ plane, which is
in the stationary coordinate system. The analysis is restricted to two
dimensional incompressible flow in the $X^* - Y^*$ plane. From a compressi-
bility standpoint it is necessary that the velocity of the plate be of a
lower order than the velocity of sound in the fluid. The harmonic oscil-
lation of the plate is $V_O = a\,\Omega\,\cos\Omega\tau$ where a is the amplitude of
vibration, Ω is the frequency of vibration, τ is time. The product
$a\,\Omega$ represents the maximum velocity of the plate and V_O represents the
velocity of the plate with respect to time.

The plate is heated to a uniform temperature, θ_O, and is main-
tained in contact with an otherwise quiescent fluid at temperature θ_∞.
The fluid has constant viscosity μ, constant thermal diffusivity α,
and constant coefficient of thermal expansion β. There exists in the
fluid a uniform force field g which in the absence of the harmonic oscil-
lation would generate a free convection flow only.

The solutions of the governing equations of momentum, energy
and mass treat the case where buoyancy forces of free convective flow
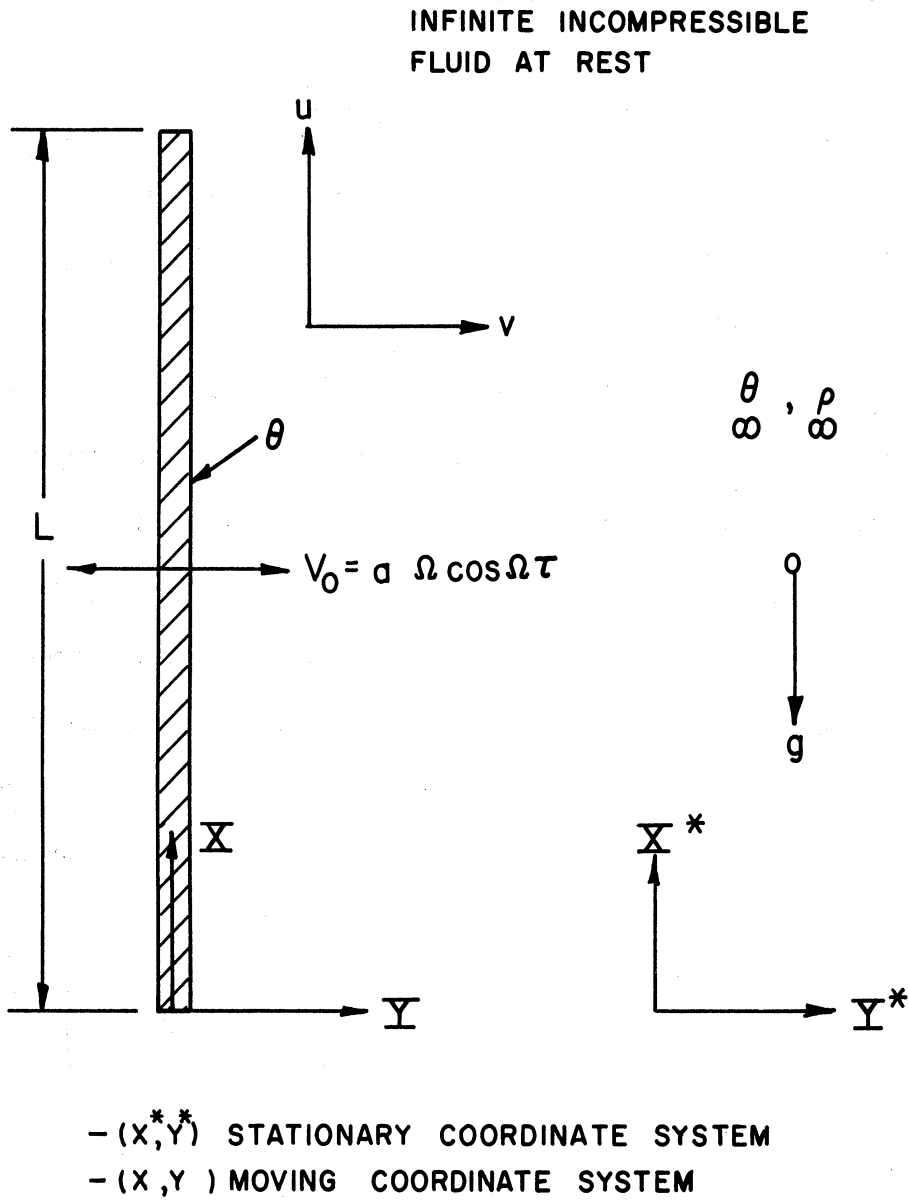
Figure 2-1.   A Sketch of Heated Thin Plate of Finite Length Oscillating Transversely in an Infinite Incompressible Fluid at Rest.

predominate over the effects of the transverse harmonic oscillations. The effects of the transverse harmonic oscillations are treated as first and second order perturbations of a free convection boundary layer flow. These first and second order perturbations result mainly from a potential flow pattern at the outer edge of the boundary layer.

Fundamental Equations and Transformation of Coordinates

At first it is necessary to look at the governing equations of conservation of mass, momentum, and energy. The flow analysis is restricted to incompressible flow, although in free convection the generating force term is due to thermal expansion of the fluid. Therefore it is necessary to investigate what restrictions are necessary to be able to use an incompressible analysis. This has been discussed by Ostrach (C-8) and Hellums (A-14).

Presented below are the governing equations for viscous compressible flow with K, μ and C_p being assumed constant and viscous dissipation and the work of compression assumed negligible. A stationary coordinate system will be considered first with the origin located at a datum plane at the bottom edge of the plate, therefore

$$\frac{DU}{DT}* = -g - \frac{1}{\rho}\frac{\partial P}{\partial X}* + \nu \left[\nabla_*^2 U + \frac{1}{3}\frac{\partial}{\partial X}* \, div \, \vec{V}\right]$$

$$\frac{DV}{DT}* = -\frac{1}{\rho}\frac{\partial P}{\partial Y}* + \nu \left[\nabla_*^2 V + \frac{1}{3}\frac{\partial}{\partial Y}* \, div \, \vec{V}\right] \qquad (2\text{-}1)$$

$$\frac{D\rho}{DT}* = -\rho \, div \, \vec{V}$$

and

$$\frac{D\Theta}{DT*} = \frac{K}{\rho C_p} \nabla_*^2 \Theta \ .$$

For air one can consider

$$\rho = \frac{\rho_\infty}{1 + \beta(\Theta - \Theta_\infty)} \tag{2-2}$$

where for an ideal gas

$$\beta = \frac{1}{\Theta_\infty} \tag{2-3}$$

Consider pressure to be composed of the following:

$$P = P_\infty + P' \tag{2-4}$$

where

P_∞ = pressure in the surrounding fluid, and

P' = pressure due to motions,

therefore, we obtain

$$\frac{\partial P}{\partial X*} = -g\rho_\infty + \frac{\partial P'}{\partial X*}$$

$$\frac{\partial P}{\partial Y*} = \frac{\partial P'}{\partial Y*} \ . \tag{2-5}$$

Since the quantity $\beta(\Theta - \Theta_\infty)$, from Ostrach, (C-8), is

$$\beta(\Theta - \Theta_\infty) \ll O(1) \tag{2-6}$$

then Equation (2-2) can be expressed as

$$P = \frac{\rho_\infty}{1+\beta(\theta-\theta_\infty)} = \rho_\infty\left[1-\beta(\theta-\theta_\infty)+\cdots_0\right] = \rho_\infty\left[1-\beta(\theta-\theta_\infty)\right] \quad (2\text{-}7)$$

and by defining T as a dimensionless variable

$$T = \frac{\theta-\theta_\infty}{\theta_w-\theta_\infty} = \frac{\theta-\theta_\infty}{\Delta\theta_0} \quad (2\text{-}8)$$

therefore Equation (2-7) is also expressed as

$$\frac{\rho_\infty}{P} = 1+\beta T \Delta\theta_0 \quad (2\text{-}9)$$

and since $\beta T \Delta\theta_0 \lll O(1)$

then $1+\beta T \Delta\theta_0 \cong 1$

$$(2\text{-}10)$$

and we have before reducing:

$$\frac{DU}{DT_*} = g\beta\Delta\theta_0 T - \frac{[1+\beta T \Delta\theta_0]}{\rho_\infty}\frac{\partial P'}{\partial X^*} + V_\infty[1+\beta T \Delta\theta_0]\left[\nabla_*^2 U +\right.$$

$$\left. +\frac{1}{3}\frac{\partial}{\partial X^*}div_* \vec{V}\right]$$

$$(2\text{-}11)$$

$$\frac{DV}{DT_*} = -\frac{[1+\beta T \Delta\theta_0]}{\rho_\infty}\frac{\partial P'}{\partial Y^*} + V_\infty[1+\beta T \Delta\theta_0]\left[\nabla_*^2 V +\frac{1}{3}\frac{\partial}{\partial Y^*}div_* \vec{V}\right]$$

$$\frac{D}{DT^*}\left[\frac{\rho_\infty}{1+\beta T \Delta\theta_0}\right] + \left[\frac{\rho_\infty}{1+\beta T \Delta\theta_0}\right]div_* \vec{V} = 0$$

$$\frac{DT}{DT^*} = \alpha\left[1+\beta T \Delta\theta_0\right]\nabla_*^2 T.$$

The set of equations have reduced to:

$$\frac{DU}{DT*} = g\beta T \Delta\theta_o - \frac{1}{\rho_\infty}\frac{\partial P}{\partial X*} + V_\infty \nabla_*^2 U$$

$$\frac{DV}{DT*} = -\frac{1}{\rho_\infty}\frac{\partial}{\partial Y*} + V_\infty \nabla_*^2 V$$

(2-12)

$$div_* \vec{V} = 0$$

$$\frac{DT}{DT} = \alpha_\infty \nabla_*^2 T$$

It is convenient to analyze the problem in a frame of reference fixed in the plate, i.e., a coordinate system moving with the plate. As pointed out by Lighthill (A-20) in the hydrodynamics of an incompressible fluid, frames of reference are equivalent if they are in a uniform, though not necessarily constant, translational motion to one another. This is because any uniform inertial force per unit volume is automatically canceled by a uniform pressure gradient. Therefore, it would appear that equivalent frames of reference could be employed on this system without changing the equations. This would be true except for the fact that there is relative acceleration between the moving system and the stationary system in the Y direction. This alters the Y-momentum equations and has been treated by Schoenhals (A-34). The alteration resulting from the shift of reference systems produces a d'Alembert or body force due to the vibratory acceleration of the fluid coupled with its own inertia. By the adoption of a coordinate system attached to the

accelerating plate, Equations (2-12) become:

$$\frac{DU}{DT} = g\beta T\Delta\theta_0 - \frac{1}{\rho}\frac{\partial P}{\partial X} + \nu\nabla^2 U$$

$$\frac{DV}{DT} = -\frac{1}{\rho}\frac{\partial P}{\partial Y} + \nu\nabla^2 V - \rho\frac{DV_0}{DT}$$

$$\frac{\partial U}{\partial X} + \frac{\partial V}{\partial Y} = 0$$

(2-13)

$$\frac{DT}{DT} = \alpha\nabla^2 T$$

According to Ostrach, (C-8), the free convection flow along a vertical plate is of the boundary-layer type for large, sub-transitional Grashof numbers. This is the case in the present investigation. For free convection boundary layer flow without oscillation the Y-momentum equation is zero, but with oscillatory perturbations it becomes:

$$\frac{\partial P}{\partial Y} = -\rho\frac{DV_0}{DT} = -\rho\frac{\partial V_0}{\partial T}$$

(2-14)

By integrating Equation (2-14) from a distance Y_1, with respect to Y, outside the boundary layer, the pressure distribution is given as

$$P = P(X, Y, T) - \rho_\infty \int_Y^{Y_1} (1 - \beta T\Delta\theta_0)\frac{\partial V_0}{\partial T} dY$$

(2-15)

Differentiation with respect to X gives the pressure gradient along

the wall to be

$$\frac{\partial P}{\partial X} = \frac{\partial P}{\partial X} + \rho_\infty \int_Y^{Y_1} \beta \Delta \theta_0 \frac{\partial T}{\partial X} \frac{\partial V_0}{\partial T} dY_0 \qquad (2\text{-}16)$$

The first term gives the pressure gradient due to the potential flow just outside the boundary layer, and the second term gives the pressure distribution due to the inertial force term. It should be noted here that in this case the thermal variation of density provides the effect necessary to effect the pressure gradient. If there were no thermal variation of density then there would be no difference between a moving coordinate system and a stationary one. Therefore the final equations to solve with boundary-layer simplifications are

$$\frac{DU}{DT} = g\beta \Delta \theta_0 T - \frac{1}{\rho_\infty} \frac{\partial P}{\partial X} - \int_Y^{Y_1} \beta \Delta \theta_0 \frac{\partial T}{\partial X} \frac{\partial V_0}{\partial T} dY$$
$$+ \nu \frac{\partial^2 U}{\partial Y^2}$$

$$\qquad (2\text{-}17)$$

$$\frac{\partial U}{\partial X} + \frac{\partial V}{\partial Y} = 0$$

$$\frac{DT}{DT} = \alpha \frac{\partial^2 T}{\partial Y^2}$$

The Potential Flow Response

Schoenhals and Clark (A-33) have obtained the potential flow response of a thin plate of finite length vibrating transversely in an

incompressible fluid at rest using Lamb's treatment to obtain the potential flow about an elliptical cylinder. They approximated the thin plate of finite length by letting the semi-minor axis of the elliptical cylinder approach zero. Only the highlights of this development will be given here, more detailed information may be found in References (A-33) and (A-34).

The coordinate system was fixed in the body as shown in Figure 2-2. Therefore the velocity of the fluid at large distances from the plate is $-a\Omega \cos \Omega T$ and at the plate it is zero.

A complex potential $W(Z)$ was utilized the Z being a complex variable. In this representation the complex velocity is written as

$$\frac{dw}{dz} = -\overline{U} + i\,\overline{V} \tag{2-18}$$

The complex potential was determined with the appropriate boundary conditions so that the components of the complex velocity are

$$\overline{U} = \frac{V_0}{\sqrt{2}}\left\{\frac{X}{2}\sqrt{\frac{\sqrt{[1-(\frac{X}{C})^2+(\frac{Y}{C})^2]^2+4(\frac{X}{C})^2(\frac{Y}{C})^2}+[1-(\frac{X}{C})^2+(\frac{Y}{C})^2]}{[1-(\frac{X}{C})^2+(\frac{Y}{C})^2]^2+4(\frac{X}{C})^2(\frac{Y}{C})^2}}\right.$$

$$\left. -\frac{Y}{2}\sqrt{\frac{\sqrt{[1-(\frac{X}{C})^2+(\frac{Y}{C})^2]^2+4(\frac{X}{C})^2(\frac{Y}{C})^2}-[1-(\frac{X}{C})^2+(\frac{Y}{C})^2]}{[1-(\frac{X}{C})^2+(\frac{Y}{C})^2]^2+4(\frac{X}{C})^2(\frac{Y}{C})^2}}\right\}$$

$$\tag{2-19}$$
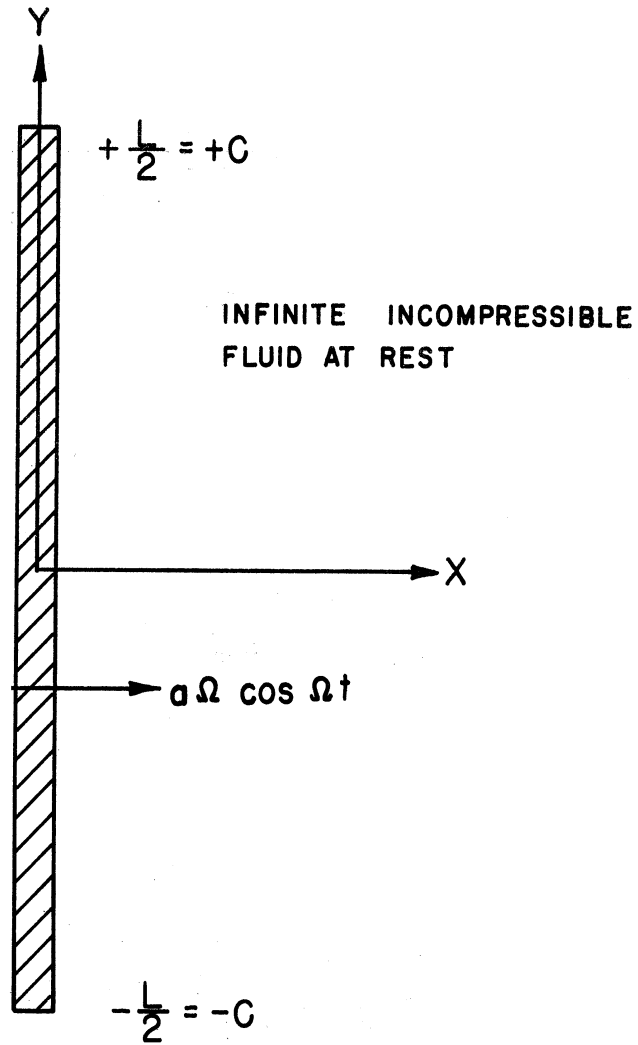
Figure 2-2. Sketch Showing a Thin Plate of Finite Length
Vibrating Transversely in an Infinite Incom-
pressible Fluid at Rest.

and

$$\overline{V} = \frac{-V_0}{\sqrt{2}} \left\{ \frac{X}{2} \sqrt{\frac{\sqrt{[1-(\frac{X}{C})^2+(\frac{Y}{C})^2]^2+4(\frac{X}{C})^2(\frac{Y}{C})^2}-[1-(\frac{X}{C})^2+(\frac{Y}{C})^2]}{[1-(\frac{X}{C})^2+(\frac{Y}{C})^2]^2+4(\frac{X}{C})^2(\frac{Y}{C})^2}} \right. $$

$$\qquad\qquad (2\text{-}20)$$

$$+ \frac{Y}{2} \sqrt{\frac{\sqrt{[1-(\frac{X}{C})^2+(\frac{Y}{C})^2]^2+4(\frac{X}{C})^2(\frac{Y}{C})^2}+[1-(\frac{X}{C})^2+(\frac{Y}{C})^2]}{[1-(\frac{X}{C})^2+(\frac{Y}{C})^2]^2+4(\frac{X}{C})^2(\frac{Y}{C})^2}}$$

The oscillating potential flow streamline pattern, taken from Schoenhals (A-34) is shown in Figure 2-3. Also values of the velocity profiles, $\overline{u}$ and $\overline{v}$, are shown as function of x/c and y/c in Figures 2-4 through 2-7.

For small values of Y, that is, the boundary layer regions, the above equations reduce to

$$\overline{V} = 0 \qquad\qquad (2\text{-}21A)$$

$$\overline{U} = \left[\frac{(X/C)}{\sqrt{1-(X/C)^2}} \right] V_0 \cos \Omega \, T \qquad\qquad (2\text{-}21B)$$

The values of the bracketed term in Equation (2-21B) are given in Figure 2-8. There are singular points at the edges of the plates where the theory would be invalid for a viscous fluid. Schoenhals, (A-34) have found good agreement with theory by using a hot-wire anemometer, except close to the singular points. This will be discussed in more detail in Chapter IV.
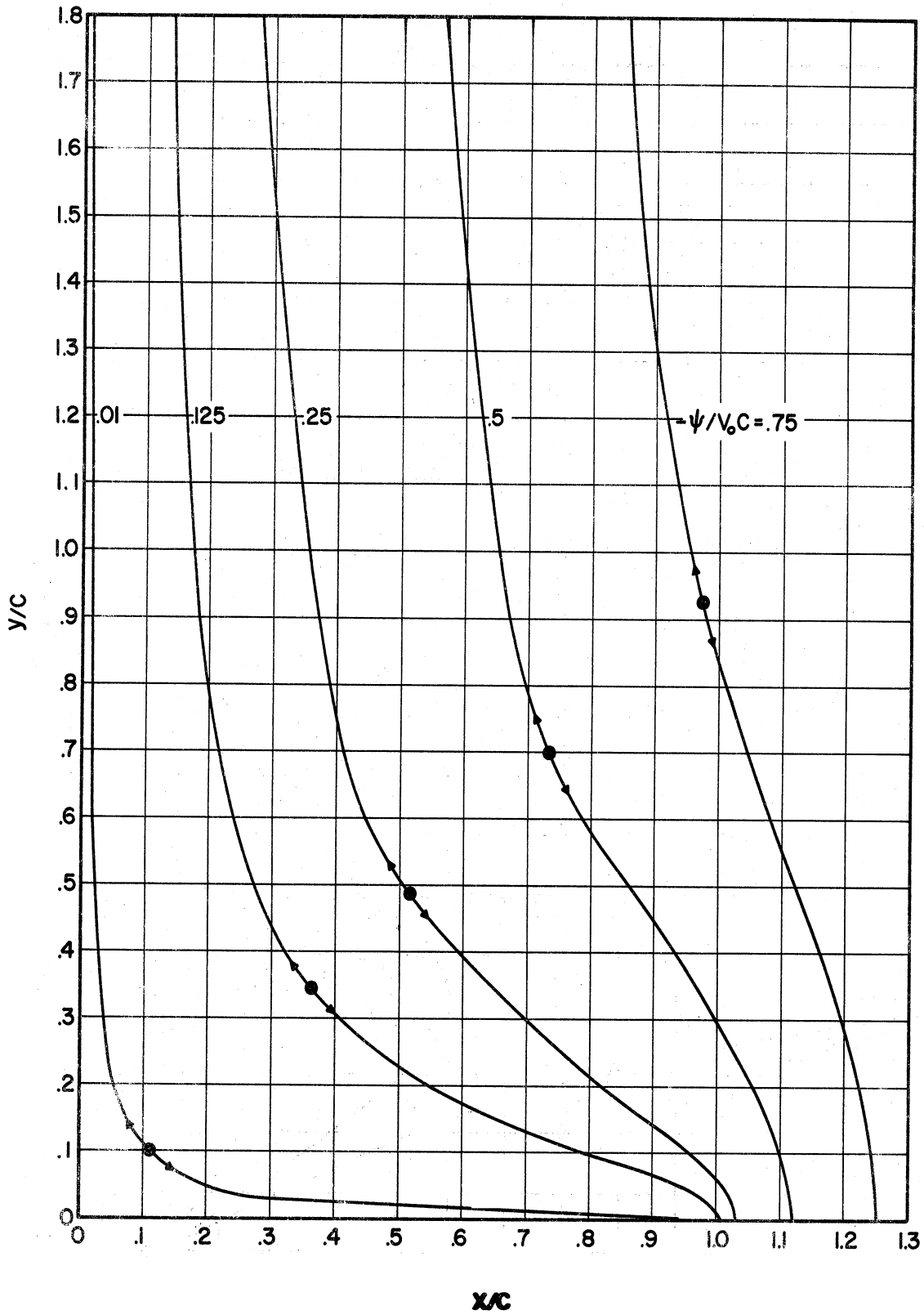
Figure 2-3. The Oscillating Potential Flow Streamline Patter for a
Plate Vibrating Transversely from Schoenhals (A-34).
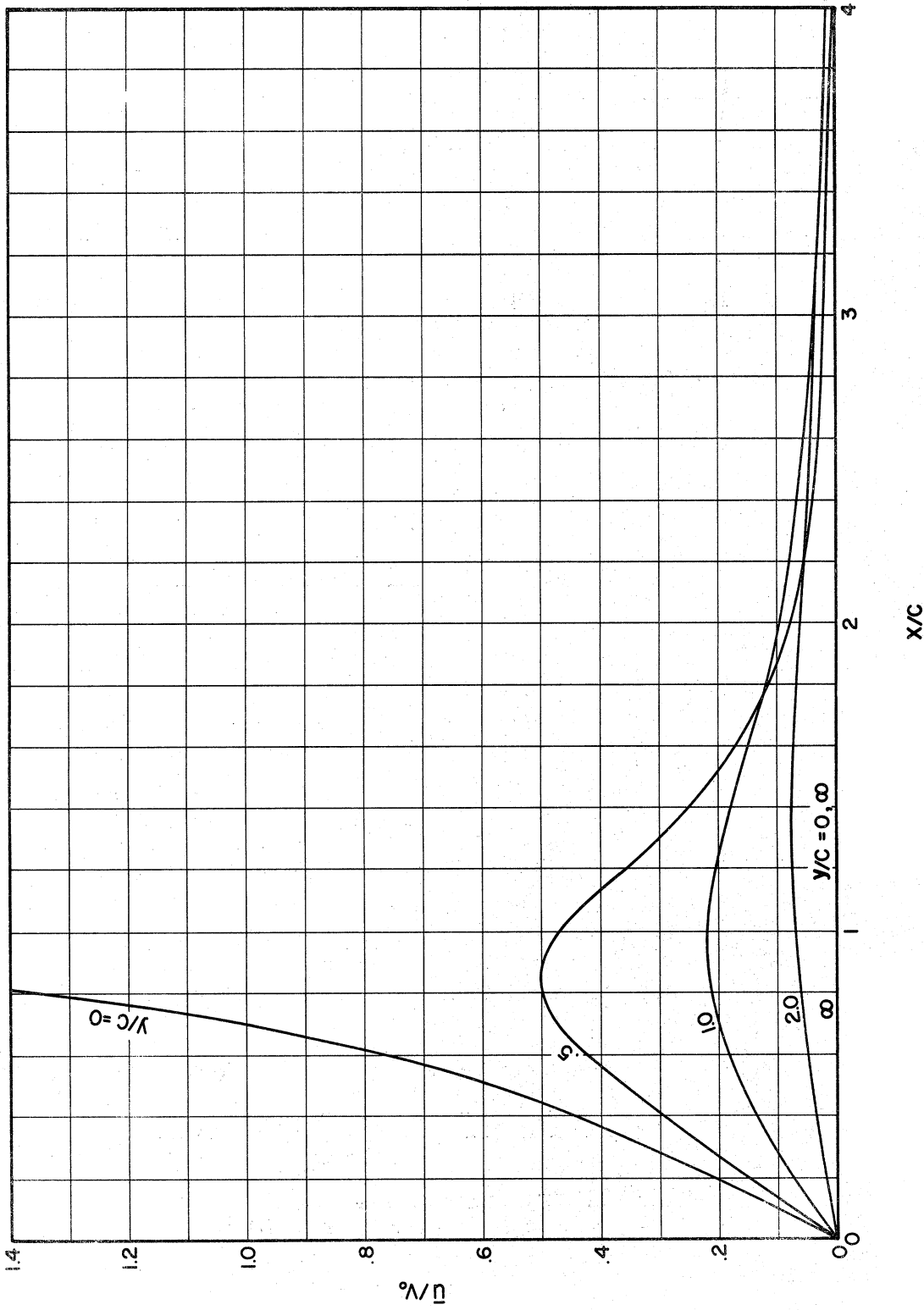
Figure 2-4. The Oscillating Potential Flow Velocity Distribution
for a Plate Vibrating Transversely from Schoenhals (A-34).
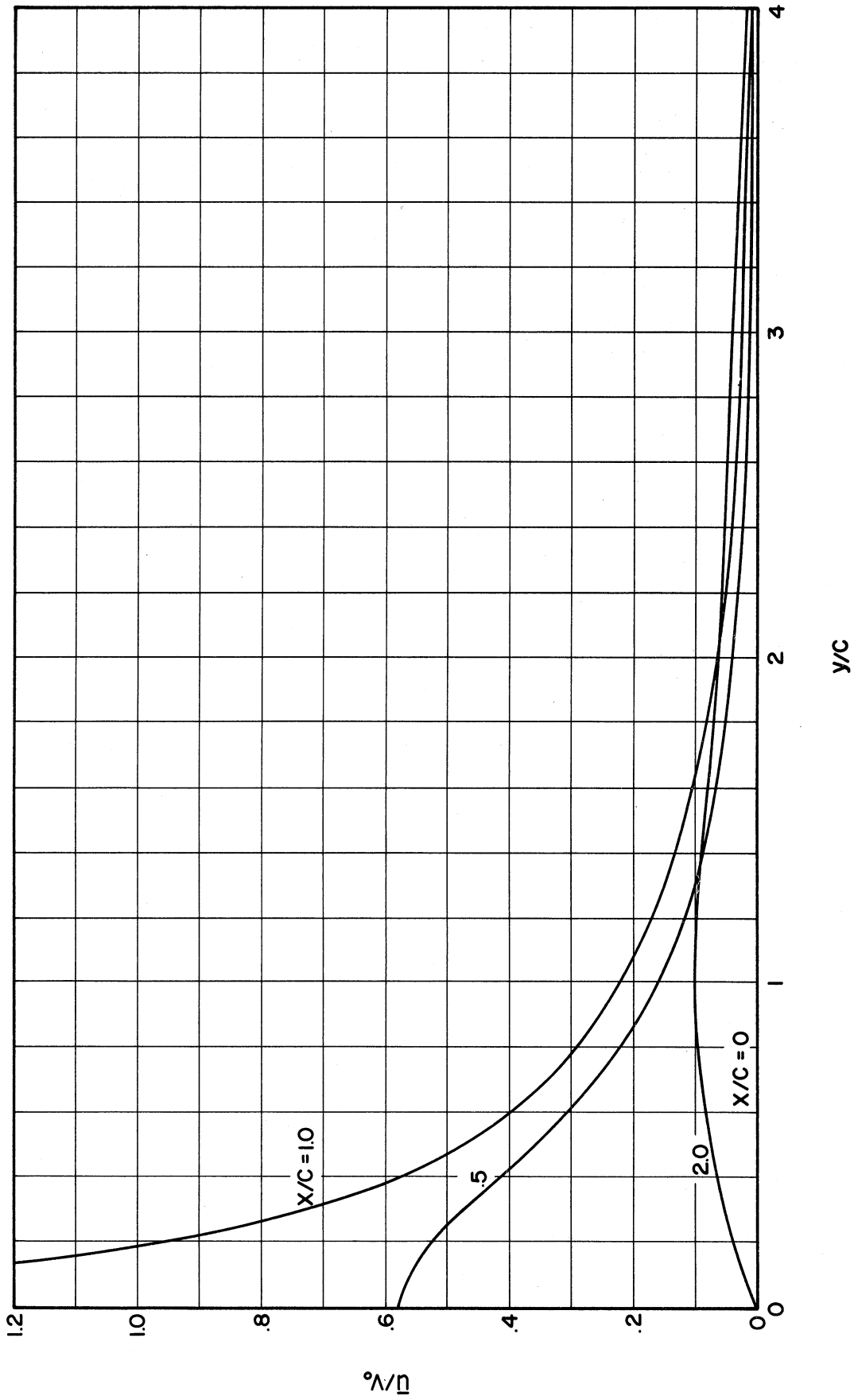
Figure 2-5. The Oscillating Potential Flow Velocity Distribution for a Plate Vibrating Transversely from Schoenhals (A-34).
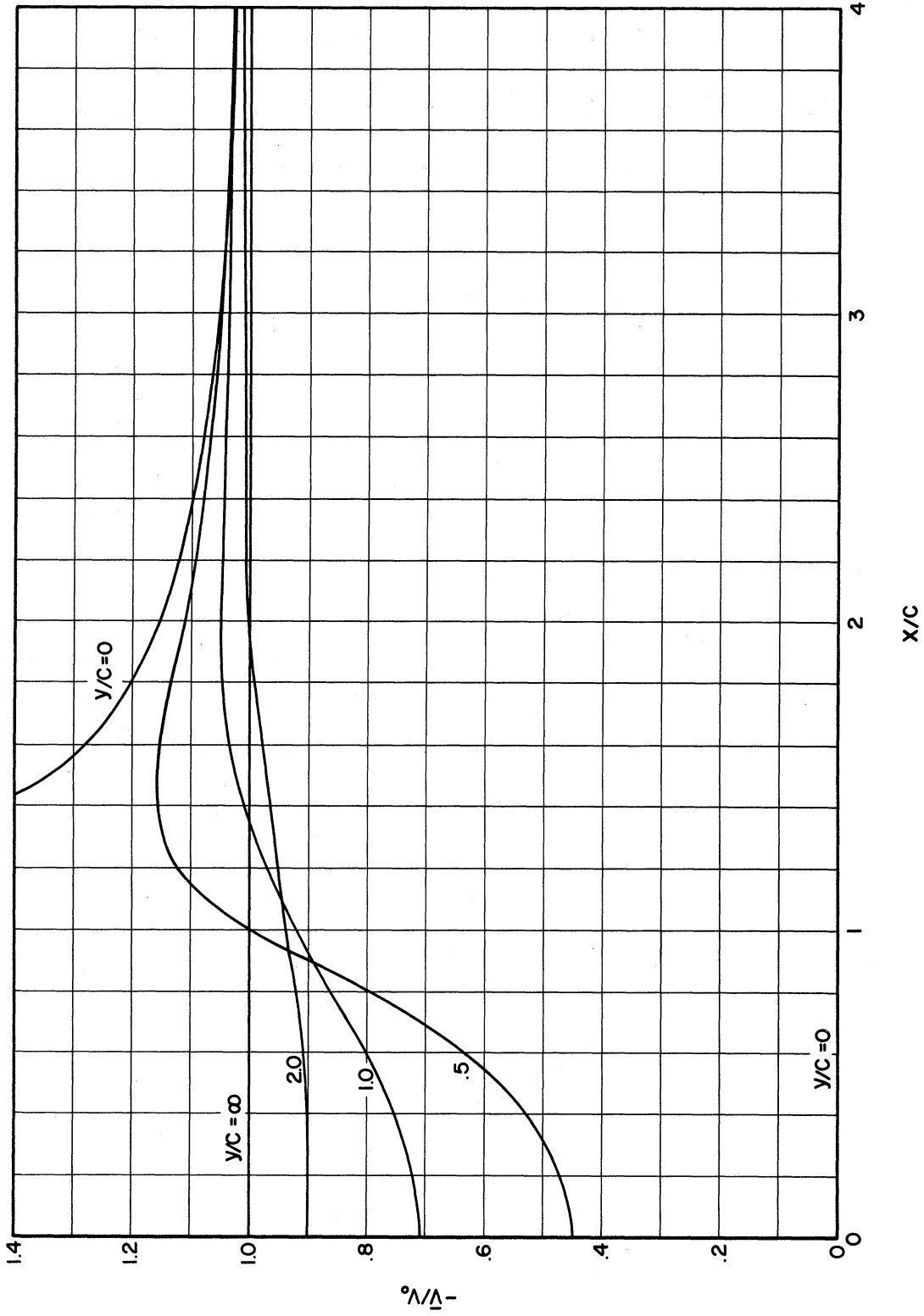
Figure 2-6. The Oscillating Potential Flow Velocity Distribution for a Plate Vibrating Transversely from Schoenhals (A-34).
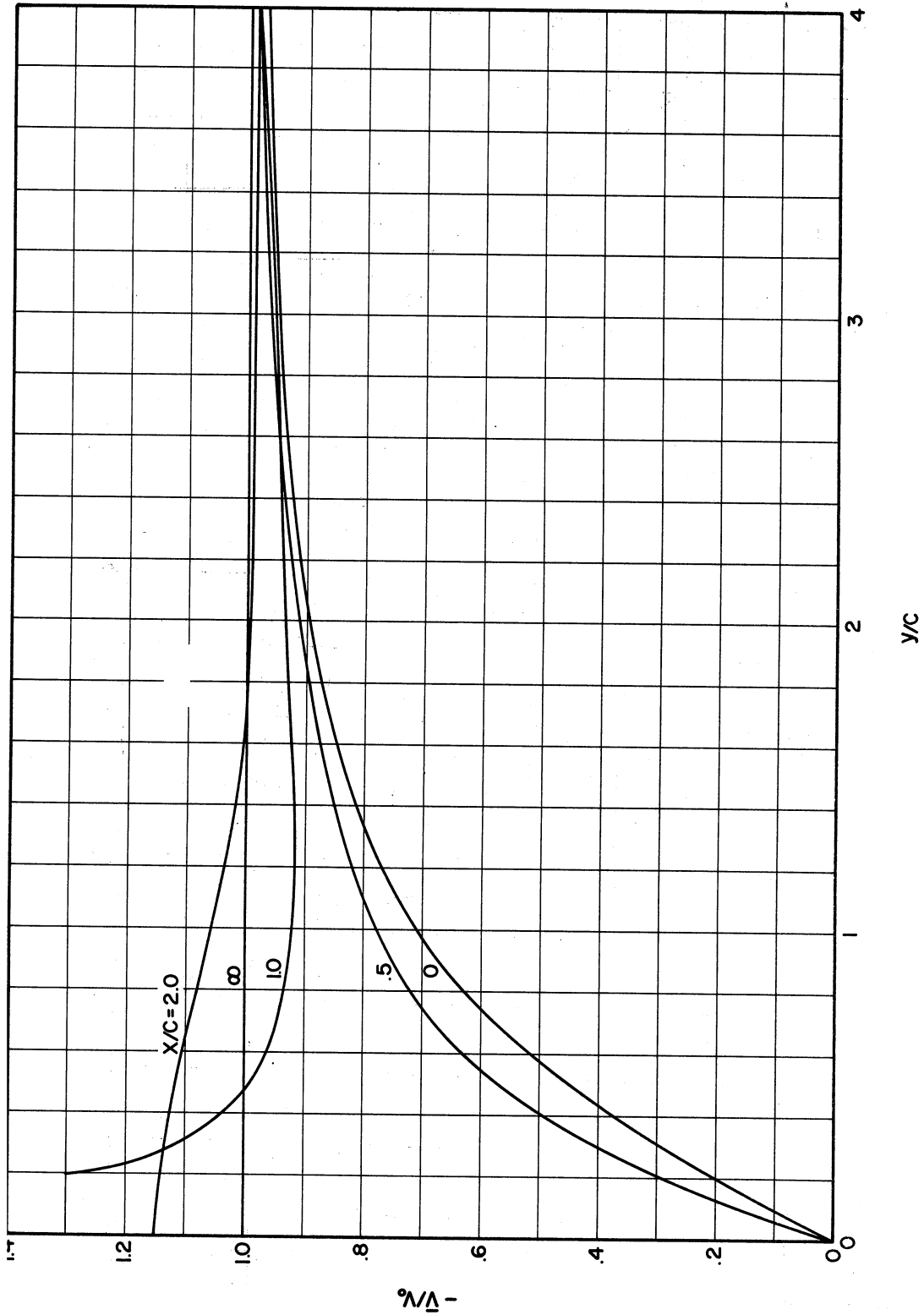
Figure 2-7. The Oscillating Potential Flow Velocity Distribution for a Plate Vibrating Transversely from Schoenhals (A-34).

$$\frac{u_o}{V_o} = \frac{X/C}{\sqrt{1-(X/C)^2}}$$
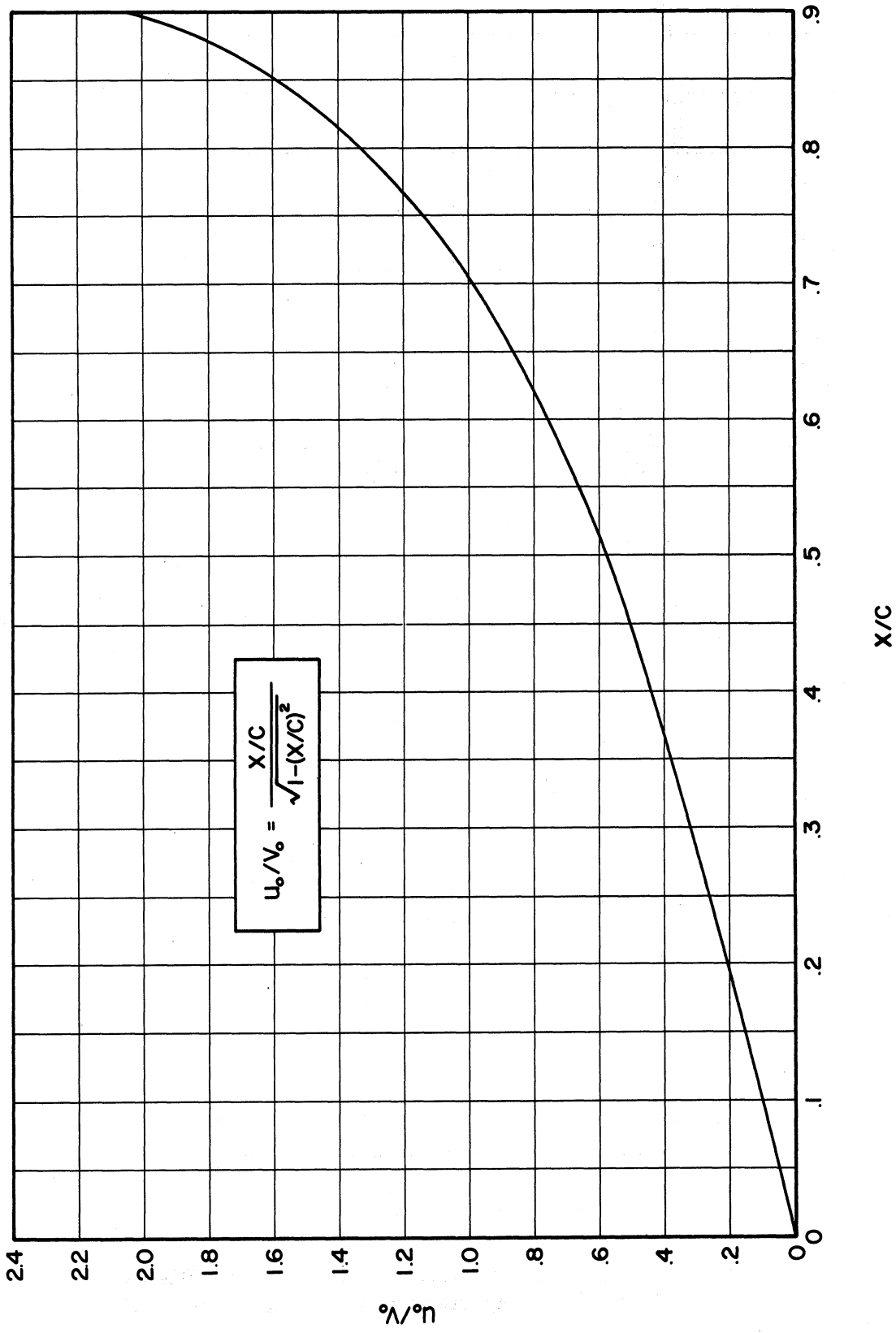
2-8   The Oscillating Potential Flow Along a Plate Vibrating
      Transversely from Schoenhals (A-34)................

Non-Dimensionalization of the Equations

Non-dimensionalization of the equations is fashioned after Ostrach (C-8). The potential flow was determined with the reference system fixed in the middle of the plate. In this problem it is more convenient to fix the coordinate system at the bottom edge of the plate, the same as the reference system of the governing equation. By defining

$$P = \frac{X/c}{\sqrt{1 - (X/c)^2}} \tag{2-22}$$

we have by shifting the coordinate X to $(X-1)$

$$P_0 = \frac{(X/c) - 1}{\sqrt{1 - ((X/c) - 1)^2}} \tag{2-23}$$

The pressure distribution is determined from the potential flow by utilizing the Euler's equations. Euler's equations are

$$-\frac{1}{\rho}\frac{\partial P}{\partial X} = \frac{\partial \overline{U}}{\partial T} + \overline{U}\frac{\partial \overline{U}}{\partial X} + \overline{V}\frac{\partial \overline{U}}{\partial Y}$$

$$\tag{2-24}$$

$$-\frac{1}{\rho}\frac{\partial P}{\partial Y} = \frac{\partial \overline{V}}{\partial T} + \overline{U}\frac{\partial \overline{V}}{\partial X} + \overline{V}\frac{\partial \overline{V}}{\partial Y}$$

and by utilizing the Equations (2-21) at the outer edge of the boundary

layer we have

$$-\frac{1}{\rho}\frac{\partial P}{\partial X} = \frac{\partial \overline{U}}{\partial \tau} + \overline{U}\frac{\partial \overline{U}}{\partial X}$$

$$-\frac{1}{\rho}\frac{\partial P}{\partial Y} = 0$$

(2-25)

The dimensionless terms used in the non-dimensionalization

are

$$X = \frac{\overline{X}}{L} \qquad\qquad \epsilon = \frac{a\omega}{L}$$

$$Y = \frac{\overline{Y}}{L}\sqrt[4]{Gr_L} \qquad\qquad K_o = \frac{\beta\Delta\Theta_0}{\sqrt[4]{Gr_L}}$$

$$Gr_L = \frac{g\beta L^3 \Delta\Theta_0}{\nu^2} \qquad\qquad U = \frac{L}{\nu\sqrt{Gr_L}}\,\mathcal{U}$$

(2-26)

$$\mathcal{W} = \frac{L^2}{\nu\sqrt{Gr_L}}\,\Omega \qquad V = \frac{L}{\nu\sqrt[4]{Gr_L}}\,\mathcal{V}$$

$$t = \frac{\nu\sqrt{Gr_L}}{L^2}\,\tau \qquad P = \frac{2X-1}{2\sqrt{X(1-X)}}$$

The dimensionless equations from Equations (2-17) are there-

fore represented as

$$\frac{DU}{Dt} = T + \frac{\partial^2 U}{\partial Y^2} + \epsilon\frac{\partial P}{\partial t}\cos\omega t + \epsilon^2 P\frac{\partial P}{\partial X}\cos^2\omega t$$

$$+ \epsilon K_o \omega \int_y^{Y_1} \frac{\partial T}{\partial X}\,dy\,\sin\omega t$$

(2-27)

$$\frac{\partial u}{\partial x} + \frac{\partial v}{\partial y} = 0$$

$$\frac{DT}{Dt} = \frac{1}{P_R} \frac{\partial^2 T}{\partial y^2}$$

Perturbation of the Equations

As stated in the preceding discussion, this problem treats the case where buoyancy forces predominate. In other words, where the flow is mainly that of free convection and the oscillations are imposed as perturbations on the free convection velocity and temperature field. This is expressed by the following expansion in terms of ϵ

$$U = U(X, Y, 0) + \frac{\partial U}{\partial \epsilon}\bigg)_{\epsilon=0} \epsilon + \frac{\partial^2 U}{\partial \epsilon^2}\bigg)_{\epsilon=0} \frac{\epsilon^2}{2!} + \cdots \qquad (2\text{-}28)$$

and is written in the form

$$U = U_0 + \epsilon U_I + \epsilon^2 U_{II} + \cdots \qquad (2\text{-}29\text{A})$$

The u_0 is the free convection velocity. This expansion is advantageous because the first term is the velocity of the free convection boundary layer which has been solved analytically by Ostrach (C-8). The expansions are therefore taken as

$$U = U_0 + \epsilon U_I + \epsilon^2 U_{II} + \cdots \qquad (2\text{-}29\text{A})$$

$$V = V_0 + \epsilon V_I + \epsilon^2 V_{II} + \cdots \qquad (2\text{-}29\text{B})$$

$$T = T_0 + \epsilon T_I + \epsilon^2 T_{II} + \cdots \qquad (2\text{-}29\text{C})$$

By substituting these expansions into Equations (2-27) and by separating terms according to the powers of ϵ^n, n = 0, 1, 2, ..., the following equations are found

Zero-order equations, ϵ^0

$$\frac{\partial U_0}{\partial X} + \frac{\partial V_0}{\partial Y} = 0$$

$$U_0 \frac{\partial U_0}{\partial X} + V_0 \frac{\partial U_0}{\partial Y} = \frac{\partial^2 U_0}{\partial Y^2} + T_0 \qquad (2\text{-}30)$$

$$U_0 \frac{\partial T_0}{\partial X} + V_0 \frac{\partial T_0}{\partial Y} = \frac{1}{P_R} \frac{\partial^2 T_0}{\partial Y^2}$$

First-order equations, ϵ^1

$$\frac{\partial U_I}{\partial X} + \frac{\partial V_I}{\partial Y} = 0 \qquad (2\text{-}31\text{A})$$

$$\frac{\partial U_I}{\partial t} + U_0 \frac{\partial U_I}{\partial X} + U_I \frac{\partial U_0}{\partial X} + V_0 \frac{\partial U_I}{\partial Y} + V_I \frac{\partial U_0}{\partial Y} = \frac{\partial^2 U_I}{\partial Y^2} \qquad (2\text{-}31\text{B})$$

$$+ T_I + \frac{\partial}{\partial t}\left[P \cos \omega t\right] + K_0 \omega \int_Y^{Y_I} \frac{\partial T_0}{\partial X} dy \sin \omega t$$

$$\frac{\partial T_I}{\partial t} + U_0 \frac{\partial T_I}{\partial X} + U_I \frac{\partial T_0}{\partial X} + V_0 \frac{\partial T_I}{\partial Y} + V_I \frac{\partial T_0}{\partial Y} = \frac{1}{P_R} \frac{\partial^2 T_I}{\partial Y^2} \qquad (2\text{-}31\text{C})$$

Second-order equations, ϵ^2

$$\frac{\partial U_{II}}{\partial X} + \frac{\partial V_{II}}{\partial Y} = 0 \qquad (2\text{-}32\text{A})$$

$$\frac{\partial U_I}{\partial t} + U_0 \frac{\partial U_I}{\partial X} + U_I \frac{\partial U_I}{\partial X} + U_{II} \frac{\partial U_0}{\partial X} + V_0 \frac{\partial U_{II}}{\partial Y} +$$

$$V_I \frac{\partial U_I}{\partial Y} + V_{II} \frac{\partial U_0}{\partial Y} = \frac{\partial^2 U_{II}}{\partial Y^2} + T_{II} + P \frac{\partial P}{\partial X} \cos^2 \omega t + \quad \text{(2-32B)}$$

$$K_0 \omega \int_Y^{Y_I} \frac{\partial T_I}{\partial X} \, dy \, \sin \omega t$$

$$\frac{\partial T_{II}}{\partial t} + U_0 \frac{\partial T_{II}}{\partial X} + U_I \frac{\partial T_I}{\partial X} + U_{II} \frac{\partial T_0}{\partial X} + V_0 \frac{\partial T_{II}}{\partial Y} +$$

$$\text{(2-32C)}$$

$$V_I \frac{\partial T_I}{\partial Y} + V_{II} \frac{\partial T_{II}}{\partial Y} = \frac{1}{P_R} \frac{\partial^2 T_{II}}{\partial Y^2}$$

The value of ϵ is chosen small so that the first three terms of the expansion will approximate the physical problem. By choice of small ϵ, terms such as $\epsilon u_I + \epsilon^2 u_{II} + \ldots$ will always be small. The quantity (a/L) must always be considered small to stay within compressibility requirements. Since ϵ includes ω, then as frequency increases (a/L) must decrease proportionately.

Zero-Order Equations

Ostrach's (C-8) solution and tabulated values were used for the zero-order equations. The non-dimensionalization of the equations was made so that the zero-order equations would yield the form used by Ostrach.

He utilized a stream function such that

$$U = \frac{\partial \Psi_0}{\partial Y} \tag{2-33A}$$

and

$$V = -\frac{\partial \Psi_0}{\partial X} \tag{2-33B}$$

so that continuity is satisfied. This produces

$$\frac{\partial \Psi_0}{\partial Y} \frac{\partial^2 \Psi_0}{\partial X \partial Y} - \frac{\partial \Psi_0}{\partial X} \frac{\partial^2 \Psi_0}{\partial Y^2} - \frac{\partial^3 \Psi_0}{\partial Y^3} - T_0 = 0$$

$$\tag{2-34}$$

$$\frac{\partial \Psi_0}{\partial Y} \frac{\partial T_0}{\partial X} - \frac{\partial \Psi_0}{\partial X} \frac{\partial T_0}{\partial Y} = \frac{1}{P_R} \frac{\partial^2 T_0}{\partial Y^2}$$

The boundary conditions are

$$\left(\frac{\partial \Psi_0}{\partial X}\right)_0 = \left(\frac{\partial \Psi_0}{\partial Y}\right)_0 = \left(\frac{\partial \Psi_0}{\partial Y}\right)_\infty = 0$$

$$\tag{2-35}$$

$$(T_0)_0 = 1, \quad (T_0)_\infty = 0.$$

Final simplification of the equations was made by transforming the coordinates using a "similarity transformation"

$$\eta = \frac{Y}{(4X)^{1/4}} \tag{2-36}$$

and a stream function

$$\psi = (4X)^{3/4} F(\eta) \qquad \qquad (2\text{-}37)$$

and a temperature function

$$T_0 = H(\eta) \, . \qquad \qquad (2\text{-}38)$$

The energy equation and the momentum equation were then reduced to the
following ordinary differential equations:

$$F''' + 3FF'' - 2F'^2 + H = 0 \qquad \qquad (2\text{-}39)$$

and

$$H'' + 2P_R F H' = 0 \qquad \qquad (2\text{-}40)$$

The boundary conditions are

$$F(0) = F'(0) = 0$$
$$H(0) = 1 \qquad \qquad (2\text{-}41)$$

and

$$F'(\infty) = H(\infty) = 0 \, .$$

Some of the results obtained by Ostrach are shown in Figures 9
through 14. His results agreed with measurements of Schmidt and Beckman
(C-11), and Eckert (C-1). Schmidt and Beckman performed experiments on
free-convection flows in which velocity measurements at various points
along the plate were made by means of a quartz-filament anemometer and
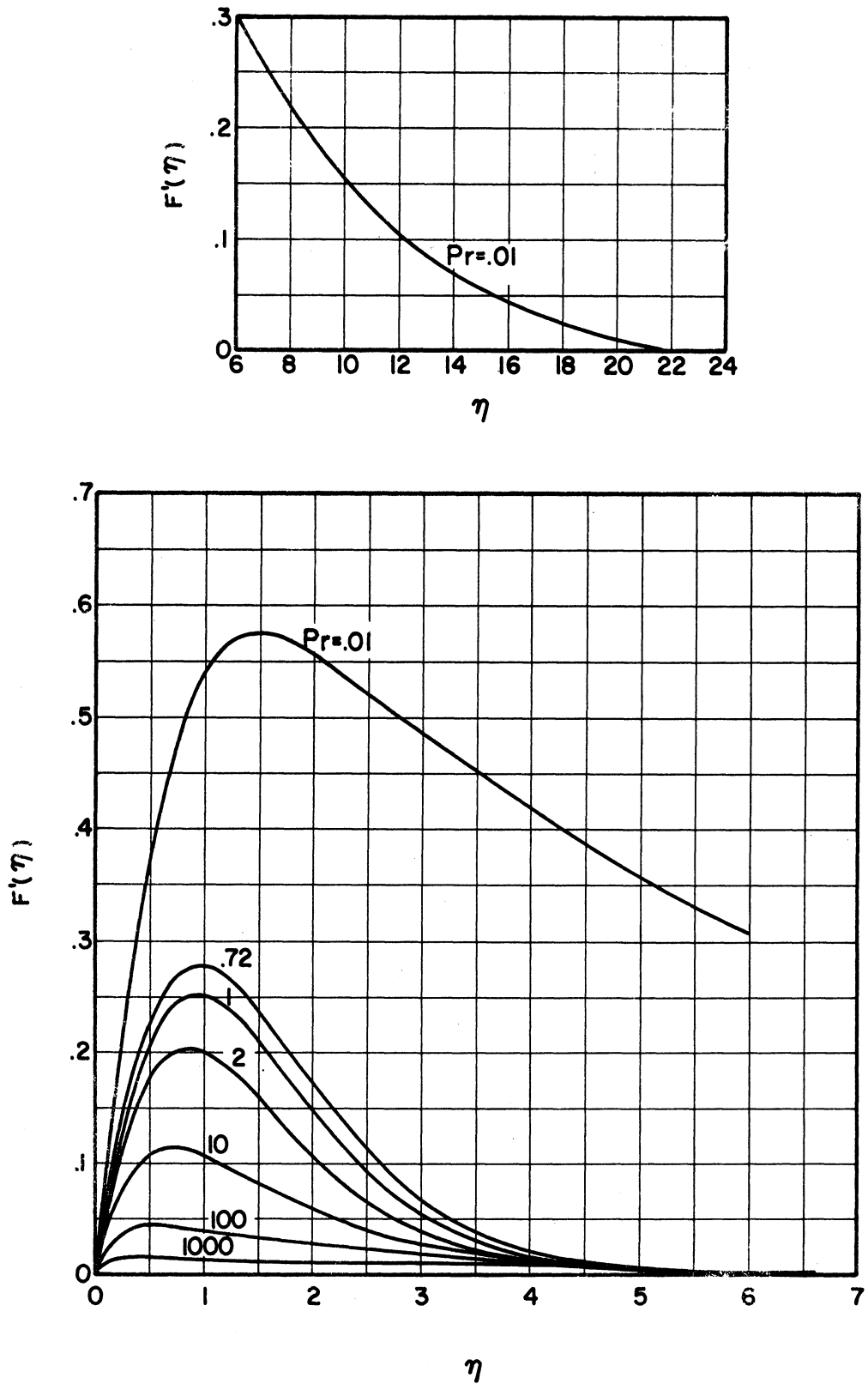
Figure 2-9.   Velocity Profiles for Laminar Free Convection Boundary
               Layers as Reproduced from Ostrach (C-8).
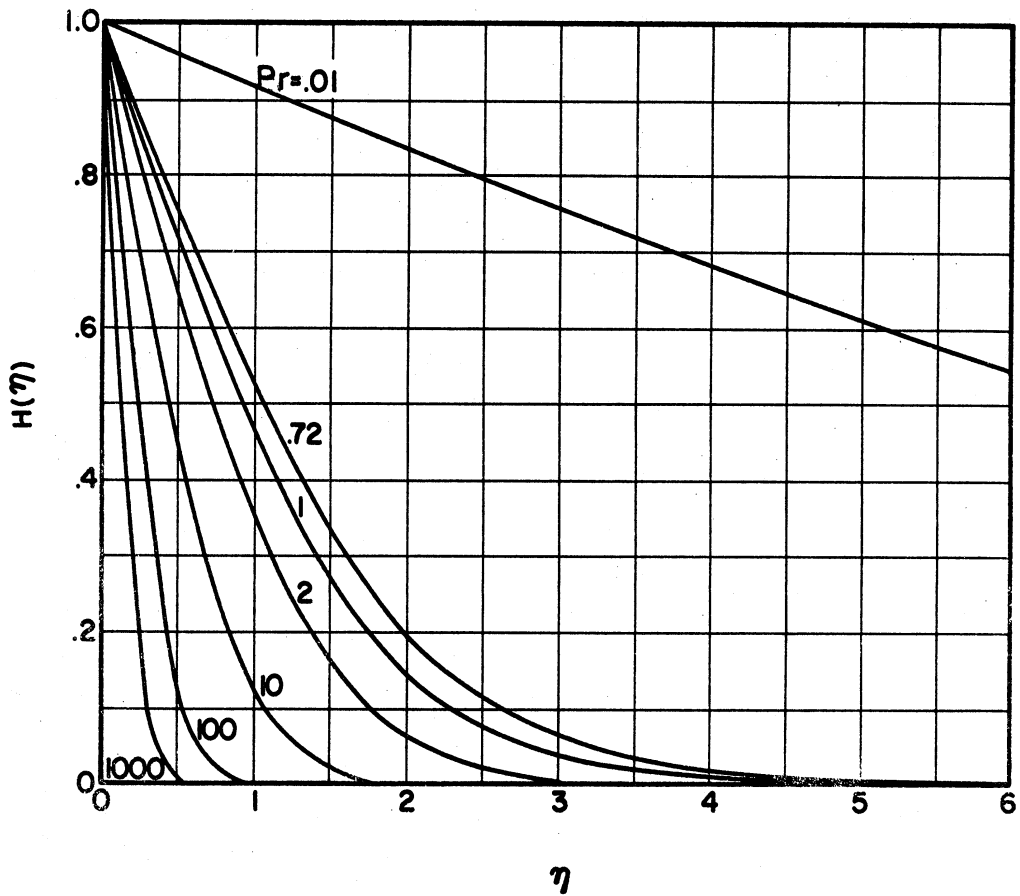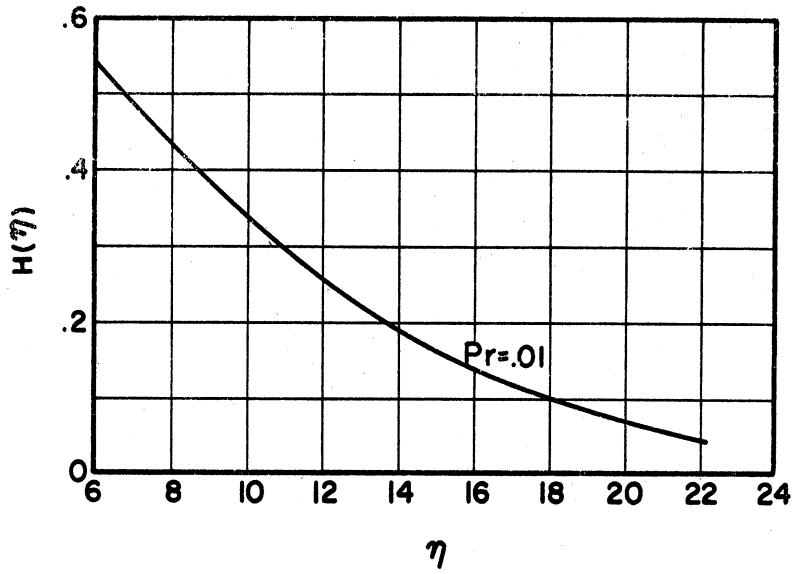
Figure 2-10. Temperature Profiles for Laminar Free Convection Boundary
Layer as Reproduced from Ostrach (C-8).
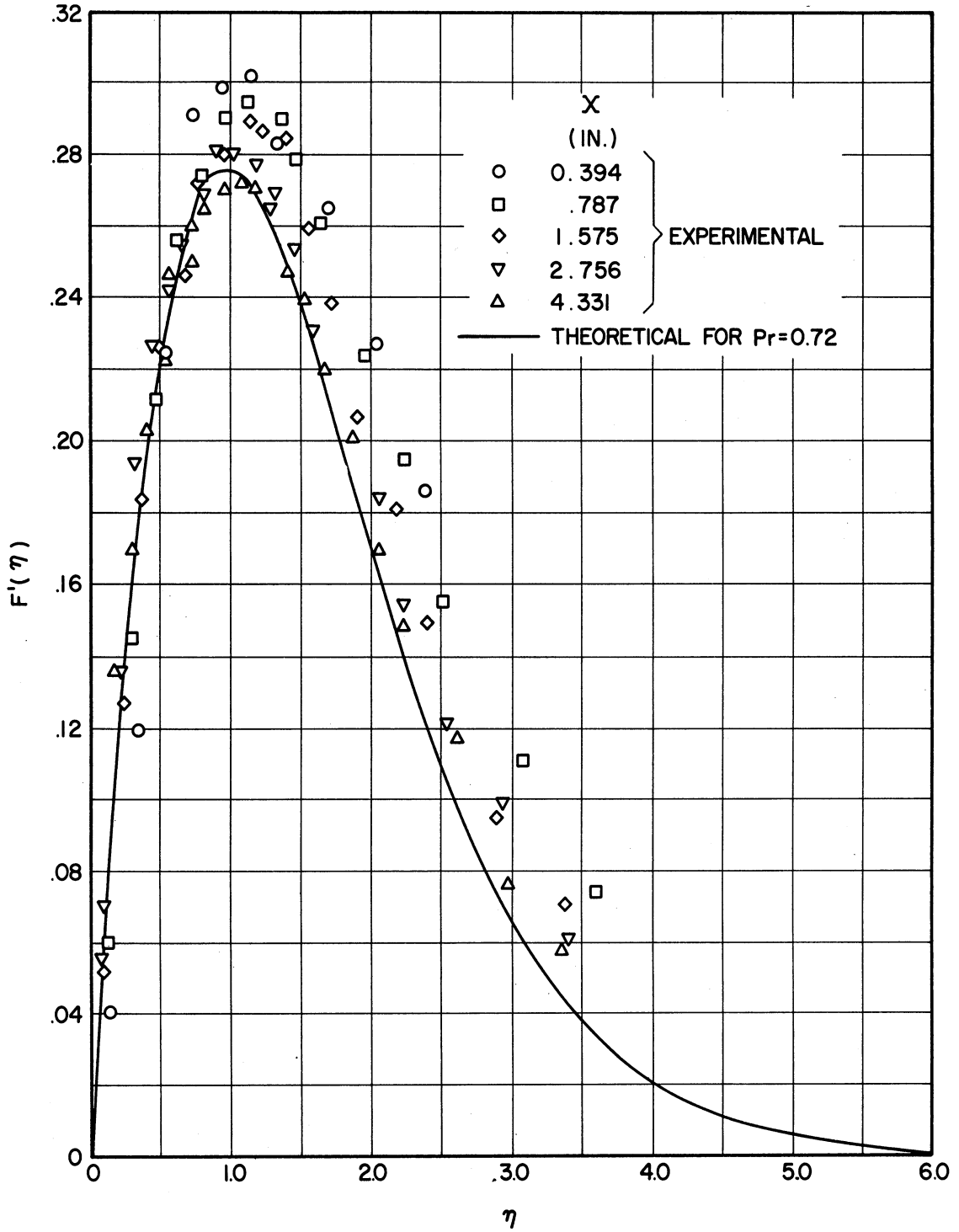
Figure 2-11. Velocity Measurements of Schmidt and Beckman (C-11) and
Comparison with Theory as Reproduced from Ostrach (C-8)
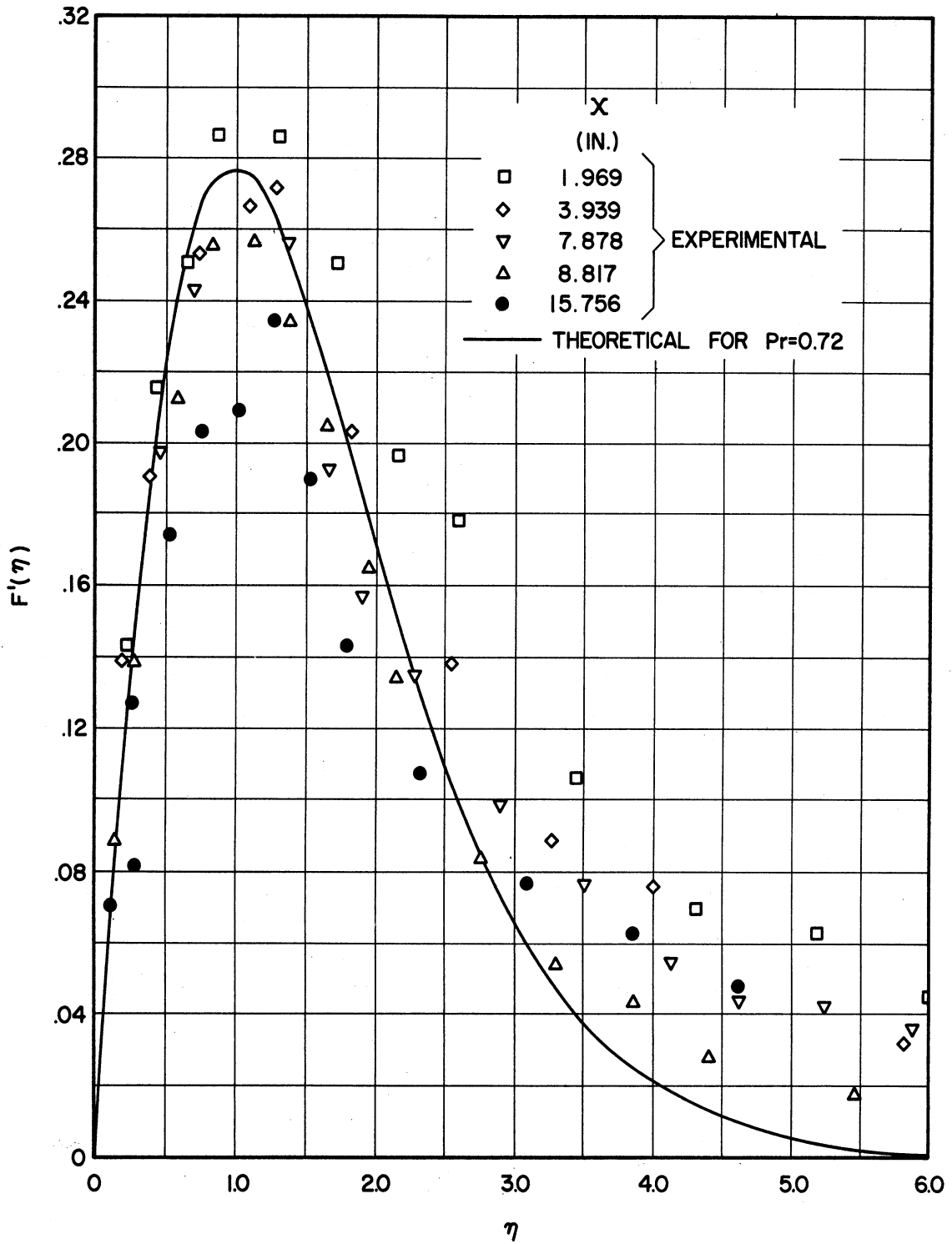
Figure 2-12. Velocity Measurements of Schmidt and Beckman (C-11) and Comparison with Theory as Reproduced from Ostrach (C-8)
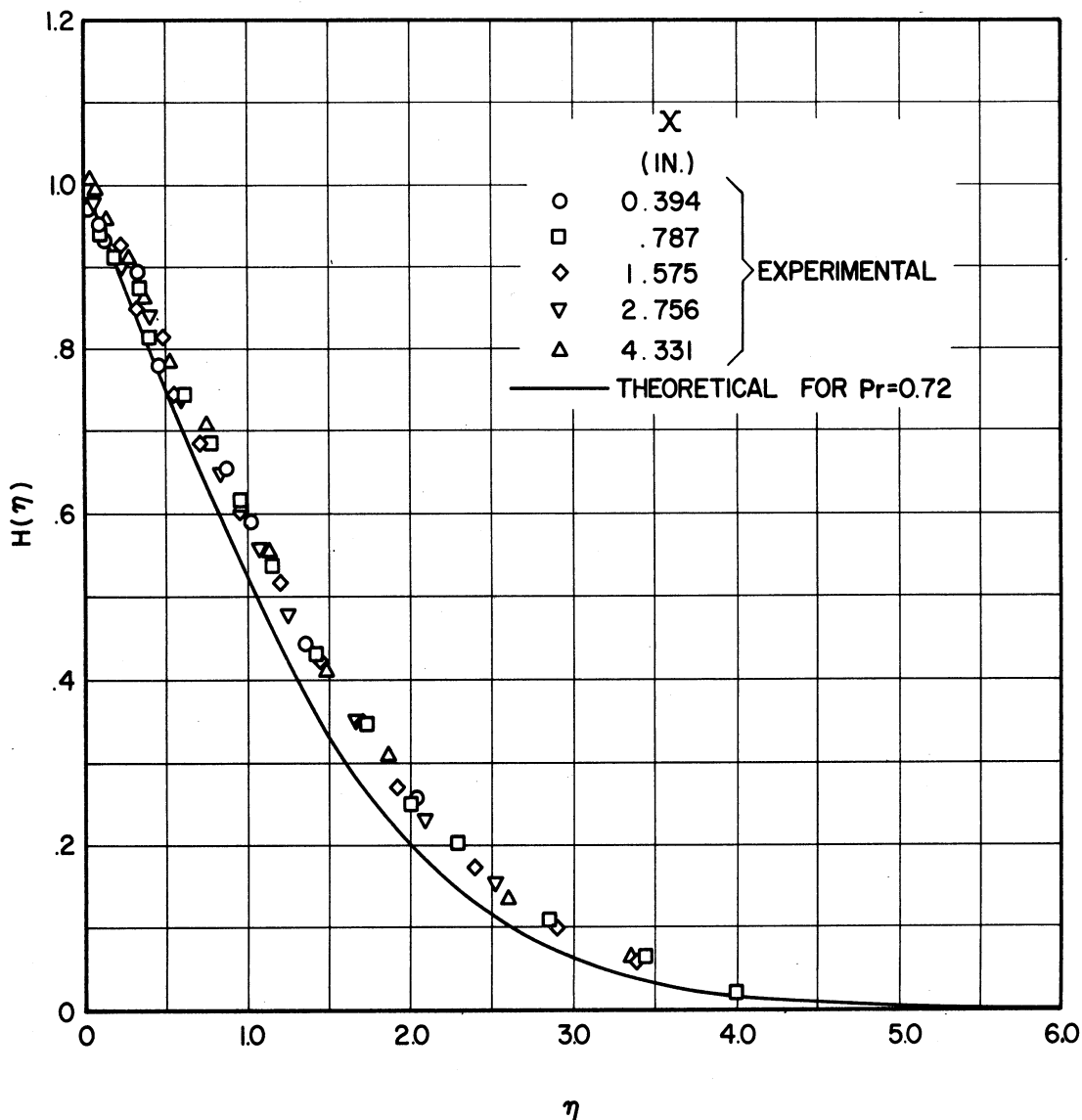
Figure 2-13. Temperature Measurements of Schmidt and Beckman (C-11) and Comparison with Theory as Reproduced from Ostrach (C-8).
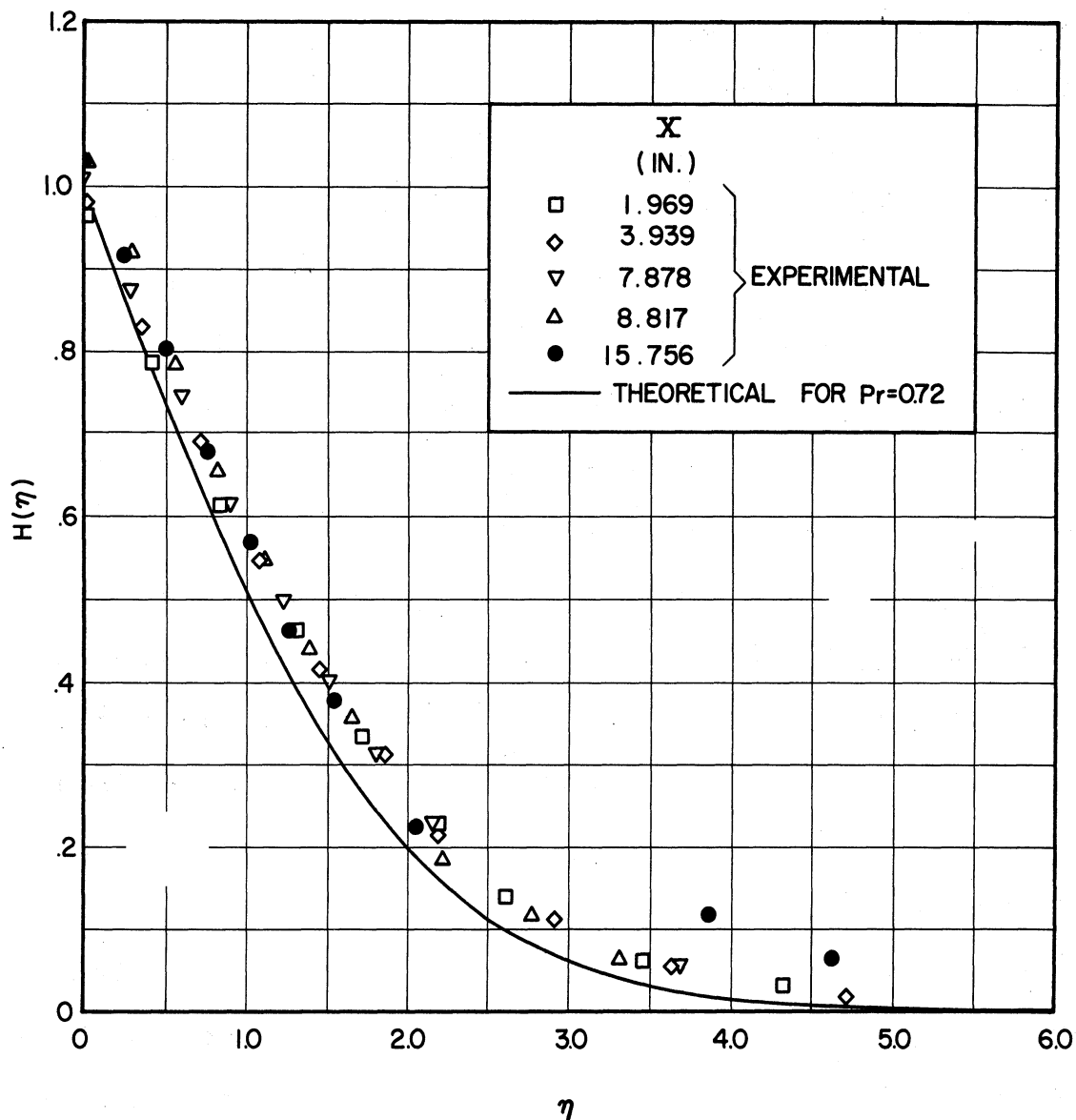
Figure 2-14. Temperature Measurements of Schmidt and Beckman (C-11) and Comparison with Theory as Reproduced from Ostrach (C-8).

the temperature measurements were obtained by means of manganese-constantan thermocouples. Eckert made similar measurements by means of a Zehnder-Mach interferometer. The lines shown in the figures are the theory of Ostrach and the data is that of Schmidt and Beckman.

The results for the small plate are nearly identical to that of theory especially for small values of η. This was attributed to the fact that for the small plates the flow was entirely laminar except near the outer edge of the boundary layer where some slight turbulence from the room air disturbed the measurements. As can be seen, in the figures for the large plate the scatter of the data is more than that of the small plate. Large periodic oscillations of the flow near the downstream edge were reported for the large plate in addition to room turbulence at the outer edge of the boundary layer. It is well known that by increasing the Grashof number the transition region from laminar to turbulent flow will move down a plate.

Heat transfer data correlate well with the theoretically computed values except for those of oil. The Prandtl number of oil in the experiment varies approximately from 90 to 500. The maximum error was reported to be approximately 20 percent. The deviations were attributed to either end effects in the measurements or to the fact that viscosity changes in oil are large for even small temperature differences.

As a result of the good correlation of the data of Schmidt and Beckman (C-11) to the theory of Ostrach (C-8) for velocity, temperature and Nusselt number, Ostrach's tabulated results were used for the zero-order solution.

Approximated Zero-Order Functions

In the first-order and second-order equations most terms depend upon functions of solutions of the zero-order equations. The zero-order solutions are tabulated values which do not lend themselves to convenient integration. The reason for their presence is due to physical interaction of the small effects of the oscillations on the free convection field arising from inertia and viscous forces in the boundary layer. Mathematically it is represented by the non-linearity of the governing partial differential equations.

The last term in the first-order momentum equation can be calculated as

$$(4X)^{1/4} \int_{y}^{\infty} \frac{\partial T_0}{\partial X} dy = (4X)^{-3/4} \int_{\infty}^{\eta} \eta \, H'(\eta) d\eta = (4X)^{-3/4} \, \Upsilon(\eta) \qquad (2\text{-}42)$$

Schoenhals (A-34) has done this, and the solid line in Figure 2-15 is values of his result. His tabulated results can be found in Appendix IIIA. In order to solve the first order momentum equation a simple but satisfactory analytical expression has been found in the present study for $\zeta(\eta)$ which adequately fits the data. These are shown as the dotted line in Figure 2-15. The equation which fits approximately the data for two Prandtl numbers is

$$\frac{\Upsilon(\eta)}{\Upsilon(0)} = K_1(P_R) \eta \, e^{-K_1(P_r)\eta} + e^{-K_1(P_r)\eta} \qquad (2\text{-}43)$$

This normalized representation is exact at $\eta = 0$. This curve approximates very well $\zeta(\eta)$ for low values of η and for extremely high values of η,
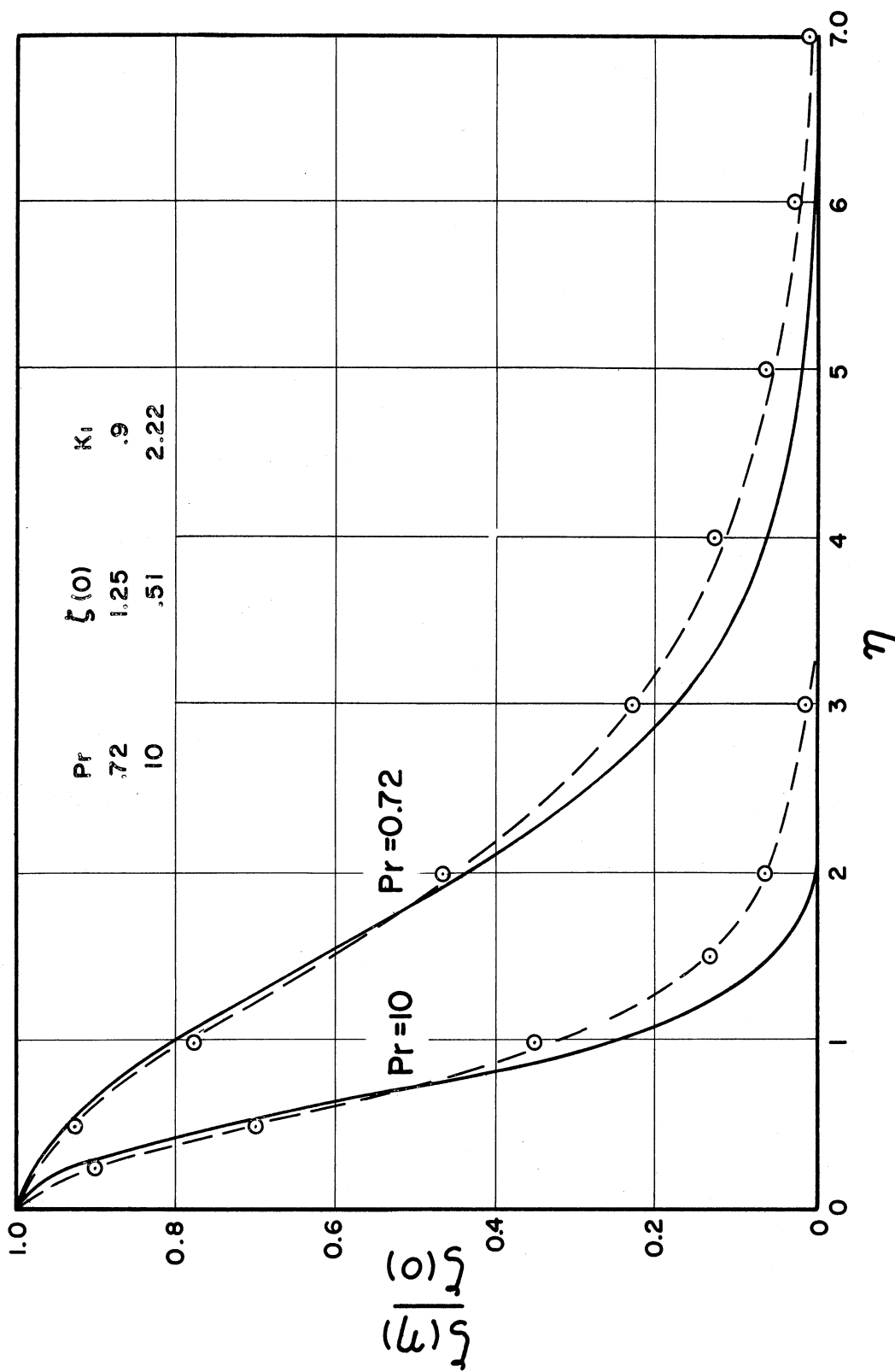
Figure 2-15. Comparison of $\zeta(\eta)/\zeta(0)$ from Schoenhals (A-34) to That of Equation (2-43).

where it approaches zero. More terms or a higher order polynomial with exponential terms would give an improved fit but the effort required compared to the additional accuracy gained would be excessive. The value of $\zeta(\eta)$ at any point in the boundary layer indicates the order of magnitude of the oscillating pressure gradient produced by wall vibration arising from thermal variation of density. In the next section the order of magnitude of this quantity will be discussed with respect to the pressure gradient arising from the potential flow. Since the derivatives of the free convection temperature can be expressed as

$$\frac{\partial T_0}{\partial X} = -\frac{\eta}{(4X)} H'(\eta)$$

$$\frac{\partial T_0}{\partial Y} = \frac{1}{(4X)^{1/4}} H'(\eta)$$

(2-44)

a simple but satisfactory expression was found in this present study which adequately approximated the curve of $H'(\eta)$. The solid line in Figure 2-16 represent the tabulated results of Ostrach (C-8) and the dashed lines are the values of

$$H'(\eta) = H'(0) e^{-K_1(P_r)\eta} - K_2(P_r)\eta e^{-K_1(P_r)\eta} .$$

(2-45)

All the coefficients K_1 and K_2 are constants for a particular Prandtl number. K_1 and K_2 are given on Figure 2-16 for two Prandtl numbers, 0.72 and 10. The values are exact for $\eta = 0$ since here it is equal to $H'(0)$. The curves for both Prandtl numbers fit well for small values of η and for large values of η. The intermediate values of η are slightly

	Pr	H'(0)	K$_1$	K$_2$
	.72	-.5046	.9	.5046
	10	-1.169	2.22	3.1

Pr = 10

Pr = 0.72
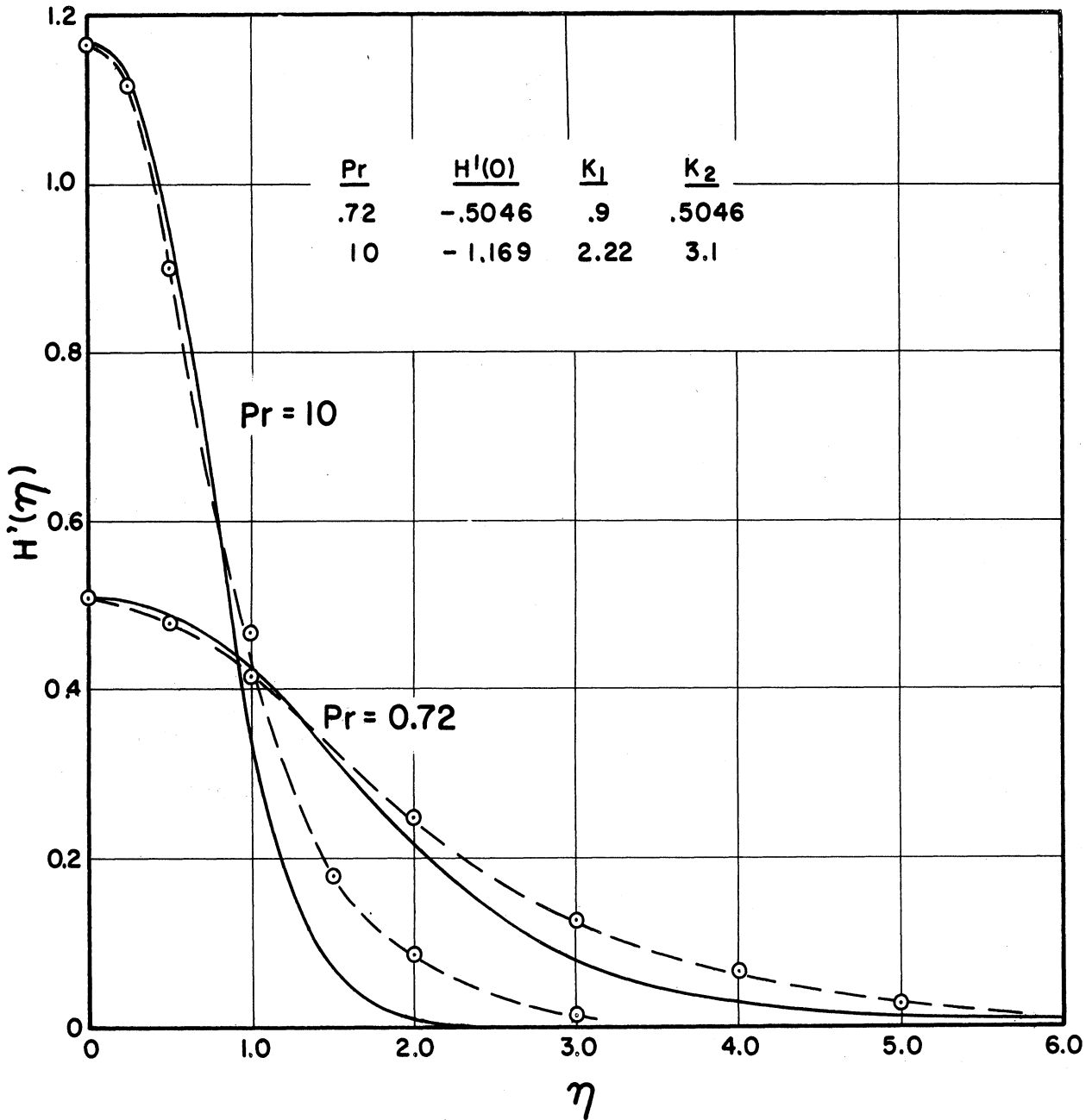
Figure 2-16. Comparison of -H'(η) from Ostrach (C-8) to that of Equation (2-45).

higher than the theoretical results of Ostrach (C-8). The approximated

expression was made specifically to fit closely for small regions of η

since this region is of more interest because it determines the Nusselt

number and shear stress. Since free convection velocity and stream func-

tion in terms of the "similarity transformation" are

$$\psi = (4x)^{3/4} F(\eta)$$

$$U = (4x)^{1/2} F'(\eta),$$

(2-46)

it was decided to fit $F'(\eta)$ also to a simple but satisfactory expres-

sion. The result can be seen in Figure 2-17. This expression was found

to be

$$F'(\eta) = K_3(P_R) \eta e^{-K_4(P_R)\eta}$$

(2-47)

This expression fits extremely well for small values of η and also

represents the peaking of $F'(\eta)$ in a very exact manner. For large

values of η, the Pr = .72 curve is higher and for Pr = 10 the

curve is lower than that of Ostrach's (C-8) results. This expression

is a better fit of the small plate data for large values of η but as

reported previously the flow was entirely laminar except near the outer

edge of the boundary-layer where slight turbulence from the room air dis-

turbed the measurements. Therefore it is well to say that $F'(\eta)$ for

Pr = 0.72 is high for large values of η. This expression is not as

important as the others, as will be brought out in the next section.
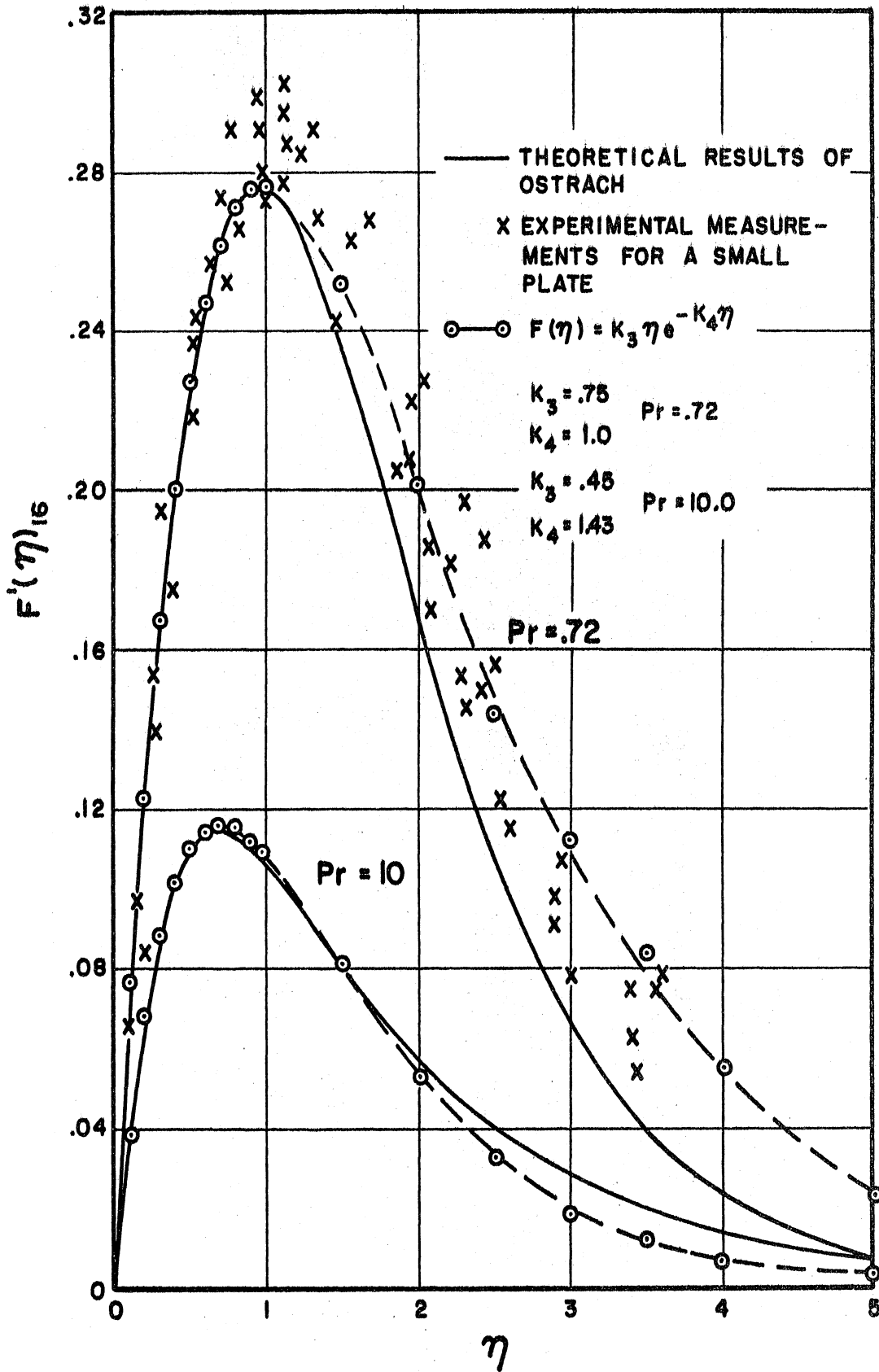
Figure 2-17. Comparison of F'(η) from Ostrach (C-8)
to that of Equation (2-47).

First-Order Velocities

The governing equations of momentum and energy are

$$\frac{\partial U_I}{\partial t} + U_0 \frac{\partial U_I}{\partial X} + U_I \frac{\partial U_0}{\partial X} + V_0 \frac{\partial U_I}{\partial Y} + V_I \frac{\partial U_0}{\partial Y} =$$

$$\frac{\partial^2 U_I}{\partial Y^2} + T_I + \frac{\partial}{\partial t} \left[P \cos \omega t \right] + \frac{K_0 W}{(4X)^{3/4}} \mathcal{Y}(\eta) \sin \omega t \qquad (2\text{-}48\text{A})$$

$$\frac{\partial T_I}{\partial t} + U_0 \frac{\partial T_I}{\partial X} + U_I \frac{\partial T_0}{\partial X} + V_0 \frac{\partial T_I}{\partial Y} + V_I \frac{\partial T_0}{\partial Y} = \frac{1}{P_R} \frac{\partial^2 T_I}{\partial Y^2} \qquad (2\text{-}48\text{B})$$

It is convenient to adopt complex notations and to write

$$U_I(X, Y, t) = \text{REAL} \left[\vec{U}_1(X, Y) e^{i \omega t} \right]$$

$$V_I(X, Y, t) = \text{REAL} \left[\vec{V}_1(X, Y) e^{i \omega t} \right]$$

$$P_0 \cos \omega t = \text{REAL} \left[P e^{i \omega t} \right] \qquad (2\text{-}49)$$

$$\mathcal{Y}(\eta) \sin \omega t = \text{REAL} \left[-i \, \mathcal{Y}(\eta) e^{i \omega t} \right]$$

$$T_I(X, Y, t) = \text{REAL} \left[\vec{T}_1(X, Y) e^{i \omega t} \right]$$

The momentum Equation (2-48A) becomes

$$i \omega \vec{U}_1 + U_0 \frac{\partial \vec{U}_1}{\partial X} + \vec{U}_1 \frac{\partial U_0}{\partial X} + V_0 \frac{\partial U_1}{\partial Y} + V_1 \frac{\partial U_0}{\partial Y} =$$

$$\frac{\partial^2 U_1}{\partial Y^2} + T_1 + i \omega P - i \frac{K_0 W}{(4X)^{3/4}} \mathcal{Y}(\eta) \qquad (2\text{-}50)$$

where $i = \sqrt{-1}$ and only the real part of $u_1(x,y)e^{i\omega t}$ has significance. This can also be written as

$$\text{REAL } \vec{U_1} e^{i\omega t} = |U_1| \cos(\omega t + \phi)$$

or

(2-51)

$$\text{REAL } \vec{U_1} e^{i\omega t} = \text{REAL } \vec{U_1} \cos \omega t - \text{IMAG. } \vec{U_1} \sin \omega t$$

where ϕ is the phase angle and $|u_1|$ is the absolute magnitude of the vector quantity u_1.

For large frequencies all convective terms and the temperature term are negligible with respect to the terms containing frequency as a factor in Equation (2-50). Therefore the terms retained are the inertia terms, the pressure gradient due to the potential flow and the forcing function $\zeta(\eta)$ which all have frequency as a factor. The highest order derivative also is retained. This has been done by Lighthill (A-20) and is in agreement with the theory of differential equation with large parameters. By dropping the vector superscript, Equation (2-50) becomes

$$i\omega U_1 = \frac{\partial^2 U_1}{\partial y^2} + i\omega P - i \frac{K_0 \omega}{(4X)^{3/4}} \mathcal{Y}(\eta)$$

(2-52)

It is convenient to find solutions in terms of the similarity variable of the zero-order equations. By the change of variable

$$\eta = \frac{y}{(4X)^{1/4}}$$

the following equation is obtained

$$\frac{d^2 U_1}{d\eta^2} - i\omega(4X)^{1/2} U_1 = -i\omega(4X)^{1/2} P + \frac{i K_0 \omega}{(4X)^{1/4}} \mathcal{Y}(\eta)$$

(2-53)

with the boundary conditions

$$U_1(0) = 0$$

$$U_1(\infty) = P \qquad (2\text{-}54)$$

We now have an ordinary differential equation which requires a particular and a homogeneous solution. The solution to this is

$$U_1 = (-P-V_1)e^{-(i\omega(4X)^{1/2})^{1/2}\eta} + P + V_1 e^{-K_1\eta} + V_2\,\eta\, e^{-K_1\eta} \qquad (2\text{-}55)$$

where

$$V_2 = \frac{i K_0 \omega \mathcal{G}(0) K_1}{(4X)^{1/4}(K_1^2 - i\omega(4X)^{1/2})} \qquad (2\text{-}56)$$

$$V_1 = \frac{i K_0 \omega \mathcal{G}(0)}{(4X)^{1/4}(K_1^2 - i\omega(4X)^{1/2})} + \frac{2 K_1 V_2}{(K_1^2 - i\omega(4X)^{1/2})}$$

Now the relative effect of the pressure gradient due to potential flow and the pressure gradient due to thermal variations can be investigated. The ratio of the pressure gradient due to potential flow to that due to thermal variations of density is

$$\frac{P(4X)^{3/4}}{K_0\,\mathcal{G}(0)} = \frac{P(4X)^{3/4}\sqrt[4]{Gr}}{\beta(\theta_w - \theta_\infty)} \qquad (2\text{-}57)$$

This quantity has very large values for all values of X except where X = 0.5 where P = 0. The reason for the large values is that

$$\beta(\theta_w - \theta_\infty) \ll O(1)$$

$$Gr \gg O(1) \qquad (2\text{-}58)$$

The expression $\beta(\Theta_W - \Theta_\infty)$ is a small quantity. The coefficient of volumetric expansion for gases is $\beta = 1/T$ and in general it is of the order of magnitude between 10^{-2} and 10^{-4}. The analysis of Ostrach (C-8) points out the fact that free convection flow is of the boundary layer type only for large Grashof numbers. The value of P, which is given as a dimensionless term in Equations (2-26), can become large. This suggests that Equation (2-57) would certainly assume large values. This was checked by numerical evaluation of the solution to u_1. The resulting values of u_1 for both finite and zero K_O were essentially identical. It is concluded that the effect on u_1 due to the thermal variation of density arising from the inertial force term is insignificant compared to the effects from an oscillating potential flow. Therefore all results given in this chapter are for $K_O = 0$. Figure 2-18 shows some representative values of ωu_1, where $K_O = 0$. For high frequencies ωu_1 is not a function of Pr number but only a function of X and ω. This is due to the fact that u_1 is responding to the potential flow which is only a function of the dimensions of the thin plate. The u_1 was multiplied by ω in order to show the frequency dependency. The multiplicative term comes from ϵ, $\epsilon = a\omega/L$. With $K_O = 0$ the first order velocity is identical to the periodic velocity of an adiabatic plate, treated by Schoenhals (A-34).

The first part of the solution and all subsequent solutions have been programmed on the 709 IBM computer at the University of Michigan Computing Center. Two representative methods of evaluation are presented in Appendix I.
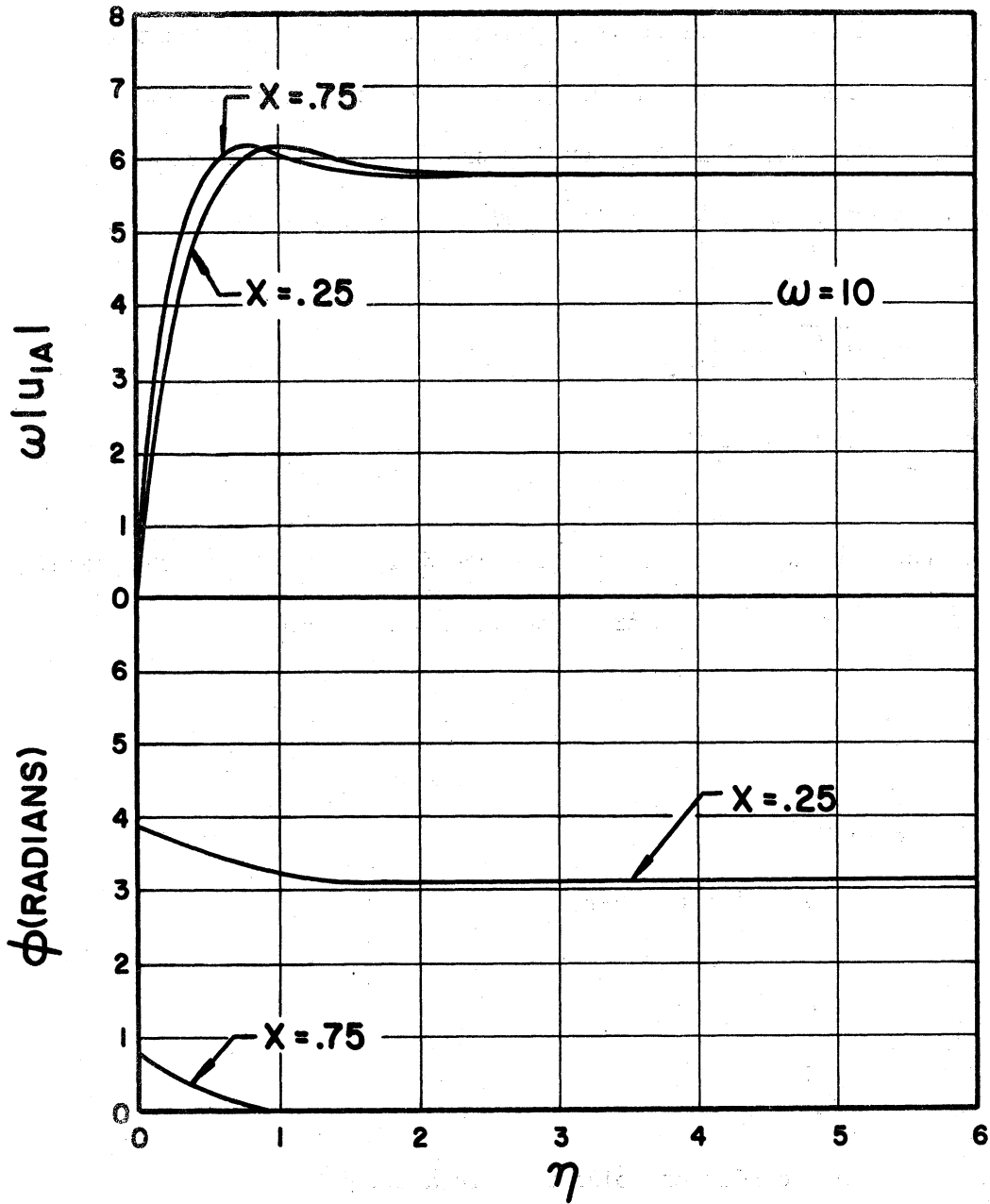
Figure 2-18. Magnitude and Phase of the First
Order Velocity, u_{1A}.

For intermediate frequencies, the whole momentum equation should be integrated with the exception of T_1. For small frequencies, the total momentum equation and the energy equation would have to be integrated together since they would be coupled. To ascertain where the high frequency case describes the flow the intermediate case was solved. This was done by assuming that the high frequency case is the first approximation to the intermediate frequency case, using the following

$$\vec{U}_{1C} = \vec{U}_{1A} + \vec{U}_{1B}$$

$$\vec{V}_{1C} = \vec{V}_{1A} + \vec{V}_{1B}$$

(2-59)

The quantity u_{1A} is u_1 of the preceding case of high frequency. The conditions here on the approximation is, of course

$$\vec{U}_{1A} > \vec{U}_{1B}$$

$$\vec{V}_{1A} > \vec{V}_{1B} .$$

(2-60)

The problem is to decide where

$$\vec{U}_{1A} \cong \vec{U}_{1C}$$

$$\vec{V}_{1A} \cong \vec{V}_{1C}$$

(2-61)

When the above condition holds this is a cut-off point and the high frequency solution describes the problem. Otherwise the solution holds for intermediate frequencies.

To find the governing equation for u_{1B}, the superscripts having been dropped for convenience, consider Equation (2-52) where $u_1 = u_{1A}$ and also substitute $u_1 = u_{1A} + u_{1B}$ into Equation (2-48A). By subtraction it is found that:

$$i\omega u_{1B} + u_0 \frac{\partial u_{1c}}{\partial x} + u_{1c} \frac{\partial u_0}{\partial x} + v_0 \frac{\partial u_{1c}}{\partial y} + v_{1c} \frac{\partial u_0}{\partial y} = \quad (2\text{-}62)$$

$$\frac{\partial^2 u_{1B}}{\partial y^2}$$

Therefore, the following is obtained.

$$\frac{\partial^2 u_{1B}}{\partial y^2} - i\omega u_{1B} = u_0 \frac{\partial u_{1c}}{\partial x} + u_{1c} \frac{\partial u_0}{\partial x} + v_0 \frac{\partial u_{1c}}{\partial y} + v_{1c} \frac{\partial u_0}{\partial y} \quad (2\text{-}63)$$

Since $u_{1A} > u_{1B}$, u_{1C} and v_{1C} are replaced by u_{1A} and v_{1A} in the right hand side of the above equation. This represents a type of forcing function. By change of variable from y to η we have

$$\frac{d^2 u_{1B}}{d\eta^2} - i\omega(4x)^{1/2} = (4x)^{1/2} \left[u_0 \frac{\partial u_{1A}}{\partial x} + u_{1A} \frac{\partial u_0}{\partial x} + v_0 \frac{\partial u_{1A}}{\partial y} + v_{1A} \frac{\partial u_0}{\partial y} \right] \quad (2\text{-}64)$$

with the boundary conditions

$$u_{1B}(0) = 0$$

$$\quad (2\text{-}65)$$

$$u_{1B}(\infty) = 0$$

so that

$$u_{1c}(0) = 0$$

$$\quad (2\text{-}66)$$

$$u_{1c}(\infty) = p$$

This is carried out by using the continuity equation to find v_{1A} and then evaluating the forcing function on the right hand side of Equation (2-64). Some characteristic results are shown in the form of graphs in Figure 2-19 through Figure 2-21. At $X = 0.5$, u_1 is zero. For $X > 0.5$ the phase angle leads by 45 degrees at $\eta = 0$ and for large values of η it is 0 degrees. For $X < 0.5$ the phase angle leads by 235 degrees at $\eta = 0$ and for large η it is 180 degrees. If the phase angle were referenced to the oscillating potential flow as has been done in Schoenhals (A-34) and Schlichting (A-34) the phase angle would be 45 degrees at the wall and 0 for large values of η. The significance of the method of plotting phase angles as used here is to preserve the absolute phase angle relationships for the first order complex vectors in the second order perturbations. The graphs reveal that for $\omega = 10$ and greater, the high frequency solution is valid. High frequency analysis is discussed in the next section in more detail. Schoenhals (A-34) using a hot wire anemometer found good agreement for periodic velocities of an adiabatic plate. For high frequencies, as discussed previously in this section, the first order velocities with $K_o = 0$ is identical with the velocities in the region of an oscillating adiabatic plate. Schoenhals experimental results are discussed in more detail in Chapter IV and graphs of his data are shown.

First Order Temperatures

The energy equation with the adopted complex notation is

$$i\omega T_1 + U_0 \frac{\partial T_1}{\partial X} + U_1 \frac{\partial T_0}{\partial X} + V_0 \frac{\partial T_1}{\partial y} + V_1 \frac{\partial T_0}{\partial y} = \frac{1}{P_R} \frac{\partial^2 T_1}{\partial y^2} \qquad (2\text{-}67)$$
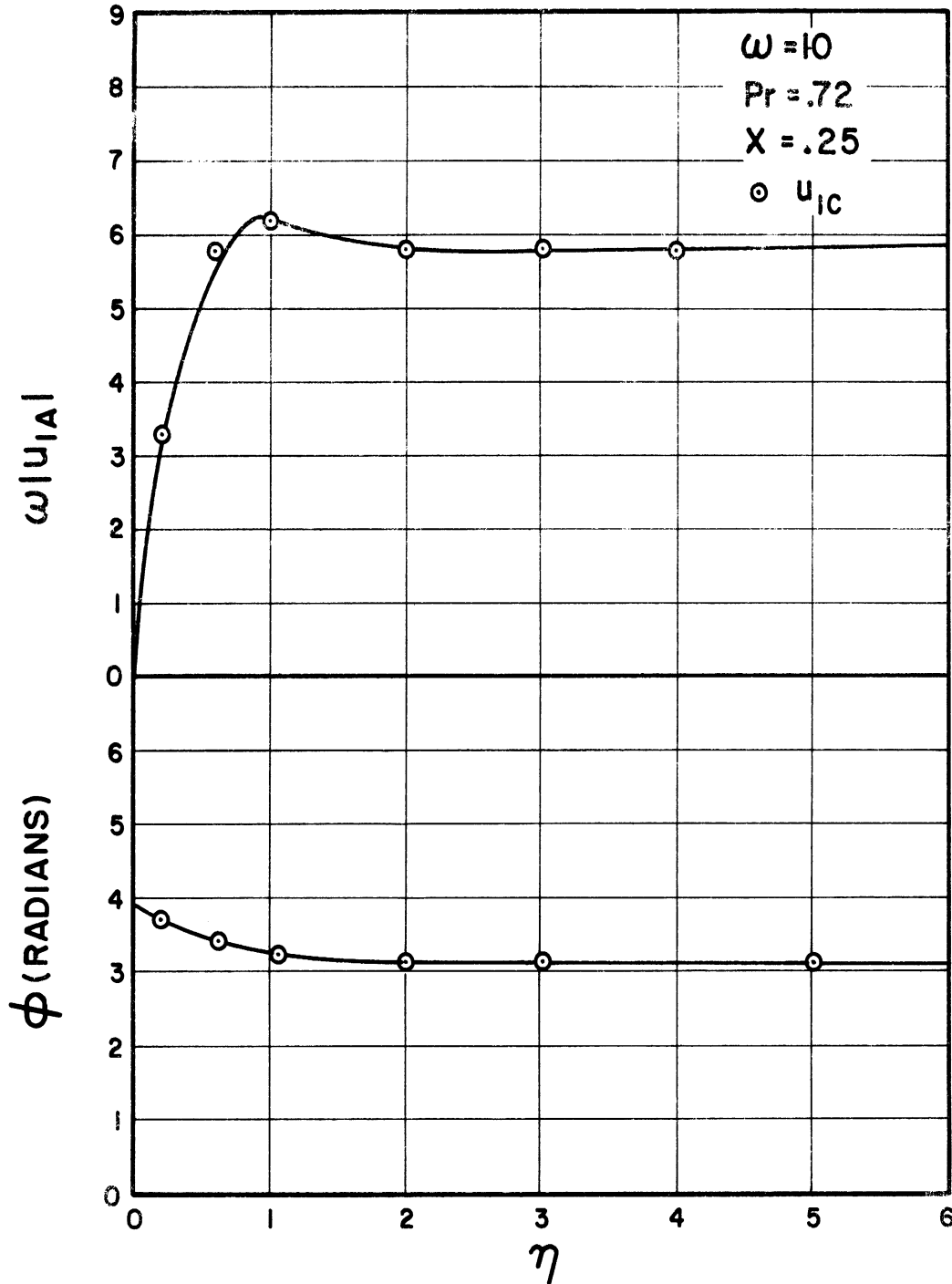
Figure 2-19. Magnitude and Phase of First Order Velocities u_{1A} and u_{1C}.

Figure 3-20. Magnitude and Phase of First Order Velocities u_{1A} an u_{1C}.
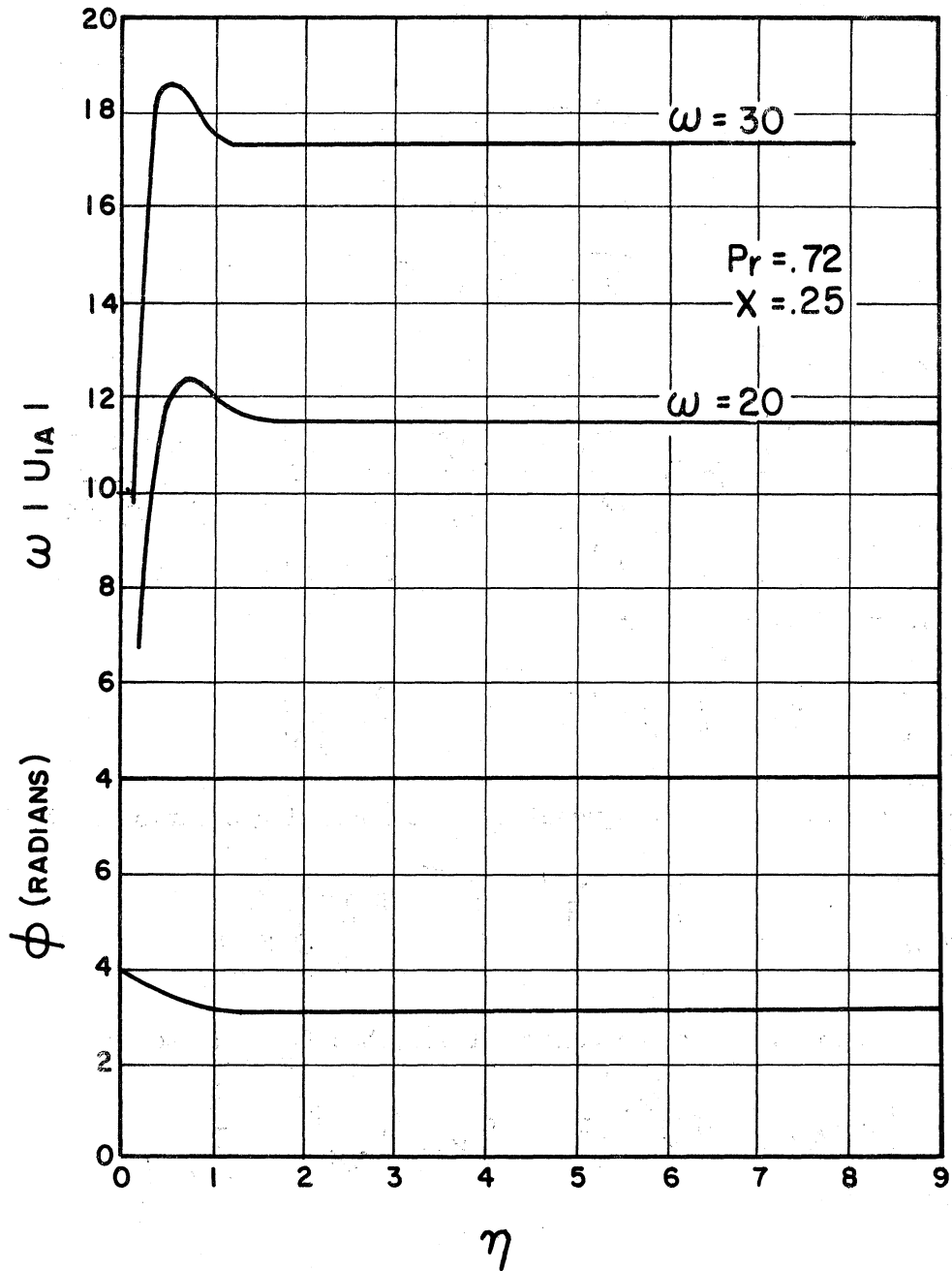
Figure 2-21. Magnitude and Phase of the First
Order Velocity, u_{1A}.

From the preceding analysis it is known that

$$U_0 \sim O(1)$$

$$V_0 \sim O(1)$$

$$U_1 \sim O(1)$$

$$V_1 \sim O(1)$$ (2-68)

$$T_0 \sim O(1)$$

$$T_1 \sim O(\omega^{-1})$$

Therefore it is found that

$$i\omega T_1 + U_0 \frac{\partial T_1}{\partial X} + U_1 \frac{\partial T_0}{\partial X} + V_0 \frac{\partial T_1}{\partial Y} + V_1 \frac{\partial T_0}{\partial Y} = \frac{1}{P_R} \frac{\partial^2 T_1}{\partial Y^2} \quad (2\text{-}69)$$

$$O(1 \cdot \tfrac{1}{\omega}) \quad O(1 \cdot 1) \quad O(1 \cdot \tfrac{1}{\omega^{1/2}}) \quad O(1 \cdot 1)$$

it is apparent then that

$$U_1 \frac{\partial T_0}{\partial X} + V_1 \frac{\partial T_0}{\partial Y} > U_0 \frac{\partial T_1}{\partial X} + V_0 \frac{\partial T_1}{\partial Y} \quad (2\text{-}70)$$

for the case of high frequencies. The governing equation is therefore

$$\frac{d^2 T_1}{d\eta^2} - i\omega P_R T_1 = P_R \left[U_1 \frac{\partial T_0}{\partial X} + V_1 \frac{\partial T_0}{\partial Y} \right] \quad (2\text{-}71)$$

which becomes, after the change of variable from Y to η,

$$\frac{d^2 T_1}{d\eta^2} - i\omega P_R (4X)^{1/2} T_1 = P_R (4X)^{1/2} \left[U_1 \frac{\partial T_0}{\partial X} + V_1 \frac{\partial T_0}{\partial Y} \right] \quad (2\text{-}72)$$

with the boundary conditions

$$T_1(0) = 0$$

$$T_1(\infty) = 0 \quad (2\text{-}73)$$

The integration has been performed and the results are shown in Figures 2-22 through 2-26. To find the cut-off point between intermediate and high frequencies it is necessary to perform the same type of process of determining where the criteria of high frequency is valid as was done for velocities therefore

$$T_{1C} = T_{1A} + T_{1B} \tag{2-74}$$

The governing equation is

$$i\omega T_{1B} + U_0 \frac{\partial T_{1C}}{\partial X} + U_{1B} \frac{\partial T_0}{\partial X} + V_0 \frac{\partial T_{1C}}{\partial Y} + V_{1B} \frac{\partial T_0}{\partial Y} = \frac{1}{P_R} \frac{\partial^2 T_{1B}}{\partial Y^2} \tag{2-75}$$

Since $T_{1A} > T_{1B}$, T_{1C} is replaced by T_{1A} in the above equation. By change of variable from Y to η, Equation (2-75) becomes

$$\frac{d^2 T_{1B}}{d\eta^2} - i\omega P_R (4X)^{1/2} T_{1B} = P_R (4X)^{1/2} \left[U_0 \frac{\partial T_{1A}}{\partial X} + \right. \tag{2-76}$$
$$\left. U_{1B} \frac{\partial T_0}{\partial X} + V_0 \frac{\partial T_{1A}}{\partial Y} + V_{1B} \frac{\partial T_0}{\partial Y} \right]$$

with zero boundary conditions at $\eta = 0$ and $\eta = \infty$.

Graphs of T_{1A} show that the phase angle at $\eta = 0$ approaches 90 degrees. The phase lag for large values of η is asymptotic to 90 degrees. For intermediate η the phase lag increases and then decreases. For the same values of ω and X the temperature profiles for $Pr = 0.72$ peak at a higher point than those of $Pr = 10$. The temperature profiles for $Pr = 10$ peak for smaller values of η than those of $Pr = 0.72$.
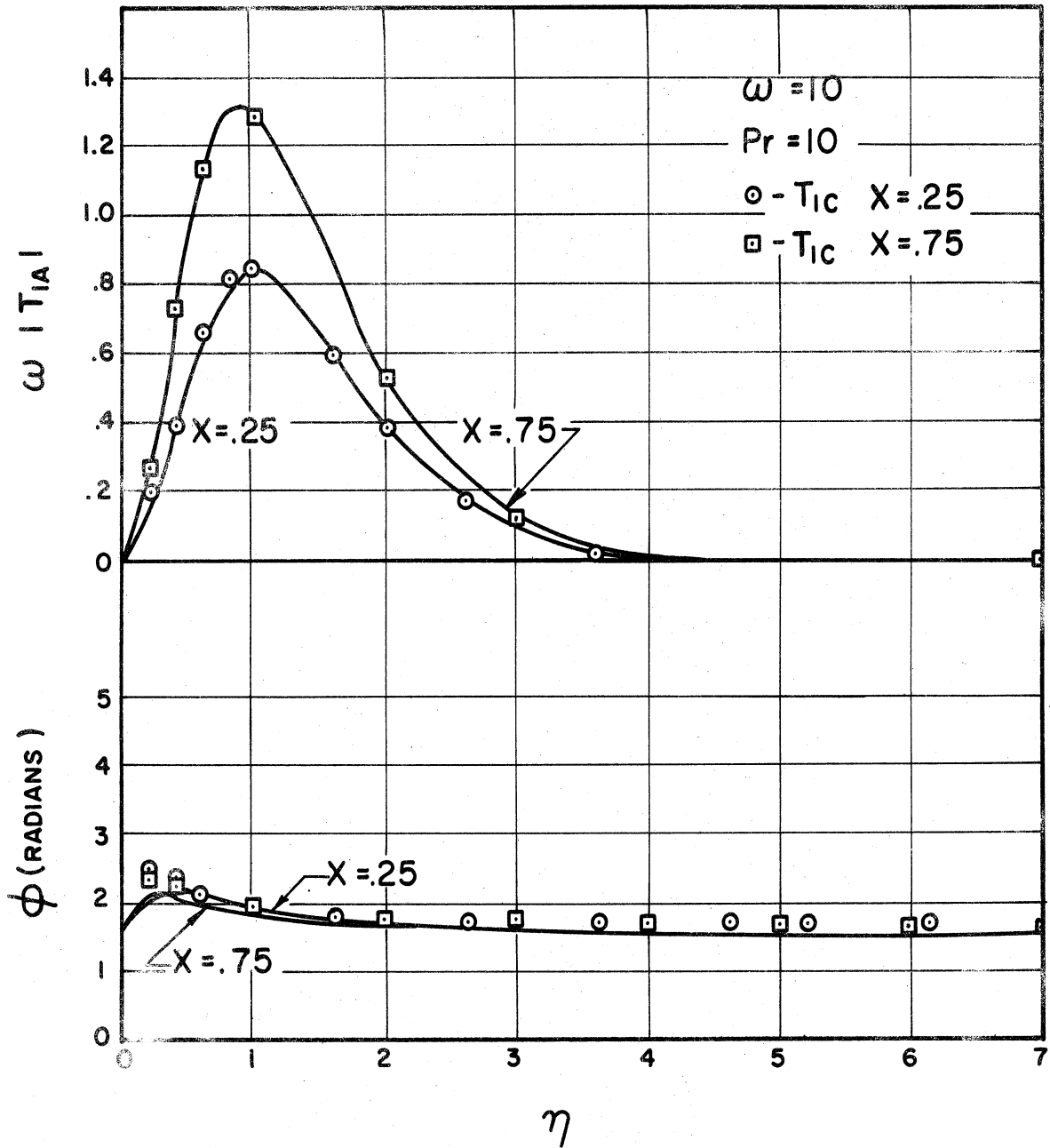
Figure 2-22. Magnitude and Phase of First Order Temperatures of T_{1A} and T_{1C}.
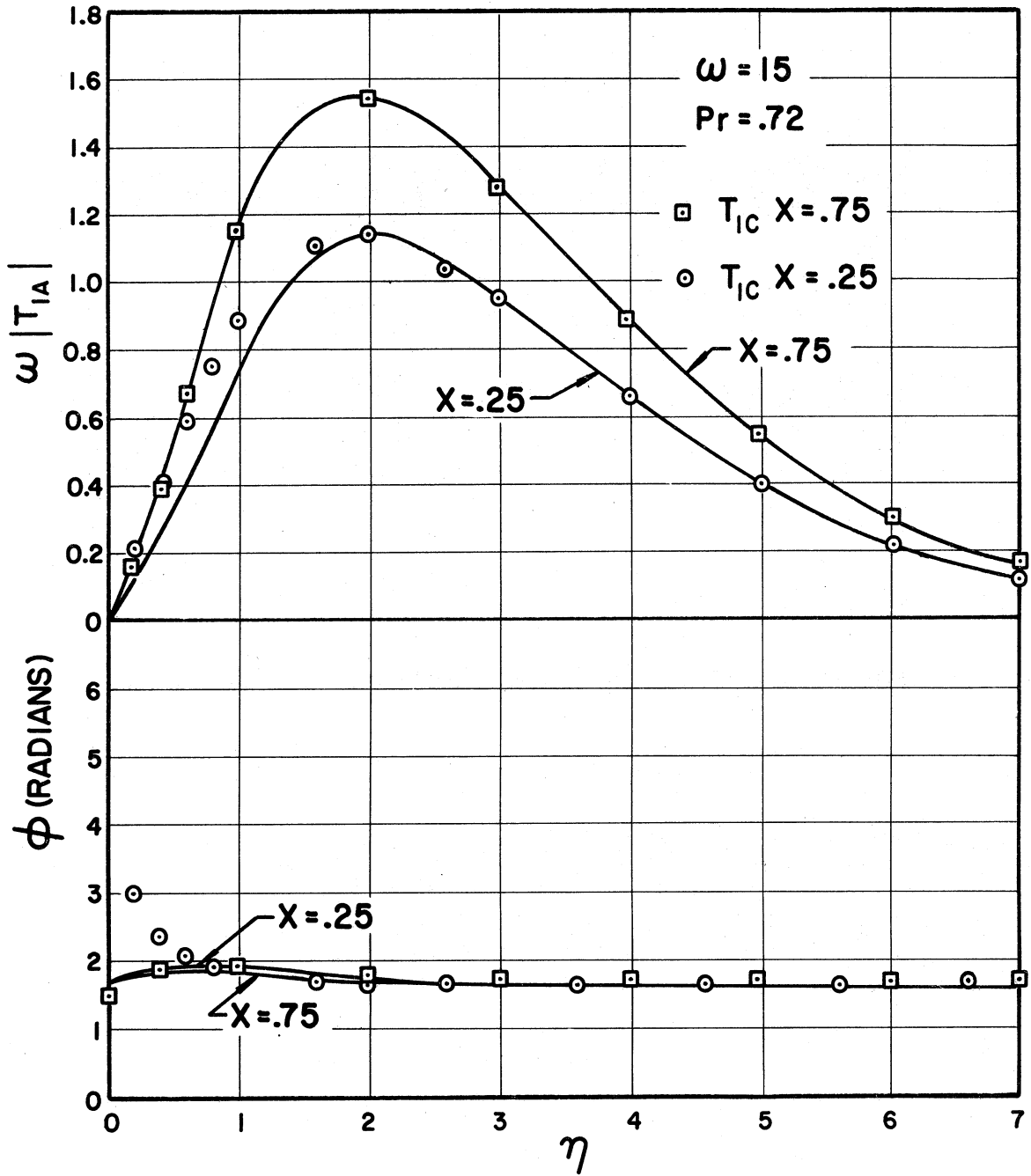
Figure 2-25. Magnitude and Phase of First Order Temperatures of T_{1A} and T_{1C}.
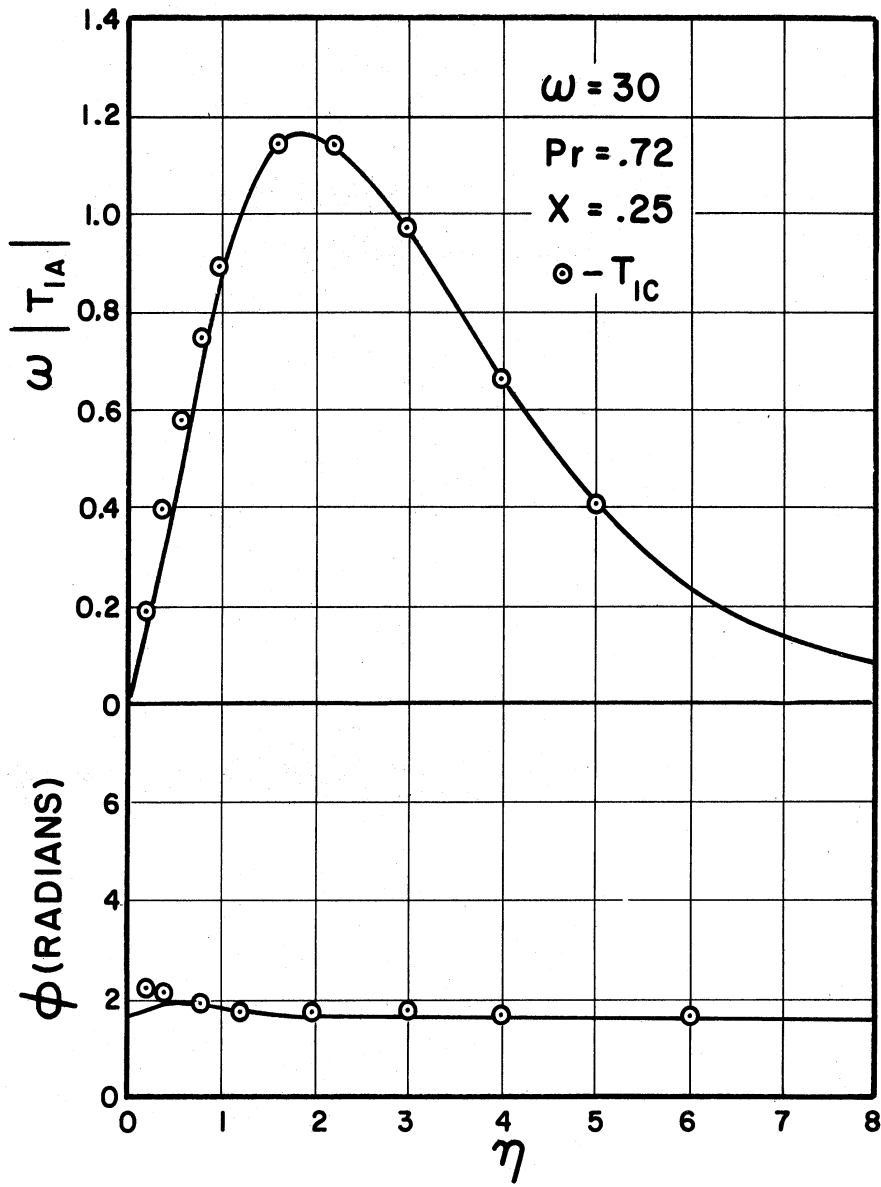
Figure 2-26. Magnitude and Phase of First Order
Temperatures of T_{1A} and T_{1C}.

This is because $H'(\eta)$, see Figure 2-15, has a smaller thermal boundary layer thickness for larger Prandtl numbers.

Figures 2-22 through 2-25 show the convergence of T_{1A} to that of T_{1C} for high frequency. The circles and squares are values of T_{1C} and the solid lines are values of T_{1A}. As can be seen in these figures, convergence is better for large values of X, Pr and ω. The graphs indicate the rate of convergence for increasing X, Pr and ω. The criteria for T_{1A} to be used in place of T_{1C} was found from the results to be

$$P_R^{0.21} \omega (4X)^{1/2} \gg 25 \qquad (2\text{-}77)$$

This represents the fact that for the high frequency solution, T_{1A}, to be valid the above group of parameters must be approximately greater than 25. The values of frequency which permit T_{1A} to describe the periodic temperature solutions are greater for low Prandtl numbers than those of high Prandtl number. Also if X becomes very small then ω would have to become very large to satisfy Equation (2-77). Figure 2-27 shows characteristic values of ωT_{1B} for two Prandtl numbers.

First-Order Shear-Stress and Nusselt Number

The shear stress will be evaluated first. The derivative of u_1 without the term $\zeta(\eta)$, described by $K_0 = 0$, which was found to be negligible, is

$$\left(\frac{\partial u_1}{\partial y}\right)_0 = P\sqrt{i\omega} = REAL\left[P\sqrt{\omega}\, e^{i(\omega t + \phi)}\right] \qquad (2\text{-}78)$$
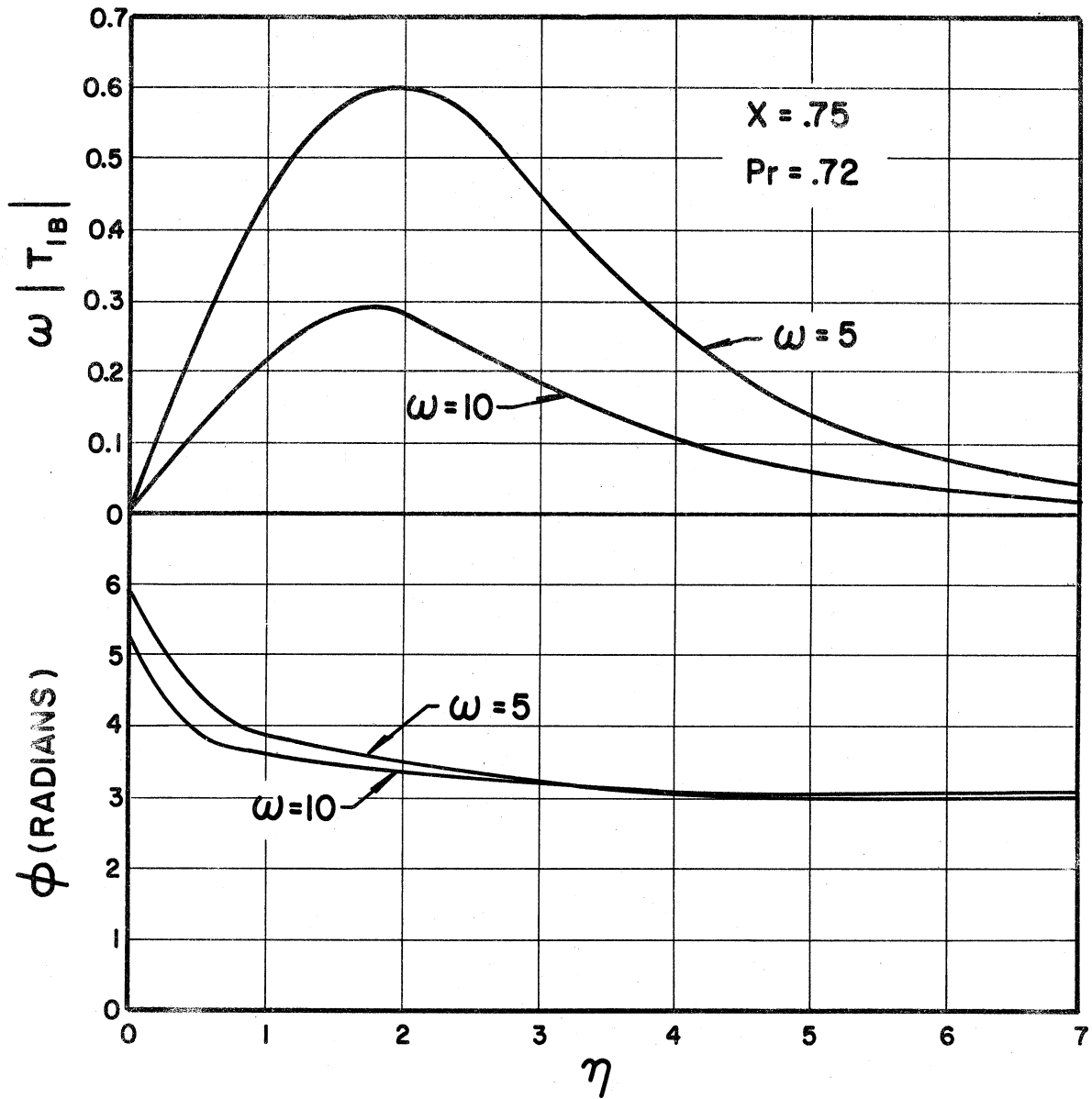
Figure 2-27. Magnitude and Phase of T_{1B}.

The expression for the zeroth and first order (periodic) velocities is

$$U = U_0 + \epsilon \, REAL \; U_1 \, e^{i\omega t} + \cdots \qquad (2\text{-}79)$$

which can be written as

$$U = U_0 + \epsilon \, |U_1| \, COS(\omega t + \phi) + \cdots \qquad (2\text{-}80)$$

The expression for the zeroth and first order (periodic) shear-stress is

$$\frac{T_s}{\mu_\infty} = (4X)^{1/4} F''(0) + \epsilon \frac{\left(\frac{\partial |U_1|}{\partial Y}\right)_0}{(4X)^{1/2}} COS(\omega t + \phi) + \cdots \qquad (2\text{-}81)$$

which can also be written as

$$\frac{T_s}{\mu_\infty} = (4X)^{1/4} F''(0) + \epsilon \frac{P\sqrt{\omega}}{(4X)^{1/2}} COS(\omega t + 45°) + \cdots \qquad (2\text{-}82)$$

The first-order contribution in the shear stress is not a function of Prandtl number, as may be seen in Equation (2-82). It is, however, a function of viscosity. It leads the disturbance by an angle of $\pi/4$. At $X = 0.5$ there is a line of symmetry for P, but the X-dependency of the first order (periodic) shear stress is not symmetrical around $X = 0.5$ because of the influence of the factor $(4X)^{1/2}$. The frequency dependency of the first order (periodic) shear stress is $\omega^{3/2}$ because ϵ is proportional to ω.

The derivative of the first-order temperature distribution is presented in the form of graphs in Figures 2-28 through 2-30. Figures 2-28 and 2-30 for $Pr = 0.72$ have the same ordinate values. The difference in the plots is in the abscissa so that the effects of frequency
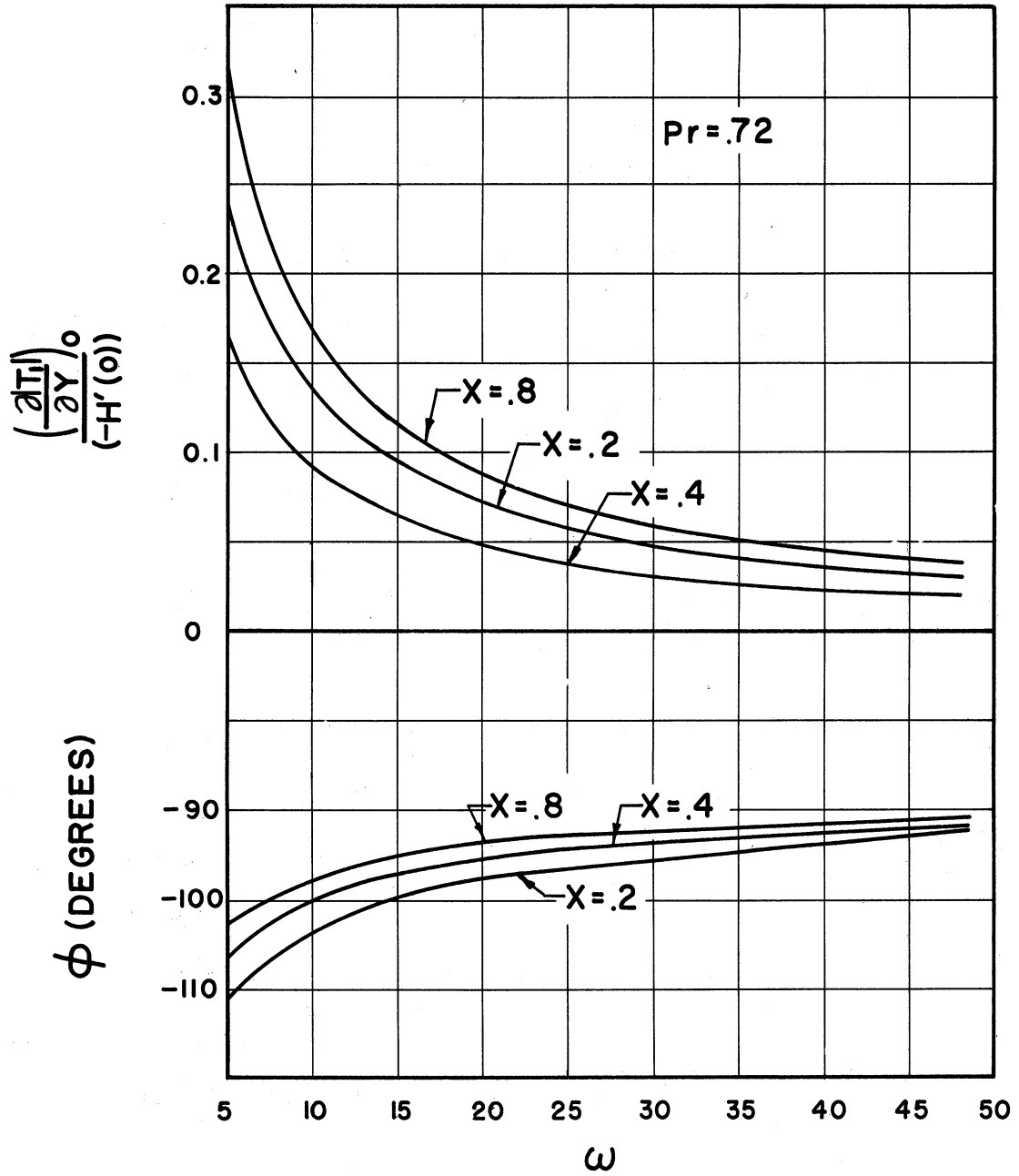
Figure 2-28. Magnitude and Phase of the First Order Temperature
Derivative Divided by the Zeroth Derivative of
Temperature.
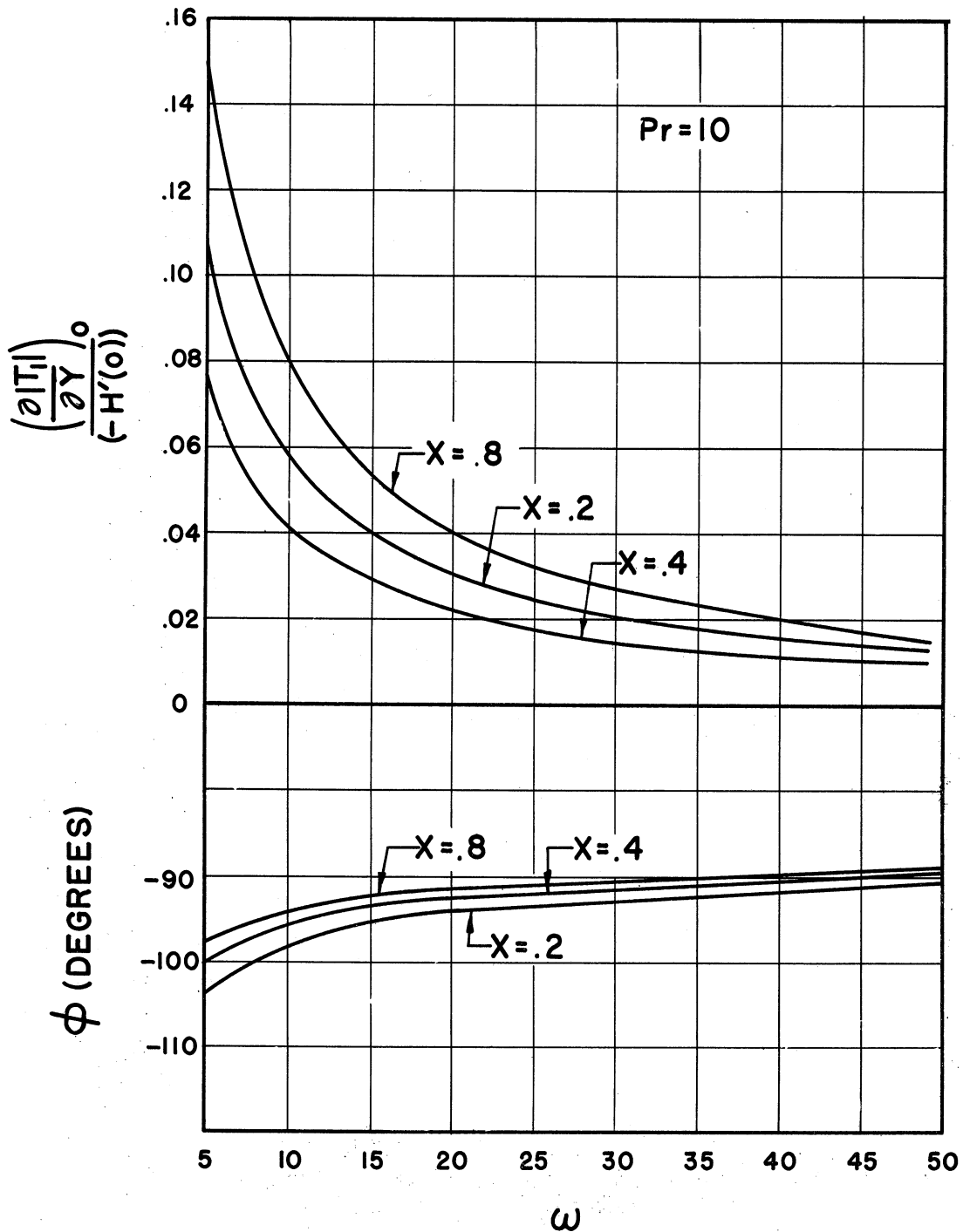
Figure 2-29. Magnitude and Phase of the First Order Temperature Derivative Divided by the Zeroth Derivative of Temperature.
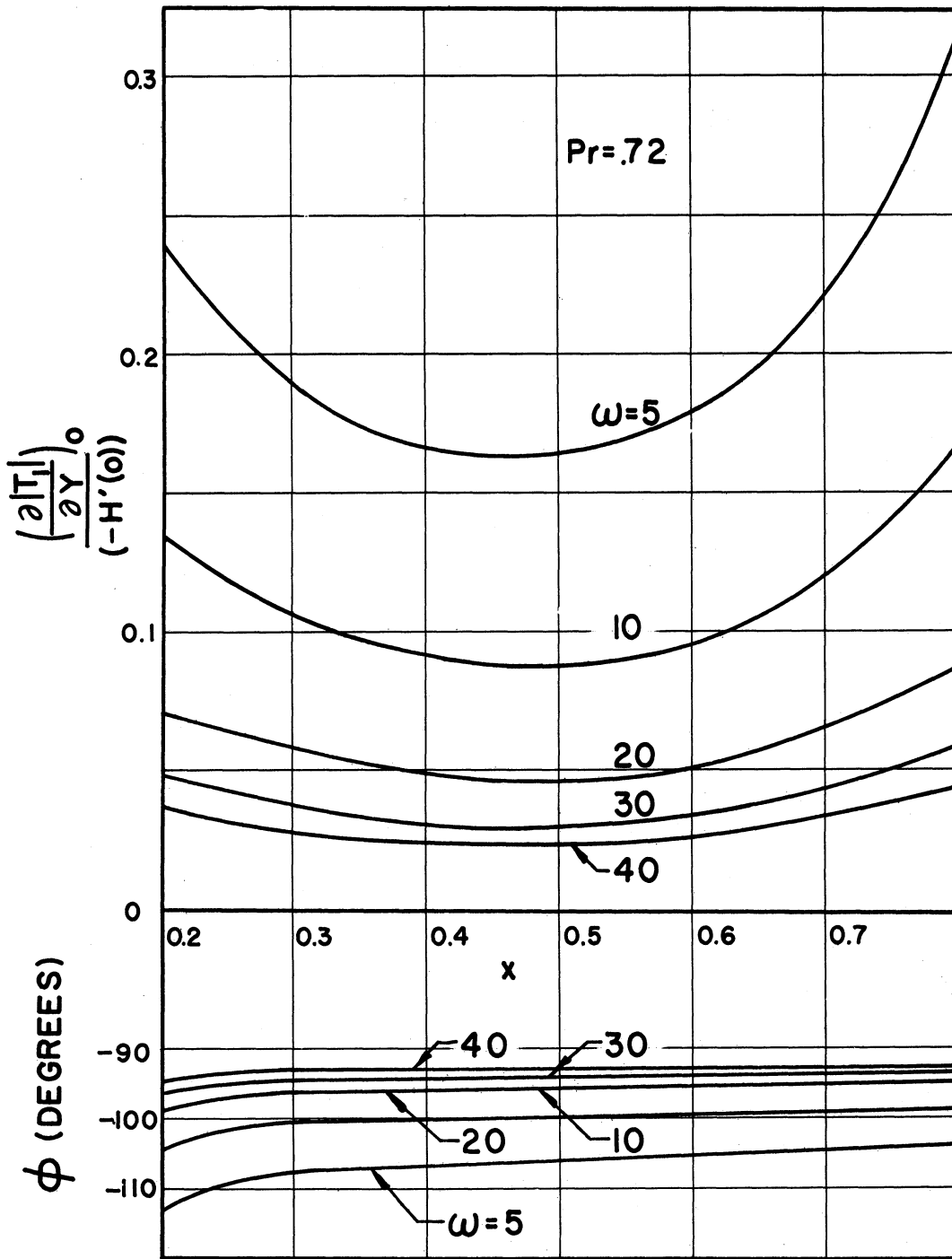
Figure 2-30. Magnitude and Phase of the First Order
Temperature Derivative Divided by the
Zeroth Derivative of Temperature.
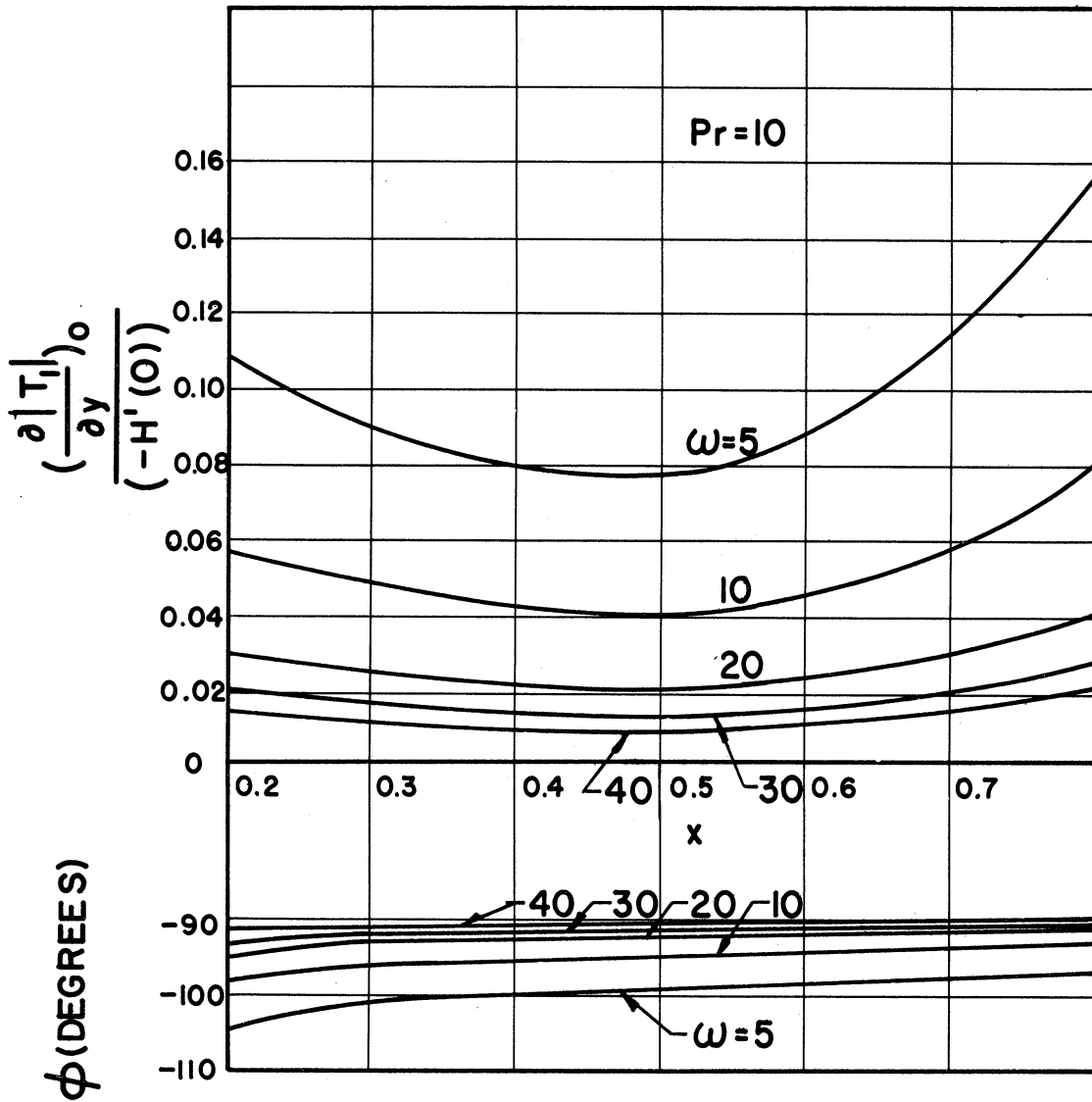
Figure 2-31. Magnitude and Phase of the First Order Temperature
Derivative Divided by the Zeroth Derivative of
Temperature.

and X can be shown separately. The same is true for Figures 2-29

and 2-31 for Pr = 10.

The expression for the zeroth and first order temperature

is

$$T = T_0 + \epsilon \, REAL \, T_1 \, e^{i\omega t} + \cdots \qquad (2\text{-}83)$$

and the derivative is

$$\frac{\partial T_1}{\partial y} = \frac{H'(\eta)}{(4X)^{1/4}} + \epsilon \frac{\partial |T_1|}{\partial y} \cos(\omega t + \phi) + \cdots \qquad (2\text{-}84)$$

The derivative was represented only in the limits from

X = 0.2 to X = 0.8. Figures 2-30 and 2-31 of the first order tempera-

ture derivative versus X show the asymmetrical character of the deriva-

tive. The limitations on X are necessary because of the existence of

singular points at X = 0 and X = 1.0. These singularity points origi-

nate in the potential flow and the solutions do not apply at or very

close to the singularity points.

For increasing frequency the phase lag approaches 90 degrees

for both Prandtl numbers and the absolute magnitude of the first order

temperature derivative decreases. For large frequency the absolute

magnitude decreases as ω^{-1}. The absolute magnitudes and phase angles

of first order temperature derivatives as a function of frequency versus

X for two Prandtl numbers are shown in Figures 2-30 and 2-31.

The local Nusselt number, in terms of dimensional quantities

of Equation (2-26), is defined as

$$Nu_X = \frac{hX}{K} = -\frac{X}{K} \left(\frac{\partial \theta}{\partial Y}\right)_0 \qquad (2\text{-}85)$$

which, in terms of the zeroth and first order temperature derivatives,

results in

$$\frac{\frac{\partial \theta}{\partial Y}}{\Delta \theta_0 \, (Gr_X)^{1/4}/X \sqrt{2}} = H'(\eta_d) + \epsilon \frac{\partial T_1}{\partial \eta_d} \cos(\omega t + \phi) + \cdots \qquad (2\text{-}86)$$

By simplification and division the following relationship is obtained

$$\frac{Nu}{(-H'(0))(Gr_X/4)^{1/4}} = 1 - \epsilon \frac{\left(\frac{\partial |T_1|}{\partial \eta_d}\right)_0}{(-H'(0))} \cos(\omega t + \phi) + \cdots \qquad (2\text{-}87)$$

Second-Order Velocities

The governing equation of momentum is Equation (2-32B) with

$K_0 = 0$. It is seen in Equation (2-32B) that certain terms will contri-

bute terms with $\cos^2 \omega t$. These terms are

$$U_I \frac{\partial U_I}{\partial X} = \text{REAL}\left(U_1 e^{i\omega t}\right) \frac{\partial}{\partial X}\left(\text{REAL } U_1 e^{i\omega t}\right)$$

$$V_I \frac{\partial U_I}{\partial Y} = \text{REAL}\left(V_1 e^{i\omega t}\right) \frac{\partial}{\partial Y}\left(\text{REAL } U_1 e^{i\omega t}\right) \qquad (2\text{-}88)$$

$$P \frac{\partial P}{\partial X} \cos^2 \omega t$$

These relationships can be reduced to terms which contain only $\cos 2\omega t$

and steady terms, as

$$U_I \frac{\partial U_I}{\partial X} = \frac{\text{REAL}}{2}\left[U_1 \frac{\partial U_1}{\partial X}\right]\cos 2\omega t + \frac{\text{REAL}}{2}\left[\overline{U_1} \frac{\partial U_1}{\partial X}\right]$$

$$V_I \frac{\partial U_I}{\partial Y} = \frac{\text{REAL}}{2}\left[V_1 \frac{\partial U_1}{\partial Y}\right]\cos 2\omega t + \frac{\text{REAL}}{2}\left[\overline{V_1} \frac{\partial U_1}{\partial Y}\right] \qquad (2\text{-}89)$$

$$P \frac{\partial P}{\partial X} \cos^2 \omega t = \frac{P}{2} \frac{\partial P}{\partial X} \cos 2\omega t + \frac{1}{2} P \frac{\partial P}{\partial X}$$

By Equations (2-89) the result can be seen why oscillations of a body in a fluid at rest induce characteristic secondary flows or streaming flows, whose nature are such that a steady motion occurs in the fluid from a purely periodic disturbance. The only conclusion that can be made is that secondary flow is a result of viscous terms and convective terms, i.e., the non-linear terms. Therefore, it may be assumed that the solution has the following form of time-dependent and time-independent solutions

$$U_{II} = U_{2S} + REAL \left(U_2 \, e^{i 2 w t} \right)$$
$$T_{II} = T_{2S} + REAL \left(T_2 \, e^{i 2 w t} \right)$$

(2-90)

The two following equations, which are obtained by substituting Equations (2-89) and (2-90) into Equation (2-32B) and separating according to time-dependency, are

$$i 2 w U_2 + U_0 \frac{\partial U_2}{\partial X} + U_2 \frac{\partial U_0}{\partial X} + V_0 \frac{\partial U_2}{\partial Y} + V_2 \frac{\partial U_0}{\partial Y} +$$

$$+ \frac{REAL}{2} \left[U_1 \frac{\partial U_1}{\partial X} + V_1 \frac{\partial U_1}{\partial Y} \right] = \frac{1}{2} P \frac{\partial P}{\partial X} + \frac{\partial^2 U_2}{\partial Y^2}$$

(2-91A)

$$U_0 \frac{\partial U_{2S}}{\partial X} + U_{2S} \frac{\partial U_0}{\partial X} + V_0 \frac{\partial U_{2S}}{\partial Y} + V_{2S} \frac{\partial U_0}{\partial Y} + \frac{Real}{2} \Big[$$

(2-91B)

$$\overline{U_1} \frac{\partial U_1}{\partial X} + \overline{V_1} \frac{\partial U_1}{\partial Y} \Big] = \frac{1}{2} P \frac{\partial P}{\partial X} + \frac{\partial^2 U_{2S}}{\partial Y^2}$$

The bar over the symbols denotes the respective conjugate complex quantities. The order of magnitude of the quantities above have been investigated previously, Equations (2-67), with the exception of u_{2s} and v_{2s}. The unsteady solution u_{2t} was not solved since it is doubly harmonic. The steady part u_{2s} was solved because of its importance to a time-steady shear stress and Nusselt number. The order of magnitude of u_{2s} cannot be greater than $O(\omega^{-1})$. The forcing terms in Equation (2-91B), the underlined terms, have the order of magnitude $O(1)$. Each integration will decrease the order of magnitude by $\sqrt{\omega}$ and since two integrations are required the resulting order of magnitude of u_{2s} will be $O(\omega^{-1})$. Then u_{2s} and v_{2s} are treated as having $O(\omega^{-1})$ and it is found that

$$\frac{\partial^2 U_{2s}}{\partial y^2} = U_0 \frac{\partial U_{2s}}{\partial X} + U_{2s} \frac{\partial U_0}{\partial X} + V_0 \frac{\partial U_{2s}}{\partial Y} + V_{2s} \frac{\partial U_0}{\partial Y}$$

$$O(1 \cdot \omega^{-1}) \quad O(\omega^{-1} \cdot 1) \quad O(1 \cdot \omega^{-1/2}) \quad O(\omega^{-1}, 1)$$

$$-\frac{1}{2} P \frac{\partial P}{\partial X} + \frac{REAL}{2} \left[\bar{U}_1 \frac{\partial U_1}{\partial X} + \bar{V}_1 \frac{\partial U_1}{\partial Y} \right] \tag{2-92}$$

$$O(1 \cdot 1) \qquad O(1 \cdot 1) \qquad O(1 \cdot \omega^{1/2})$$

By retaining only the higher-order terms for large frequency Equation (2-92) reduces to

$$\frac{\partial^2 U_{2s}}{\partial y^2} = \frac{REAL}{2} \left[\bar{U}_1 \frac{\partial U_1}{\partial X} + \bar{V}_1 \frac{\partial U_1}{\partial Y} \right] - \frac{1}{2} P \frac{\partial P}{\partial X} \tag{2-93}$$

Equation (2-93) was found by inspection to be that first solved by Schlichting (A-32) for an adiabatic plane executing harmonic wall motion. He applied the result to a circular cylinder. Equation (2-93) was

also solved by Schoenhals (A-34) for an adiabatic finite plate executing

harmonic transverse motion. The potential flow is, of course, different

for both cases. Their similarity results from the fact that the solu-

tions to each are restricted to high frequency. Schlichting obtained

u_{2s} as the product of a x-dependent function (potential flow) and a y-

dependent function, as shown in Equations (2-94) and (2-95). Although

Equation (2-93) was not solved here in this way, the y-dependent results

are the same as given by Schlichting. The form of Equation (2-94), par-

ticularly convenient for plotting the stream function, is

$$U_{2s} = \frac{1}{\omega} P \frac{\partial P}{\partial X} \chi'(\xi) \tag{2-94}$$

where

$$\xi = y \left(\frac{\omega}{2}\right)^{1/2} \tag{2-95}$$

$\chi(\xi)$ satisfies

$$-\chi''' = \frac{1}{2} - \chi_0' \overline{\chi_0'} + \frac{1}{4}\left(\chi_0 \overline{\chi_0''} + \overline{\chi_0} \chi_0''\right) \tag{2-96}$$

where $p\chi_0$ is the first-order velocity. The solution in terms of ζ'

and ξ is

$$\chi' = -\frac{3}{4} + \frac{1}{4} e^{-2\xi} + 2 e^{-\xi} \sin\xi + \frac{1}{2} e^{-\xi} \cos\xi \tag{2-97}$$
$$- \frac{\xi}{2} e^{-\xi}(\cos\xi - \sin\xi).$$

This is plotted in Figure 2-32. The steady velocity can only satisfy

boundary conditions at the wall. At distances outside the boundary layer
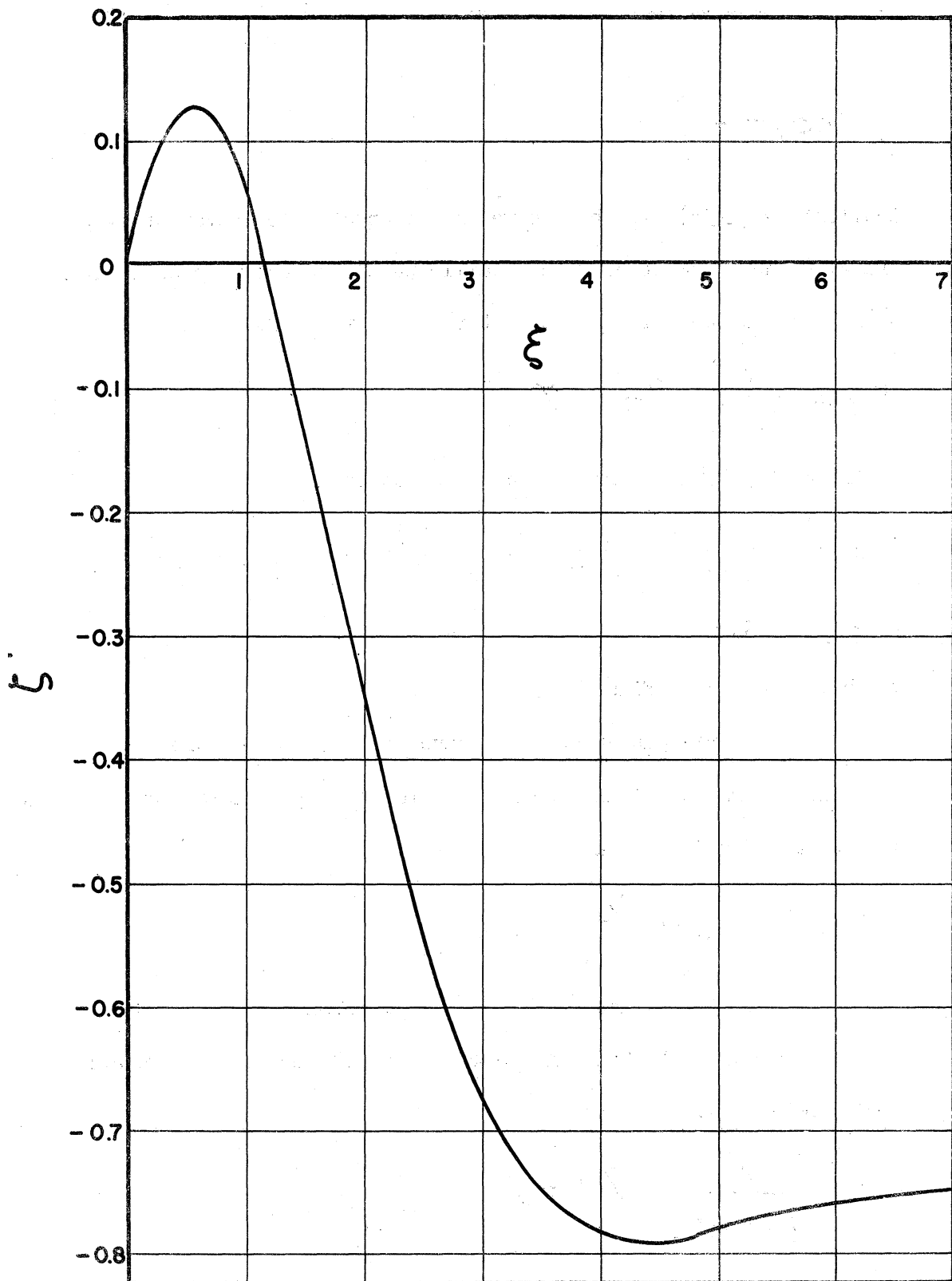
Figure 2-32.   Values of $\zeta'(\xi)$ of Equation   (2-97).

it is possible to make the velocity finite but not zero. The value of ζ' is

$$\chi'(\infty) = -\frac{3}{4} \qquad (2\text{-}98)$$

Schlichting (A-34) was able to verify secondary flow movement by photo-graphing the movement of fine metallic particles about an oscillating cylinder in a tank filled with water. The stream function is

$$\psi_{2S} = \frac{\sqrt{2}}{\omega^{3/2}} P \frac{\partial P}{\partial X} \chi . \qquad (2\text{-}99)$$

By integrating χ' the result was found to be

$$\chi = \frac{13}{8} - \frac{3}{4}\zeta - \frac{1}{8} e^{-2\zeta} - \frac{3}{2} e^{-\zeta} \cos \zeta - e^{-\zeta} \sin \zeta \qquad (2\text{-}100)$$
$$- \frac{1}{2} \zeta e^{-\zeta} \sin \zeta$$

which is plotted in Figure 2-33.

The previous discussion leaves the stream function in a very convenient form for finding constant values of ψ, the streamlines. A new variable is defined as

$$\psi = \psi_{2S} (\omega)^{3/2} / \sqrt{2} . \qquad (2\text{-}101)$$

By shifting the coordinate of P from the bottom edge of the plate to the middle and by letting $X/L = X/C$ for this development Equation (2-99) reduces to

$$\psi = \frac{X}{[1-X^2]^2} \chi(\zeta) \qquad (2\text{-}102)$$
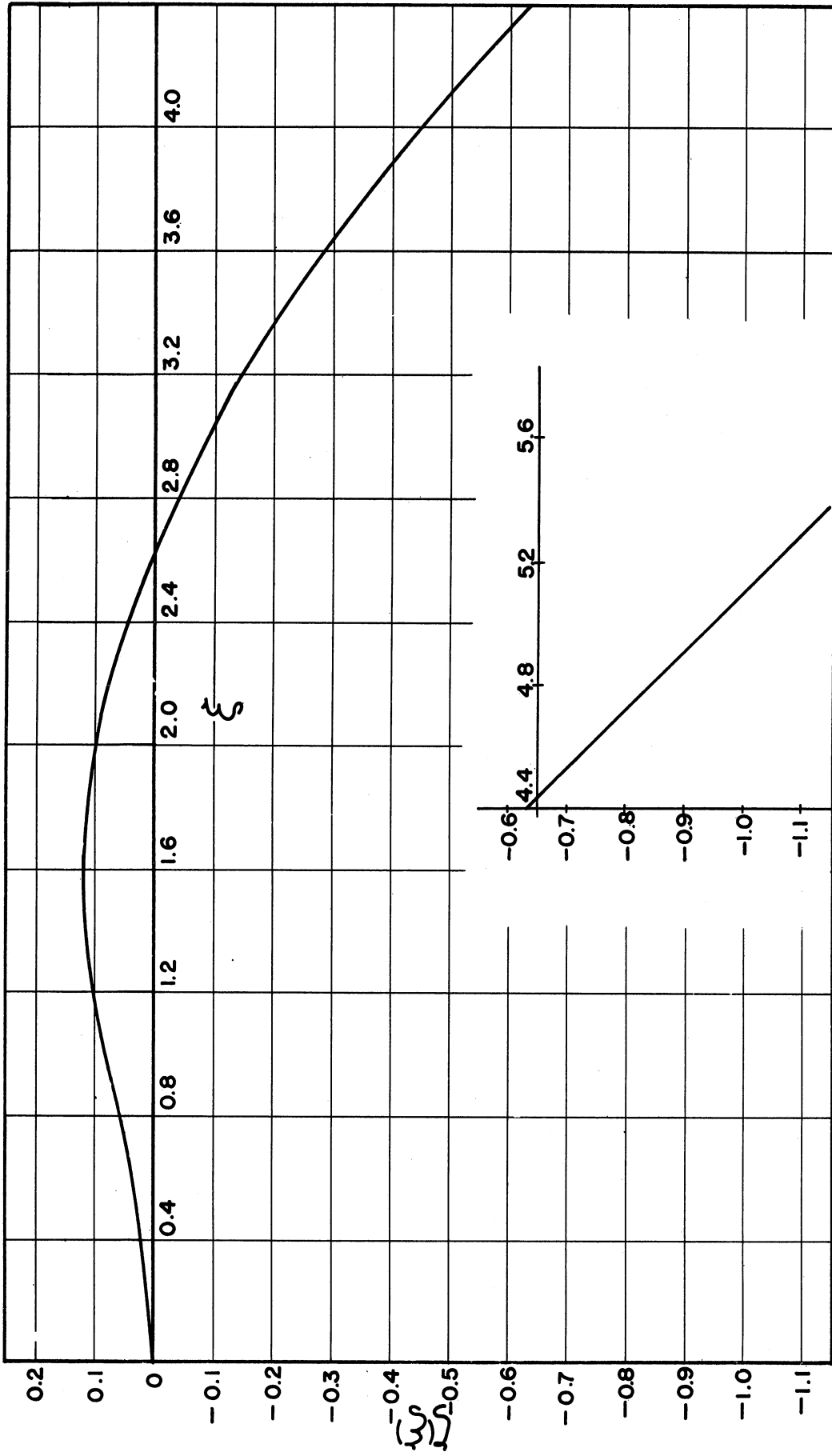
Figure 2-33. Values of $\zeta(\xi)$ of Equation (2-100).

which is written as

$$1 - 2X^2 + X^4 = X \, \zeta(\xi)/\psi \qquad (2\text{-}103)$$

For a chosen ψ there are particular values of X and ξ which satisfy this equation.

The solution of Equation (2-103) can be done in several ways. One way is to select values of ξ and ψ and then solve for the fourth order roots of X. This method is difficult. A more convenient way has been ascertained by realizing that the root-locus method from automatic control theory can be applied here. It was realized that Equation (2-103) has the form of a closed-loop transfer function for a feed-back system. A brief account of root-locus theory will be given here as explanation. The root-locus method represents, through simple and analytic techniques, the changes in position of the poles and zeros of the closed-loop transfer function as the gain of the open-loop transfer function is varied. From this point on X is replaced by Z, a complex variable, where only X, the real part, has significance. The closed-loop transfer function can be written as

$$\frac{1}{D} = \frac{\psi}{X} = \frac{Z}{[Z^2 - 1]^2} = G \qquad (2\text{-}104)$$

where D represents the gain. Root-locus will yield where

$$1 - GD = 0 \qquad (2\text{-}105)$$

G has a zero at $Z = 0$, double order poles at $Z = \pm 1$ and a third

order zero at ∞. With this known and by utilizing the rules for the asymptotes of the root-locus, the root-locus plots were made and are shown in Figure 2-34.

As can be ascertained from the root-locus plots there will be, on one side of the plate, four regions of ψ. In Figure 2-34 is shown one of these areas and in Figure 2-35 is shown the right half side of the plate.

The streamline, ψ_{2s}, of Equation (2-99) decreases by $\omega^{-3/2}$ and u_{2s} of Equation (2-44) decreases by ω^{-1}. Since the second-order time-independent contribution to velocity is $\epsilon^2 u_{2s}$ ($\epsilon = a\omega/L$) the frequency dependency of velocity is ω. The inner vortex of Figure 2-36 on the upper quadrant goes up and the one on the lower quadrant goes down, near the plate. The result is that free convection (time-independent) velocities are increased in the upper quadrant and decreased in the lower quadrant near the wall due to time-independent second-order perturbations. Also for increasing frequencies the vortices move inward toward the plate. The streamlines touch at $X = 1$ and $\xi = 0$ and 2.63 due to the approximations imposed on the potential flow. In reality these would not touch but would be close together in these regions.

Second-Order (Time-Independent) Shear Stress and Nusselt Number

Taking the expression from the steady velocity and differentiating it, the time-independent derivative is found to be

$$\left(\frac{\partial u_{2s}}{\partial Y}\right)_0 = \frac{1}{(2\omega)^{1/2}} P \frac{\partial P}{\partial X}$$

(2-106)

ROOT-LOCUS PLOTS

$Z^4 - 2Z^2 - [\ \zeta/\psi\ ]Z + 1$

$Z = x/c + i\ r/c$

PLOT "A": NEGATIVE ζ/ψ

PLOT "B": POSITIVE
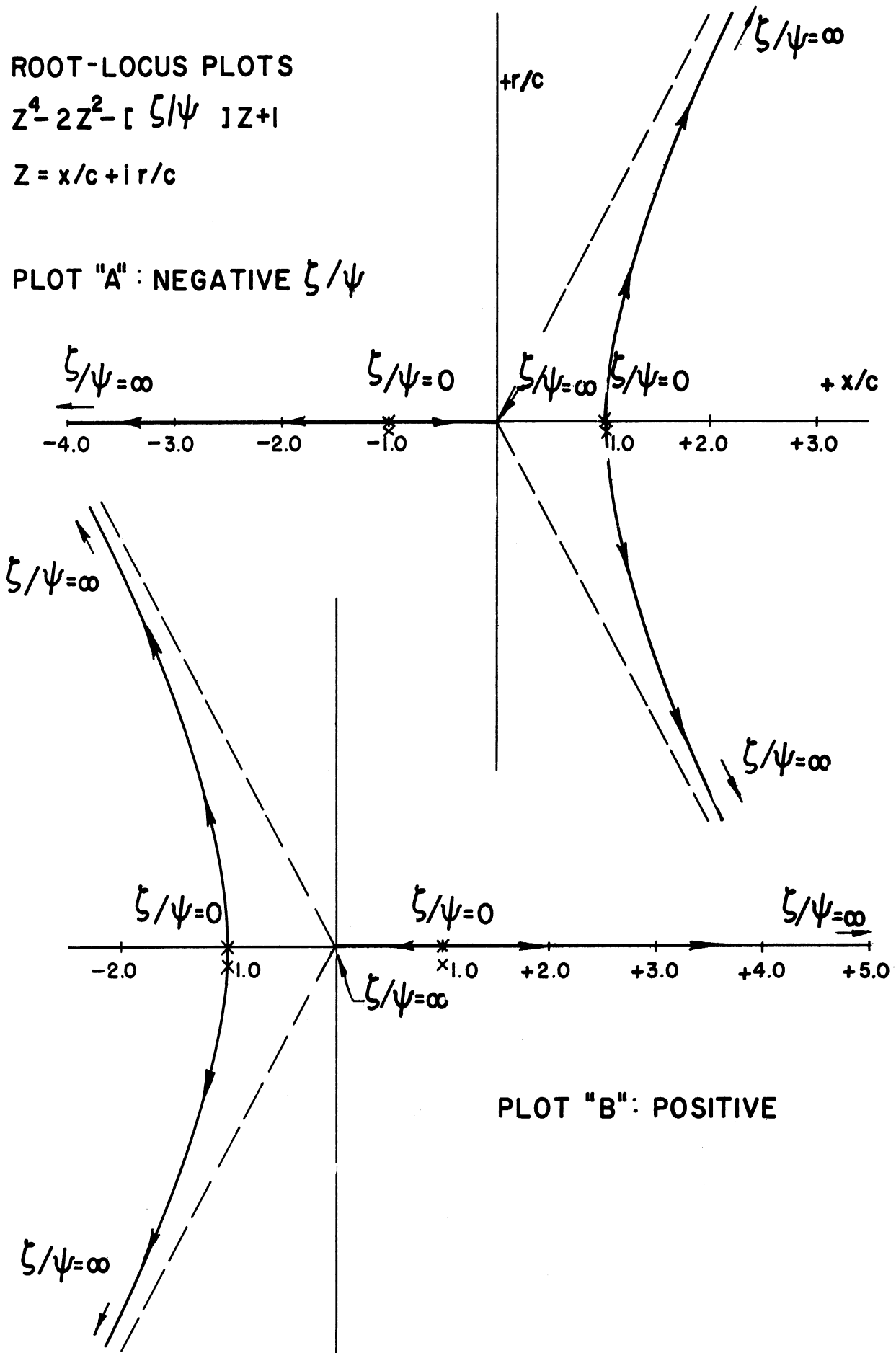
Figure 2-34. Root-Locus Plots for Determination of the
Streamlines of Equation (2-102).
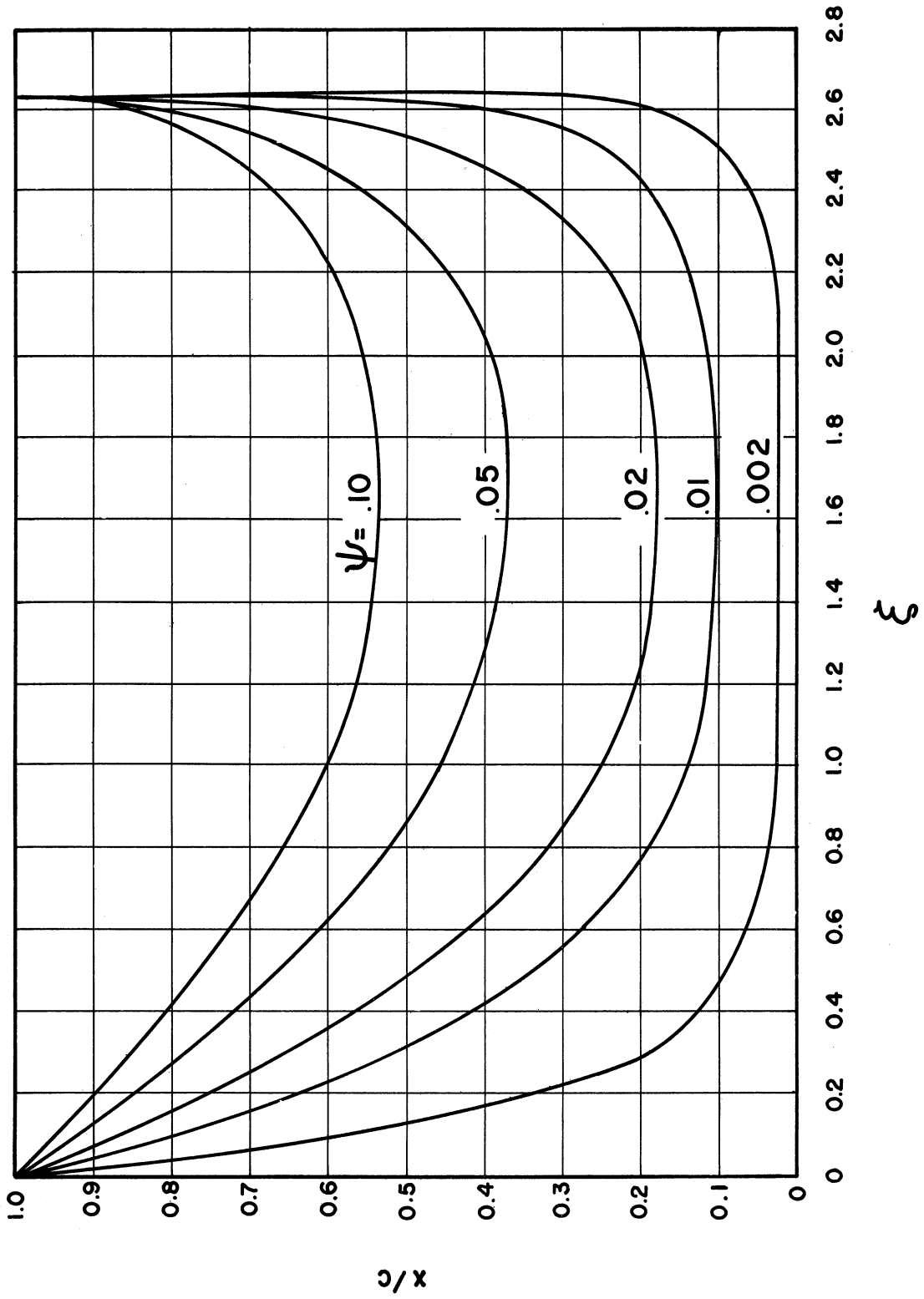
Figure 2-35. Time-Independent (Secondary) Streamline in the Top Inner Region of the Plate.
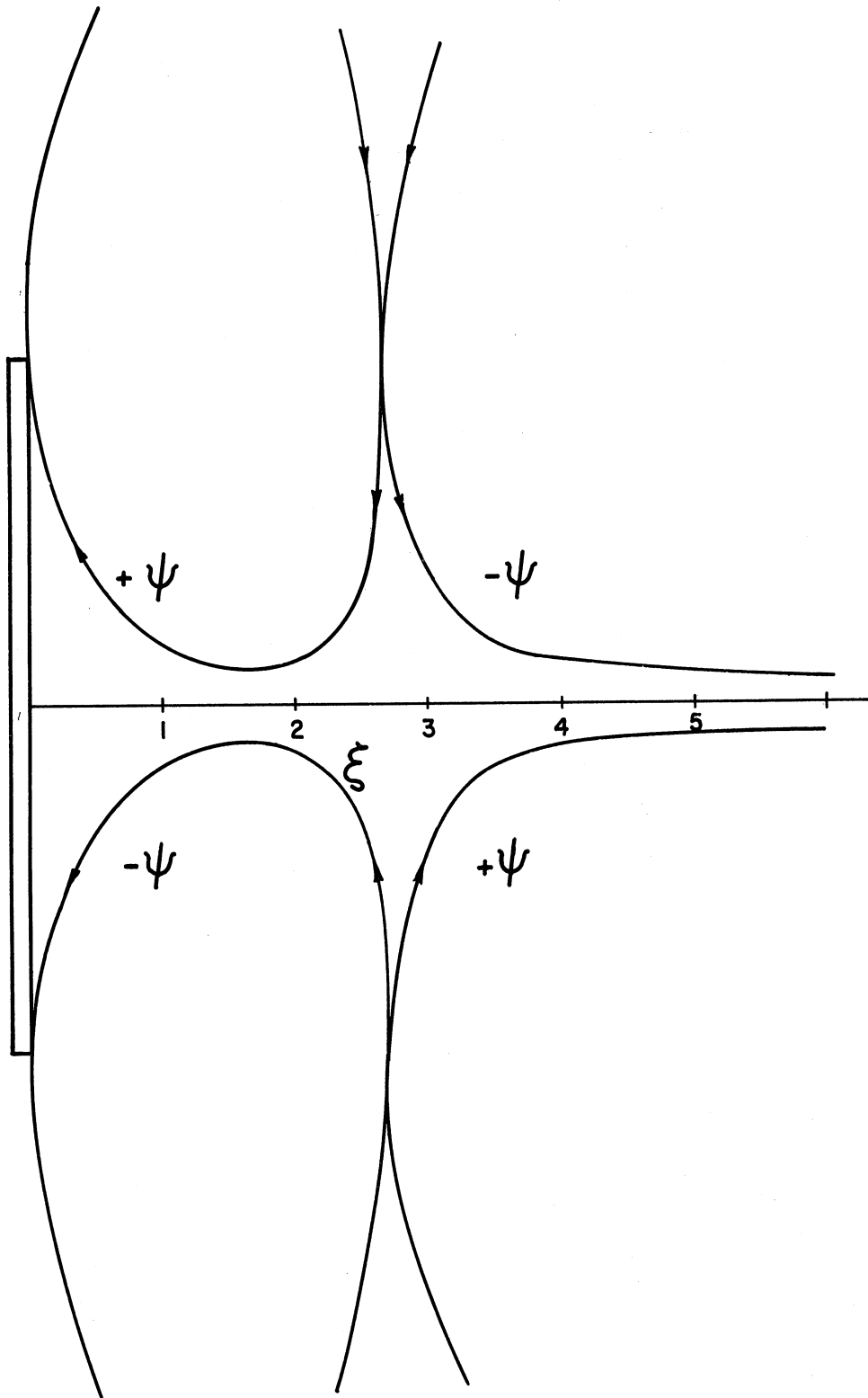
Figure 2-36. A Representative Plot of Time-Independent
             Flow Streamlines.

Therefore the second-order or time-independent contribution, τ_{2s}, can be written as

$$\frac{\tilde{T}_{2s}}{\mu_\infty} = \epsilon^2 \frac{P \frac{\partial P}{\partial X}}{(2\omega)^{1/2} (4X)^{1/2}} \tag{2-107}$$

This result is not a function of the Prandtl number since for high frequency the non-negligible terms in Equation (2-92) are independent of Prandtl number. The result in Equation (2-106) decreases for increasing frequency as $\omega^{-1/2}$. τ_{2s}, however, increases as $\omega^{3/2}$ since $\epsilon = a\omega/L$. Except for the $(4X)^{1/2}$ in the denominator, the contribution to τ_s/μ_∞ $(4X)^{1/2}$ for $X < 0.5$ is equal and of opposite sign to that of $X < 0.5$.

It is appropriate at this point to investigate the second-order energy equation. The governing Equation (2-31C) will yield terms which contribute $\cos^2\omega t$ terms. These were reduced to terms which contained only $\cos 2\omega t$ and steady terms exactly like the procedure used for the steady velocities. The two resulting time-dependent and time-independent equations are

$$i2\omega T_2 + U_0 \frac{\partial T_2}{\partial X} + U_2 \frac{\partial T_0}{\partial X} + V_0 \frac{\partial T_2}{\partial Y} + V_2 \frac{\partial T_0}{\partial Y} +$$

$$\frac{REAL}{2}\left[U_1 \frac{\partial T_1}{\partial X} + V_1 \frac{\partial T_1}{\partial Y}\right] = \frac{1}{P_R} \frac{\partial^2 T_2}{\partial Y^2}$$

$$\tag{2-108}$$

$$U_0 \frac{\partial T_{2s}}{\partial X} + U_{2s} \frac{\partial T_0}{\partial X} + V_0 \frac{\partial T_{2s}}{\partial Y} + V_{2s} \frac{\partial T_0}{\partial Y} + \frac{REAL}{2}\left[\overline{U_1} \frac{\partial T_1}{\partial X}\right.$$

$$\left. + \overline{V_1} \frac{\partial T_1}{\partial Y}\right] = \frac{1}{P_R} \frac{\partial^2 T_{2s}}{\partial Y^2}$$

where the bar over the symbols denotes the respective complex conjugate quantities. Only the steady equation is treated because of its importance as a steady contribution to the Nusselt number. The order of magnitude is

$$U_0 \frac{\partial T_{2s}}{\partial X} + U_{2s} \frac{\partial T_0}{\partial X} + V_0 \frac{\partial T_{2s}}{\partial Y} + V_{2s} \frac{\partial T_0}{\partial Y} +$$

$$O(1 \cdot \quad) \quad O(\omega^{-1} \cdot 1) \quad O(1 \cdot \quad) \quad O(\omega^{-1} \cdot 1)$$

$$+ Real \frac{1}{2} \left[\bar{U}_1 \frac{\partial T_1}{\partial X} + \bar{V}_1 \frac{\partial T_1}{\partial Y} \right] = \frac{1}{P_R} \frac{\partial^2 T_{2s}}{\partial Y^2}$$

$$O(1 \cdot \omega^{-1}) \quad O(1 \cdot \omega^{-1/2})$$

(2-109)

Therefore we conclude that T_{2s} will be approximately of the order of magnitude of $\omega^{-3/2}$. By change of variable from Y to η and retaining only higher order terms Equation (2-109) reduces to

$$\frac{\partial^2 T_{2s}}{\partial \eta^2} = P_R (4X)^{1/2} \left[\frac{Real}{2} \left[\bar{U}_1 \frac{\partial T_1}{\partial X} + \bar{V}_1 \frac{\partial T_1}{\partial Y} \right] + \right.$$

$$\left. U_{2s} \frac{\partial T_0}{\partial X} + V_{2s} \frac{\partial T_0}{\partial Y} \right] .$$

(2-110)

This was integrated to $(\partial T_{2s}/\partial \eta)_0$. By one simple integration and evaluation at $\eta = 0$ some of the burdensome algebra was eliminated. Furthermore the steady-state contribution to the Nusselt number is the prime objective and $(\partial T_{2s}/\partial \eta)_0$ yields this information. The zeroth and second-order Nusselt number is

$$\frac{Nu}{(-H'(0))\left(\frac{Gr_X}{4}\right)^{1/4}} = 1 - \epsilon^2 \frac{\left(\frac{\partial T_{2s}}{\partial \eta}\right)_0}{(-H'(0))}$$

(2-111)

The steady-state contribution is shown in Figures 2-37 through 2-40. As can be seen in these figures, there is an asymmetrical nature to the gradient along the X-direction. This asymmetry is due to the fact that the potential flow is symmetrical about the middle of the plate and the free convection (zero-order) part is similar from the leading edge up and the net effect is a non-symmetrical result. The gradient is positive and therefore the second-order contribution is to decrease the Nusselt number. The gradient $(\partial T_{2s}/\partial \eta)_0$ increases approximately as ω^{-1} as frequency is increased. Since $\epsilon = a\omega/L$ the second order perturbation dependency on frequency is ω which decreases as ω increases. Also the second order dependency on amplitude is $(a/L)^2$ and the Nusselt number decreases as $(a/L)^2$. The Nusselt number in Equation (2-111) decreases at higher Prandtl number.

Solutions Up to Second Order

The velocity in dimensional quantities is

$$\frac{V}{2\sqrt{g\beta \Delta\theta_0 X}} = F'(\eta) + \epsilon \frac{|U_1|}{(4X)^{1/2}} \cos(\omega t + \phi) + \epsilon^2 \frac{U_{2s}}{(4X)^{1/2}} \qquad (2\text{-}112)$$

To express $(\partial U/\partial Y)_0$ in terms of the known functions, there is obtained by substitution of these functions into Equation (2-112) the following equation

$$\frac{\partial V}{\partial Y} = (4 G_{rx})^{1/4} \frac{V_\infty}{X^2} \left[F''(\eta_d) + \epsilon \frac{\left(\frac{\partial |U_1|}{\partial \eta_d}\right)}{(4X)^{1/2}} \cos(\omega t + \phi) \right.$$

$$\left. + \epsilon^2 \left(\frac{\partial U_{2s}}{\partial \eta_d}\right) \frac{1}{(4X)^{1/2}} \right. \qquad (2\text{-}113)$$
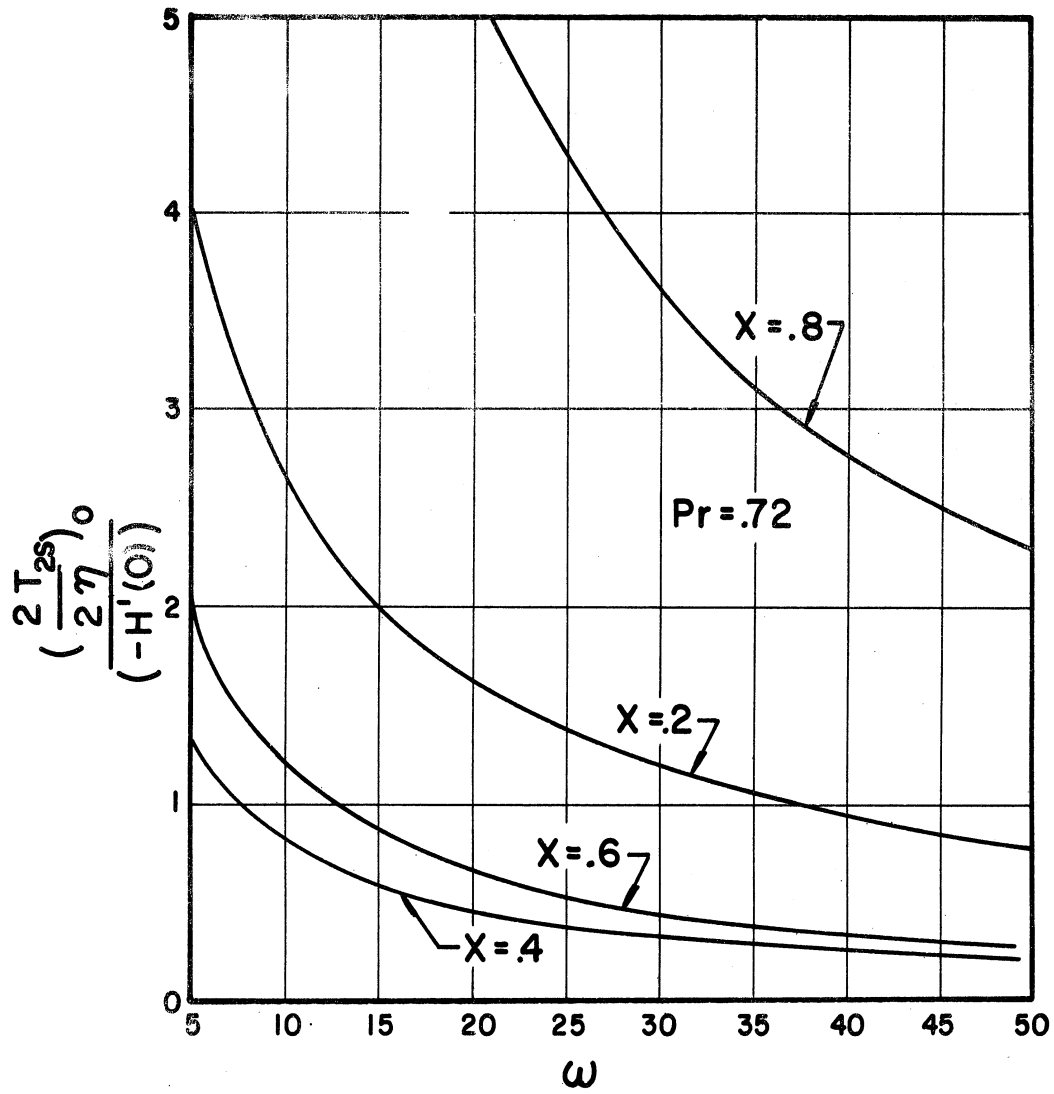
Figure 2-37. Magnitude of the Time-Independent Temperature
Derivative Divided by the Zeroth Derivative
of Temperature.
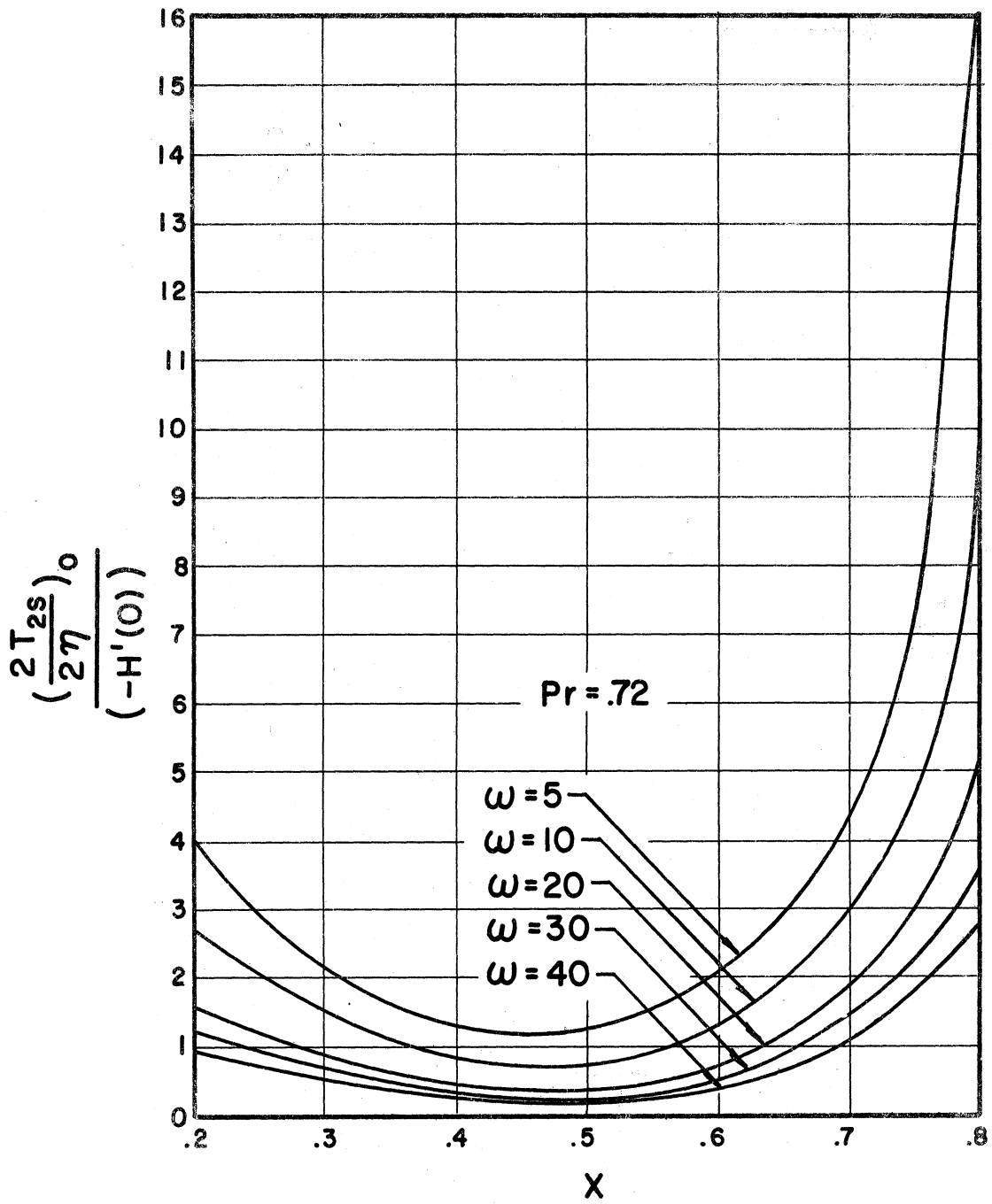
Figure 2-38. Magnitude of the Time-Independent Temperature
Derivative Divided by the Zeroth Derivative
of Temperature.
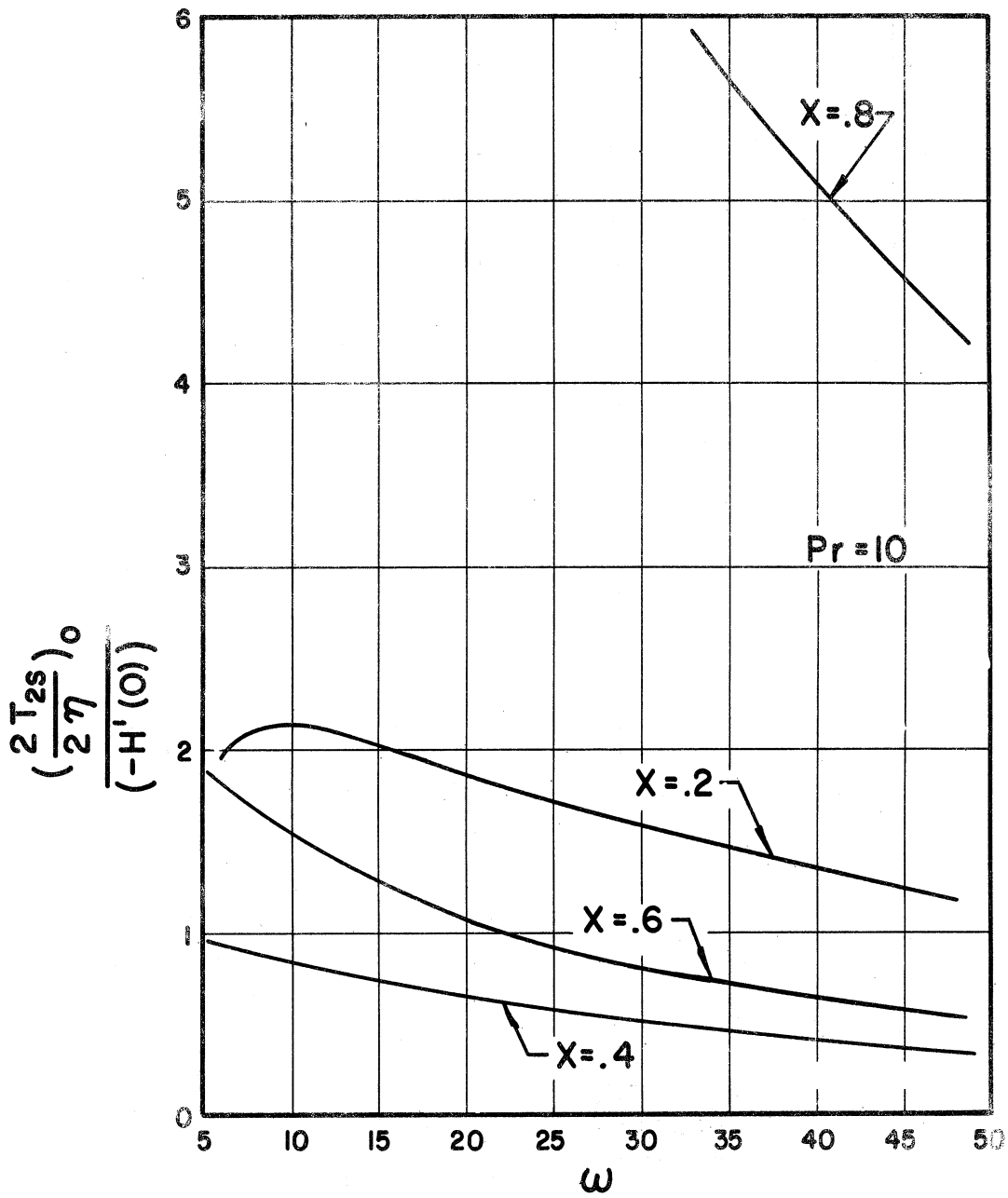
Figure 2-39. Magnitude of the Time-Independent Temperature Derivative Divided by the Zeroth Derivative of Temperature.
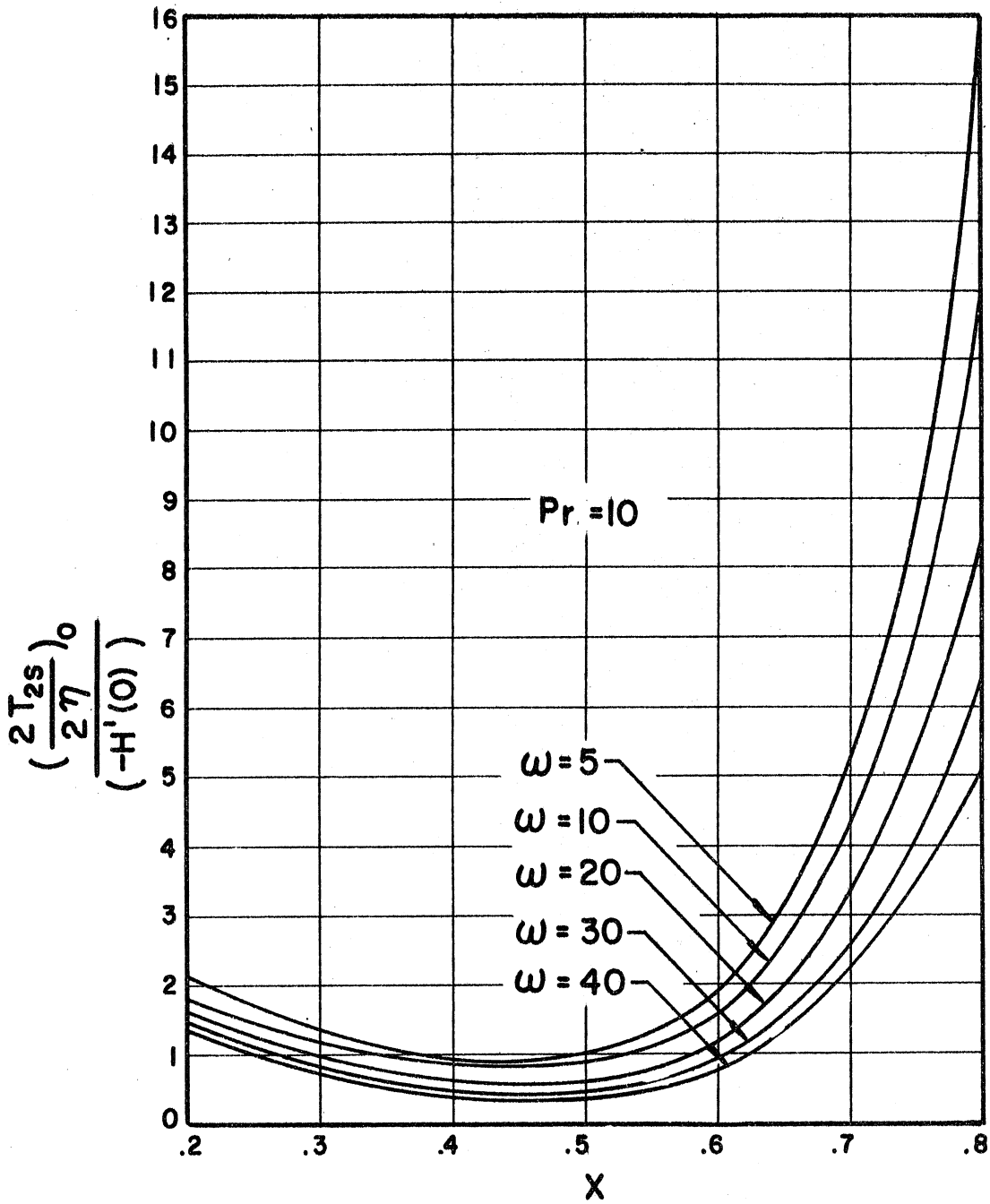
Figure 2-40. Magnitude of the Time-Independent Temperature
Derivative Divided by the Zeroth Derivative
of Temperature.

By definition the shear stress is

$$\mathcal{T} = \mu_\infty \left(\frac{\partial U}{\partial Y} \right)_0 \tag{2-114}$$

so that substitution of Equation (2-113) into Equation (2-114) will

yield

$$\frac{\mathcal{T}}{(4G_{RX}^3)^{\frac{1}{4}} \left(\frac{V_\infty \mu_\infty}{X^2} \right)} = F''(0) + \epsilon \frac{\left(\frac{\partial |U_{1}|}{\partial \eta} \right)_0}{(4X)^{\frac{1}{4}}} \cos(\omega t + \phi) \tag{2-115}$$

$$+ \epsilon^2 \left(\frac{\partial U_{2s}}{\partial \eta} \right)_0 \frac{1}{(4X)^{\frac{1}{4}}} + \cdots$$

The steady-state shear stress is Equation (2-115) without the
second term on the right hand side of the equation. The periodic middle
term will contribute nothing when integrated over a whole cycle.

The local Nusselt number is defined as

$$N_u = \frac{hX}{K} = \frac{-X}{\Delta\theta_0} \left(\frac{\partial \theta}{\partial Y} \right)_0 \tag{2-116}$$

and to express $(\partial\theta/\partial Y)_0$ in terms of the known functions, there is ob-
tained by substitution of these functions into the derivative of the
zeroth, first and second order temperatures the following equation

$$\frac{\partial\theta}{\partial Y} = \frac{\Delta\theta_0}{X} \left(\frac{G_{RX}}{4} \right)^{\frac{1}{4}} \left[H'(\eta_d) + \epsilon \frac{\partial |T_1|}{\partial \eta_d} \cos(\omega t + \phi) \right. \tag{2-117}$$

$$\left. + \epsilon^2 \left(\frac{\partial T_{2s}}{\partial \eta_d} \right) \right]$$

so that substitution of Equation (2-117) evaluated at $\eta = 0$ into Equation (2-116) yields

$$\frac{Nu}{(Gr_x/4)^{1/4}(-H'(0))} = 1 - \epsilon \frac{\left(\frac{\partial |T_1|}{\partial \eta_d}\right)}{(-H'(0))} \cos(\omega t + \phi)$$

$$- \epsilon^2 \left(\frac{\partial T_{2s}}{\partial \eta_d}\right)_0 \frac{1}{(-H'(0))} + \cdots$$

(2-118)

Again the middle term contributes nothing to the steady-state value. The values for all of these expressions are presented in the previous sections either in the form of graphs or the expression itself.

Discussion of Results

In the preceding sections an analysis of the effects of transverse vibrations of a finite, vertical flat plate in an otherwise free convection field was presented. The case treated was that of free convection with a perturbing effect from a potential flow of small $a\Omega$ and high frequency. The external periodic potential flow induces oscillations of temperature and velocity in the boundary layer. The phase angle and magnitude of these oscillations as well as the secondary or steady-state alterations of the free convection boundary layer were obtained. These were present in the second-order perturbations and arise from the inertia terms of the governing equations of momentum and energy.

Also studied were shear stress and Nusselt number changes due to the external potential flow oscillations. These effects were both periodic and steady-valued. The effect of oscillations produced a slight

decrease in the heat transfer coefficient. Experimental observations, discussed in Chapter IV, support this result and explain a phenomenon which is prevalent in experimental data in the literature. This phenomenon is reported to be a transition from a laminar to a turbulent flow at a critical condition of vibration.

CHAPTER III

FIRST AND SECOND ORDER PERTURBATION
OF A LAMINAR FREE CONVECTION BOUNDARY LAYER DUE
TO TRANSVERSE HARMONIC OSCILLATIONS OF AN INFINITE PLATE

Introduction

This chapter is an extension of work on the subject of
vibrational effects in heat transfer completed recently by the Heat
Transfer and Thermodynamics Laboratory (A-34). Schoenhals and Clark
reference (A-33) treated the first order perturbation. The present
results disclose the existence of a steady streaming or secondary
flow phenomena. Shear stress and Nusselt number are presented in
the form of series solutions. A revision is made in the analysis
from that of reference (A-33) in that mathematical relations are
fitted to the important variable functions and the derivates of the
free convection boundary layer. This revision is found to allow more
freedom in the solution. The present results and those found earlier
(A-34) are identical in these regions where both are applicable. This
revision was found also to be more convenient for utilization in the
second order perturbation.

Formulation of the Problem

The physical problem is that of a vertical heated flat plate
in an otherwise quiescent fluid. The surface of the plate is maintained
at a constant temperature Θ for $X \geq 0$, Figure 3-1. In the absence of
oscillations the problem would be that of free convection previously
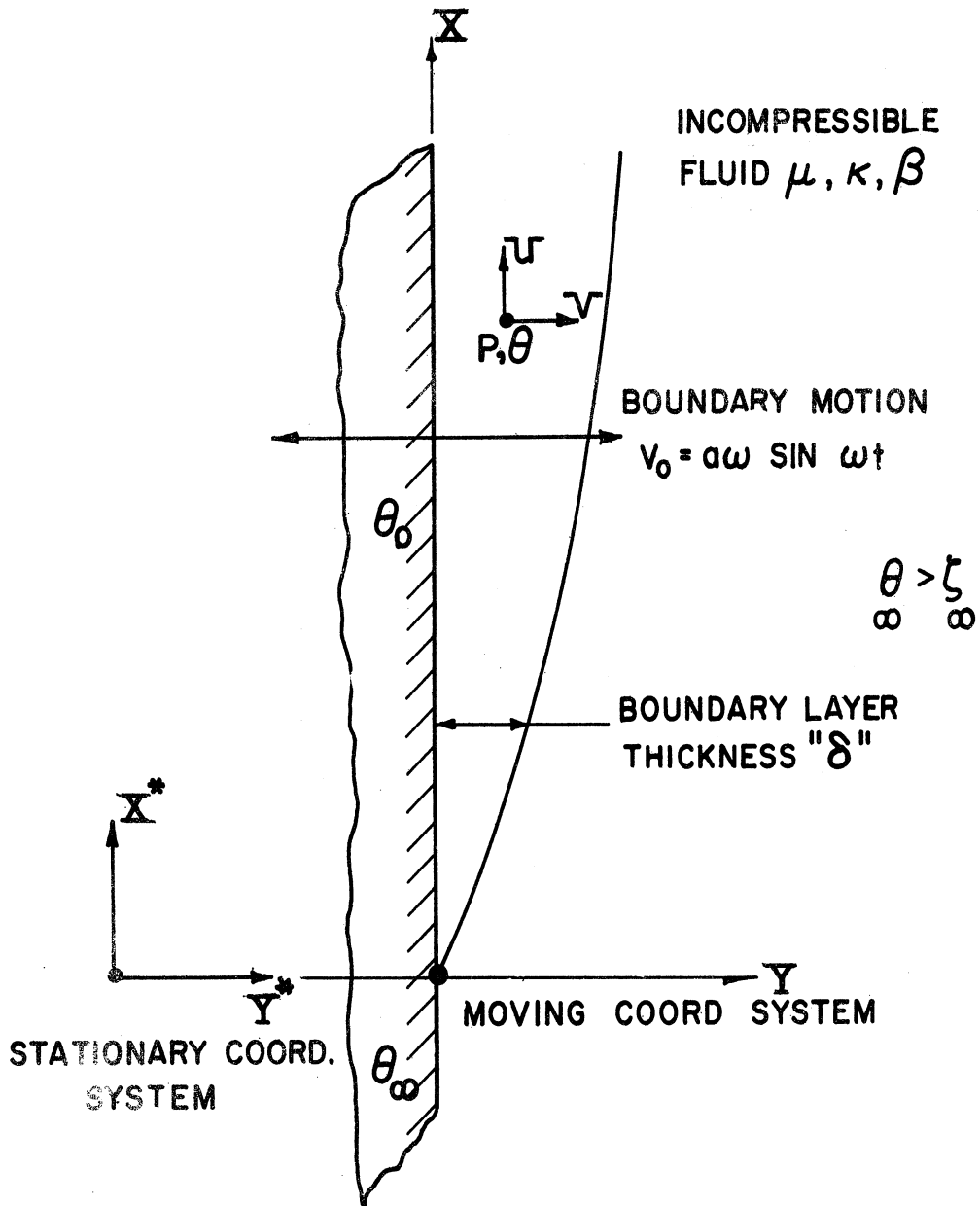
Figure 3-1. Laminar Free Convection Boundary Layer
Adjacent to a Heated Wall with Transverse
Vibration.

treated by Schmidt and Beckman (C-11) and Ostrach (C-8). Their results will be called herein the zeroth-order solution.

For transverse sinusoidal oscillation the first-order approximation has been determined (A-34), and has a periodic character. The plate is considered to be of infinite extent. In a practical case this would require that edge effects be negligible in the central portions of the plate. If the plate were of finite extent the problem would be that of Chapter II.

This chapter is concerned with the effects of transverse wall vibration on a free convection flow at high frequencies for an infinite plate. The perturbation method of solution used linearizes the governing of equations. Therefore by the nature of the solution the effects of vibration are expected to be small. It is in this way the problem can be rendered mathematically amenable.

The analysis is concerned with incompressible flow. The question of compressibility is examined in reference (A-34) and is repeated here. The motion of the plate is $V_O = a \Omega \sin\Omega_T$. If the plate is considered to be the source of a sound wave propagating normal to its surface with velocity V_s and frequency Ω, then the acoustic wave length normal to the wall is $\lambda = V_s/2\pi \Omega$. It was found that compressibility is not important as long as $a_O\Omega$ is small compared to the velocity of sound of the surrounding fluid. For example with air let $a_O = 1$ inch and $\Omega = 30$ cps then the relative compressiblity is about 0.1 per cent.

The problem is formulated in a frame of reference fixed
to the oscillating plate. The governing equations of momentum,
energy and mass are (A-34)

$$\rho \frac{DU}{DT} = -\frac{\partial P}{\partial X} - \rho g + \mu \nabla^2 U \qquad (3\text{-}1\text{A})$$

$$\rho \frac{DV}{DT} = -\frac{\partial P}{\partial Y} + \mu \nabla^2 V - \rho \frac{DV_0}{DT} \qquad (3\text{-}1\text{B})$$

$$\text{div } \vec{V} = 0 \qquad (3\text{-}1\text{C})$$

$$\frac{D\Theta}{DT} = \alpha \nabla^2 \Theta \qquad (3\text{-}1\text{D})$$

If there were no oscillations the last term of Equation (3-1B)
would be zero. Utilizing the usual boundary layer assumptions these
equations reduce, from reference (A-34), to

$$\rho \frac{DU}{DT} = -\frac{\partial P}{\partial X} - \rho g + \mu \frac{\partial^2 U}{\partial Y^2} \qquad (3\text{-}2\text{A})$$

$$\frac{\partial P}{\partial Y} = -\rho a \Omega^2 \cos \Omega T \qquad (3\text{-}2\text{B})$$

$$\text{div } \vec{V} = 0 \qquad (3\text{-}2\text{C})$$

$$\frac{D\Theta}{DT} = \alpha \frac{\partial^2 \Theta}{\partial Y^2} \qquad (3\text{-}2\text{D})$$

with the boundary conditions

$$Y=0 \quad U=V=0, \quad \Theta=\Theta_0$$
$$Y=\infty \quad U=0, \quad \Theta=\Theta_\infty \tag{3-3}$$

Equation (3-2) introduces the influence of the oscillation. Should the frequency be zero then Equations (3-2) would describe the laminar free convection heat transfer. In Chapter II the method is described for treating the pressure distribution due to the thermal variations of density. This is not repeated here and it is seen from Chapter II that

$$\frac{DU}{DT} = g\beta(\Theta-\Theta_\infty) + V\frac{\partial^2 U}{\partial Y^2} + a\Omega^2\beta\int_Y^\infty \frac{\partial\Theta}{\partial X}dY\cos\Omega T \tag{3-4}$$

is the governing equation for momentum.

The governing equations are non-dimensionalized by the same relationships used in Chapter II. The result is

$$\frac{DU}{Dt} = T + \frac{\partial^2 U}{\partial Y^2} + \left(\frac{a\Omega^2}{g\,(G_{RL})^{1/4}}\right)\int_Y^\infty \frac{\partial T}{\partial X}dy\cos\omega t$$

$$\frac{\partial U}{\partial X} + \frac{\partial V}{\partial Y} = 0 \tag{3-5}$$

$$\frac{DT}{DT} = \frac{1}{P_R}\frac{\partial^2 T}{\partial Y^2}$$

with the boundary conditions

$$Y=0 \quad U=V=0, \quad T=1$$
$$Y=\infty \quad U=T=0 \tag{3-6}$$

The quantity in parenthesis in Equation (3-5) is defined as

$$\epsilon = \frac{a_o \Omega^2}{g} \frac{1}{(G_{RL})^{1/4}} = \left(\frac{a_o}{L}\right) \frac{\beta \Delta T_o}{(G_{RL})^{1/4}} \omega^2 \tag{3-7}$$

This chapter treats small ϵ and high frequencies. It can be seen that ϵ will be small even if ω is high because of the extremely small magnitude of the coefficient of ω^2 in Equation (3-7). It should be noted that a_o/L has to be small because of the compressibility restraint. Considering the requirements of compressibility and free convection flow it can be stated that

$$\left(a_o/L\right) << O(1)$$

$$a_o \Omega << O(1) \tag{3-8}$$

$$\beta \Delta T_o << O(1)$$

$$G_R >> O(1)$$

The first three are related with compressiblity restraints. The last two are conditions that are necessary for the treatment of free convection as used by Ostrach (C-8) which are inherent to this problem as previously explained in Chapter II.

Perturbations of the Equations

Equations (3-5) are coupled, non-linear partial differential equations. Owing to these complexities a solution is sought using the perturbation technique. The solution is a convergent series expansion in the following form

$$U = U_0 + \epsilon\, U_I + \epsilon^2\, U_{II} + \cdots \tag{3-9A}$$

$$V = V_0 + \epsilon\, V_I + \epsilon^2\, V_{II} + \cdots \tag{3-9B}$$

$$T = T_0 + \epsilon\, T_I + \epsilon^2\, T_{II} + \cdots \tag{3-9C}$$

These expansions are discussed in Chapter II in the section concerning the perturbations of the equations.

The n-number of differential equations are found by substituting Equations (3-9) into Equations (3-5) and separating according to powers of ϵ. The continuity equation is, of course, linear. The equation found with ϵ' as the common coefficient is called the first-order equation, that with ϵ^2 the second-order approximation, etc. The results up to second-order are as follows:

Zeroth order, ϵ^0

$$U_0 \frac{\partial U_0}{\partial X} + V_0 \frac{\partial U_0}{\partial Y} = T_0 + \frac{\partial^2 U_0}{\partial Y^2}$$

$$U_0 \frac{\partial T_0}{\partial X} + V_0 \frac{\partial T_0}{\partial Y} = \frac{1}{P_R} \frac{\partial^2 T_0}{\partial Y^2} \tag{3-10}$$

$$\frac{\partial U_0}{\partial X} + \frac{\partial V_0}{\partial Y} = 0$$

with the boundary conditions

$$Y = 0 \qquad U_0 = V_0 = 0 \; ; \; T_0 = 1$$

$$Y = \infty \qquad U_0 = T_0 = 0 \tag{3-11}$$

first order, ϵ'

$$\frac{\partial U_I}{\partial t} + U_0\frac{\partial U_I}{\partial X} + U_I\frac{\partial U_0}{\partial X} + V_0\frac{\partial U_I}{\partial Y} + V_I\frac{\partial U_0}{\partial Y} = \tag{3-12A}$$

$$T_I + \frac{\partial^2 U_I}{\partial Y^2} + \int_Y^\infty \frac{\partial T_0}{\partial X}\, dy \cos \omega t$$

$$\frac{\partial T_I}{\partial t} + U_0\frac{\partial T_I}{\partial X} + U_I\frac{\partial T_0}{\partial X} + V_0\frac{\partial T_I}{\partial Y} + V_I\frac{\partial T_0}{\partial Y} = \frac{1}{P_R}\frac{\partial^2 T_I}{\partial Y^2} \tag{3-12B}$$

$$\frac{\partial U_I}{\partial X} + \frac{\partial V_I}{\partial Y} = 0 \tag{3-12C}$$

with the boundary conditions

$$Y = 0 \quad U_I = V_I = T_I = 0$$
$$Y = \infty \quad U_I = T_I = 0 \tag{3-14}$$

second-order, ϵ^2

$$\frac{\partial U_{II}}{\partial t} + U_0\frac{\partial U_{II}}{\partial X} + U_I\frac{\partial U_I}{\partial X} + U_{II}\frac{\partial U_0}{\partial X} + V_0\frac{\partial U_{II}}{\partial Y} + V_I\frac{\partial U_I}{\partial Y} \tag{3-15A}$$

$$+ V_{II}\frac{\partial U_0}{\partial Y} = T_{II} + \frac{\partial^2 U_{II}}{\partial Y^2} + \int_Y^\infty \frac{\partial T_I}{\partial X}\, dy \cos \omega t$$

$$\frac{\partial T_{I\!I}}{\partial t} + U_0 \frac{\partial T_{I\!I}}{\partial X} + U_I \frac{\partial T_I}{\partial X} + U_{I\!I} \frac{\partial T_0}{\partial X} + V_0 \frac{\partial T_{I\!I}}{\partial Y} + V_I \frac{\partial T_I}{\partial Y} +$$

$$V_{I\!I} \frac{\partial T_0}{\partial Y} = \frac{1}{P_R} \frac{\partial^2 T_{I\!I}}{\partial Y^2} \tag{3-15B}$$

$$\frac{\partial U_{I\!I}}{\partial X} + \frac{\partial V_{I\!I}}{\partial Y} = 0 \tag{3-15C}$$

with the boundary conditions

$$Y = 0 \qquad U_{I\!I} = V_{I\!I} = T_{I\!I} = 0$$

$$Y = \infty \qquad U_{I\!I} = T_{I\!I} = 0 \tag{3-16}$$

Except for the zeroth-order equations, the solution of the governing non-linear equations, valid only for high frequencies are formed from a convergent series of linear solutions. To have convergence it is necessary that

$$U_0 > \epsilon\, U_I > \epsilon^2 U_{I\!I} > \cdots$$

$$V_0 > \epsilon\, V_I > \epsilon^2 V_{I\!I} > \cdots$$

$$T_0 > \epsilon\, T_I > \epsilon^2 T_{I\!I} > \cdots \tag{3-17}$$

Zero-Order Solution

The zero-order solutions are exactly those of Ostrach (C-8) and were discussed in Chapter II. It is appropriate here to recall the similarity variable

$$\eta = Y/(4X)^{1/4} \tag{3-18}$$

and

$$\psi_0 = (4X)^{3/4} F(\eta) \tag{3-19}$$

$$T_0 = H(\eta)$$

where ψ_0 is the stream function. $F(\eta)$ and $H(\eta)$ are tabulated values of Ostrach (C-8) and are listed in Appendix III.

First-Order Solutions

Two solutions desired are of a steady-periodic nature. This is facilitated by the use of a complex variable time function as was done in Chapter II. By realizing the trignometric relationship

$$\cos \omega t = REAL\ e^{i \omega t} \tag{3-20}$$

we can therefore say

$$u_I = REAL\ (u_1\ e^{i \omega t}) \tag{3-21}$$

where u_I is a complex quantity. Then the solution can be written in the form

$$u_I = |u_1| \cos (\omega t + \phi) \tag{3-22}$$

where ϕ is the phase lag and $|u_I|$ is the absolute magnitude of the vector quantity u_I. Therefore we have

$$\frac{\partial u_I}{\partial t} = REAL\ i \omega\ u_1 e^{i \omega t}$$
$$\frac{\partial T_I}{\partial t} = REAL\ i \omega\ T_1 e^{i \omega t} \tag{3-23}$$

By substitution of these two relationships into Equations (3-12) it is

seen that the exponential term drops out. For large frequencies all

convective terms are negligible in the momentum equation for a first

approximation. In view of this the terms retained are the inertia terms

involving ω, the highest order derivative and the forcing function $\zeta(\eta)$.

This method has been used by Lighthill (A-20) and is in agreement with

the theory of differential equations with large parameters. For the

energy equation the two underlined terms of Equation (3-12B) are retained

along with the inertia term involving ω and the highest order derivative.

The two underlined terms represent a type of forcing function for the

energy equation. This was done because the subscripted zero terms have

approximately the same order of magnitude and u_1 and v_1 are larger than

T_1. This results in

$$\frac{\partial^2 u_1}{\partial y^2} - i\,\omega\, u_1 = -(4x)^{-3/4}\, \mathcal{Y}(\eta) \tag{3-24}$$

and

$$\frac{1}{P_R}\frac{\partial^2 T_1}{\partial y^2} - i\,\omega\, T_1 = u_1 \frac{\partial \overline{T_0}}{\partial x} + v_1 \frac{\partial \overline{T_0}}{\partial y} \tag{3-25}$$

By changing from the variable y to η they become

$$\frac{\partial^2 u_1}{\partial \eta^2} - i\,\gamma\, u_1 = -(4x)^{-1/4}\, \mathcal{Y}(\eta) \tag{3-26A}$$

$$\frac{1}{P_R}\frac{\partial^2 T_1}{\partial \eta^2} - i\,\gamma\, T_1 = (4x)^{1/2}\left[u_1 \frac{\partial \overline{T_0}}{\partial x} + v_1 \frac{\partial \overline{T_0}}{\partial y}\right] \tag{3-26B}$$

where

$$\gamma = \omega (4X)^{1/2}.$$

(3-27)

The solution to the first-order momentum equation is

$$U_1 = V_1 e^{-K_1 \eta} - V_1 e^{-\sqrt{i\gamma'}\,\eta} + V_2 \gamma e^{-K_1 \eta}$$

(3-28)

By introducing the variable $\mathcal{H}$

$$\mathcal{H} = \frac{K_1^2}{i\gamma}.$$

(3-29)

V_1 and V_2 are complex functions which can be described as

$$V_1 = \frac{-\mathscr{Y}(0)}{(4X)^{1/4} i\gamma} \left[1 + \sum_0^\infty \mathcal{H}^{m+1} \right]$$

(3-30)

$$V_2 = \frac{-\mathscr{Y}(0)}{(4X)^{1/4} i\gamma} \sum_0^\infty \mathcal{H}^m.$$

The solution of reference (A-33) for u_1 is

$$U_1 = \frac{\mathscr{Y}(0)}{i\gamma(4X)^{1/4}} \left[\frac{\mathscr{Y}(\gamma)}{\mathscr{Y}(0)} - e^{-\sqrt{i\gamma'}\,\eta} \right]$$

(3-31)

By replacing $\zeta(\eta)/\zeta(0)$ by the fitted curve in Chapter II this function is

given as

$$U_1 = \frac{\mathscr{Y}(0)}{i\gamma(4X)^{1/4}} \left[e^{-K_1 \eta} + K_1 \gamma e^{-K_1 \eta} - e^{-\sqrt{i\gamma'}\,\eta} \right]$$

(3-32)

It was found that solution (3-28) and that obtained by

Schoenhals (A-33) are identical for large values of γ and hence small

values of $\mathcal{H}$, as is easily seen by letting $\mathcal{H} \to 0$ in Equation (3-29).

In solution (3-28) V_1 and V_2 are evaluated completely by a numerical

method and are not approximated by the series of Equations (3-30).

The series were used only to compare solutions (3-28) and (3-31). The

solution of reference (A-33) treats large γ and ω therefore moderately

large values of X. The present solution treats large ω and therefore

almost any value of γ and X. Although X cannot be too small, because

the non-oscillating free convection boundary layer solution is not

valid in that region and $\zeta(\eta)$ is dependent on its results. The reason

the present solution, Equation (3-28), was derived was to have a form

which is not dependent upon the tabulated results of the free convection

solution. Solution (3-28) is in closed form and has been evaluated for

numerical results on an IBM 709 digital computer. Two typical programs

for the computation are given in Appendix I.

Figure 3-2 shows how Equations (3-28) and (3-31) compare for a

moderate value of $\gamma = 10$. The agreement is quite good for small values

of η and it is fair for large values of η. For smaller values of X the

comparison would not be as favorable, but for moderately large values of

η the two solutions coincide within the limits of the fitted curve and

the assumption for the solution of reference (A-33). For this value of

γ the phase angle appears to oscillate. This is due to the fact that

$\zeta(\eta)$ is actually zero but the fitted curve is not.

Figures 3-2 through 3-6 show some representative values of the

first-order velocities. They are represented in the form of ω^2 times
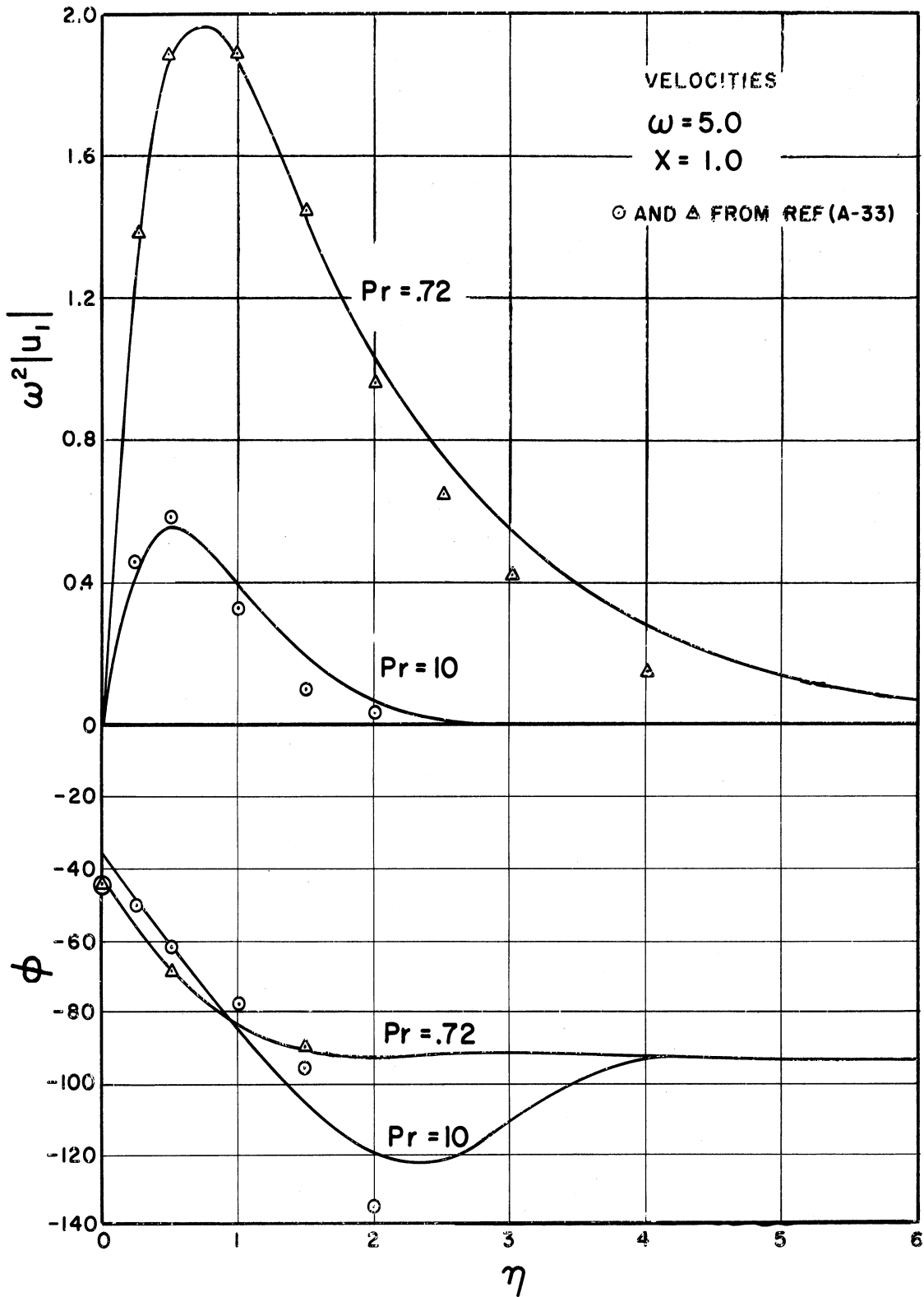
Figure 3-2. Magnitude and Phase of First Order Velocities With Comparison to that of Schoenhals and Clark (A-33).
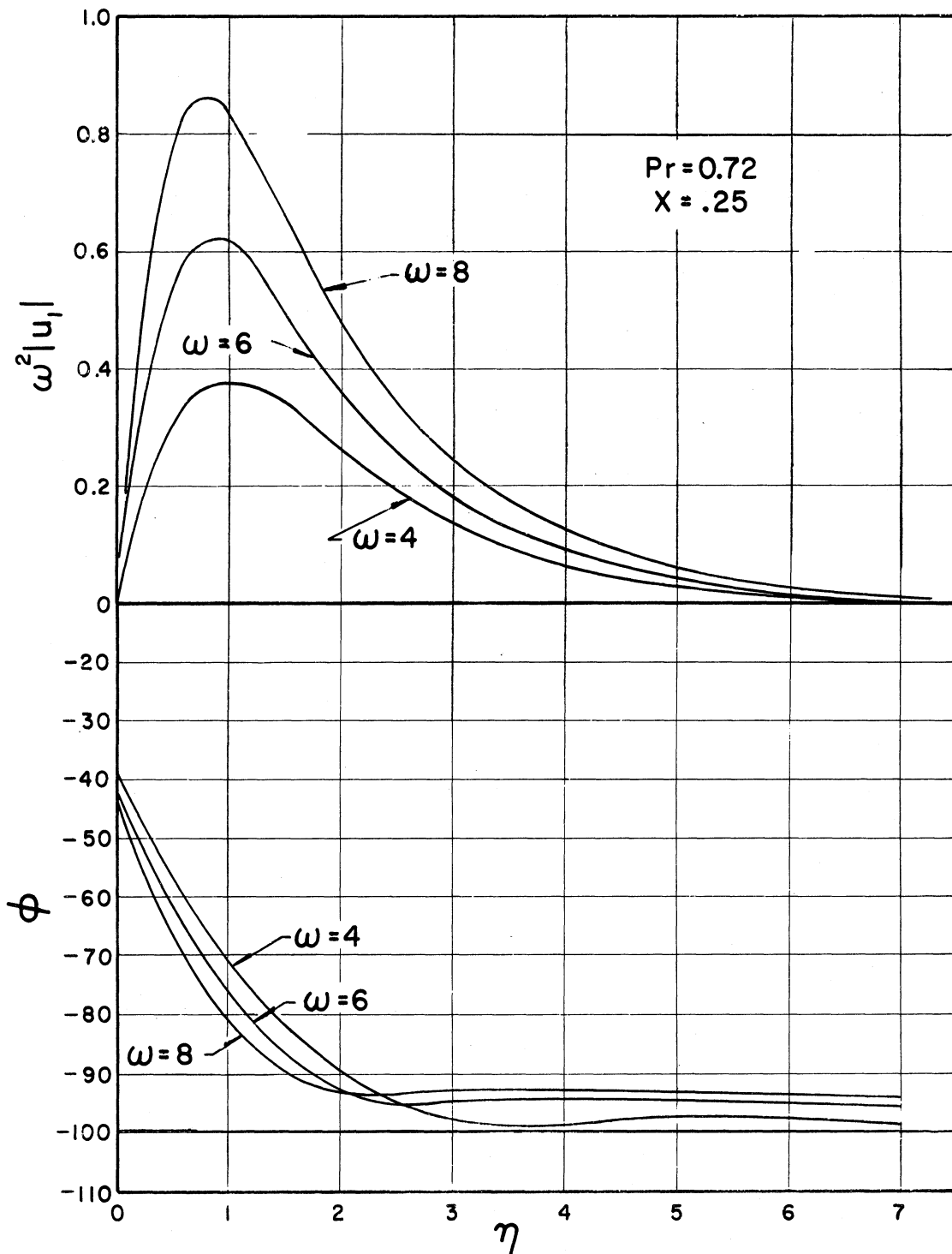
Figure 3-3. Magnitude and Phase of First Order Velocities.
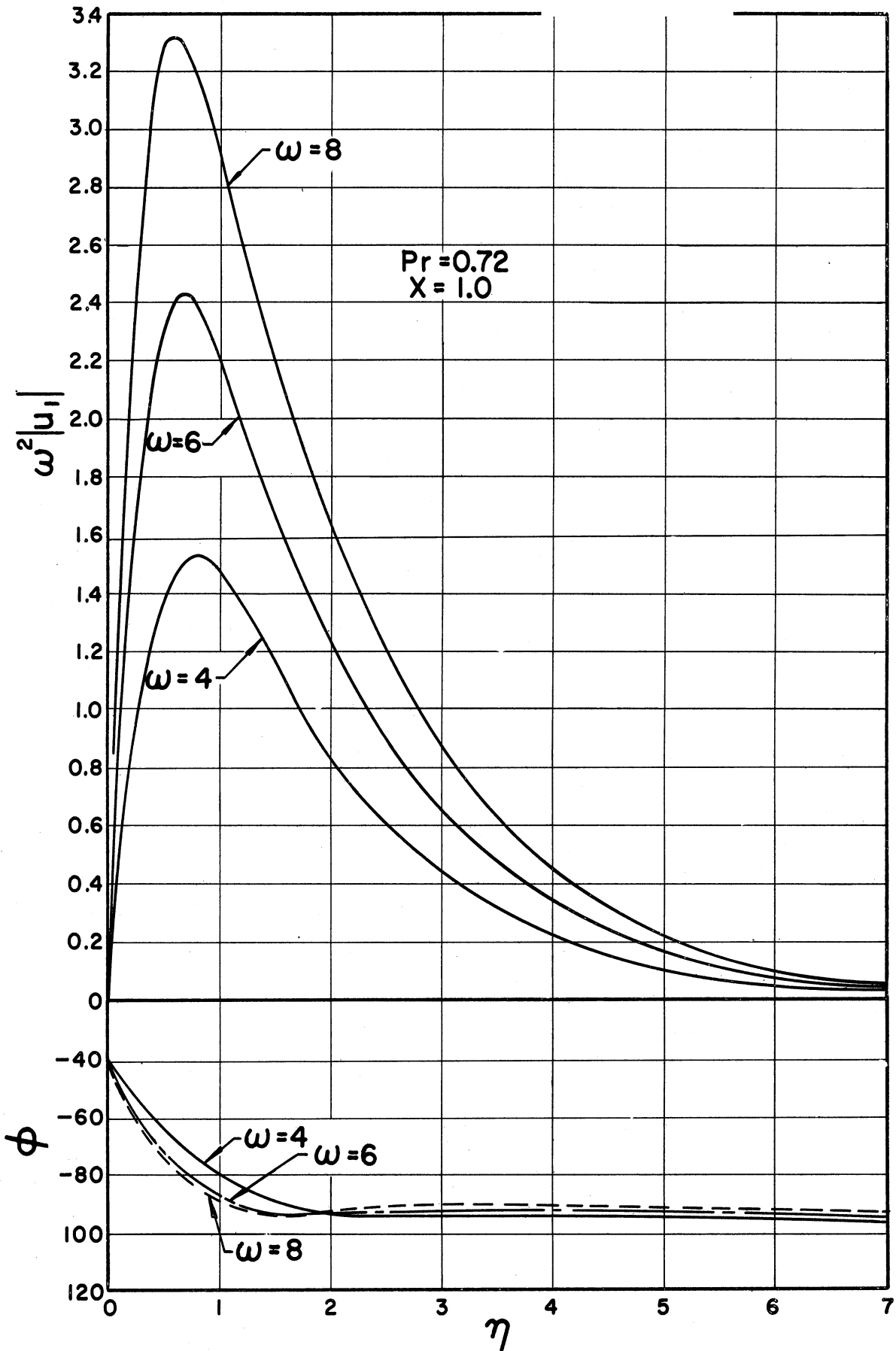
Figure 3-4. Magnitude and Phase of First Order Velocities.
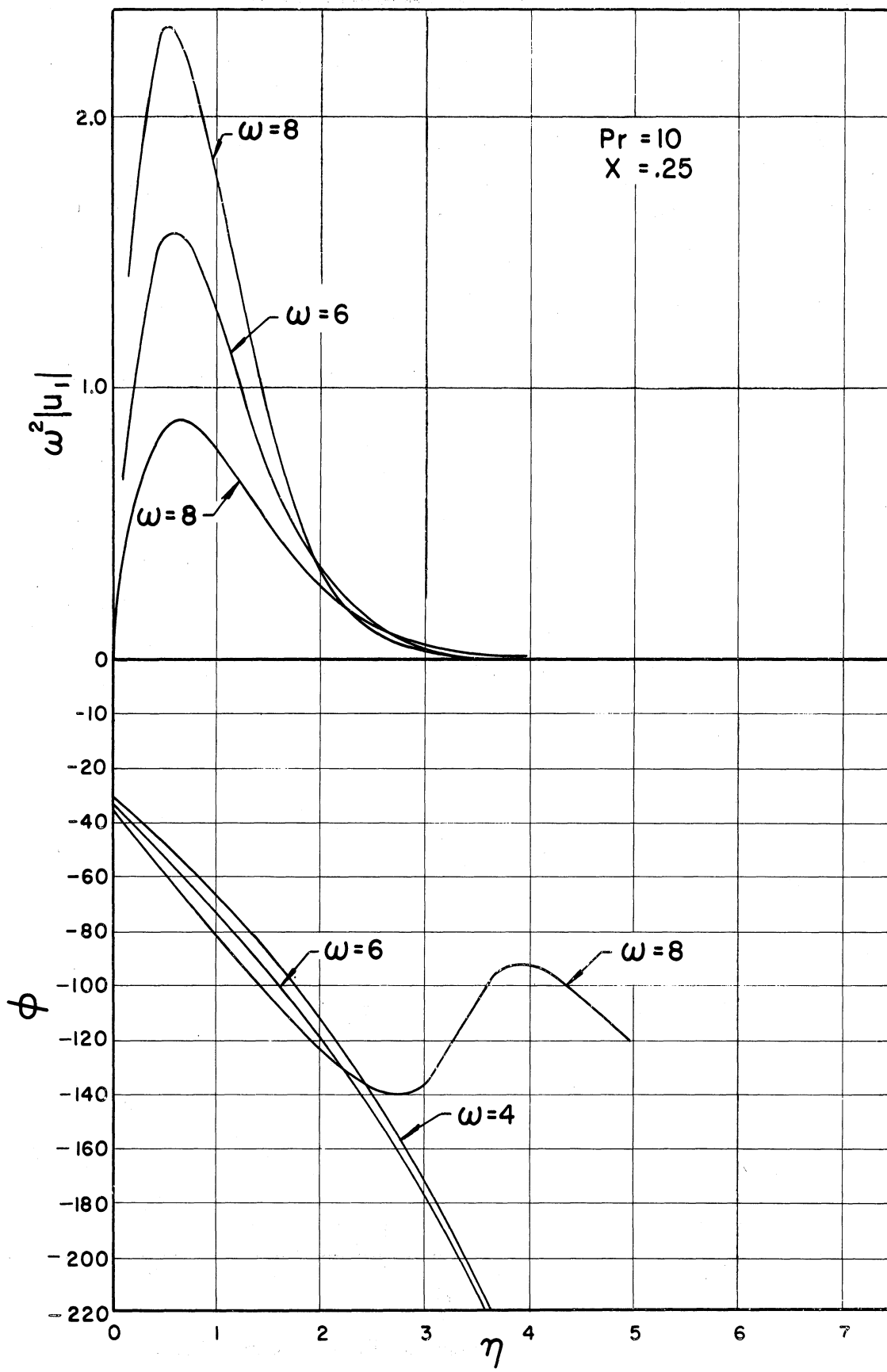
Figure 3-5. Magnitude and Phase of First Order Velocities.
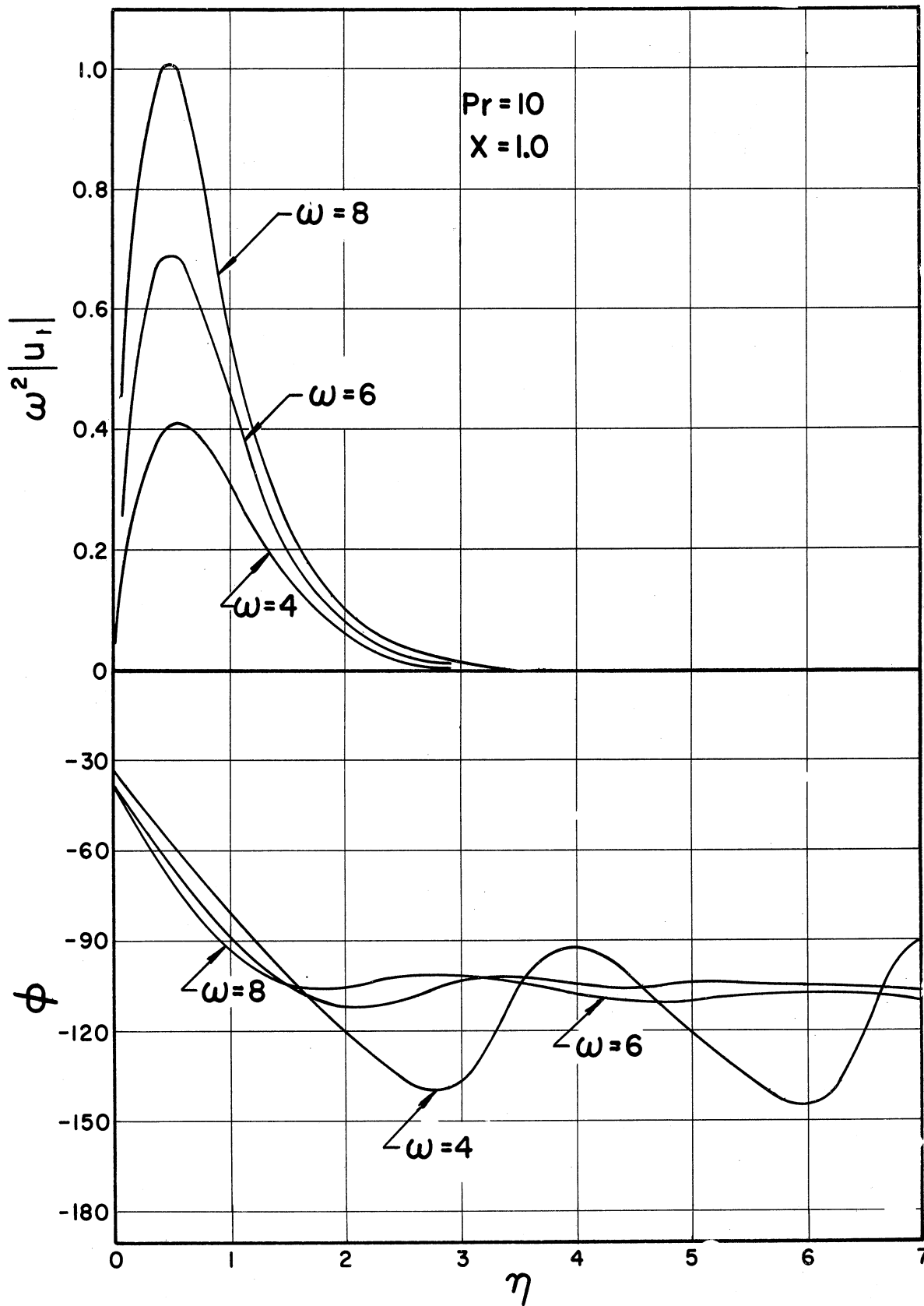
Figure 3-6. Magnitude and Phase of First Order Velocities.

absolute magnitude and phase angle. The absolute magnitude was

multiplied by the ω^2 taken from ϵ in order to show the whole effect

of frequency. The motion of the plate is $\sin\Omega\tau$ and the oscillating

pressure distribution has a timewise variation of $\cos\Omega\tau$. The solu-

tion is represented as

$$\text{Real } U_1 e^{i\omega t} = \text{Real} |U_1| e^{i(\omega t + \phi)} = |U_1| \cos(\omega t + \phi) \qquad (3\text{-}33)$$

so that in this case phase lag refers to the oscillating pressure

gradient.

The phase lag of Pr = 0.72 some distance out in the boundary

layer has a value of 90° for sufficiently large values of ω and X. For

smaller values of X for the same frequency the phase lag is greater and

for the same value of X with increasing frequency the phase lag is

approximately 90°. A similar phenomena is observed for Pr = 10 except

that larger values of frequency and X are required for the phase angle

to approach 90° as an asymptotic value.

It can be seen in Figures 3-2 through 3-6 that the absolute

magnitude of velocity decreases as X increases. This is explained by

considering the fact that the oscillating pressure distribution is de-

pendent upon thermal density variations which are a result of the non-

oscillating free convection boundary layer temperature distribution.

The derivative of the free convection temperature distribution decreases

with increasing X and therefore the oscillating pressure distribution

decreases. Since this serves as a type of forcing function for the

first-order momentum equation the velocity will decrease with increasing

X. With everything else being constant it was found from Figures 3-2

through 3-6 that the magnitude of velocity decreases for increasing

Prandtl number.

To solve the energy equation of Equations (3-20) use was made

of the simple curve of the derivative of the free convection temperature

distribution which is given in Figure 2-16 of Chapter II. Rather than

fitting a curve to the free convection temperature and then having to

differentiate it which has a large possibility of error, a curve was

fit to the derivative of free convection temperature, $H'(\eta)$. This is

very convenient because

$$\frac{\partial T_0}{\partial X} = -\frac{\eta}{(4X)} H'(\eta)$$

$$\frac{\partial T_0}{\partial Y} = \frac{1}{(4X)^{1/4}} H'(\eta)$$

(3-34)

which requires only one fitted curve for both derivatives. By the use of

this fitted curve it was possible to get a solution for all values of η

whereas in reference (α-33) the solution for temperature was valid for

small values and large values of η only. Then with these two regions an

intermediate region of η was approximated. The present solution applies

to all values of η. By performing the necessary operations on the energy

Equation (3-26B) the following solution was found to be

$$T_1 = V_3 e^{-\sqrt{18'}\eta} + (V_4 + V_5\eta)e^{-K_2\eta} + (V_6 + V_7\eta +$$

$$V_8\eta^2)e^{-(K_1+\sqrt{18'})\eta} + (V_9 + V_{10}\eta + V_{11}\eta +$$

$$V_{12}\eta^3)e^{-2K_1\eta}$$

(3-35)

The V's in this equation are complex quantities due to the exponential time factor and consist of real and imaginary parts. The boundary conditions are zero at $\eta = 0$ and $\eta = \infty$ so that $V_3 = V_4 - V_6 - V_9$. This solution is evaluated numerically in the computer program which is discussed in Appendix I.

Figures 3-7 through 3-11 show representative values of the first-order temperature distribution. Figure 3-7 shows the relationship of the temperature distribution for two different Prandtl numbers, Figures 3-7 through 3-11 show the relationship of the first-order temperature distribution for different X, ω and Prandtl number.

The first-order temperature perturbations show that for higher Prandtl numbers, with everything else constant, there is less temperature response to the same oscillation. This is due to the fact that both viscosity and thermal diffusivity are having an effect. A more viscous fluid cannot respond with the same velocities as that of a less viscous fluid and therefore the temperature field is less. The thermal diffusivity being lower in higher Prandtl numbers may also keep the temperature response low. The smaller response of first-order temperature for higher Prandtl numbers actually originates in the non-oscillating temperature field which causes the thermal density variations thereby producing with the oscillations an oscillating pressure distribution, which decreases for increasing Prandtl numbers. The quantity $\omega^2 |T_1|$ increases with frequency for the values of frequency given in Figures 3-7 through 3-11. The quantity $\omega^2 |T_1|$ for larger values of frequency approaches an asymptotic constant value. The ratio of peak values of temperature to velocity
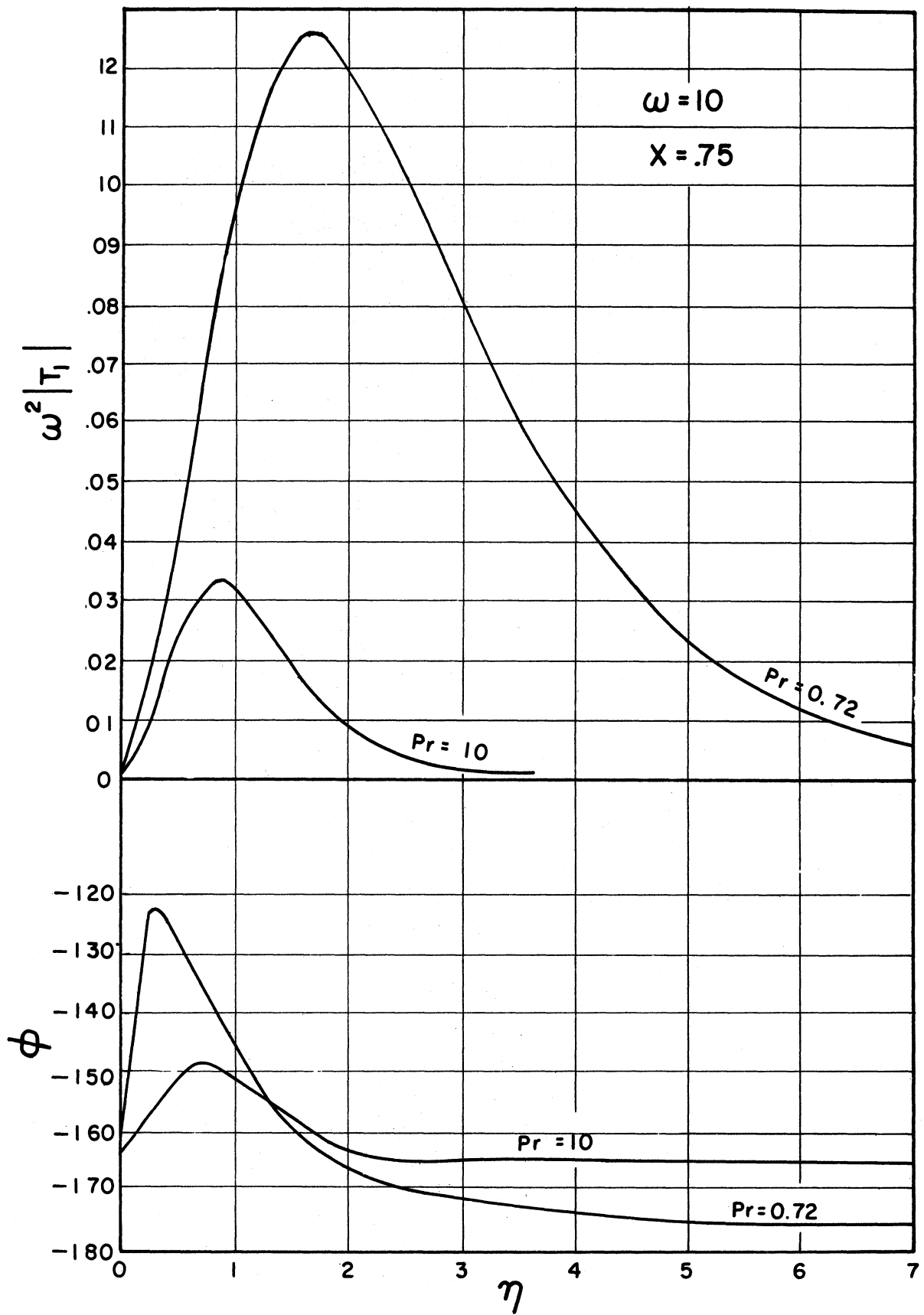
Figure 3-7. Magnitude and Phase of First Order Temperatures.
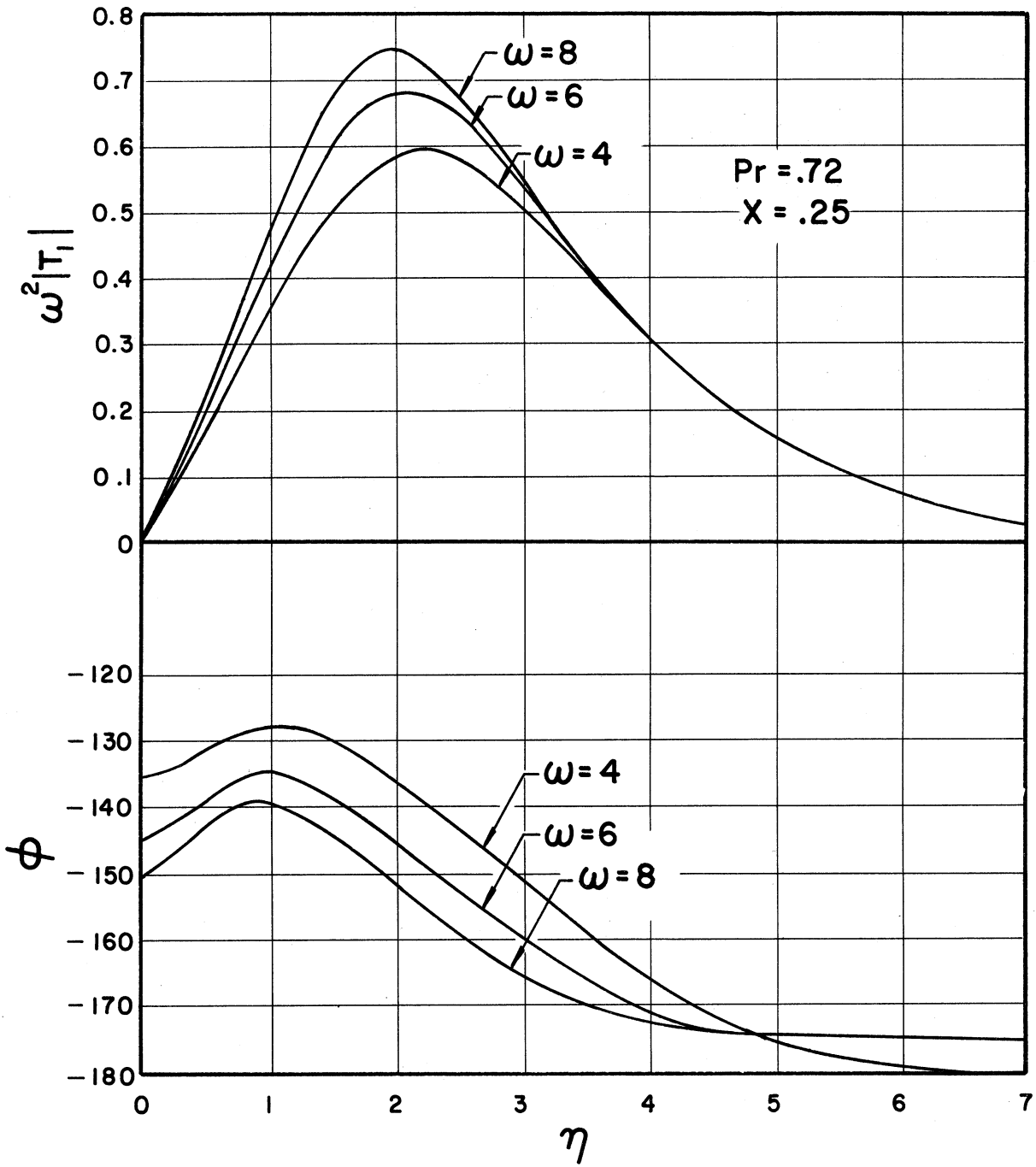
Figure 3-8. Magnitude and Phase of First Order Temperatures.
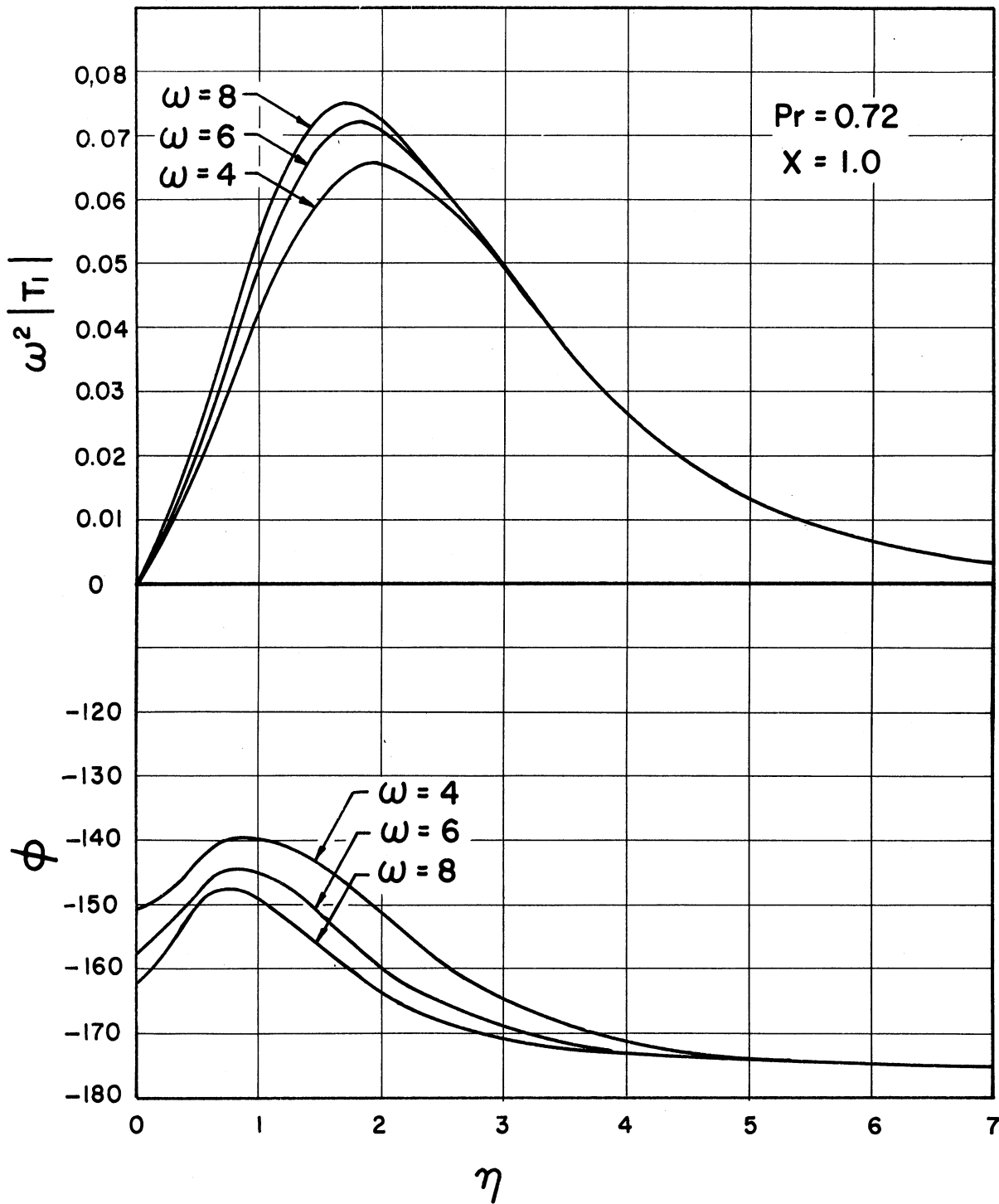
Figure 3-9. Magnitude and Phase of First Order Temperatures.
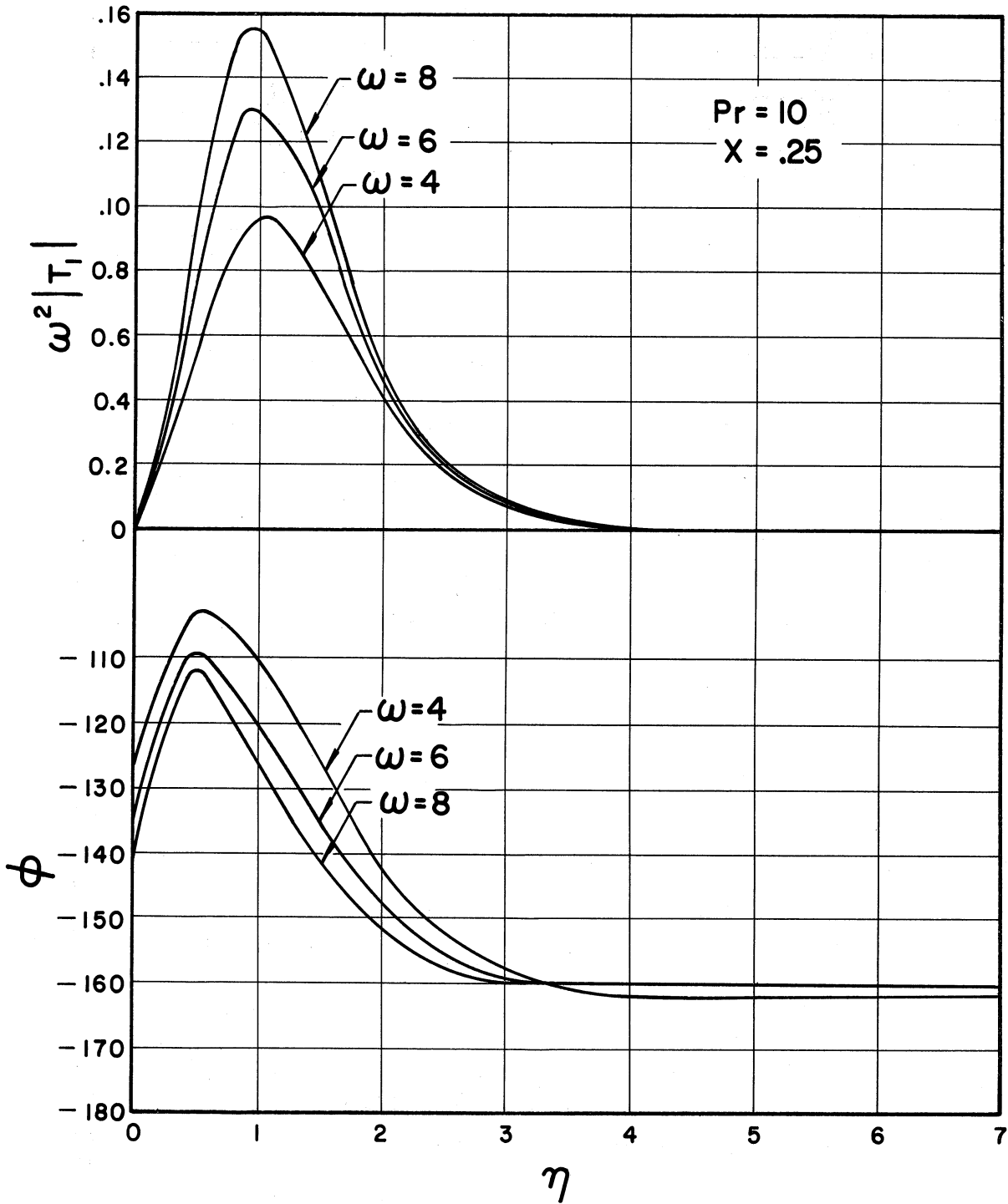
Figure 3-10. Magnitude and Phase of First Order Temperatures.
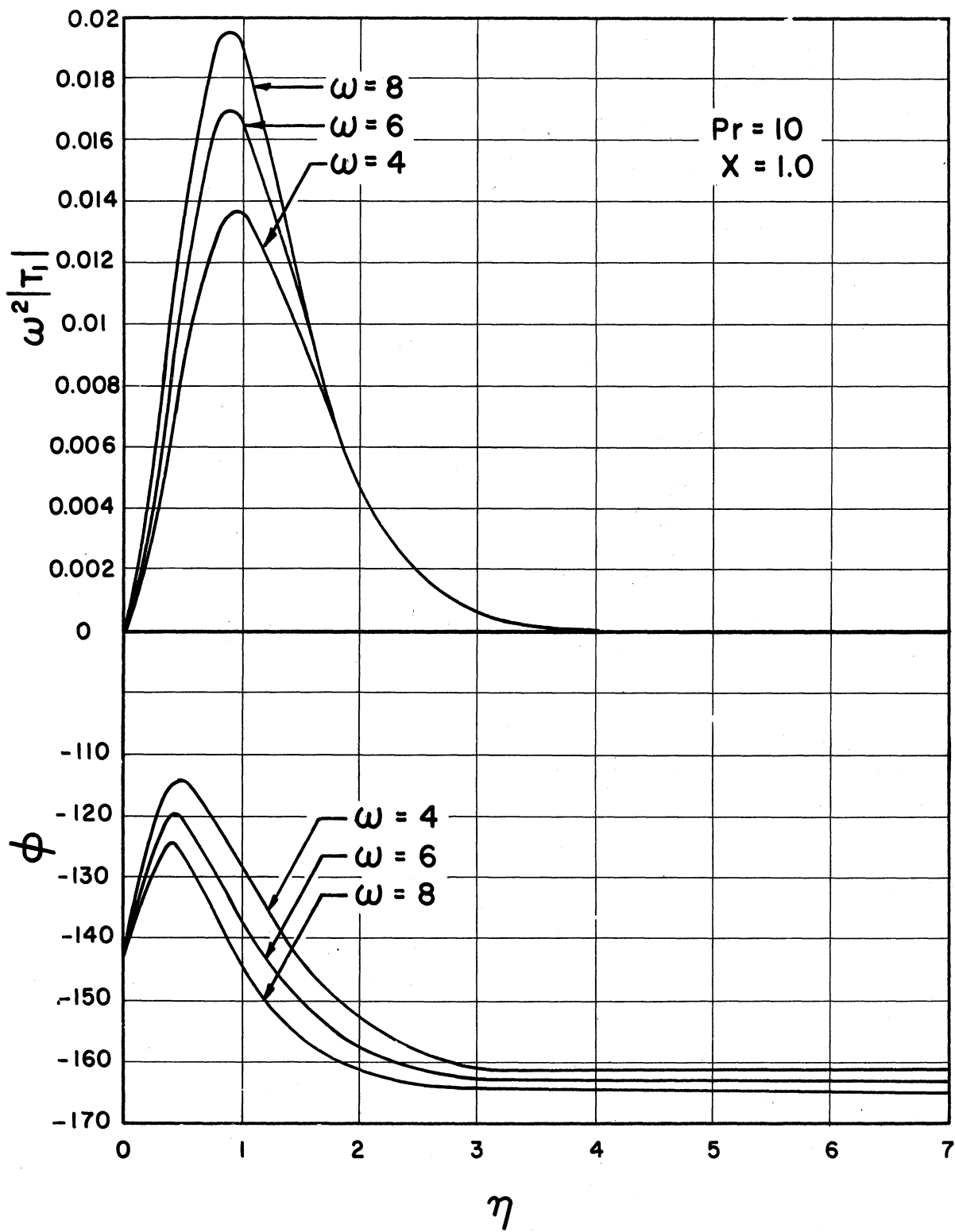
Figure 3-11. Magnitude and Phase of First Order Temperatures.

magnitudes for Pr = 0.72; ω = 8 and X = .25 is less than 10 per cent, for X = 1.0 the ratio is less than 3 per cent. The ratio of peak values of temperature to velocity magnitudes for Pr = 10, ω = 8 and X = 1.0 is less than 3 per cent. For X = 1.0 the ratio is less than 2 per cent. This proves the original assumption that at high frequencies the momentum equation and the energy equation would not be coupled. First-order temperature decreases with increasing X due originally to the fact that the oscillating pressure distribution decreases.

Phase angles for the first-order temperature solutions at $\eta \to 0$ are around -150° to -180°. As η increases the phase angles increase for a while, peak and then decrease again. As ω and X are both increased the values of ϕ at η = 0 and large η both asymptotically approach -180°. The peaking of the phase angles is higher for larger Prandtl numbers.

Second-Order Solutions

Utilizing the exponential time factor with double harmonics and the theory of differential equations with large parameters, the second-order momentum Equation (3-15A) reduces to

$$\left[i2\omega U_2 + U_1 \frac{\partial U_1}{\partial X} + V_1 \frac{\partial U_1}{\partial Y} - \frac{\partial^2 U_2}{\partial Y^2} \right] e^{i2\omega t} =$$

$$= \frac{\partial}{\partial X} \int_Y^\infty T_1 \, dy \, e^{i\omega t} \cos \omega t. \tag{3.36}$$

It is useful to repeat that only the real part of the solutions considered here have significance. Therefore it is necessary to note that

$$REAL\left[\frac{\partial T_i}{\partial X}e^{iwt}\right]\cos wt = \frac{REAL}{2}\left[\frac{\partial T_i}{\partial X}+\frac{\partial T_i}{\partial X}e^{2iwt}\right]$$

$$REAL\left[U_ie^{iwt}\right]REAL\left[\frac{\partial U_i}{\partial X}e^{iwt}\right]=\frac{1}{4}\left[U_i\frac{\partial \overline{U_i}}{\partial X}+\right.$$

$$\left.\overline{U_i}\frac{\partial U_i}{\partial X}\right]+\frac{REAL}{2}\left[U_i\frac{\partial U_i}{\partial X}e^{2iwt}\right]=$$

$$=\frac{REAL}{2}\left[\overline{U_i}\frac{\partial U_i}{\partial X}+U_i\frac{\partial U_i}{\partial X}e^{2iwt}\right],$$

(3-37)

where the bar denotes the complex conjugate. This is true also for all first-order products. Realizing this, the second-order momentum equation is separable into two equations, a time-dependent equation and a time-independent equation. The time-independent solution of the momentum equation is what has been called the secondary-flow velocity or "streaming" velocity. This has its origin in the convective terms and is due to the interaction between the effects of inertia and viscosity. Therefore it is plausible to write

$$U_2 = U_2 + U_{2S}$$

(3.38)

$$T_2 = T_2 + T_{2S}$$

The following time-dependent and time-independent equations result from

Equation (3-15A) with the change of variable from y to η

$$\frac{\partial^2 U_2}{\partial \eta^2} - i\, 2\omega \sqrt{4X'}\, U_2 = \frac{\sqrt{4X'}}{2} REAL \left[U_1 \frac{\partial U_1}{\partial X} + V_1 \frac{\partial U_1}{\partial y} - \int_y^\infty \frac{\partial T_1}{\partial X} dy \right]$$

$$\frac{\partial^2 U_{2S}}{\partial \eta^2} = \frac{\sqrt{4X'}}{2} REAL \left[\overline{U_1} \frac{\partial U_1}{\partial X} + \overline{V_1} \frac{\partial U_1}{\partial y} - \int_y^\infty \frac{\partial T_1}{\partial X} dy \right] \text{.}$$

(3.39)

The convective terms which were omitted from Equation (3-15A) are those

containing u_2 and u_{2s}. A solution was found only for u_{2s} because of its

time-independent nature and therefore the alteration of the steady

velocity of free convection. For this to be true u_{2s} should decrease

in accordance with ω^{-2} for increasing frequency. This was found to be

the case. This solution will consider large X and large frequency.

The boundary conditions, zero at the wall and at infinity,

for the second harmonic perturbation can be satisfied at the wall and

at infinity. The steady-state contribution can be satisfied at the

wall, and at large distances the value can be made finite but not zero.

This is the manner of Schlichting (A-32) who was the first to give this

type of flow an analytical treatment and also observed this flow experi-

mentally. The steady-state Equation (3-39) was solved completely. The

solution is in the form

$$U_{2S} = REAL \left[V_{13} + V_{14}\, e^{-\sqrt{i\gamma'}\,\eta} + V_{15}\, e^{-\sqrt{2\gamma'}\,\eta} + \right.$$

$$V_{16}\, e^{-\sqrt{i\gamma P_R'}\,\eta} + \left(V_{17} + V_{18}\, \eta + V_{19}\, \eta^2 \right) e^{-(K_1 + \sqrt{i\gamma'})\,\eta} +$$

$$\left(V_{20} + V_{21}\, \eta + V_{22}\, \eta^2 + V_{23}\, \eta^2 \right) e^{-(K_1 + \sqrt{i\gamma'})\,\eta} + \left(V_{24} + V_{25}\, \eta \right.$$

$$\left. + V_{26}\, \eta^2 \right) e^{-K_1 \eta} + \left(V_{27} + V_{28}\, \eta + V_{29}\, \eta^2 + V_{30}\, \eta^3 \right.$$

(3-40)

$$\left. + V_{31}\, \eta^4 \right) e^{-2K_1 \eta} \text{,}$$

where the V_n quantities are complex quantities with real and imaginary parts. Figures 3-12 through 3-14 show how the streaming velocity varies with frequency, position and Prandtl number. Figure 3-12 shows the relationship of $\omega^4 u_{2s}$ for two different Prandtl numbers. Figures 3-13 and 3-14 show how $\omega^4 u_{2s}$ varies for different values of X and frequency for two different Prandtl numbers. $\omega^4 u_{2s}$ was plotted since this represents completely the frequency dependency. The larger the Prandtl numbe the smaller the streaming velocity as Figure 3-12 represents. Large values of X result in small values of velocity.

Performing the same operations on the energy Equation (3-15B) as were done on the momentum equation the following equations result

$$\frac{1}{P_R}\frac{\partial^2 T_2}{\partial Y^2} - i 2 \omega T_2 = \frac{REAL}{2}\left[U_1\frac{\partial T_1}{\partial X} + V_1\frac{\partial T_1}{\partial Y} + \right.$$
$$\left. 2U_{2s}\frac{\partial T_0}{\partial X} + 2V_{2s}\frac{\partial T_0}{\partial Y}\right] \tag{3-41A}$$

$$\frac{1}{P_R}\frac{\partial^2 T_{2s}}{\partial Y^2} = U_{2s}\frac{\partial T_0}{\partial X} + V_{2s}\frac{\partial T_0}{\partial Y} + \frac{REAL}{2}\left[\overline{U_1}\frac{\partial T_1}{\partial X} + \overline{V_1}\frac{\partial T_1}{\partial Y}\right] \tag{3-41B}$$

The terms left out were the terms containing T_{2s} in the convective terms. Since $T_{2s} < v_{2s} < u_{2s}$ the two terms left out will be negligible compared to the first two terms on the right hand side. As in the case of the momentum equation only the steady equation was considered. The steady equation becomes, after the change of variable from Y to η

$$\frac{1}{P_R\sqrt{4X}}\frac{\partial^2 T_{2s}}{\partial \eta^2} = U_{2s}\frac{\partial T_0}{\partial X} + V_{2s}\frac{\partial T_0}{\partial Y} + \frac{REAL}{2}\left[\overline{U_1}\frac{\partial T_1}{\partial X} + \overline{V_1}\frac{\partial T_1}{\partial Y}\right] \tag{3-42}$$
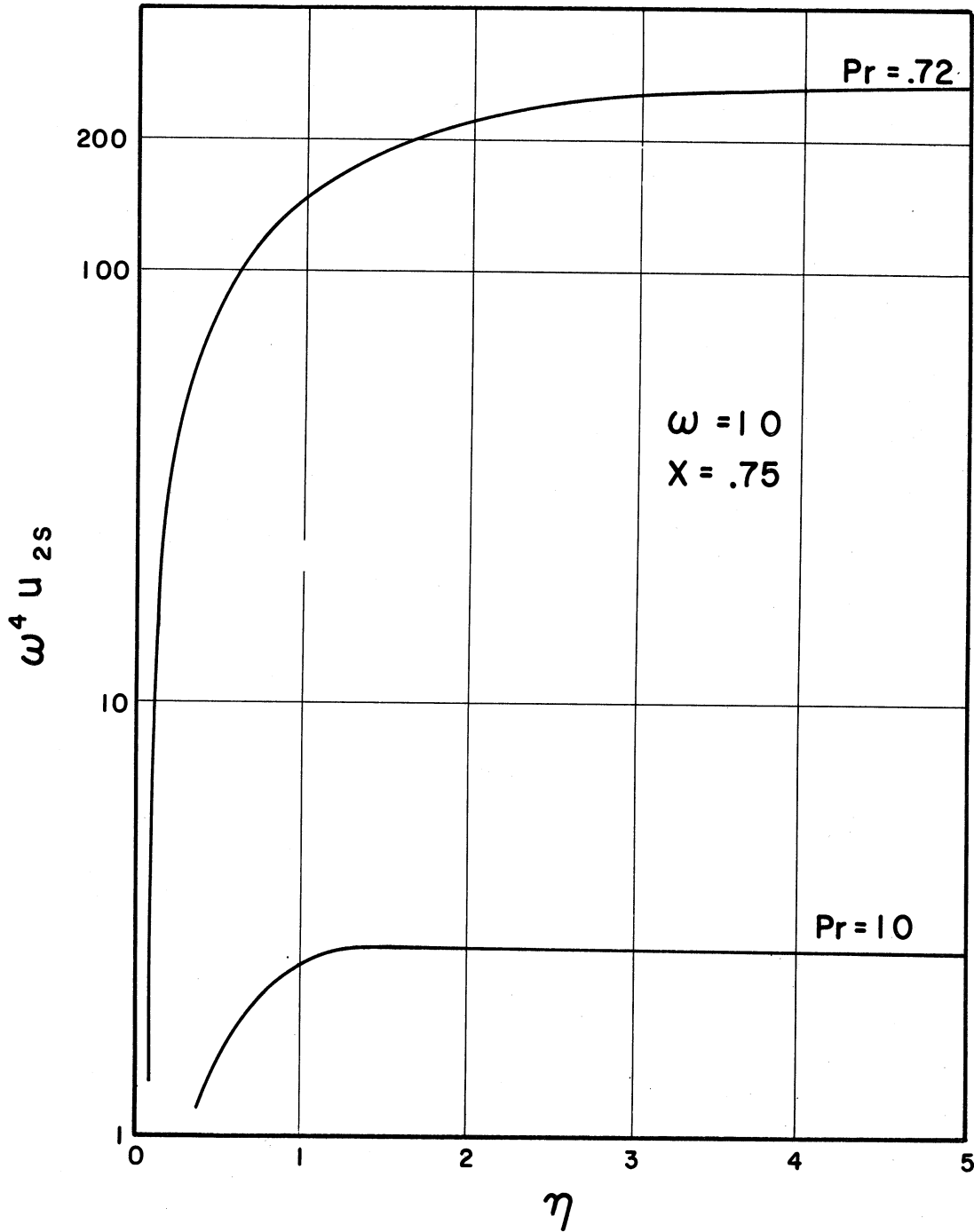
Figure 3-12. Magnitude of Second Order, Time-Independent, Velocities.
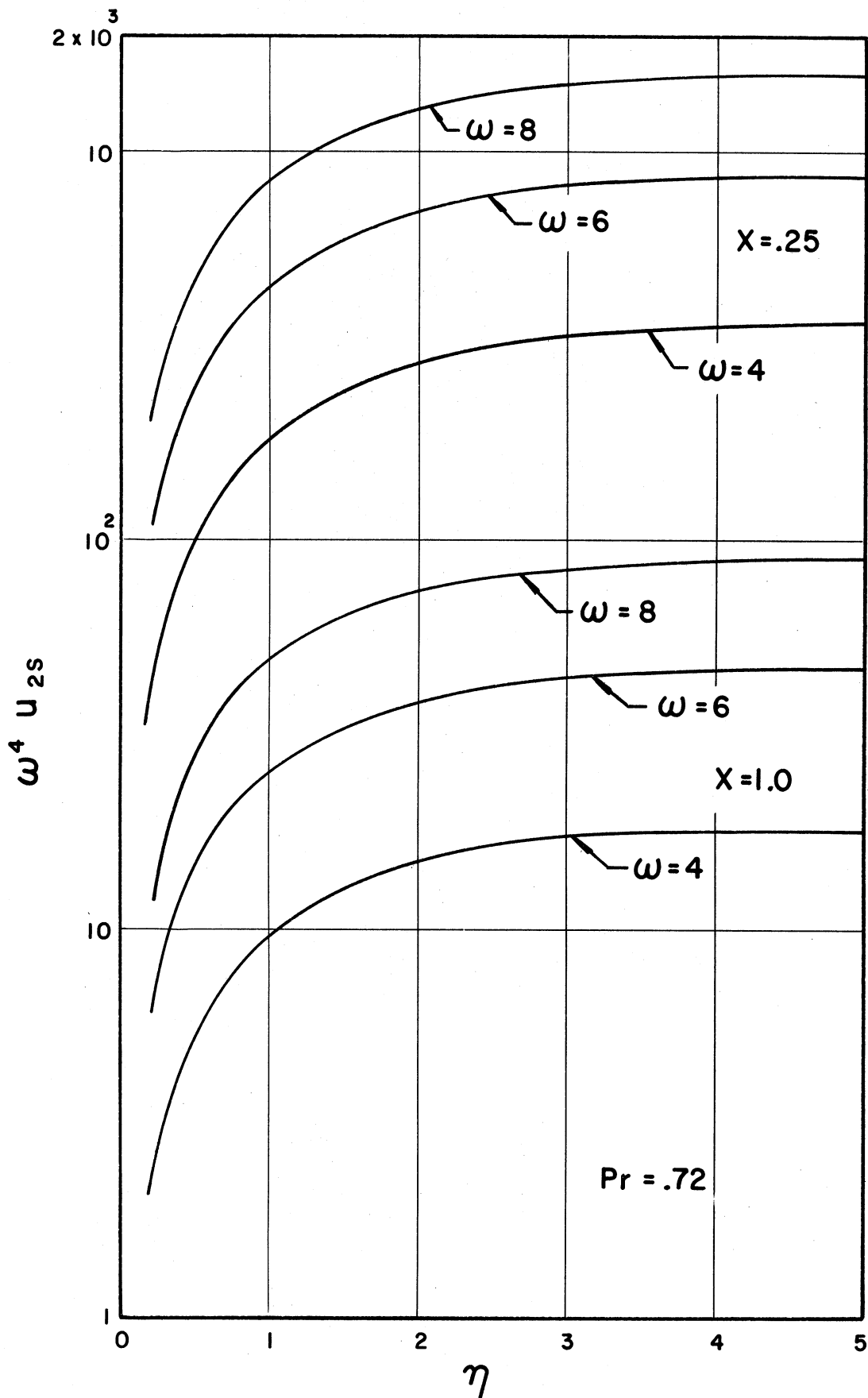
Figure 3-13. Magnitude of Second Order, Time-Independent, Velocities.
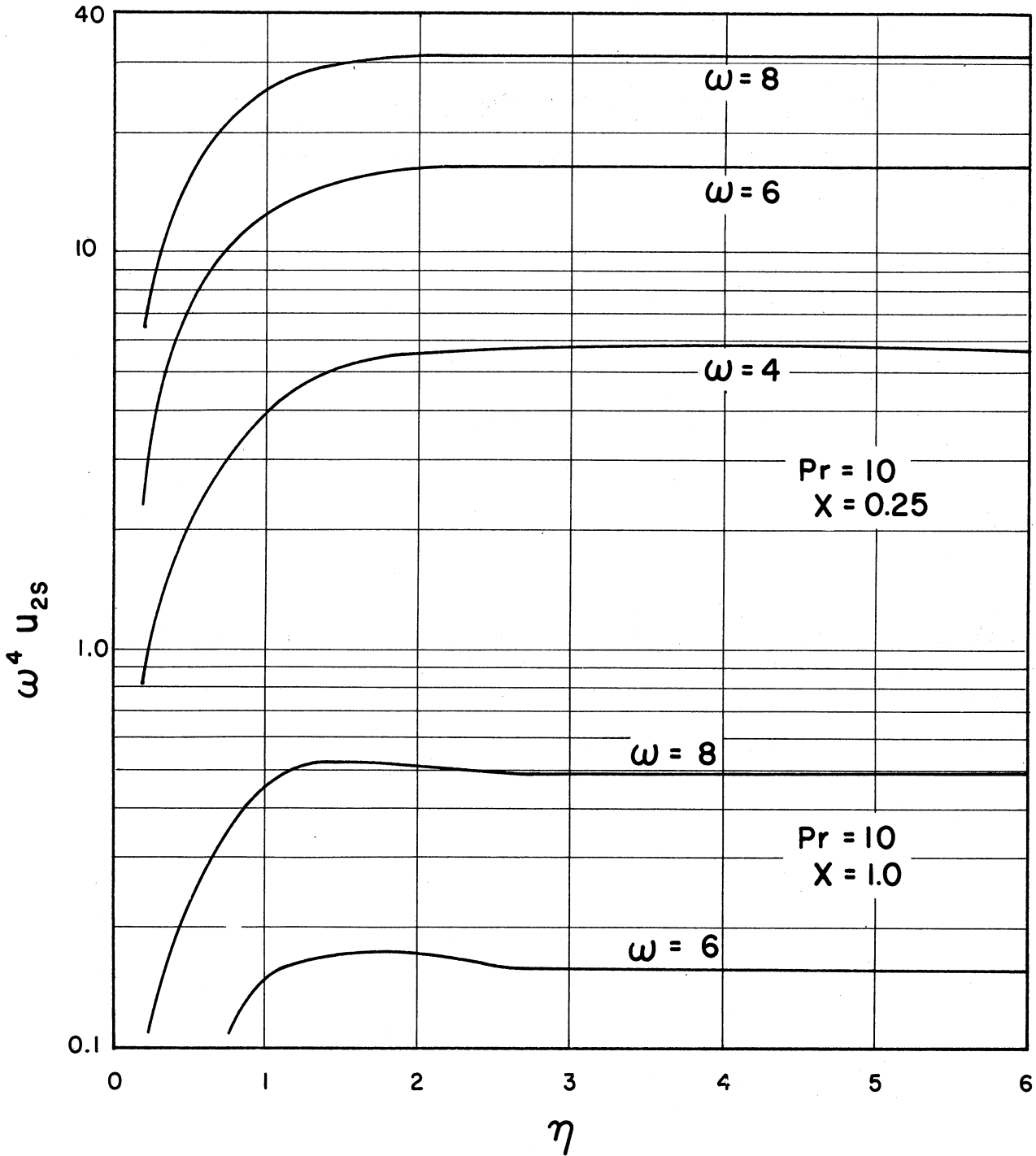
Figure 3-14. Magnitude of Second Order, Time-Independent, Velocities.

This equation was solved to the first derivative at $\eta = 0$. It was not carried further due to the excessive amount of computation that would be necessary.

Effect of Oscillation on Heat Transfer and Shear Stress

For free convection alone the shear stress by definition is

$$\tau_S = \mu_\infty \left(\frac{\partial U}{\partial Y} \right)_0 \tag{3-43}$$

By utilizing the dimensionless parameters and the tabulated results in Ostrach (C-8) this relationship of shear stress is

$$\frac{\tau_S}{\left(4 G_{rx}^3\right)^{1/4} \left(\frac{\nu_\infty \mu_\infty}{X^2} \right)} = F''(0). \tag{3-44}$$

With oscillations and the perturbation type of solution the local shear stress (time-dependent) derived by taking the derivative of Equation (3-9A) and making the terms dimensional is

$$\frac{\tau_i}{(F''(0))\left(4 G_{rx}^3\right)^{1/4}\left(\frac{\nu_\infty \mu_\infty}{X^2} \right)} = 1 + \epsilon \frac{\left(\frac{\partial |u_1|}{\partial Y} \right)_0}{F''(0)(4X)^{1/2}} \cos(\omega t + \phi) \tag{3-45}$$

$$+ \epsilon^2 \left[\frac{\left(\frac{\partial u_{2s}}{\partial Y} \right)_0}{(4X)^{1/2} F''(0)} + \frac{\left(\frac{\partial |u_2|}{\partial Y} \right)_0}{(4X)^{1/2} F''(0)} \cos(2\omega t + \phi) \right] + \cdots$$

The time-averaged local shear stress from Equation (3-45) is

$$\frac{\tau}{F''(0)\left(4G_{RX}^3\right)^{\frac{1}{4}}\left(\frac{V_\infty \mu_\infty}{X^2}\right)} = 1 + \epsilon^2 \frac{\left(\frac{\partial U_{2S}}{\partial Y}\right)_0}{(4X)^{\frac{1}{2}} F''(0)} + \cdots \qquad (3\text{-}46)$$

The values of $\left(\frac{\partial |U_1|}{\partial Y}\right)_0 \omega^2$ and ϕ are shown in Figures 3-15 and 3-16 for

different values of frequency, position, and Prandtl number.

The plots of $\left(\frac{\partial |U_1|}{\partial Y}\right)_0 \omega^2$ in Figures 3-15 and 3-16 show that

the local, oscillating shear stress increases with frequency more than

linearly but not as fast as ω^2. The oscillating shear stress will

increase linearly with amplitude if frequency is held constant. If the

oscillating pressure distribution is held constant corresponding to a

particular value of ϵ then the amplitude of the oscillating shear stress

will decrease with increasing frequency. Since ϵ is a function of both

vibration amplitude and frequency, increasing the latter requires a

corresponding decrease in the former in order to maintain constant ϵ.

The local oscillating shear stress is largest near the leading edge.

The analysis is still valid in regions close to the leading edge. The

smaller the Prandtl number the greater the magnitude of the oscillating

(time-dependent) shear stress. The phase lag for increasing frequency

for both Prandtl numbers approaches 45°. The phase lag is greater for

smaller Prandtl numbers.

The time-independent contributions to the shear stress to be

used in Equations (3-45) and (3-46) are shown in Figures 3-17 and 3-18.

The values given in these figures are found by the computer evaluation

method described in Appendix I.
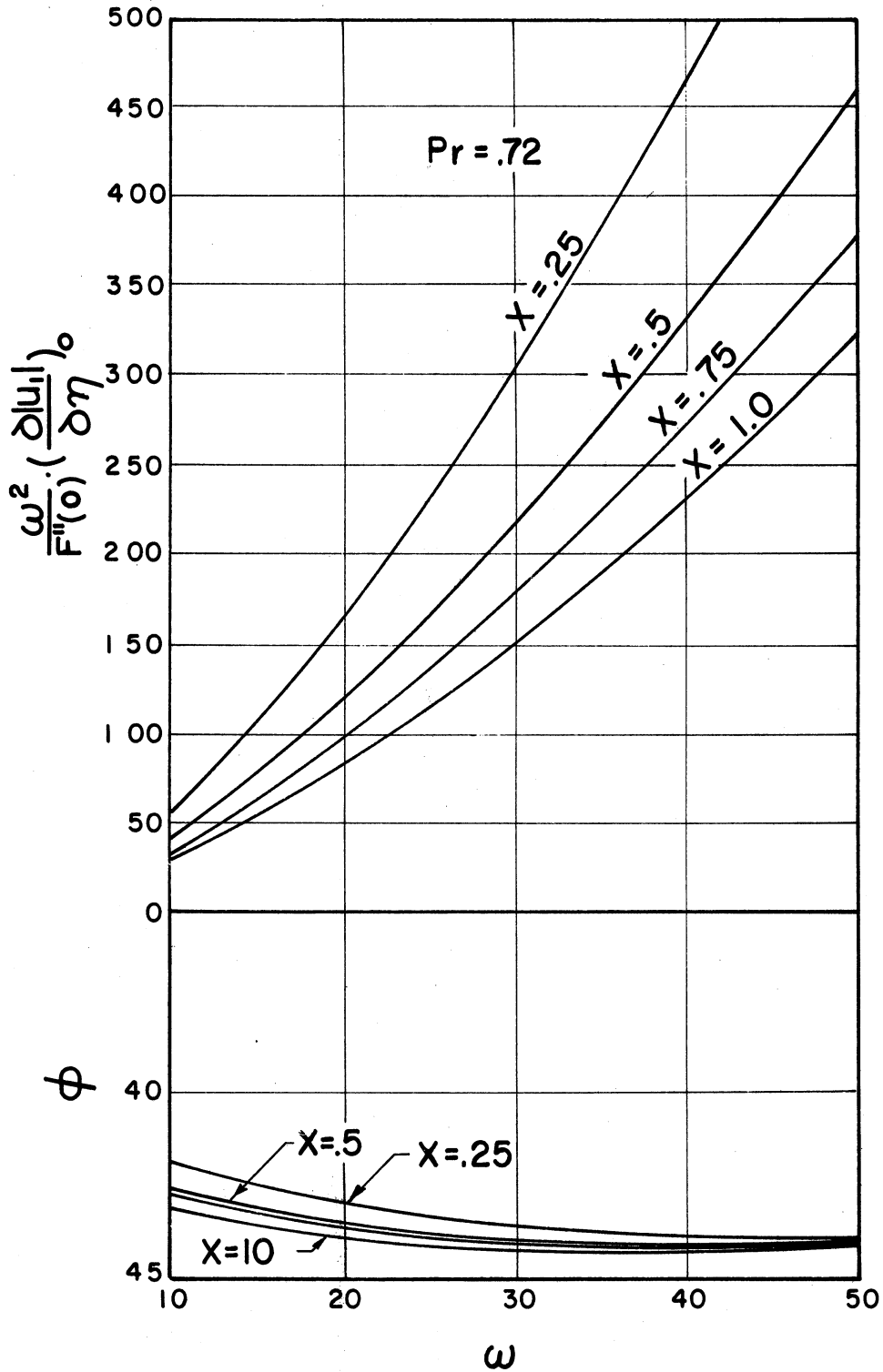
Figure 3-15. Magnitude and Phase of First Order Velocity
Derivatives Divided by the Zeroth Derivative
of Velocity.
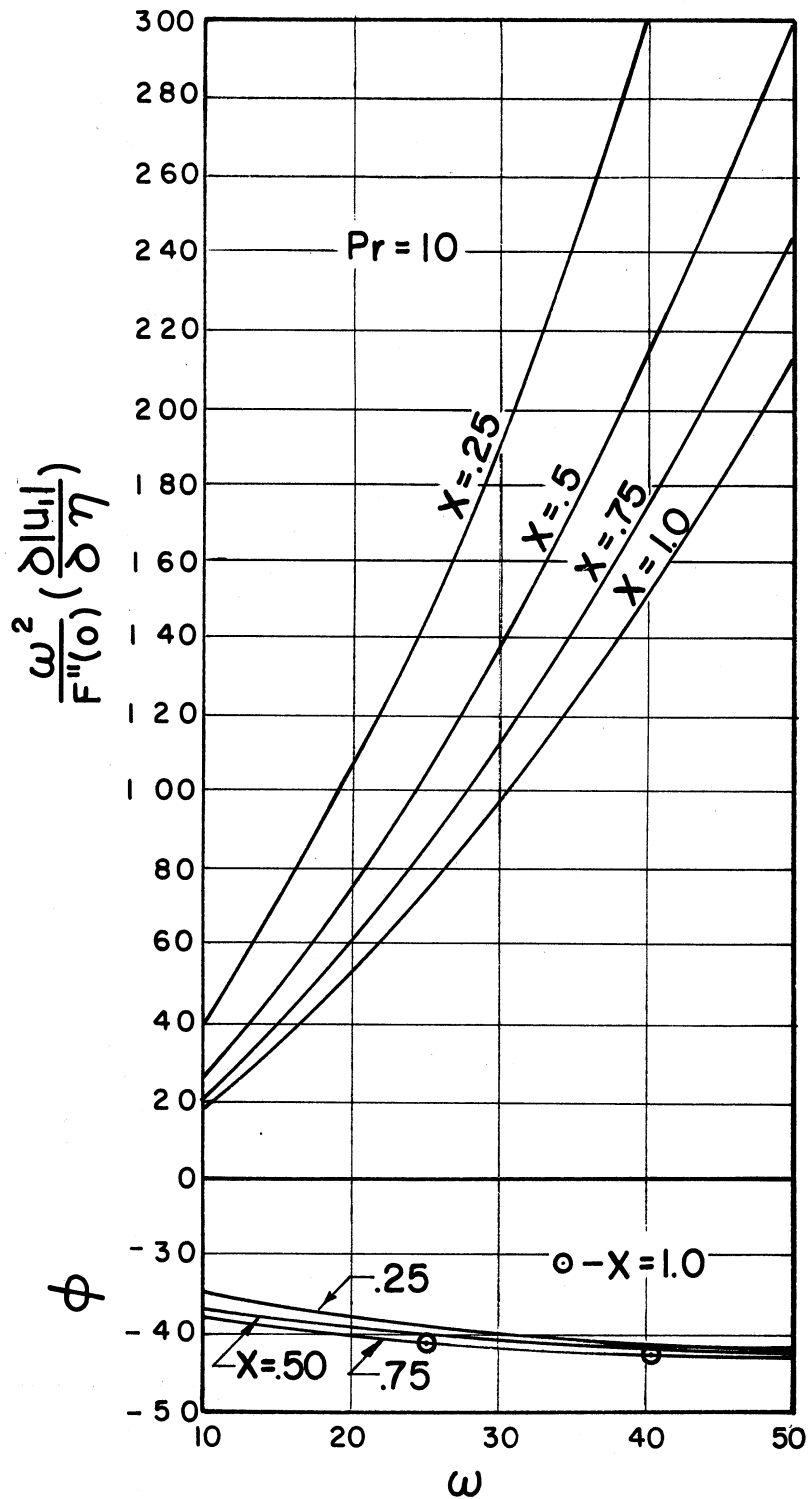
Figure 3-16. Magnitude and Phase of First Order Velocity Derivatives Divided by the Zeroth Derivative of Velocity.
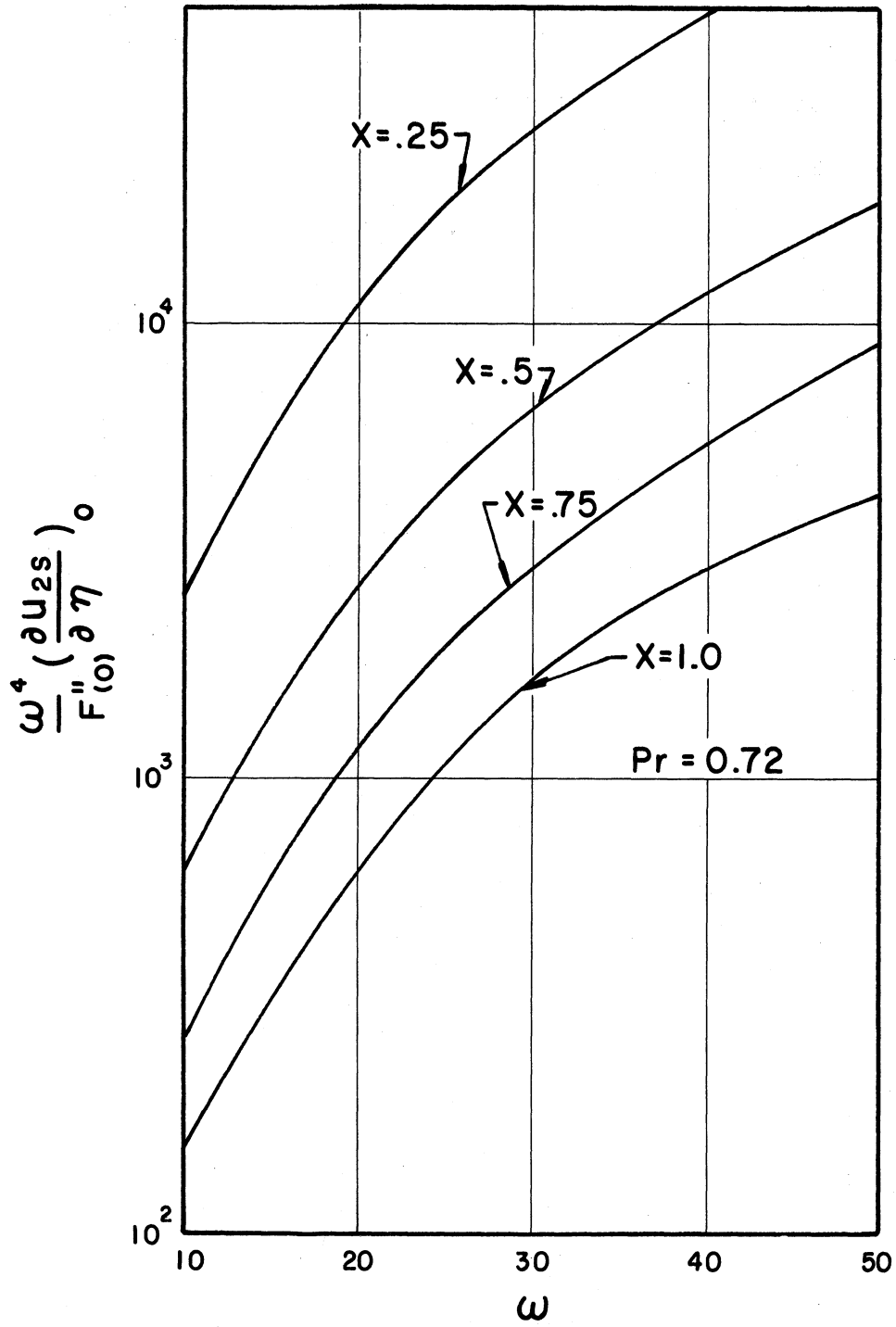
Figure 3-17. Magnitude of the Second Order, Time-Independent,
Velocity Derivatives Divided by the Zeroth
Derivative of Velocity.
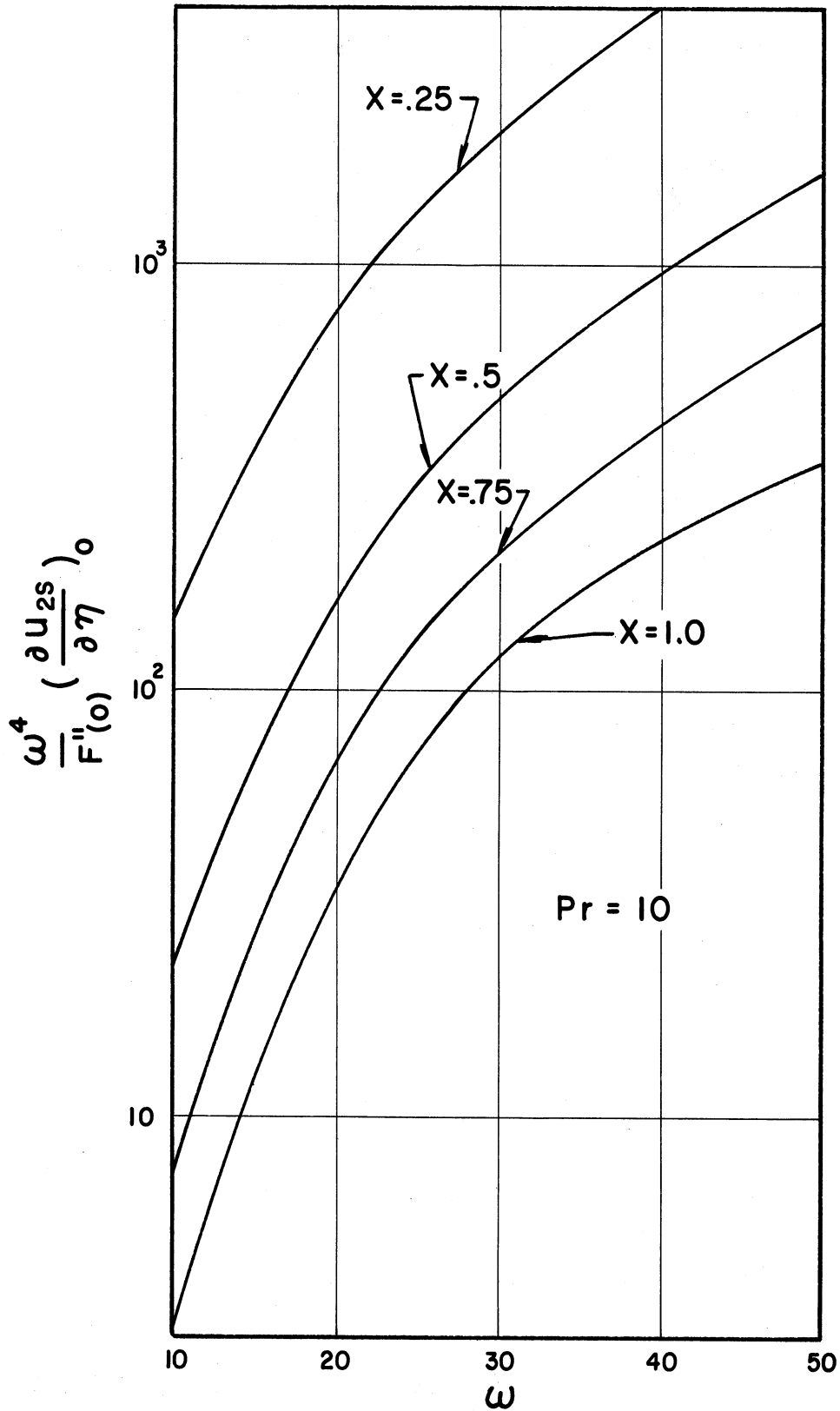
Figure 3-18. Magnitude of the Second Order, Time-Independent, Velocity Derivatives Divided by the Zeroth Derivative of Velocity.

The values of $\left(\dfrac{\partial U_{2s}}{\partial \eta}\right)_0 \omega^4$ in Figures 3-17 and 3-18 show that the local time-independent contribution to the shear stress increases with increasing frequency. The multiplicative factor ω^4 comes from ϵ^2. The derivative $\left(\dfrac{\partial U_{2s}}{\partial \eta}\right)_0$ decreases approximately the same as ω^{-2}. As the Prandtl number decreases $\left(\dfrac{\partial U_{2s}}{\partial \eta}\right)_0$ increases. The local steady shear stress also is greater the closer one is to the leading edge. Consideration of the fact that ϵ contains amplitude asserts that the local steady contribution increases with the square of the amplitude. It should be kept in mind that the ω^4 was included in the plot to show the effect of frequency and comes from ϵ^2 which is restricted to small values.

For free convection alone the local Nusselt number is defined as

$$N_u = \frac{hX}{K} = \frac{-X}{(\theta_0 - \theta_\infty)}\left(\frac{\partial T_0}{\partial X}\right)_0 \tag{3-47}$$

By utilizing the dimensionless parameters and the tabulated results in Ostrach (C-8) the relationship is

$$\frac{N_u}{(G_{RX}/4)^{1/4}} = -H'(0) \tag{3-48}$$

The solution for the temperature distribution is

$$T = T_0 + \epsilon T_1 + \epsilon^2 T_2 + \cdots$$
$$= H + \epsilon T_1 + \epsilon^2 T_2 + \cdots \tag{3-49}$$

where H is the zeroth order solution due to Ostrach (C-8), T_1 is the solution to Equation (3-26B) and T_2 is the solutions to Equations (3-41).

Therefore with oscillations and the perturbation-type of solution

the local Nusselt number, time-dependent and time-independent, is

$$\frac{Nu}{(-H'(0))(G_{RX}/4)^{1/4}} = 1 + \epsilon \frac{\left(\frac{\partial /T_1/}{\partial \eta}\right)_0}{(-H'(0))} \cos(\omega t + \phi) +$$

$$\epsilon^2 \left[\frac{\left(\frac{\partial T_{2s}}{\partial \eta}\right)_0}{(-H'(0))} + \frac{\left(\frac{\partial /T_2/}{\partial \eta}\right)_0}{(-H'(0))} \cos(2\omega t + \phi) \right] + \cdots$$

(3-50)

The time-independent local Nusselt number is

$$\frac{Nu}{(-H'(0))(G_{RX}/4)^{1/4}} = 1 + \epsilon^2 \frac{\left(\frac{\partial T_{2s}}{\partial \eta}\right)_0}{(-H'(0))} + \cdots$$

(3-51)

The plots of the derivative of T_1 and its phase angle are

shown in Figures 3-19 and 3-20 for two different Prandtl numbers. It

is seen that the magnitude of the oscillating Nusselt number multiplied

by ω^2, taken from ϵ, increases with increasing frequency for small values

of X and remains essentially constant for larger values of X. This holds

true for both Prandtl numbers. Without the multiplicative factor of ω^2

then the derivative decreases with increasing frequency. In Figures

3-19 and 3-20 it can be seen that the smaller the Prandtl number or X

the greater is the magnitude of the Nusselt number. The phase lag

approaches 180° asymptotically for larger values of frequency.

The time-independent contributions to the Nusselt number as a

function of X, Prandtl number and frequency are shown in Figures 3-21

and 3-22 for both Prandtl numbers. The steady-state contribution to the

Nusselt number is seen to decrease as compared to the non-oscillating
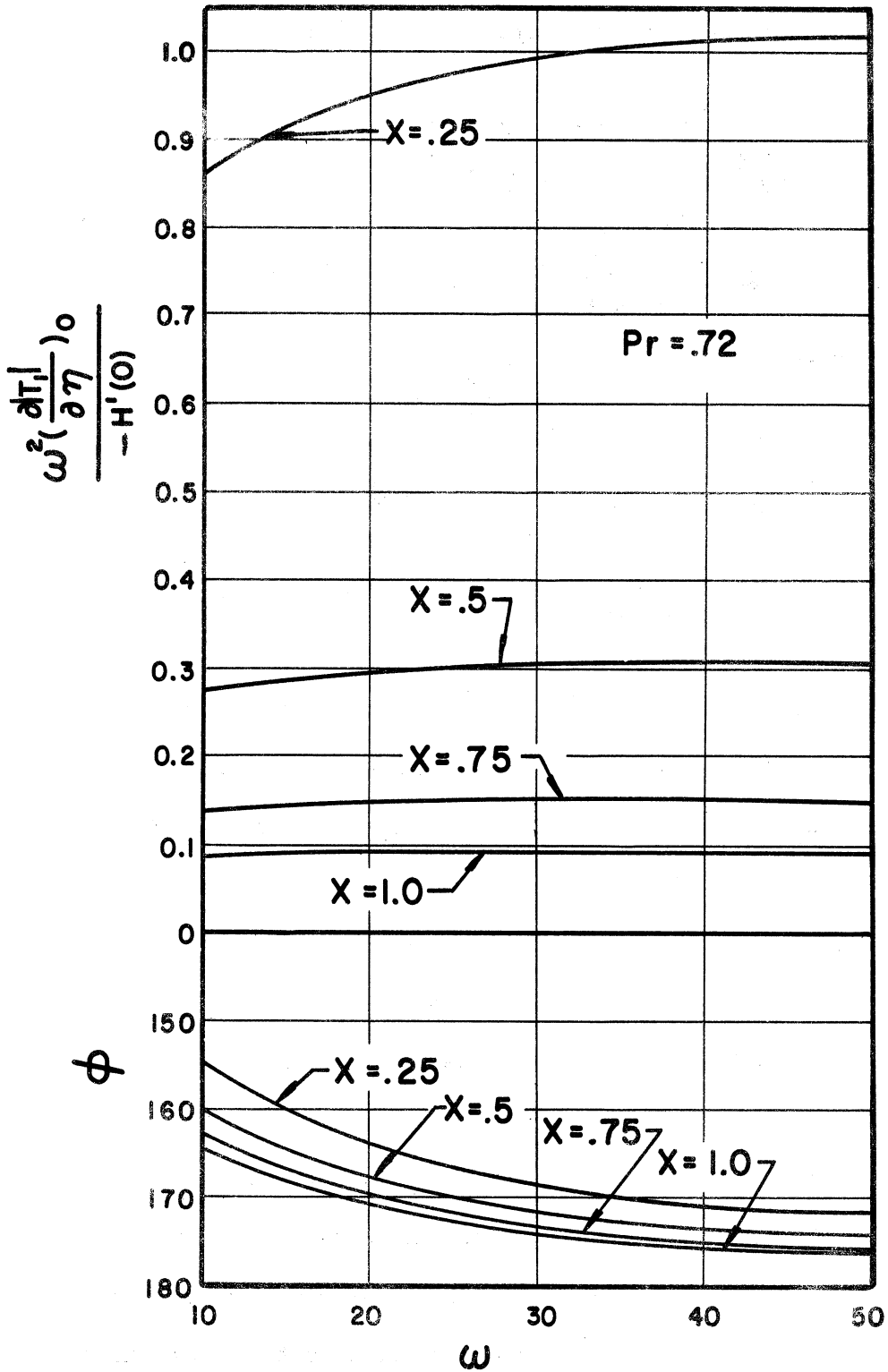
Figure 3-19. Magnitude and Phase of the First Order Temperature
Derivatives Divided by the Zeroth Derivative of
Temperature.
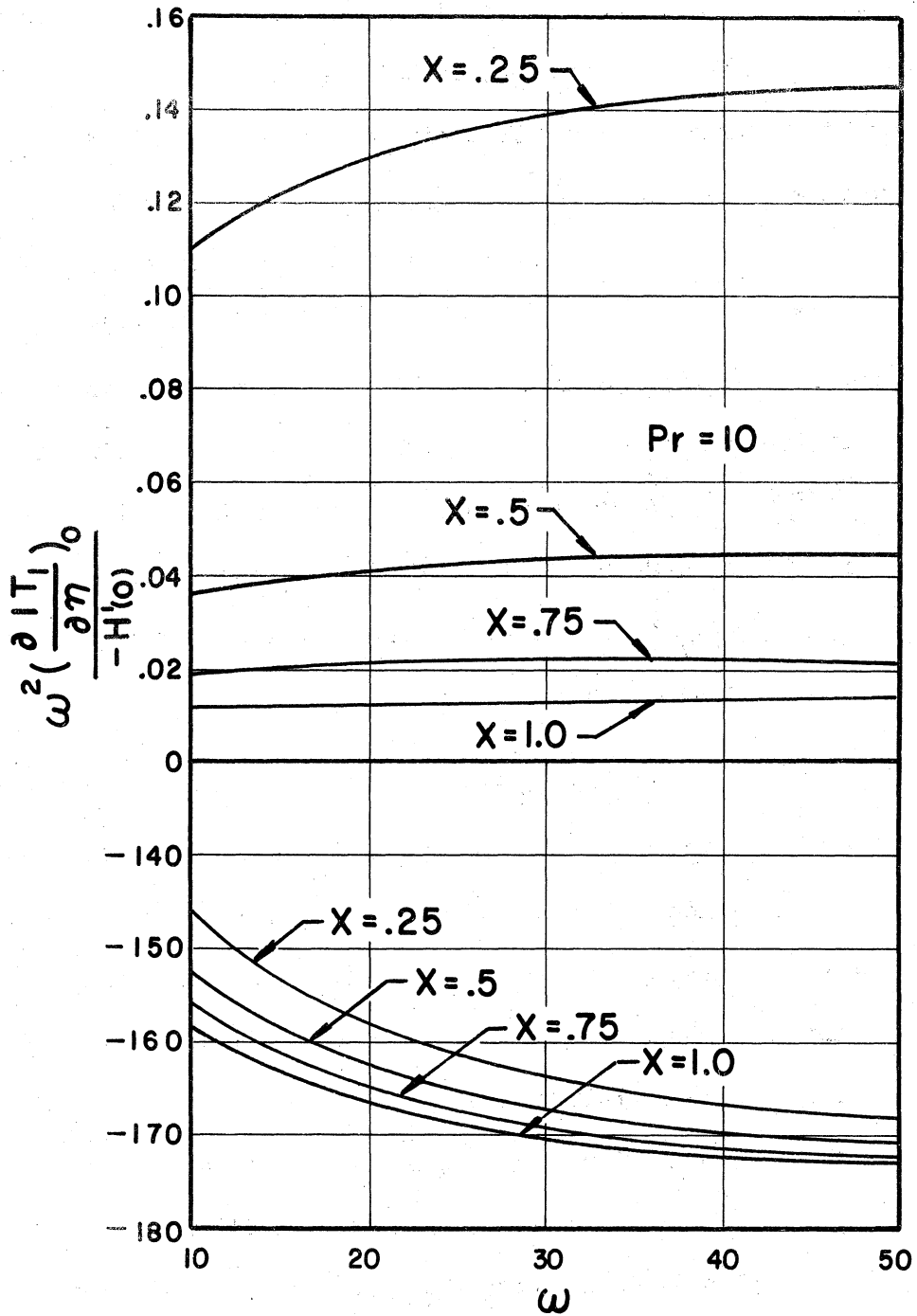
Figure 3-20. Magnitude and Phase of the First Order Temperature
Derivatives Divided by the Zeroth Derivative of
Temperature.

free convection case. From these results it is at once evident that

Reynold's analogy does not hold for oscillating flows with heat transfer.

The physical reason for the decrease, is believed to be a result of the

phase lag of the boundary layer. If conditions were such that the

temperature were oscillating as a primary effect then temperature would

be similar to the streaming velocity which creates an increase in the

shear stress. Then it seems probable an increase in the Nusselt number

would be found. Also the order of magnitude of the decrease in the

Nusselt number is small because of the multiplicative factor ϵ^2. The

fact that $\left(\frac{\partial T_{2s}}{\partial \eta} \right)_0 \Big/ \left(-H'(0) \right)$ decreases less with increasing frequency

can be seen in Figures 3-20 and 3-21. For smaller Prandtl numbers the

magnitude of $\left(\frac{\partial T_{2s}}{\partial \eta} \right)_0 \Big/ \left(-H'(0) \right)$ is greater. This would correspond to

a greater decrease in the Nusselt number.

Discussion of Results

Schoenhals and Clark, (A-33) with a physical system approximat-

ing the mathematical model of this present invention could find no effect

on the time-averaged Nusselt numbers. The analysis of this chapter supports

these experimental findings in that the decrease of the time-independent

Nusselt number is so small that it would seem to be practically impossible

to measure. As an example, for Gr = 10^8, Pr = 0.72, ΔT = 100°F and

(a /L) = 0.01, the percentage decrease in the non-oscillating Nusselt

number for ω = 20, 50 and 100 are less than 0.01, 0.03 and 0.1 percent,

respectively.
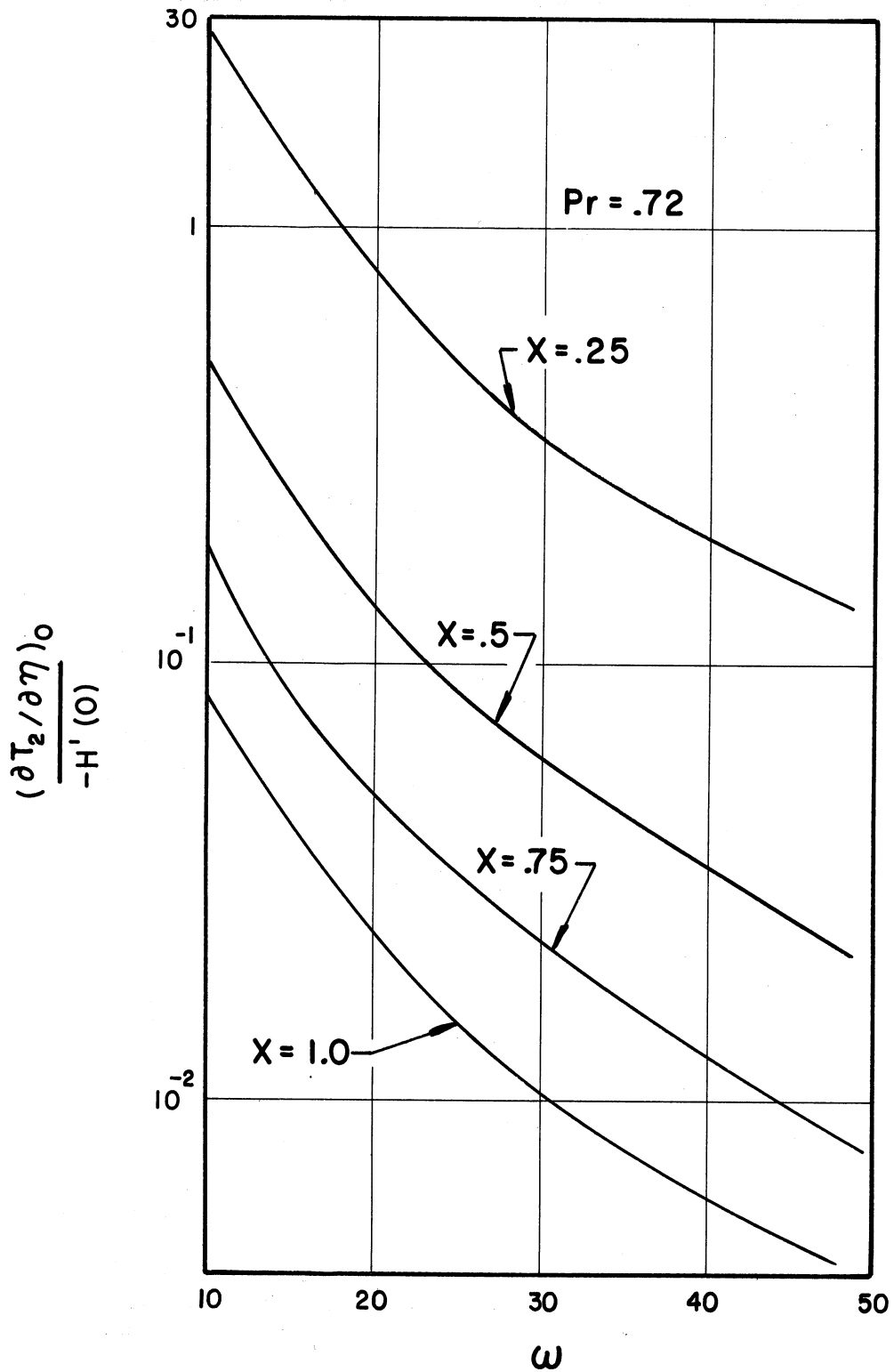
Figure 3-21. Magnitude of the Second Order, Time-Independent, Temperature Divided by the Zeroth Derivative of Temperature.
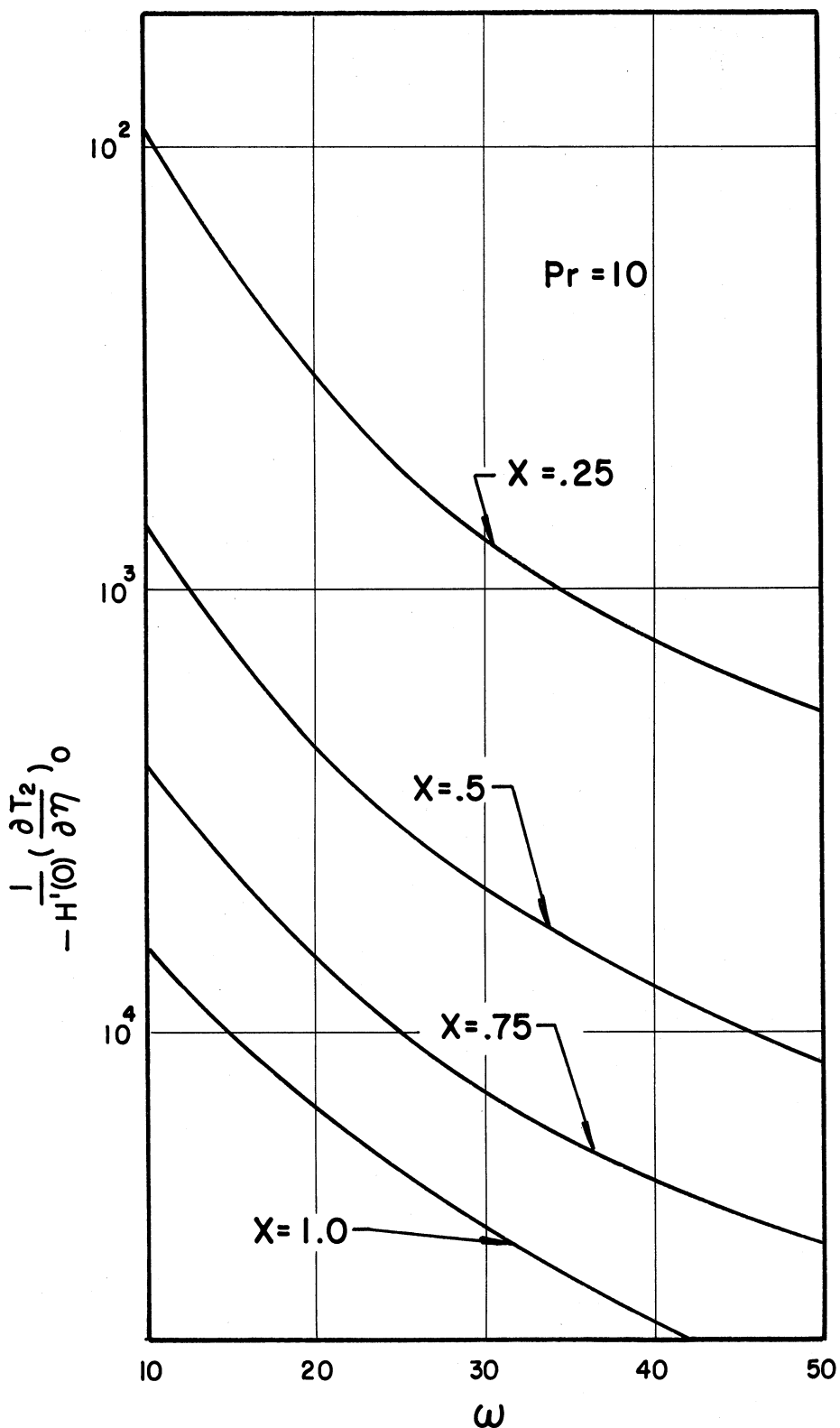
Figure 3-22. Magnitude of the Second Order, Time-Independent, Temperature Divided by the Zeroth Derivative of Temperature.

CHAPTER IV

EXPERIMENTAL WORK

Introduction

This chapter describes additional experimental work on the
subject of vibrational effects in heat transfer and extends research
completed recently by Schoenhals (A-34). The experimental apparatus
constructed by Schoenhals (A-34) was adapted to these particular exper-
iments. His results included data obtained from velocity measurements
made with a hot wire anemometer under adiabatic conditions and some
heat transfer data taken to determine the effect of wall vibration on
the time averaged heat transfer rate.

Air was the fluid used for all experimental work. In the
latter part of this chapter the combined results obtained by Schoenhals
(A-34) and those obtained here will be compared to other experimental
work which have appeared in the literature. These measurements also
will be compared to the theoretical work of the first two chapters.

The results of this chapter involve heat transfer data in the
form of nusselt number as a function of a vibrational Reynolds number
and Grashof-Prandtl number product. The Nusselt number was found to be
essentially uninfluenced by vibration for laminar conditions. A maxi-
mum decrease of 2% was found for smaller value of vibration Reynolds
number. For large values of Reynolds number a sharp increase in the
Nusselt number was obtained experimentally. The experimental results
confirm the theoretical results of an almost negligible decrease in

-143-

time-independent heat transfer. The sharp increase in Nusselt number was concluded to be a result of a flow transition from a laminar to a turbulent flow. Smoke studies were made to investigate this possibility more thoroughly. These clearly showed that this phenomena exists. Some photographs are presented of different flow conditions. A correlation in terms of a vibrational Reynolds number, amplitude ratio and Grashof number was also made.

Experimental Apparatus

The experiment is designed to produce a two dimensional boundary layer on a vertical, finite, flat plate undergoing transverse vibrations.

General views of the test apparatus are shown in Figures 4-1 and 4-2.

The test section is a 10 inch square plate 3/4 of an inch thick with a 6 inch square heated section in the center. During test conditions this heated section is maintained at a constant temperature in a manner which will be described later. The heated section consists of two highly polished aluminum plates on the outside with a heater contained between them. The heater is made up of a heating element which is chromel ribbon 1/8 of an inch wide by 0.002 inches thick wound on a thin mica sheet. A mica sheet was placed on each side of the heating element to protect it from the aluminum plates. These plates are clamped together by four hex nuts at the corners which thread onto four support rods which hold the plate in a vertical position. Construction of the test plate is shown in Figure 4-3. As can be seen in this figure, the

time-independent heat transfer. The sharp increase in Nusselt number
was concluded to be a result of a flow transition from a laminar to a
turbulent flow. Smoke studies were made to investigate this possibility
more thoroughly. These clearly showed that this phenomena exists. Some
photographs are presented of different flow conditions. A correlation
in terms of a vibrational Reynolds number, amplitude ratio and Grashof
number was also made.

Experimental Apparatus

The experiment is designed to produce a two dimensional
boundary layer on a vertical, finite, flat plate undergoing transverse
vibrations.

General views of the test apparatus are shown in Figures 4-1
and 4-2.

The test section is a 10 inch square plate 3/4 of an inch thick
with a 6 inch square heated section in the center. During test conditions
this heated section is maintained at a constant temperature in a manner
which will be described later. The heated section consists of two highly
polished aluminum plates on the outside with a heater contained between
them. The heater is made up of a heating element which is chromel
ribbon 1/8 of an inch wide by 0.002 inches thick wound on a thin mica
sheet. A mica sheet was placed on each side of the heating element to
protect it from the aluminum plates. These plates are clamped together
by four hex nuts at the corners which thread onto four support rods
which hold the plate in a vertical position. Construction of the test
plate is shown in Figure 4-3. As can be seen in this figure, the

Figure 4-1. General View of the Experimental Apparatus.
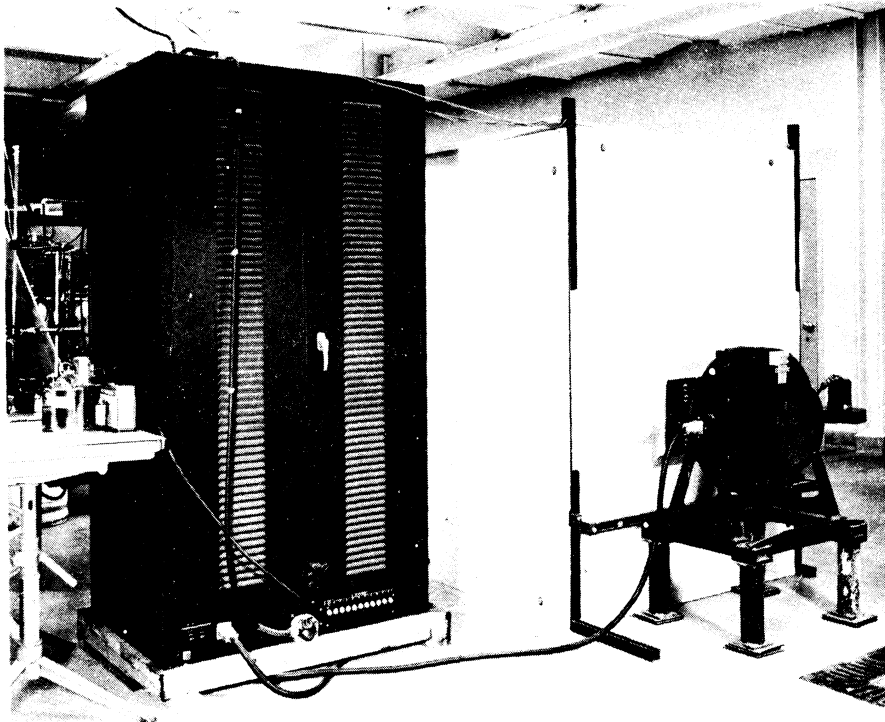
Figure 4-2 Rear View of the Experimental Apparatus.
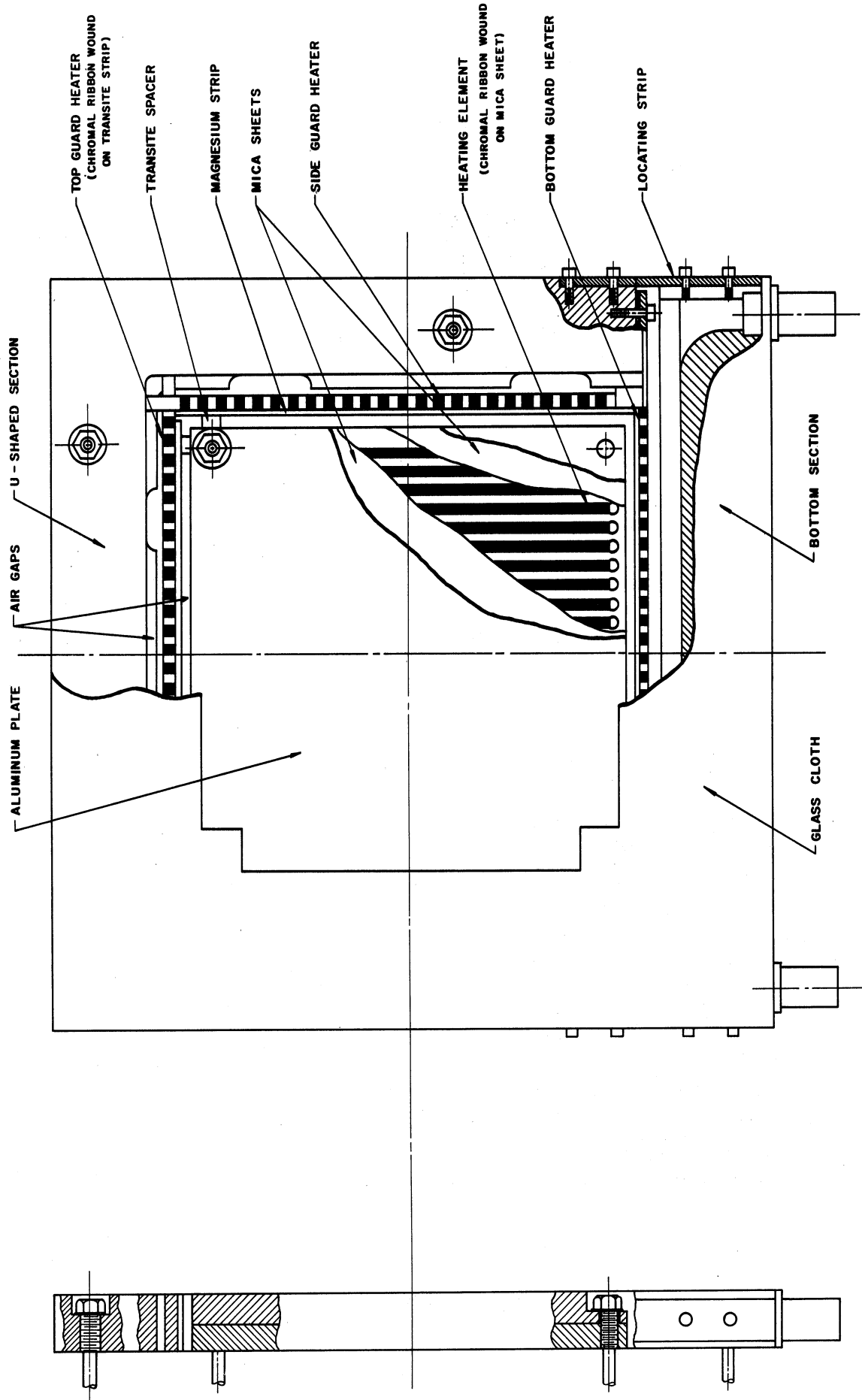
Figure 4-3.   Construction of the Test Plate.

TOP GUARD HEATER (CHROMAL RIBBON WOUND ON TRANSITE STRIP)

TRANSITE SPACER

MAGNESIUM STRIP

MICA SHEETS

SIDE GUARD HEATER

HEATING ELEMENT (CHROMAL RIBBON WOUND ON MICA SHEET)

BOTTOM GUARD HEATER

LOCATING STRIP

U - SHAPED SECTION

AIR GAPS

ALUMINUM PLATE

BOTTOM SECTION

GLASS CLOTH

center section is supported independently of the rest of the apparatus except for very small transite spacers which maintain an air gap of approximately 1 inch.

Surrounding this air strip are thin magnesium strips which have been glued to transite strips. A thin mica sheet insulates the magnesium strips from the guard heater elements directly behind them. There are four guard heaters and they are made of thin chromal ribbon wound on transite strips. There also are air gaps behind these guard heaters. The purpose of the guard heaters is to prevent heat loss from the edge of the plate by maintaining the temperature of the magnesium strips equal to that of the edges of the plate. Each magnesium strip, since it has low thermal resistance, achieves essentially an isothermal condition and is controlled by the power input to the guard heaters. The electrical circuit for measurement of energy input and control of the heater element is shown in Figure 4-4. This has been achieved by utilizing differential thermocouples between the plate and the strips and the details of the circuit for doing this will be discussed later in this chapter. These air gaps, on both sides of the heater, provide a high thermal resistance. The housing or remaining portion of the test plate consists of two sections. The top section is U-shaped while the bottom section is straight. To reduce the weight of these parts they were made out of magnesium. The U-shaped section is supported by 4 rods and the bottom section is supported by 2, thus making the whole test section have 10 support rods. The top section is connected to all 4 of the transite strips, thereby causing its temperature to increase slightly during operation.
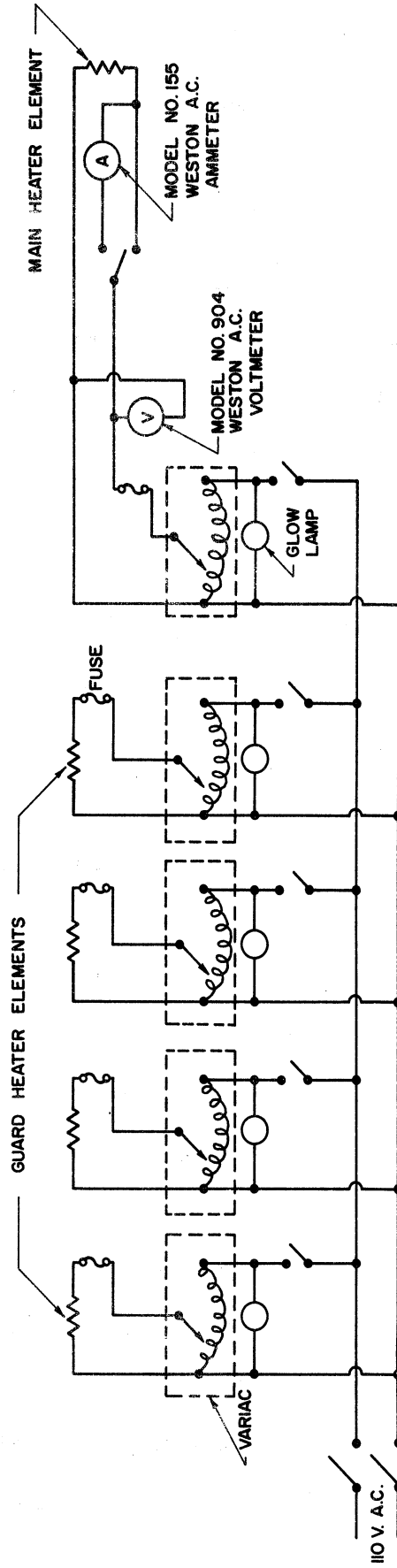
Figure 4-4. Electrical Circuit for Measurement of Energy Input and
Control of Heater Elements.

time-independent heat transfer. The sharp increase in Nusselt number was concluded to be a result of a flow transition from a laminar to a turbulent flow. Smoke studies were made to investigate this possibility more thoroughly. These clearly showed that this phenomena exists. Some photographs are presented of different flow conditions. A correlation in terms of a vibrational Reynolds number, amplitude ratio and Grashof number was also made.

Experimental Apparatus

The experiment is designed to produce a two dimensional boundary layer on a vertical, finite, flat plate undergoing transverse vibrations.

General views of the test apparatus are shown in Figures 4-1 and 4-2.

The test section is a 10 inch square plate 3/4 of an inch thick with a 6 inch square heated section in the center. During test conditions this heated section is maintained at a constant temperature in a manner which will be described later. The heated section consists of two highly polished aluminum plates on the outside with a heater contained between them. The heater is made up of a heating element which is chromel ribbon 1/8 of an inch wide by 0.002 inches thick wound on a thin mica sheet. A mica sheet was placed on each side of the heating element to protect it from the aluminum plates. These plates are clamped together by four hex nuts at the corners which thread onto four support rods which hold the plate in a vertical position. Construction of the test plate is shown in Figure 4-3. As can be seen in this figure, the

Figure 4-5. View of the Test Plate.

section is contained in a celotex enclosure as shown in Figure 4-2.
This enclosure was necessary to prevent stray currents of air from
disturbing the experiment.

To vibrate the test section a MB Vibration Exciter was used.
It is an electromagnetic force generator. The vibration exciter is a
model C5B and its control unit is a model T51-D. This system consists
of an oscillatory power amplifier and oscillator to supply the variable-
frequency power to the driver coil of the vibration exciter. The DC
field supply furnishes the power for the vibration exciter's field
coil. The control cabinet is operated from a 480 volt, three-phase,
sixty-cycle line. Control circuits are operated from a 115 volt,
single-phase, sixty-cycle line. In this system the frequency is set
on the control unit and the amplitude is raised to the desired amount.

The arrangement of the components of the apparatus are shown
in Figure 4-6. The rod support system which is carried in the bearing
wall by the teflon bushings are bolted together to one piece. This
piece is then connected to the vibration exciter by means of small
threaded rod. The test plate was adjusted until it was perpendicular
to the floor and its top was level. The bearing wall fits into the
wall of the celotex enclosure. The large overhang of the rod support
system into the enclosure is necessary so that symmetry can be obtained.
On the side of the rod support system there are 8 support rods inside
the 2 side plates. Ideally the plate should oscillate in an infinite
space without any supports. Experimentally this is almost achieved.

Seven thermocouples were used in each aluminum plate. They
were imbedded to within 3/32 inch of the polished surface by drilling
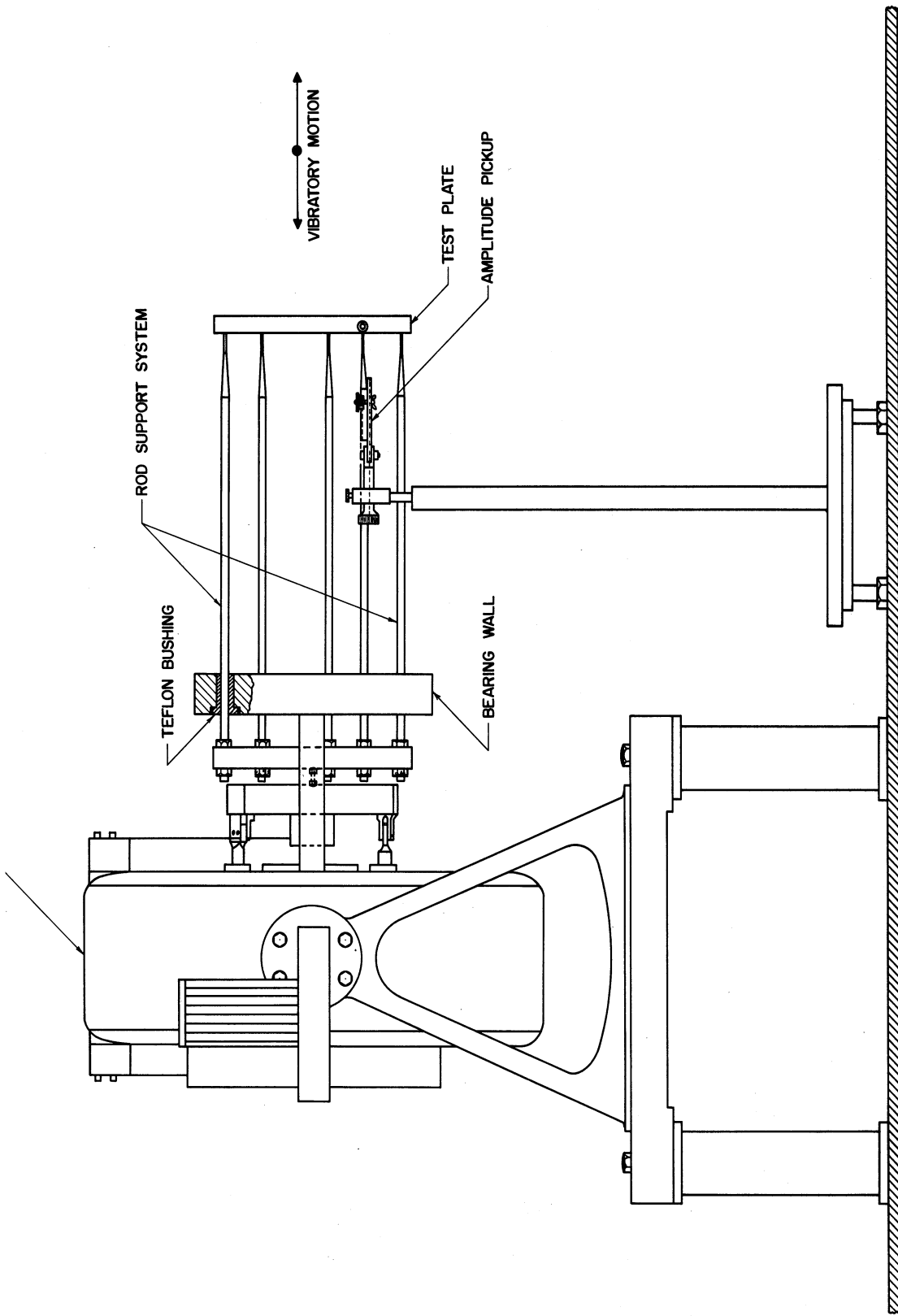
Figure 4-6. Sketch Showing the Arrangement of the Vibratory Components of the Apparatus.

holes in the back of the plate and gluing the thermocouples with epoxy thermosetting resin. Slots were drilled on the back of the plates to provide space for the wires to be taken out of the bottom of the test section. These wires were connected to a system of rotating switches so that a single thermocouple could be read at one time. The thermocouples were made from number 24 gauge copper-constantan wire. A Leeds and Northrup Model 8662 Portable Precision Potentiometer was used to read the indicated output voltage. Distilled ice water was used for the reference junction. The thermocouple wire has been calibrated in the laboratory at the steam and tin points.

A Honeywell Visicorder Model 1012 was used to monitor instantaneous temperature excursions. In the range of experimental values of amplitude and frequency it was found that the surface temperature oscillated only very slightly. This corroborates what R. J. Schoenhals (A-34) assumed in constructing the apparatus. This is due to the large thermal inertia and low thermal resistance of the aluminum plates and the relatively low heat transfer coefficient at the surface.

The power input to the heater between the two aluminum plates is controlled by a variac. The current and voltage drop are measured to obtain the power supplied, as shown in Figure 4-4. The four guard heaters are also controlled by variacs. Calibration of the ammeter and voltmeter was done in the calibration laboratory of the Electrical Engineering Department to an accuracy of 0.1%.

The galvanometer circuit for monitoring the guard heater elements is shown in Figure 4-7. A thermocouple was imbedded in each

THERMOCOUPLE ON MAGNESIUM STRIP

THERMOCOUPLE IMBEDDED IN ALUMINUM PLATE

CONSTANTAN

COPPER

G-M LABORATORIES INC.
GALVANOMETER CATALOG NO.570-204
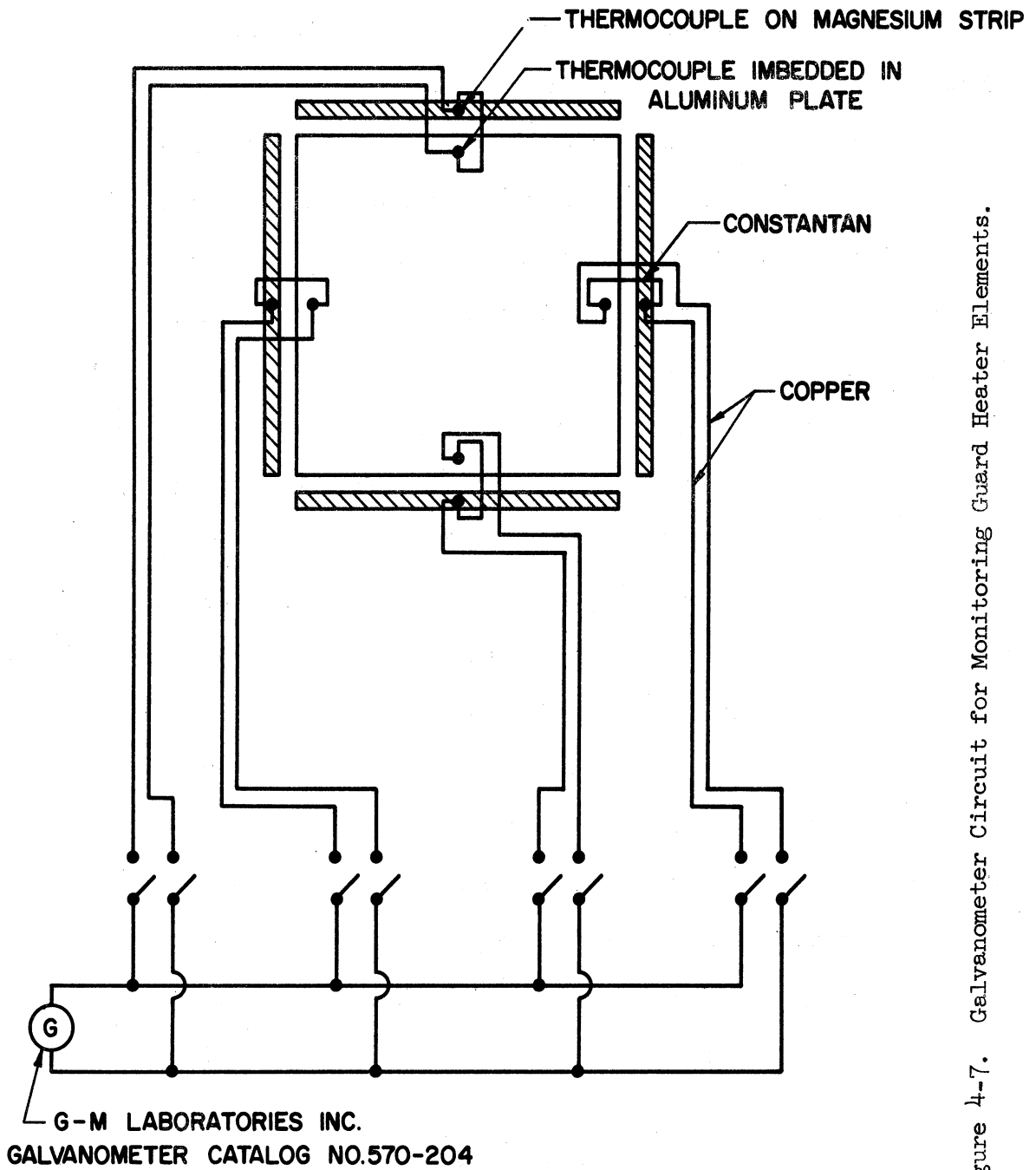
Figure 4-7. Galvanometer Circuit for Monitoring Guard Heater Elements.

magnesium strip. These four thermocouples and four thermocouples

from the aluminum plates were used to form four differential thermo-

couples. By closing one knife switch at a time the deflection of a

sensitive galvanometer indicates whether the strip or the plate is at

the higher temperature. If a null is indicated both have equal

temperature. With this monitoring system and the ten guard heaters

heat loss at the edges was largely eliminated. Two thermocouples

were imbedded in each of two stainless steel support rods, as shown

in Figure 4-7. These thermocouples were used to determine the

magnitude of the energy lost by conduction down the rods.

In Figures 4-8 and 4-9 are shown some of the instruments

used during operation.

Frequency of oscillation is controlled by setting the desired

value on the dial, and was calibrated by using a General Ratio Type

631-B strobotac. The oscillation amplitude was measured in two ways.

One means made use of a Schaevitz Linear Differential Transformer

Model 100-AS-L. The transformer was placed on a platform which has a

stationary mounting and a fine adjustment which allows a sliding member

to be controlled by a threaded shaft. The movable core of the trans-

former system was attached to the plate by means of a brass rod. This

can be seen in Figure 4-10. The differential transformer is composed

of a primary coil and two secondary coils spaced on a hollow ceramic

cylinder. The movable core moves axially within the cylinder in response

to a mechanical input. When the movable core is in the center or null

position, the voltage induced in the secondary coils will be equal.

Figure 4-8. View of Some of the Instruments.

Figure 4-9. View of Some of the Instruments.

SCHAEVITZ LINEAR DIFFERETIAL
TRANSFORMER MODEL IOO-AS -L

DUMONT MODEL 304-H
OSCILLOSCOPE

BRASS ROD ATTACHED
TO TEST PLATE

MOVABLE CORE

IO KILOCYCLES

HEWLETT-PACKARD
MODEL 200 CD
AUDIO OSCILLATOR
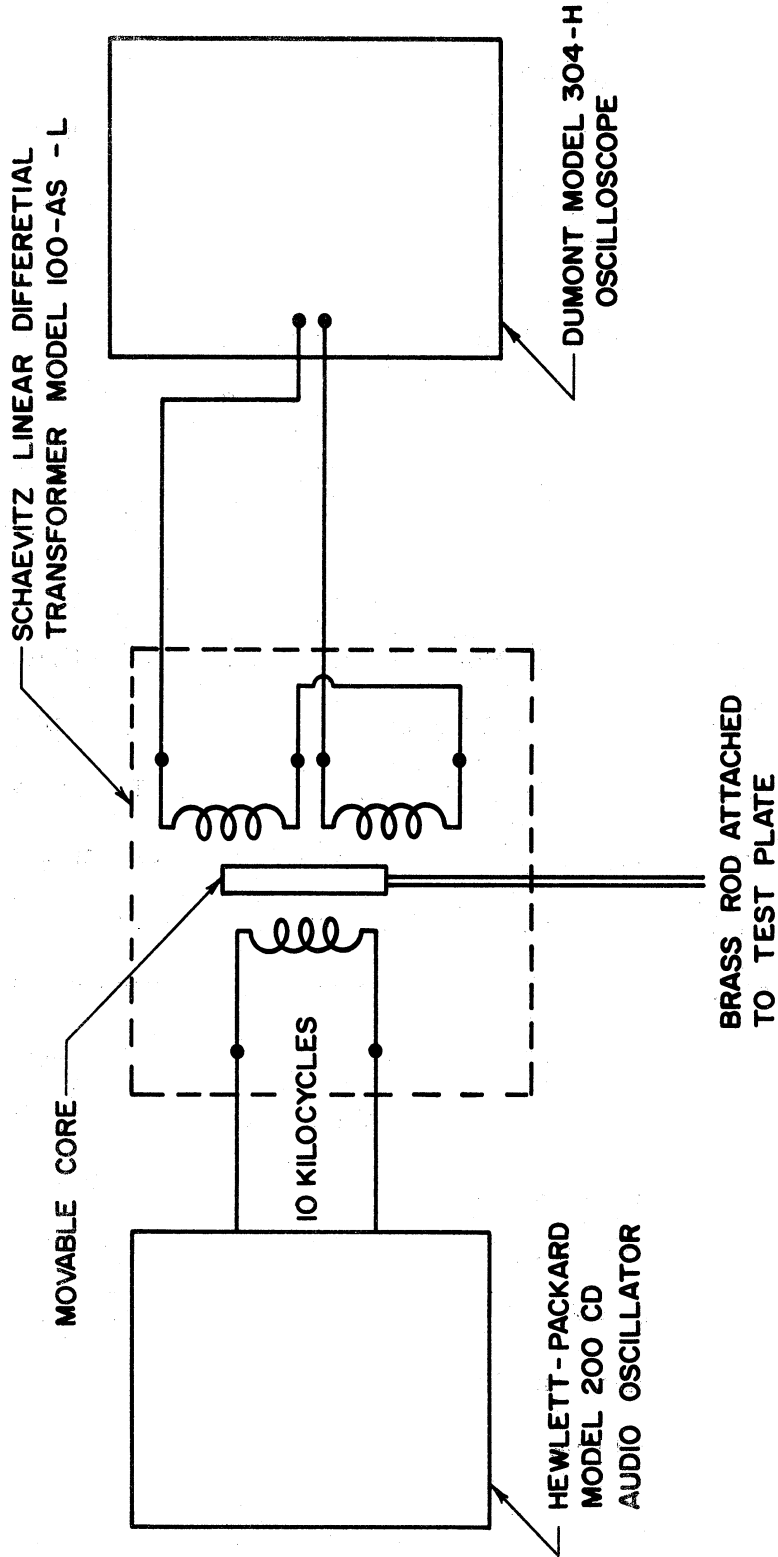
Figure 4-10. Linear Differential Transformer Circuit for Measurement
of Amplitude of Vibration.

If the core is moved away from null position a net AC output voltage

will be produced with the amplitude proportional to the displacement

from null. For the differential transformer it is known that the

output voltage is a highly linear function of core displacement. This

was experimentally verified. A Hewlett-Packard Model 200 CD Audio

Oscillator provided 10 Kilocycles carrier frequency for input to the

transformer. The output was displayed on a Dumont Type 304-H

Oscilloscope. The linearity of this oscilloscope was determined by

using a General Radio type 1800-A electron-tube voltmeter and variac.

To measure amplitude it is necessary to find the null position

by adjusting the position of the transformer. This would be seen as a

thin line on the oscilloscope. For a specific amplitude a feeler gage

of this thickness is used with the fine adjustment to displace the

transformer and thereby cuase a blurred signal in the form of a rectangle

on the oscilloscope screen, as shown in Figure 4-11. In this way a specific

amplitude corresponds to a predetermined displacement on the oscilloscope.

During vibration the output voltage from the transformer is varied so

that the modulation envelope accurately portrays the waveform frequency

and amplitude of the applied vibration. The carrier frequency in all

cases was maintained at least 50 times the highest frequency measured.

When motion of the core occurs equally on both sides of null position

of the transformer the modulated output voltage appears as the envelope

of a sine. This can be seen in Figure 4-12. The amplitude of vibration

is the calibrated distance on the oscilloscope screen. The other method

for determining amplitude was to accurately measure two converging lines
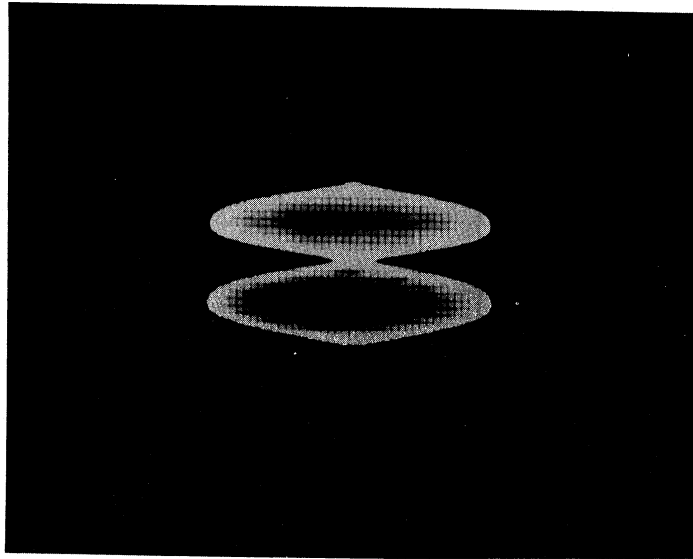
Figure 4-12. Output Signal of the Linear Differential Transformer Under Vibratory Conditions as Displayed on an Oscilloscope.
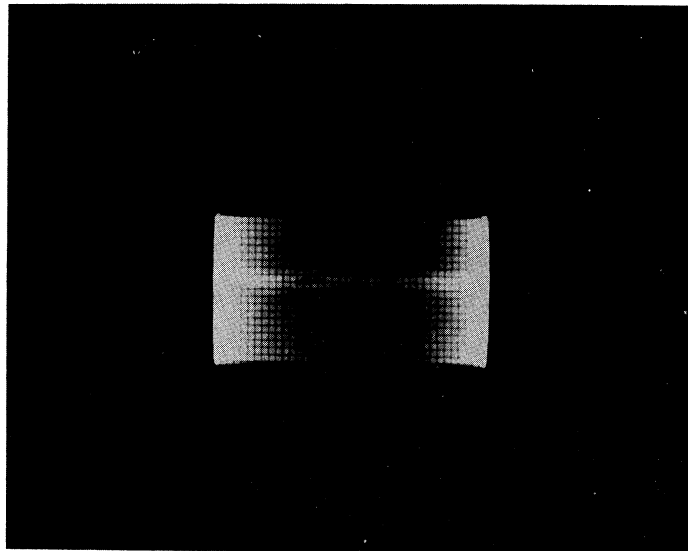
Figure 4-11. Output Signal of the Linear Differential Transformer with the Core Displaced from the Null Position as Displayed on an Oscilloscope.

shown in Figure 4-5 on the side plate and during vibration the image of where the lines crossed indicated amplitude.

One of the heat losses in this experimental apparatus is that of radiation. To evaluate the emissivity of the polished aluminum plate in order to find the heat loss by radiation a type 810C69 Cenco Thermopile was used. A black body constructed from 1/8 inch thick copper plate formed into a cone of square cross-sections, was used to calibrate the thermopile. Soldered onto this were additional copper plates 1/4 of an inch thick. The open end of the black body was 6 inches square and the included angle was approximately 12 degrees. The inside of this cone was blackened with carbon deposit from an acetylene torch. This type of geometry at the opening simulates a black body at the inside temperature. The cone was insulated with a layer of asbestos paper. High resistance wire was wound around the cone on this paper and was connected to a 110 VAC variac for heater control. Heavy fiberglas surrounded the cone and its heating element. A Leeds and Northrup Model 8662 portable Precision Potentiometer was used to read the indicated output voltage of the thermopile. A Honeywell Visicorder Model 1012 was used to find the minimum response time of the thermopile to steady-state values. The black body can be seen in Figure 4-1.

By experimentation the maximum distance was found where the thermopile could be placed away from the black body and the aluminum plate. This distance occurred when the solid angle viewed by the thermopile was entirely subtended by the radiating surface of the plate.

A maximum distance was determined so that the possibility of convection currents entering the thermopile was elminated. To determine emissivity the indicated output voltages of the thermopile for that of the plate divided by that of the black body at the same temperatures were evaluated. The emissivity was found to be essentially constant, 0.065 for a range of temperatures from 80° to $210^\circ F$.

The following procedure was used during the course of the experiments. A specified voltage and amperes were supplied to the test section by adjusting the variac. A period of usually three or four hours was required to establish steady-state, non-oscillating conditions. After steady-state conditions were attained the desired frequency was set on the control unit. Next, the differential trans- former was calibrated and the test section was vibrated at the desired amplitude. During a period of from one to two hours the variacs were adjusted periodically until a steady-state oscillatory condition was obtained. This condition was determined to be steady-state when the temperature of the thermocouples in the plates were constant and equal and the differential thermocouples of the guard heaters and the plates were null. At that time voltage, ampere, four temperatures of the support rods, temperatures of the plate and ambient temperature were recorded. Periodically during operation a Model 11-A Televiso Vibration Meter with a manual vibration pickup was used to check the uniformity of vibration of the test plate.

The smoke studies made use of a smoke generator. A schematic diagram of the smoke generator is shown in Figure 4-13. The smoke from

LOW PRESSURE
COMPRESSED AIR

REGULATING
VALVE

OIL SOAKED CIGARS

TO INJECTORS

TO EXHAUST

STEEL WOOL
FILTER

ICE BATH

WATER
FILTER
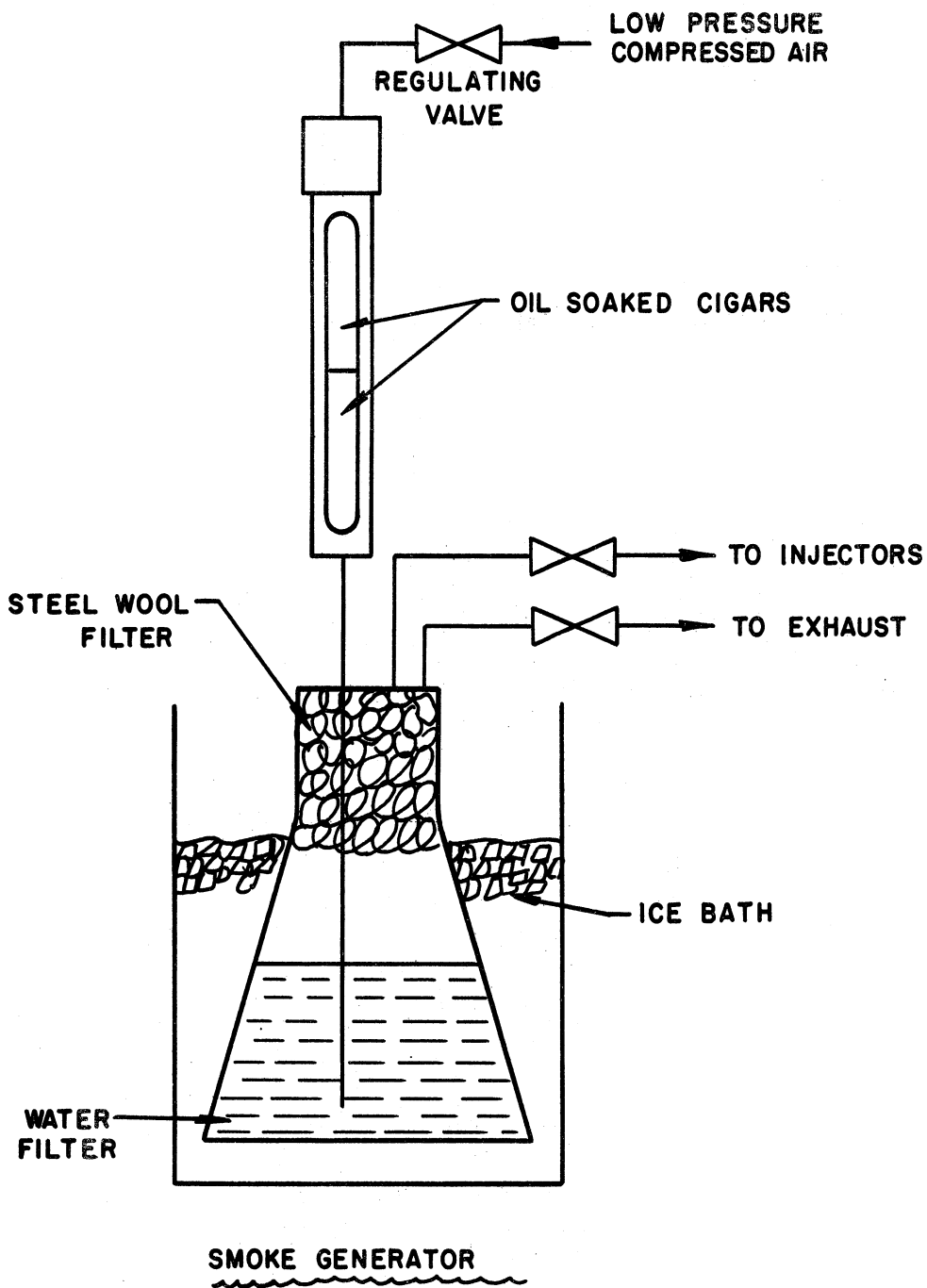
SMOKE GENERATOR

Figure 14-13. Sketch of the Smoke Generator.

cigars impregnated with oil was used as the indicating medium. The

smoke was generated by blowing compressed air down over two cigars

in a steel tube. Each cigar was loaded with approximately 6 cc of

light lubrication oil. The smoke from the cigars was then bubbled

through about 2 inches of water in the bottom of a 1000 cc Erleyemeyer

Flask. This flask was in an ice bath in order to settle out some of

the unburned oil and tar from the cigars. The smoke then filtered

out through a steel wool filter to go to the injecting nozzles

located on the test section, as shown in Figure 4-14. The injectors

consisted of ten small nozzles of approximately 0.032 inches diameter,

attached to the plate by clamps. The edges of the nozzles were adjusted

to coincide with the beginning of the thermal boundary layer. The smoke

was adjusted so that its velocity was as low as possible and yet great

enough so that the smoke filaments could be visualized.

The experimental procedure consisted of permitting the plate

to achieve different temperatures for different power inputs. Once the

plate temperature had stabilized the smoke generator was started. An

optimum smoke velocity was found after ignition of the cigars by adjust-

ing the compressed air and the various valves, to make the smoke visual

to an observer looking transversely at the injectors through a sight

glass which was inserted into one of the side plates. An observer,

by sitting next to the test section and looking through the sight glass,

observed changes in the flow as frequency and amplitude were varied.

This was done to observe the transitional phenomena. Visualization

was made possible by employing a General Radio Type 631-B Strobotac.
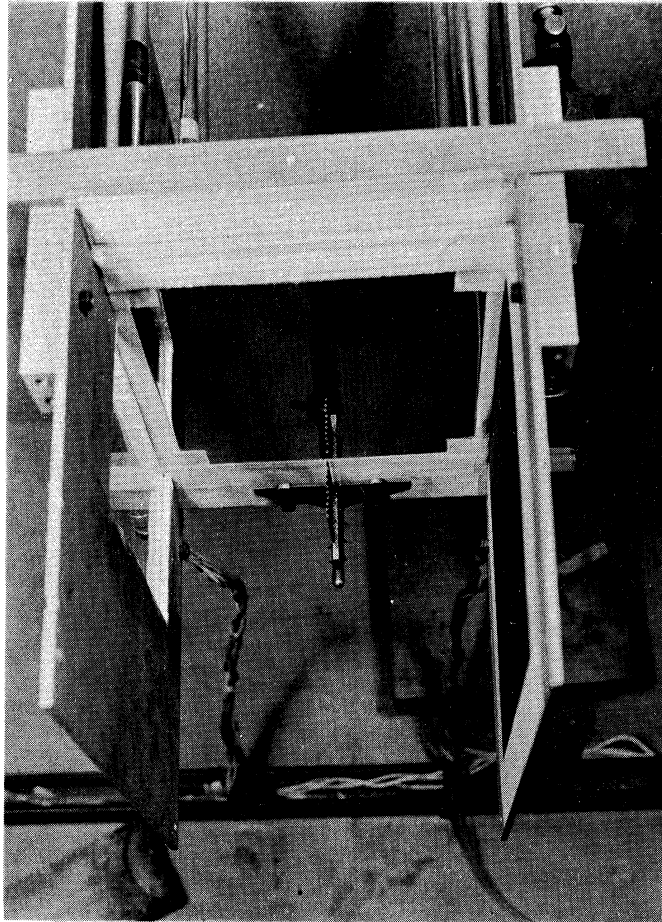
Figure 4-14. View of the Smoke Injections.

The strobotac, when its frequency matched that of the plate, froze the transverse motion. When the strobotac was not employed only a fuzzy image was observed due to double images.

Discussion of Results

As mentioned previously the undesired losses in the system are by conduction and radiation. The method used for correlating the data is by accounting for four heat transfer quantities, natural convection, radiation, conduction, and the heat transferred due to the vibration. For steady-state conditions and no vibrations this would be

$$q_{T_0} = q_{C_0} + q_{L_0} \qquad (4\text{-}1)$$

and for steady-state conditions under the effect of vibration this would be

$$q_T = q_c + q_L + q_V \qquad (4\text{-}2)$$

Non-vibrational conditions have a temperature difference which is called $\Delta\Theta_0$ and the temperature difference under vibratory condition is $\Delta\Theta$. The emissivity of the aluminum plates was 0.065 for the range of experimental temperatures used. The heat lost by the plates due to radiation is

$$q_R = \varepsilon \sigma A (T_P^4 - T_A^4) \qquad (4\text{-}3)$$

For purposes of convenience in reducing the data a coefficient of heat transfer is defined as

$$q_R = h_R A \Delta \theta \tag{4-4}$$

and therefore

$$h_R = \frac{\epsilon \sigma (T_p{}^4 - T_A{}^4)}{(T_p - T_A)} \tag{4-5}$$

For conduction losses of the support rods attention is focused on Figure 4-15. Points 1 and 2 are where thermocouples are located on the support rods. This can be considered to be a fin problem with known boundary conditions at two ends. The first law of thermodynamics yields

$$\frac{d^2 \Delta \theta_R}{d x_R{}^2} - m_R{}^2 \Delta \theta_R = 0 \tag{4-6}$$

where

$$m_R = \frac{4 h_s}{D K_r} \tag{4-7}$$

The heat lost at the base of one of the support rods is found by the first derivative of the temperature distribution as

$$\left(q_K\right)_{x_R = 0} = -K_R \frac{\pi D^2}{4} \left(\frac{d\theta_R}{d x_R}\right)_{x_R = 0} \tag{4-8}$$

For convenience in reducing experimental data a heat transfer coefficient is defined as

$$q_K = h_K A \Delta \theta \tag{4-9}$$

where for all rods

$$h_K = \frac{2\pi D \sqrt{h_s K_r D}}{A \Delta \theta} \left[\frac{(\Delta \theta_R)_1 \cosh m_R L - (\Delta \theta_R)_2}{\sinh m_r L} \right] \tag{4-10}$$
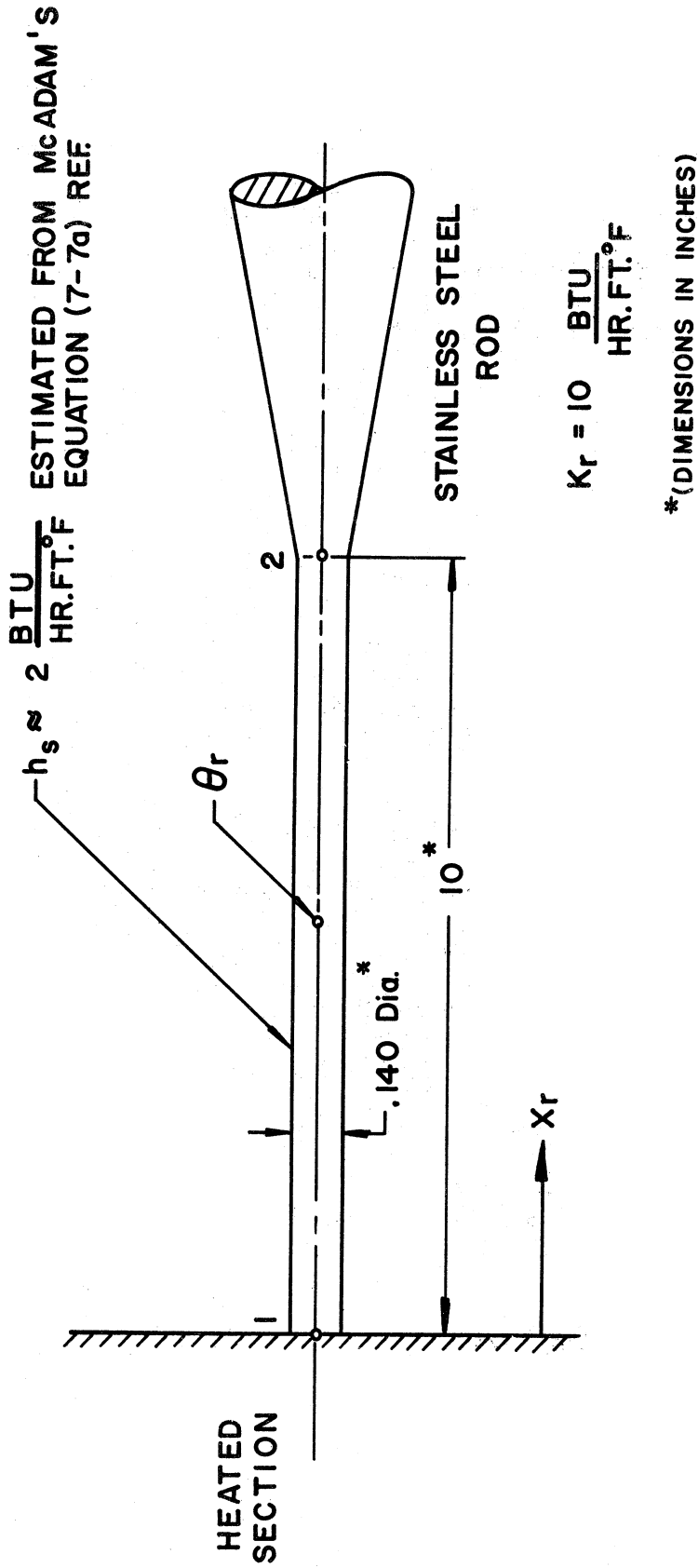
Figure 4-17. Sketch Showing One of the Four Rods Attached to the Corners of the Heated Section.

An assumption made here is that h_s is the same under vibratory and non-vibratory conditions. There is no potential flow along the length of the rod and therefore there would be no appreciable change in the time-averaged heat transfer coefficient. A cylinder vibrating along its axis will not have a pressure distribution due to potential flow. This type of problem would be similar to that in Chapter III where no significant change in heat transfer was found.

Therefore,

$$h_L = h_R + h_K \tag{4-11}$$

and, for steady-state

$$h_C = \frac{q}{A\Delta\theta} - h_L \tag{4-12}$$

A steady-state correlation was experimentally determined, as

$$h_C = 0.385 (\Delta\theta)^{1/4} \tag{4-13}$$

Schoenhals (A-34) found for this case and experimental apparatus a value of 0.4 instead of 0.385. The value of 0.385 is slightly higher than Equation (7-4B) of McAdams, (C-5). A plot of this correlation and the experimental points are shown in Figure 4-16.

The power input is the same for vibratory and non-vibratory conditions, therefore

$$\left(h_{C_0} + h_{L_0} \right) \Delta\theta_0 = \left(h_C + h_L + h_V \right) \Delta\theta \tag{4-14}$$

realizing

$$\frac{h_{C_0}}{h_C} = \left(\frac{\Delta\theta_0}{\Delta\theta} \right)^{1/4} \tag{4-15}$$
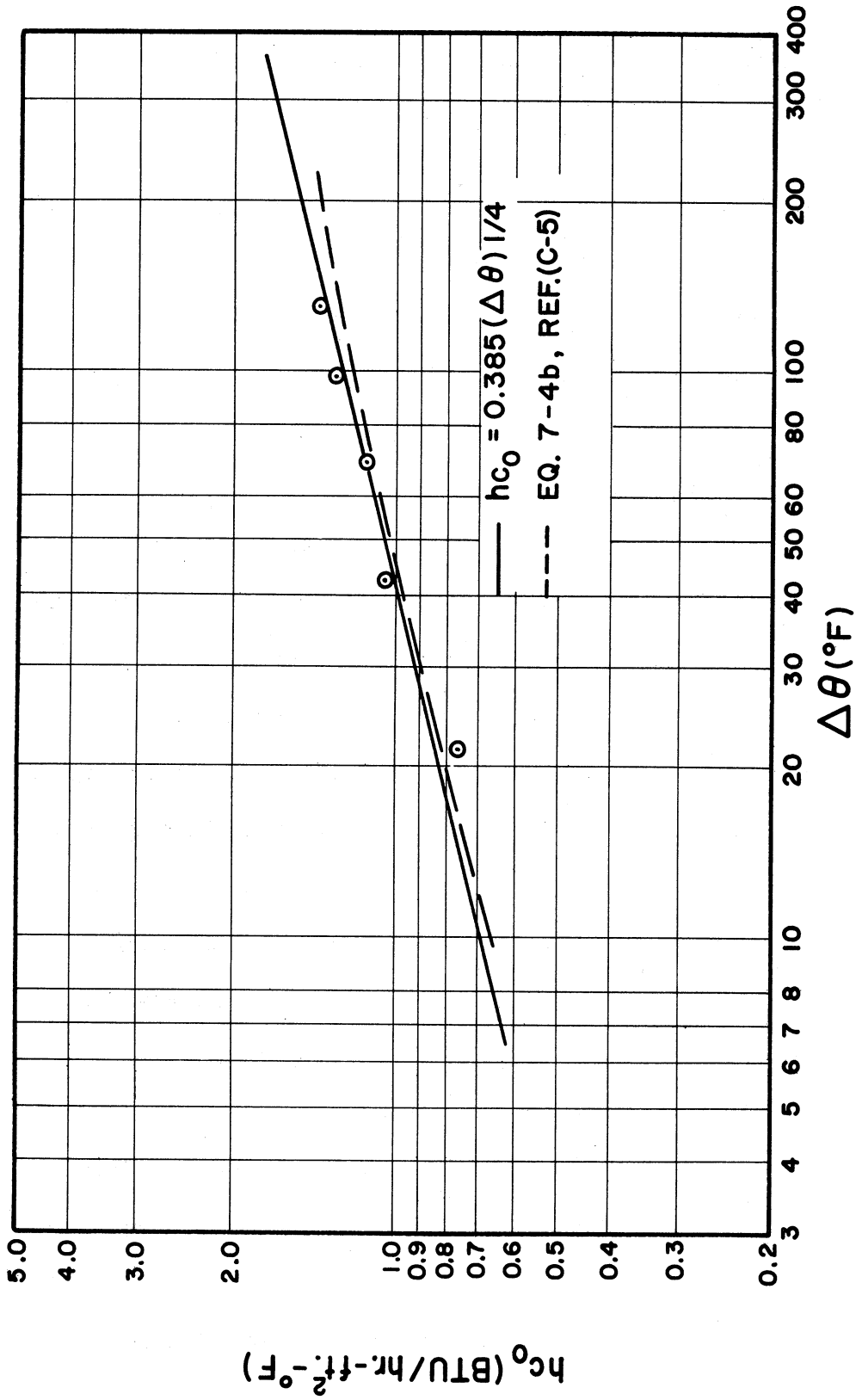
Figure 4-16. Steady-State (Non-Vibratory) Heat Transfer Correlation.

so

$$\frac{h_V}{h_C} = \left[\left(\frac{\Delta\theta_o}{\Delta\theta}\right)^{5/4} - 1 \right] + \frac{h_L}{h_C} \left[\frac{h_{Lo}}{h_L} \left(\frac{\Delta\theta_o}{\Delta\theta}\right) - 1 \right] \qquad (4\text{-}16)$$

The ratio h_L/h_C was found to have a value approximately constant at 0.11. The ratio h_{Lo}/h_C was approximately equal to 1. The advantage of reducing the data in this way is that it is dependent primarily on temperature differences only. Temperature can be measured accurately and temperature difference is a very convenient way of determining the heat transfer coefficient quickly and accurately.

Schoenhals, (A-34) made hot wire measurements of transverse vibration of the test section used in this experiment for adiabatic conditions. His potential flow measurements are reproduced in Figures 4-17 and 4-18. For the potential flow measurements fair agreement was found between theory and experiment, as can be seen. The discrepancies may be, due to four possible causes. First, theory assumes an infinitely thin plate which is the degenerate case of an ellipse while the plate is actually 3/4 of an inch thick. Second, viscous effects are ignored at the edges. Third, the assumption of two dimensional flow may not hold at the edges, and fourth, the probe and mounting structure have some effect on the flow. It is believed that in a vibrating plate such as this there probably exists small vortices which may influence hot wire readings. The experimental values tend to be lower than that of theory for higher values of X/C. But if vortices were large it would seem impossible to get the results that Schoenhals (A-34) obtained. Standing vortices may exist at the edge of the plate but apparently
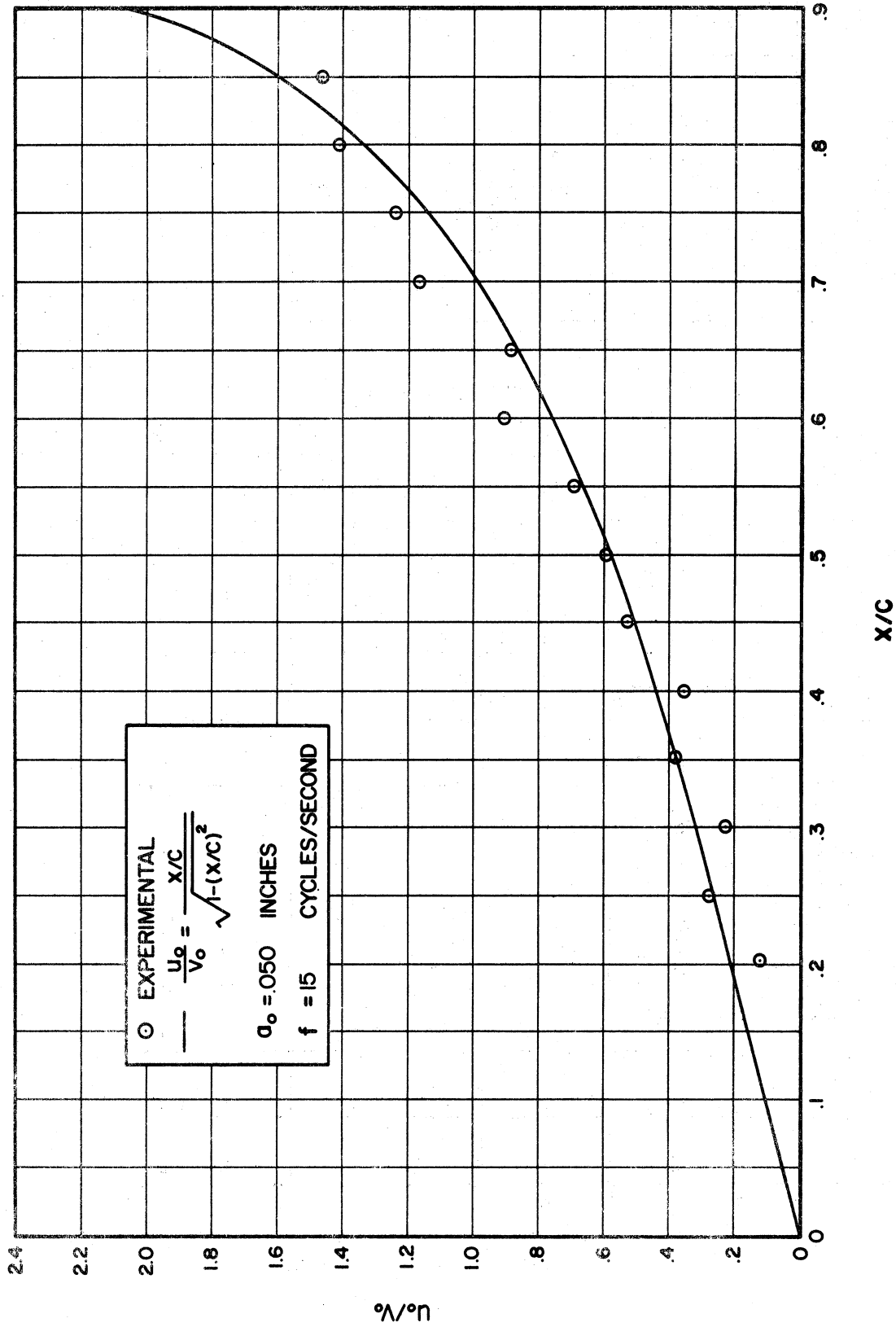
Figure 4-17. Experimental Potential Flow Velocity Measurements and Comparison with Theory from Schoenhals (A-34).
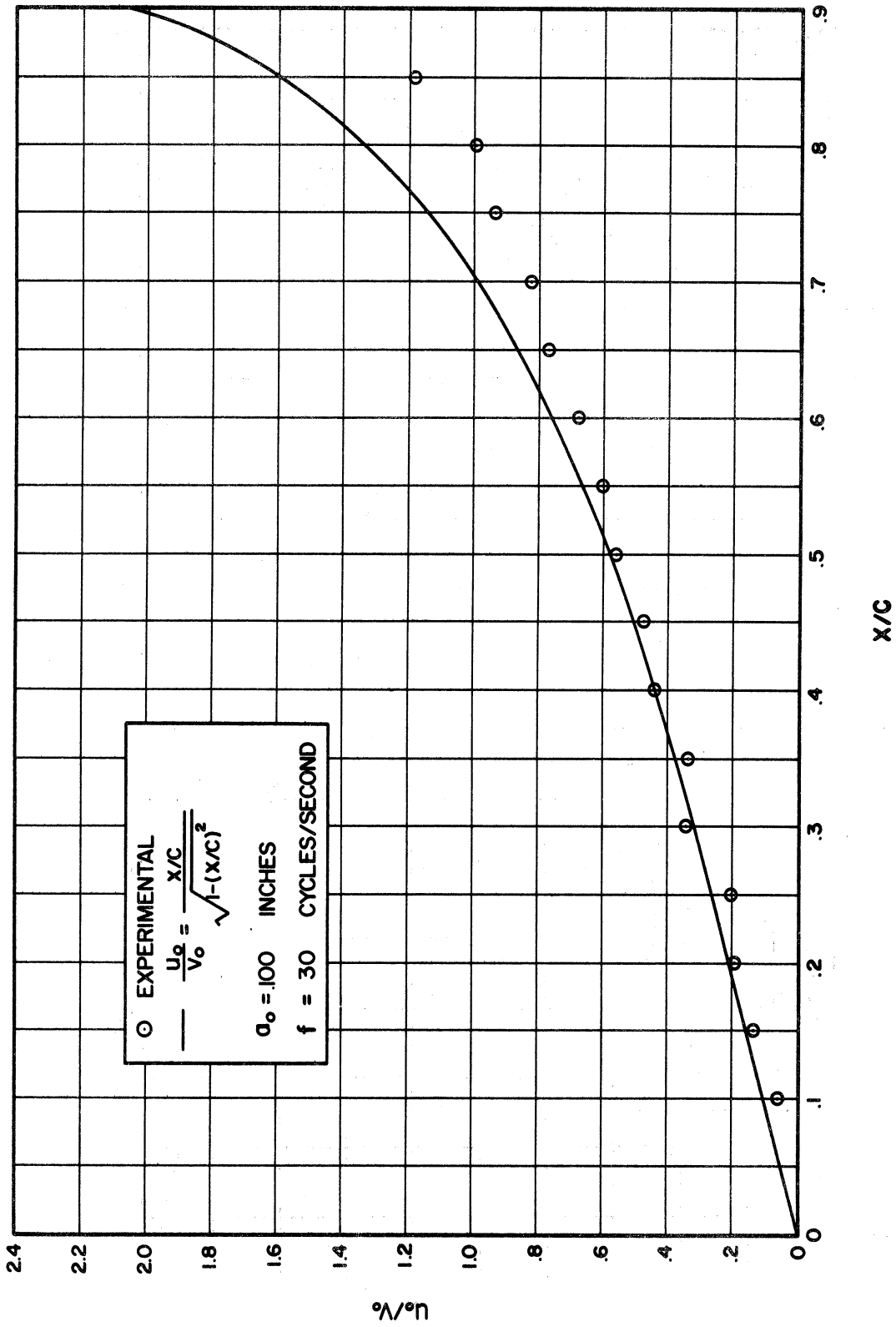
Figure 4-18. Experimental Potential Flow Velocity Measurements and
Comparison with Theory from Schoenhals (A-34).

are insignificant. The agreement of theory and experiment can be described as good for most values of X/C. The potential flow and its agreement with theory of Schoenhal (A-34) were carefully considered since this potential flow is identical to that used in Chapter II.

Oscillating velocities in the boundary layer were also obtained by Schoenhals using a hot wire anemometer for adiabatic conditions. The experimental values agree very well with that of his theory, as shown in Figures 4-19 and 4-20. The η_1 in these figures is dimensionless, $\eta_1 = y\sqrt{\Omega/\nu}$. The $|u|/v_0$, the ordinate of Figures 4-19 and 4-20 is the absolute magnitude of the periodic velocity for an adiabatic finite plate. The significance is that the oscillating potential flow and the oscillating boundary-layer flow of Schoenhals experiments agree with his theory for an oscillating adiabatic finite plate. Also of significance is that this potential flow is identical to the potential flow of the case treated here, Chapter II, of an oscillating finite plate with heat transfer.

It is well known that one of the reasons for the neglect of experimental free convection boundary layer transitional data is that it is virtually impossible to probe and measure the flow for various quantities of interest. Schoenhals (A-34) was able to probe the oscillating velocity and oscillating potential flow as related previously, but this was without heat flow. The analysis of Chapter II is directed to a problem in which the main consideration is free convection heat transfer with first and second order perturbations of velocity and temperature
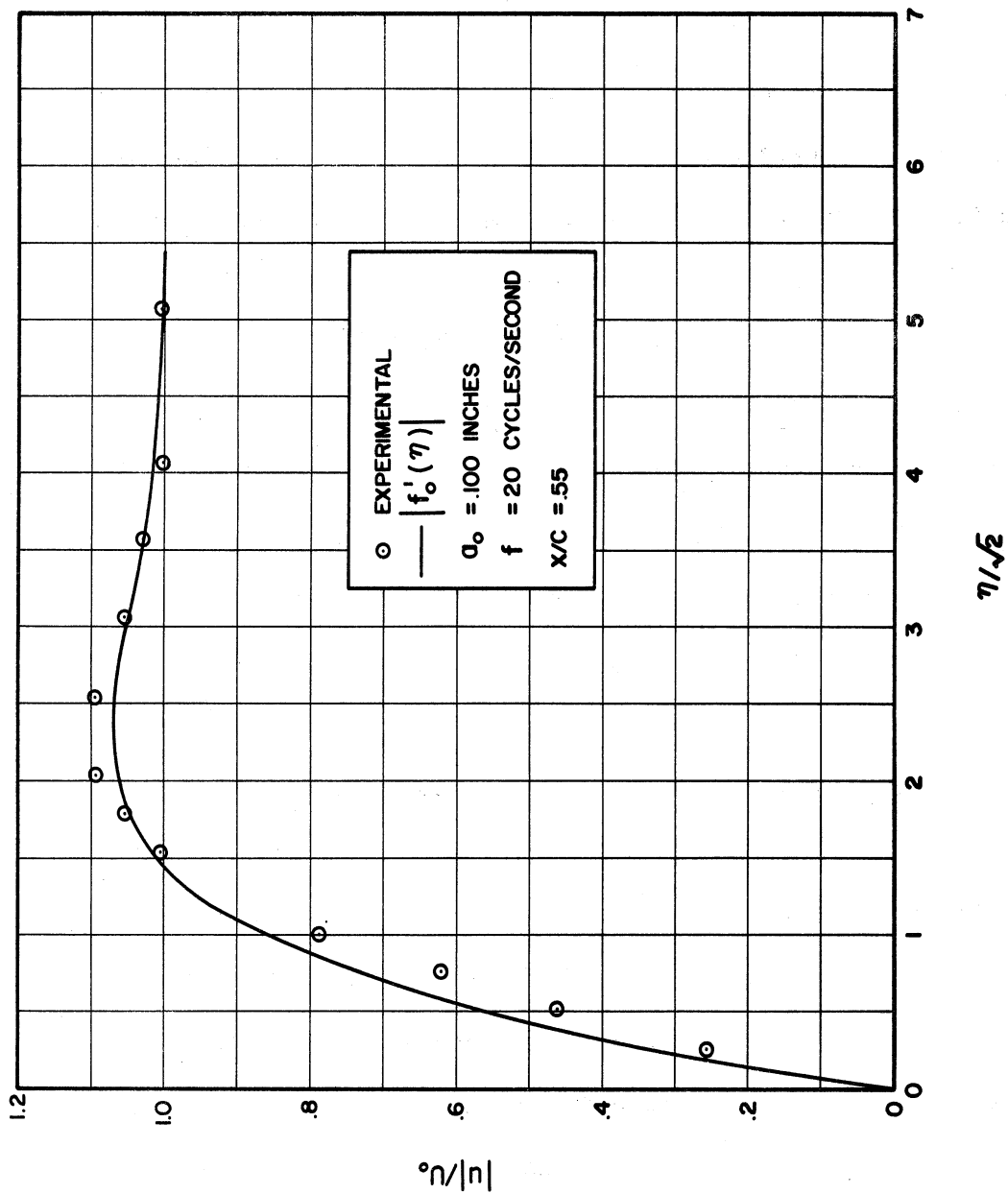
Figure 4-19. Experimental Velocity Measurements Made in the Boundary Layer on an Adiabatic Plate Vibrating Transversely and the Comparison with Theory from Schoenhals (A-34).
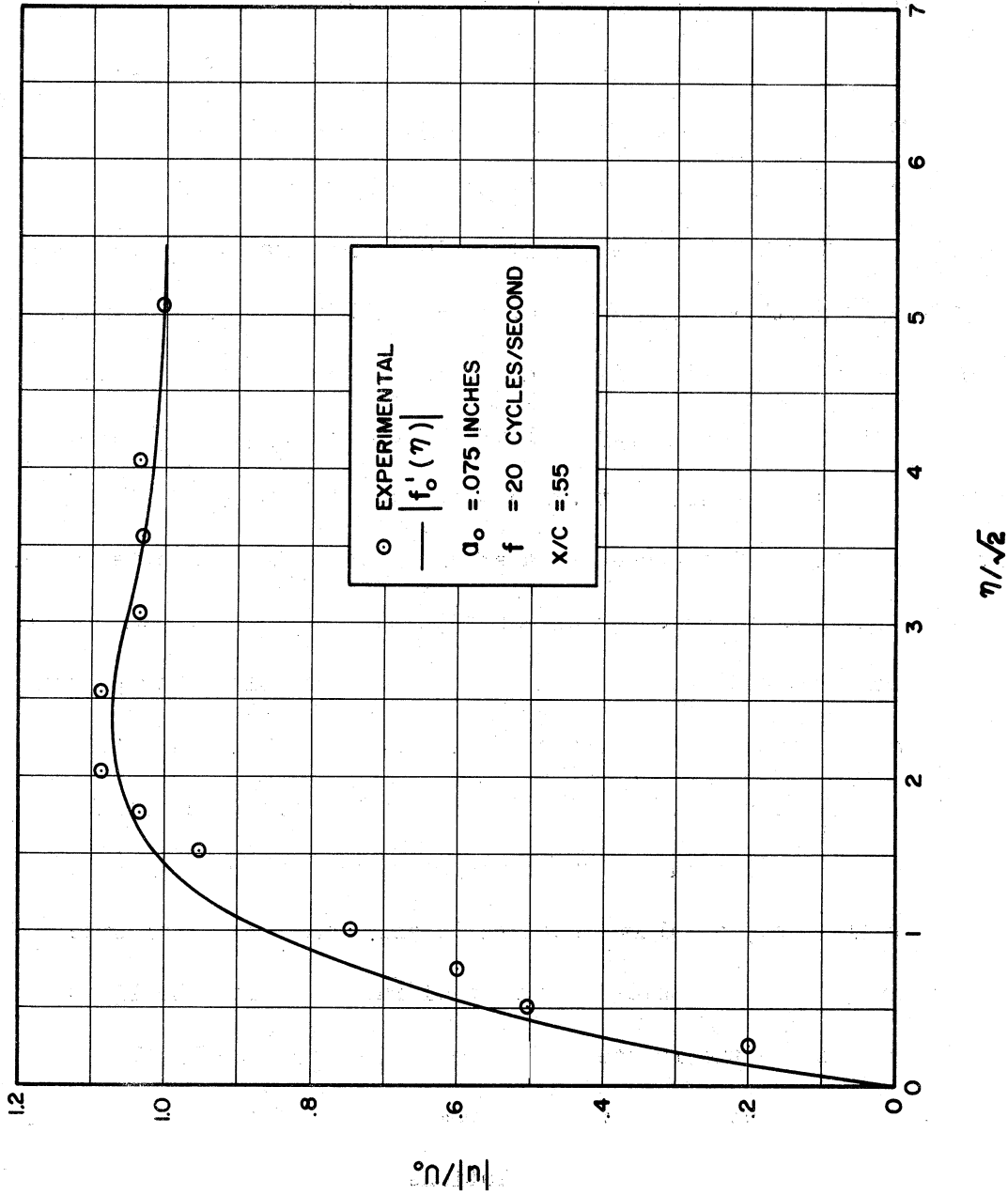
Figure 4-20. Experimental Velocity Measurements Made in the Boundary Layer on an Adiabatic Plate Vibrating Transversely and the Comparison with Theory from Schoenhals (A-34).

having been determined. Neglecting the free convection velocities
and temperatures for the moment, the problem of trying to measure an
oscillating temperature and an oscillating velocity with a hot wire
anemometer will be examined. A hot-wire depends upon the heat loss
between itself and the environment. The rate of heat loss depends
upon geometry, flow conditions and physical properties. Schoenhals
(A-34) was able to make measurements because he was dealing with an
isothermal system which allowed calibrations to be made. In this
case there are both varying and steady velocities and temperatures.
The presence of a hot-wire vibrating back and forth in its own path
in the boundary layer may very well affect the results. For these
reasons a hot-wire measurement was not attempted. Two possible methods
left to investigate the boundary layer are smoke and an interferometer.

The heat transfer results are plotted as Nusselt number versus
a vibrational Reynolds number with the Grashof-Prandtl number product
as a parameter. These results are given in Figure 4-21. A critical
vibration Reynolds number was observed. Up to a certain critical
value of this Reynolds number the data follow the theoretical results
of Chapter II, i.e., an almost negligible influence but a definite
decrease in the heat transfer rate with vibration. With the limits
of the perturbation theory used, the theory is confirmed by these
results. The conclusion, therefore, from analytical and experimental
results is that the effect of oscillations on laminar free convection
boundary layer heat transfer is negligible if the boundary layer remains
laminar.

However, from an inspection of the heat transfer data in Figure 4-21 it is apparent that vibrations and flow oscillations do cause a significant increase in the steady rate of heat transfer. Since the theory assuming laminar flow conditions does not disclose this behavior and, in fact, even predicts a decrease in the heat transfer rate, it is evident that a completely new influence is being introduced by the oscillating flow. It seems probable that this new influence is in the form of a disturbance in the flow which causes a transition from a laminar to a turbulent condition in the boundary layer. That such is likely the case is reasonable from the standpoint of the stability of boundary layer flow where it is known that disturbances can be amplified in an existing laminar boundary causing it to become turbulent. Furthermore, it can be expected that such a condition of transition would depend on the mechanics of the laminar force convection boundary layer; namely, its state of stability as indicated by the Grashof number or Grashof-Prandtl number product in a manner similar to that describing the stability of a forced convection laminar boundary layer in terms of its Reynolds number.

This threshold condition was found for the transition of the free convection laminar boundary layer to a turbulent boundary layer and is described in terms of a critical vibratory Reynolds number dependent on the Grashof-Prandtl number of the laminar boundary layer. The experimental results of this transition phenomenon are given in Figures 4-22, 4-23 and 4-24. The transition region is very difficult to ascertain from heat transfer data alone. At this point in
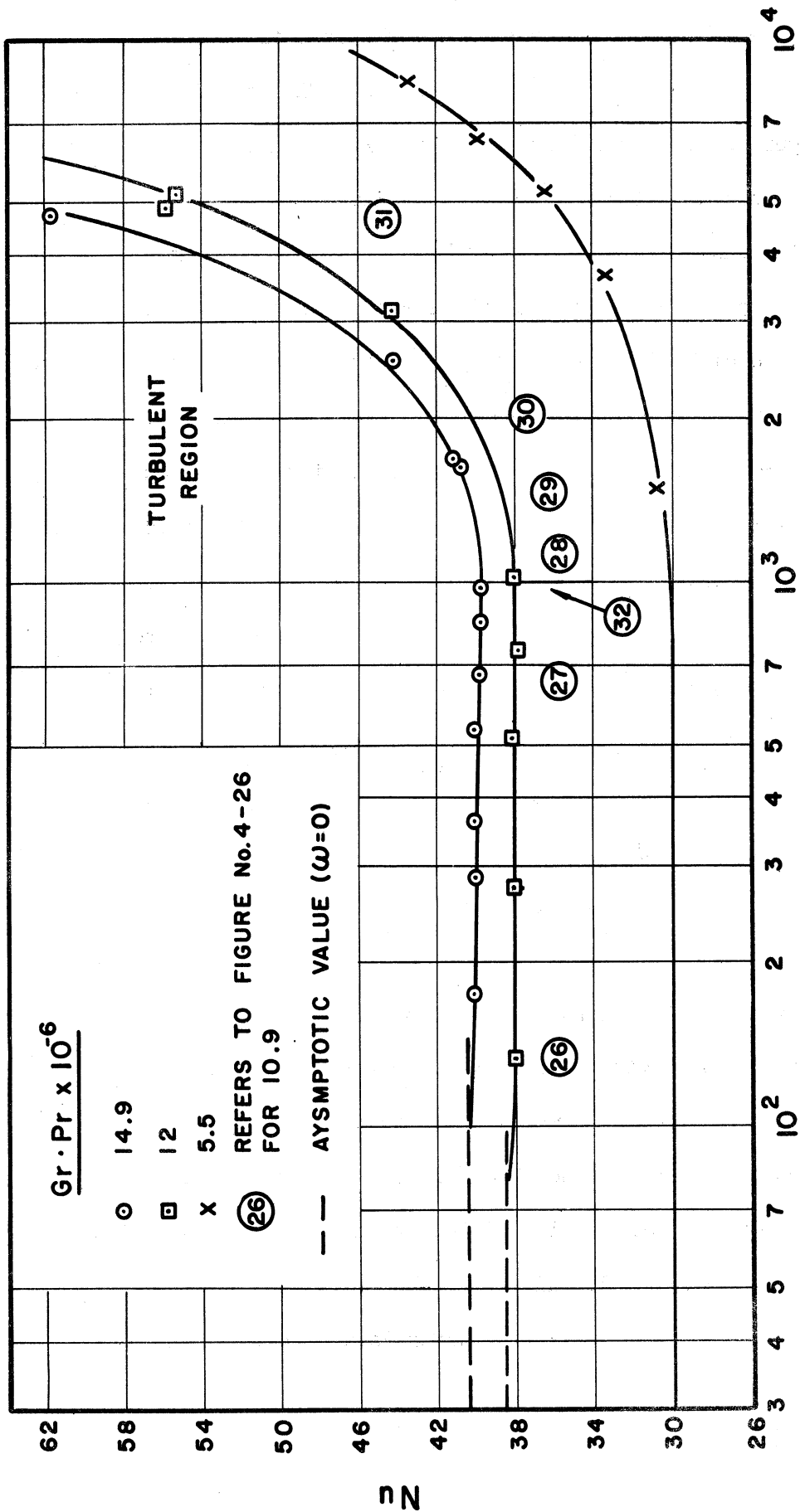
Figure 4-21.   Experimental Time-Independent Heat Transfer Data for a Heated Plate Oscillating Transversely.
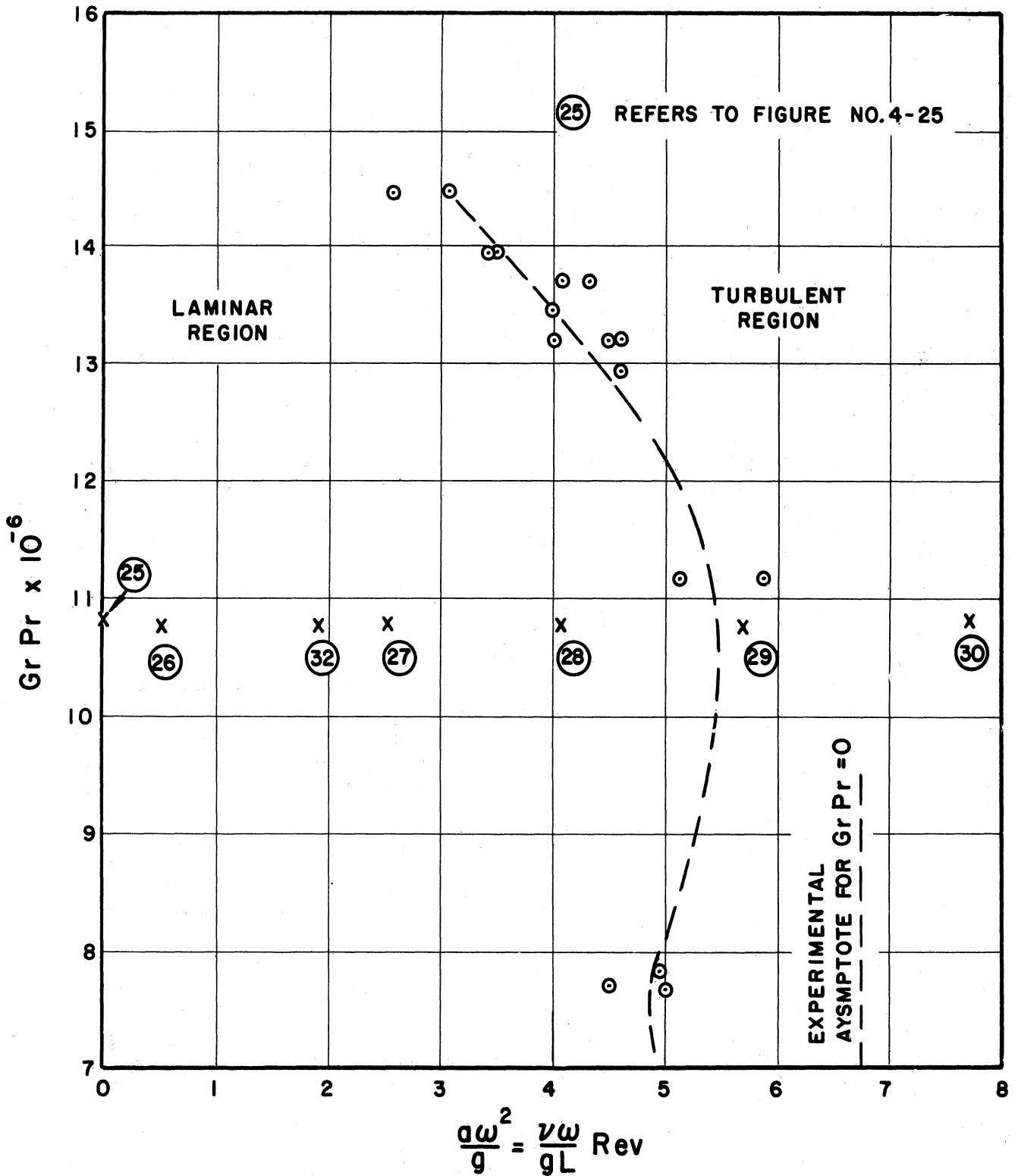
Figure 4-22. Experimental Smoke Study Data for Determining the Condition of Transition.
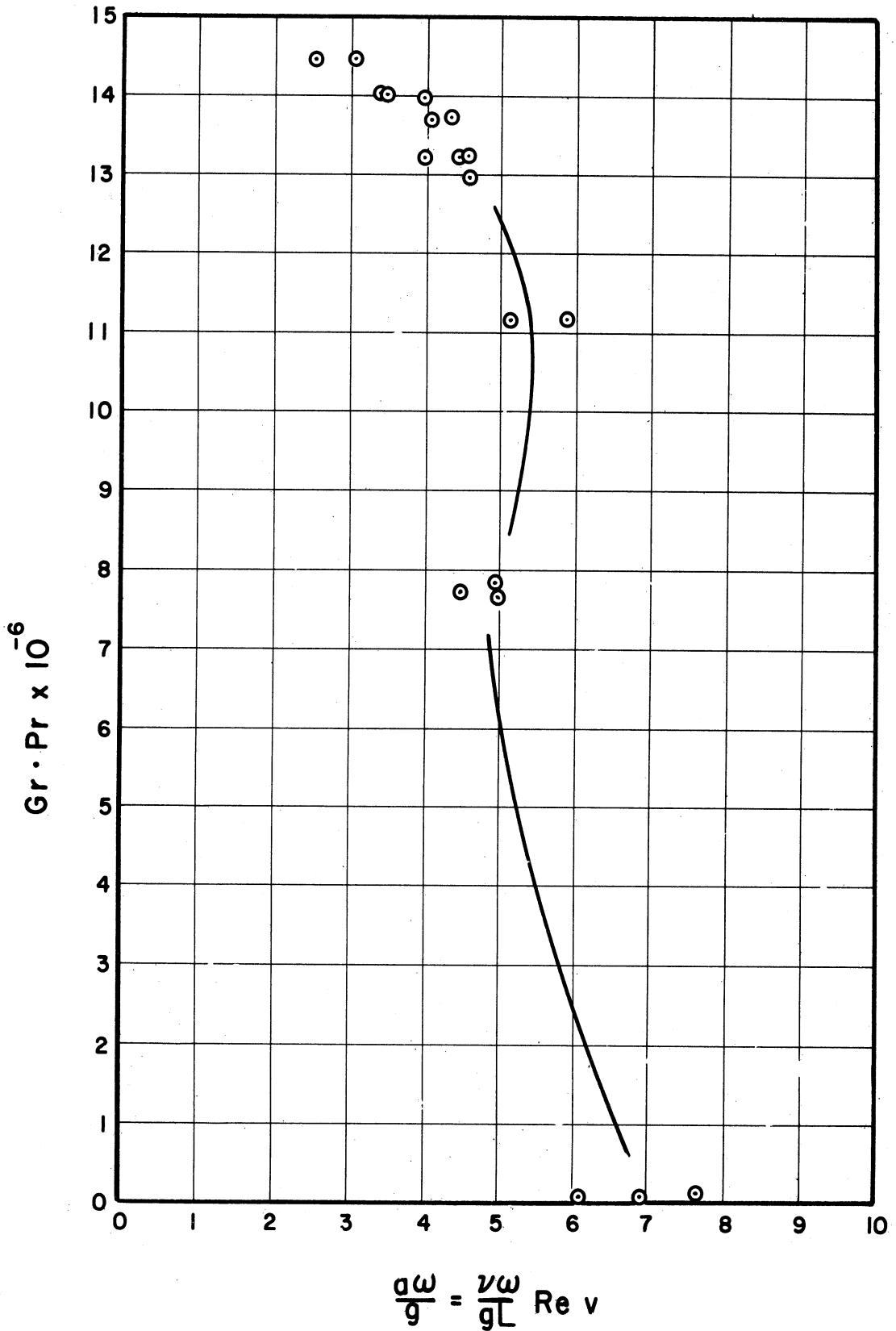
Figure 4-23.   Experimental Smoke Study Data for Determining the Condition
of Transition.
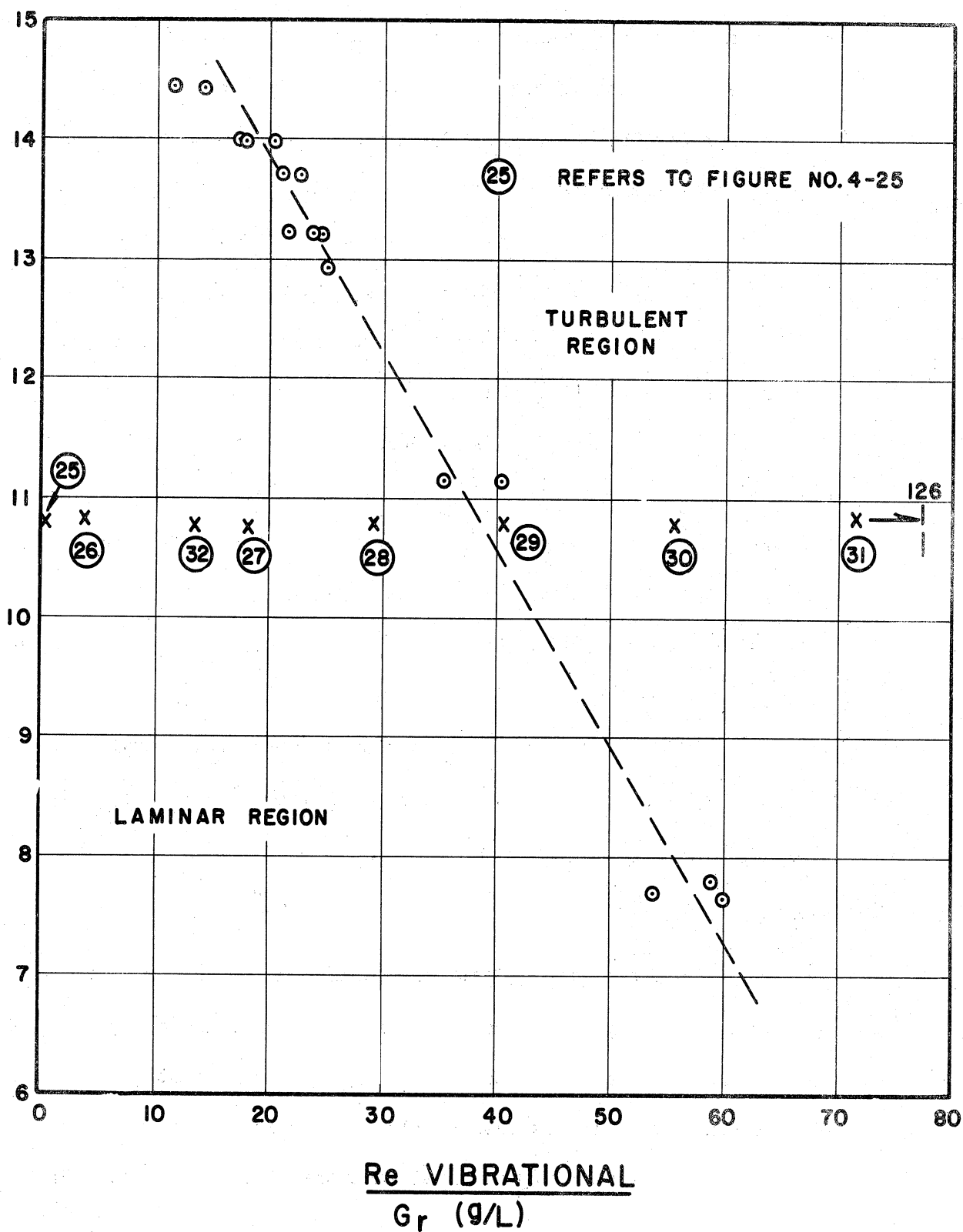
Figure 4-24. Experimental Smoke Study Data for Determining the
Condition of Transition.

the investigation another experimental method of attack was taken.

Smoke studies were used to determine the transition region of laminar flow to turbulence. The smoke filaments were observed and when under different values of amplitude and frequency the pattern in the boundary layer changed, the pertinent data were taken. The velocity of the smoke was attempted to be excluded as a factor in this experiment by taking each set of readings at a low smoke velocity. The condition of change in the smoke pattern seems to be the onset of turbulence. This condition occurred for different values of amplitude, frequency and ΔT (Grashof number).

The data correlate with GrPr product versus $a\omega^2$ not as $a\omega$ as appears to be indicated from the heat transfer data. This can be interpreted to mean that the instability of a laminar free convection boundary layer is dependent upon, for mechanically induced vibrations, an acceleration of the boundary layer or a disturbing force per pound-mass of boundary layer fluid. Considering again the governing differential Equation (2-27) for x-momentum of Chapter II and again disregarding thermal variations of density as being negligible we see that

$$ -\frac{a\omega^2}{L}\rho \sin \omega t + \left(\frac{a\omega}{L}\right)^2 \rho \frac{\partial P}{\partial x} \cos^2 \omega t $$

are the terms due to the effects of oscillation. The first term of the above has the proper terms to cause the transition and most likely causes the transition to occur. The data also show that for higher GrPr products the flow is less stable to the disturbances. This ties in with the well-known experimental fact that the higher the GrPr

product the free convection flow is less stable and less disturbance would be required to cause transition. This experimental fact also suggests that if the non-oscillatory free convection flow were initially turbulent due to large GrPr product then oscillation would show an immediate effect. Unfortunately the test apparatus could not create turbulence, without burning out the test section, to experimentally prove this one point. It should be noted here that air was the only fluid used and the Prandtl number in the GrPr product is not data. The equality of the Grashof number establishes dynamic similarity for different flows. Equality of Grashof and Prandtl numbers establish similarity for velocity and temperature distributions of free convection flow for geometrically similar bodies and therefore the Nusselt number. On this basis it was found desirable to use GrPr product in reporting the data.

Figures 4-25 through 4-32 are photographs of the smoke studies. These photographs are representative of what was seen without a camera but with the aid of a strobatac to freeze the motion. These pictures were taken through the sight window in the side plate, shown in Figure (4-5). Two spotlights were focused on the smoke. One light was focused at a small angle from the line of sight of the camera. The other light was placed above the smoke at a slight angle to a line parallel to the smoke injectors pointing toward the camera. This lighting arrangement was found to yield the best pictures. A 4 x 5 Crown Graphic Graflex Optor camera was used with a setting of 1/400 second at f/4.7. The film was Polaroid Polapan 200 type 52.

Figure 4-26. Smoke Photograph for $a = 0.002$ in., $\omega = 50$ cycle/sec., $GrPr = 1.08 \times 10^7$, $a\omega^2/g = 0.51$, $q/A = 92$ BTU/hr ft^2, $R_e{}^2{}_V/Gr(a/L) = 3.7$.

Figure 4-25. Smoke Photograph for $a = 0$, $\omega = 0$, $GrPr = 1.08 \times 10^7$, $q/A = 92$ BTU/hr ft^2, $a\omega^2/g = 0$, $R_e{}^2{}_V/Gr(a/L) = 0$.

Figure 4-28. Smoke Photograph for $a = 0.016$ in., $\omega = 50$ cycle/sec., GrPr $= 1.08 \times 10^7$, $a\omega^2/g = 4.09$, $q/A = 92$ BTU/hr ft2, $R_e^2{}_V/Gr(a/L) = 29.5$.
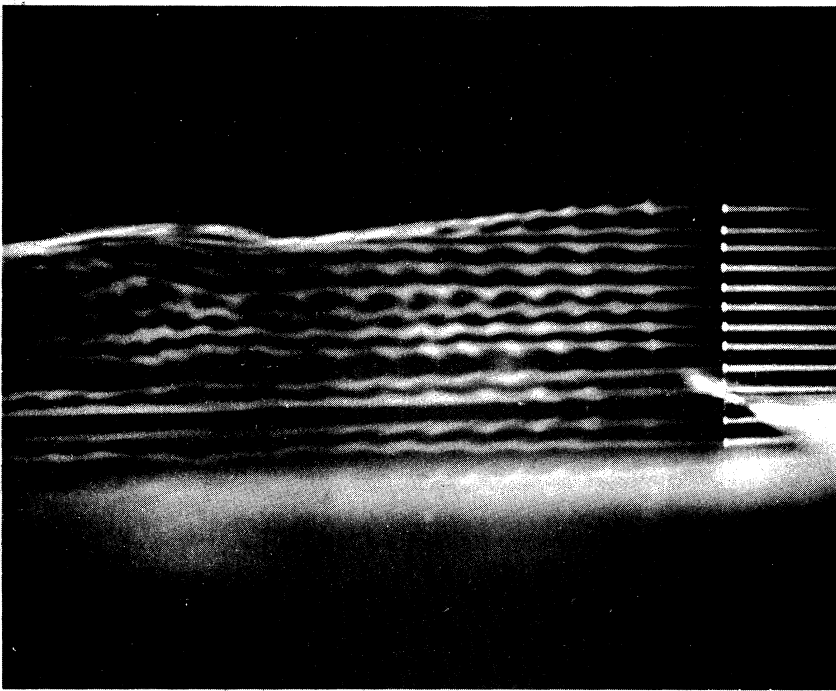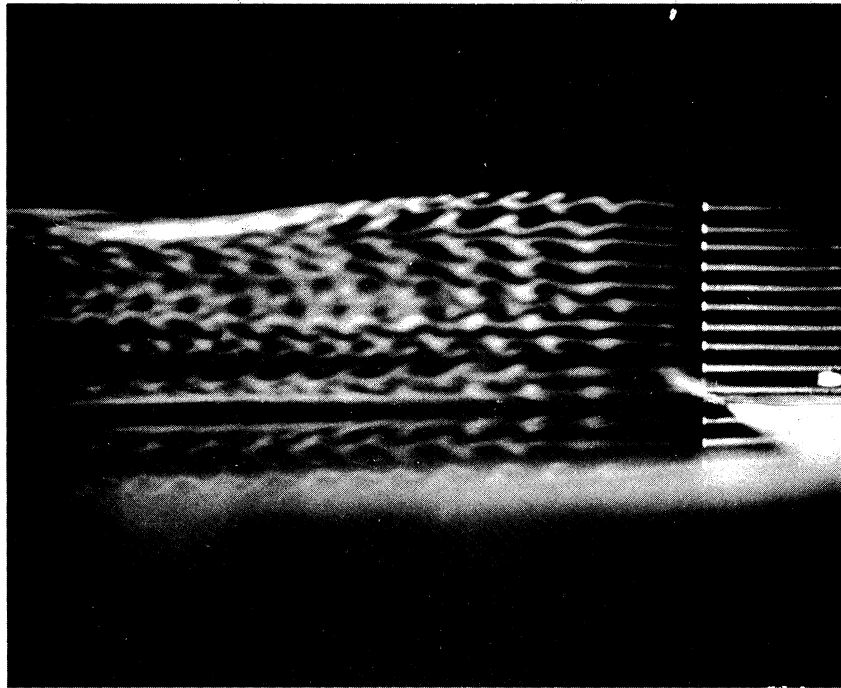
Figure 4-27. Smoke Photograph for $a = 0.01$ in., $\omega = 50$ cycle/sec., GrPr $= 1.08 \times 10^7$, $a\omega^2/g = 2.54$, $q/A = 92$ BTU/hr ft2, $R_e^2{}_V/Gr(a/L) = 18.4$.

Figure 4-30. Smoke Photograph for $a = 0.03$ in., $\omega = 50$ cycle/sec., GrPr $= 1.08 \times 10^7$, $a\omega^2/g = 7.69$, $q/A = 92$ BTU/hr ft^2, $R_e^2 \sqrt{Gr(a/L)} = 55.7$.

Figure 4-29. Smoke Photograph for $a = 0.022$ in., $\omega = 50$ cycle/sec., GrPr $= 1.08 \times 10^7$, $a\omega^2/g = 5.62$, $q/A = 92$ BTU/hr ft^2, $R_e^2 \sqrt{Gr(a/L)} = 40.7$.
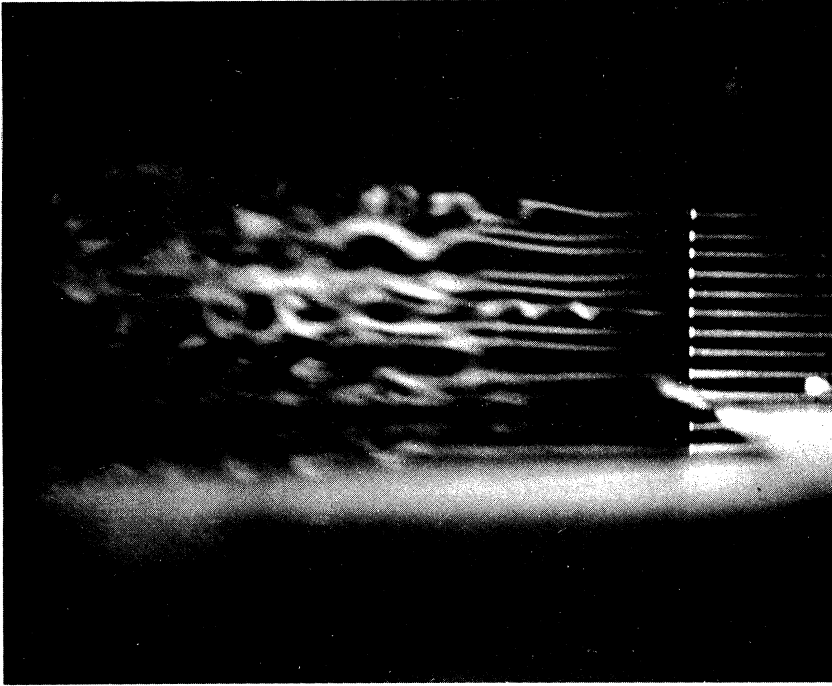
Figure 4-30. Smoke Photograph for $a = 0.03$ in., $\omega = 50$ cycle/sec., $GrPr = 1.08 \times 10^7$, $a\omega^2/g = 7.69$, $q/A = 92$ BTU/hr ft^2, $R_e{}^2{}_V/Gr(a/L) = 55.7$.

Figure 4-29. Smoke Photograph for $a = 0.022$ in., $\omega = 50$ cycle/sec., $GrPr = 1.08 \times 10^7$, $a\omega^2/g = 5.62$, $q/A = 92$ BTU/hr ft^2, $R_e{}^2{}_V/Gr(a/L) = 40.7$.
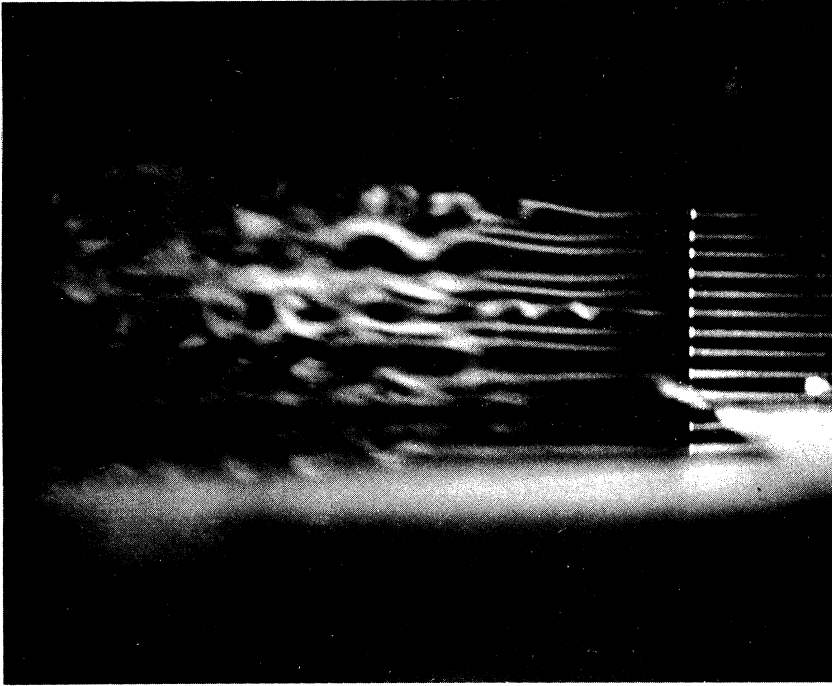
These photographs for different values of the pertinent parameters, listed on the figures, have also been related to Figures 4-21, 4-22, and 4-24. The conditions corresponding to the photographs are shown on these figures. The photographs, correlation data and this discussion attempt to disclose the source and mechanics of propagation of the vibratory disturbance. The significance of these results is that they definitely show the gross effect of a transitional phenomenon.

The method for obtaining data for Figures 4-22, 4-23 and 4-24 was to vary both amplitude and frequency for a given heater input to the plate. The inner smoke filaments were observed closely. When the inner filaments, approximately in the boundary layer, began to mix with each other. This was considered to be the start of transition. It was observed from the photographs that a disturbance originated outside the boundary layer in the potential flow region and propagated in toward the plate causing transition in the boundary layer. Also it was observed that this transition process depended on the Grashof-Prandtl number which is a product measure of the stability of the free convection flow. The critical condition was always found to occur at the top of the plate where the flow stability may be expected to be less.

Figures 4-26 through 4-31 are not to be interpreted as streamlines, pathlines or streak lines. What is seen in these photographs is a rather complicated phenomenon. In these photographs the smoke has an upward velocity which is superimposed on the velocity of the fluid. Outside the boundary-layer the effects of the potential flow can be seen.

The potential flow is oscillating with time at different angles, depending on location, with respect to the velocity of the flow. A smoke particle outside the boundary layer moving upward, due to its initial velocity is subjected to accelerations and decelerations from the potential flow thereby causing the smoke patterns. The flow in the boundary layer is predominately oscillating up and down and causes patterns in the boundary-layer to be different from those outside of the boundary-layer in the potential flow. This difference can be seen in the photographs. The flow was considered to be laminar as long as the smoke pattern in the boundary-layer was regular. When the pattern in the boundary-layer became irregular and smoke filaments mixed with each other, this condition was considered to be the critical condition. As the photographs indicate the disturbance originated outside the bounary-layer and propagated inwards causing a transional phenomenon to occur.

The laminar boundary layer can be distinguished in Figures 4-25, 4-26, 4-27, 4-28 and 4-32 because the patterns are still visible. Figure 4-29 represents what can be described as the beginning of this critical condition. The finer filaments of smoke are seen to start mixing with each other and the smoke outside the boundary-layer is irregular. Figures 4-30 and 4-31 are definitely in the turbulent region. Figure 4-30 indicates a large degree of turbulence outside the boundary-layer. The inner smoke filaments appear very turbulent. Figure 4-31 represents a high degree of turbulence and indicates apparently a churning action.

In the experimental work performed in this study a critical condition of transition was found. A correlation was experimentally found to determine the transition region from a laminar flow to what appears to be a turbulent flow. This condition was determined in two ways, first, by being indicated in the heat transfer experimental results and secondly, by the smoke studies. The transition region was found to be a function of the stability of the free convection boundary layer and a disturbance which propagates inward from the potential flow.

It is of value at this point in this study to investigate some other experimental results from the literature.

Discussion of Other Experimental Results

Kestin, Maeder and Sogin, reference (A-44) discussed the influence of turbulence on the heat transfer to cylinders near the stagnation point. They observed from experiment that when the boundary layer is laminar near the forward stagnation point there are large increases in heat transfer rate when the free stream velocity is large and when there exists a large downstream gradient in the amplitude of oscillation. A net decrease in the heat transfer rate for this type of oscillating system was predict by Kestin, Maeder and Wang, reference (A-17). In view of these conflicting results it is apparent that their theoretical model imperfectly represents the physical system. Two possibilities are suggested. First, the system of equations solved (A-17) does not properly represent the physical phenomena in the stagnation region in that normal-direction momentum effects are ignored. Second, turbulence may be encountered in the boundary layer which is not accounted for in the theoretical description.

Shine (A-35) used an Zehnder-Mach interferometer to study the boundary layer on a vertical, heated plate as it vibrates. His results showed that as the product of amplitude times frequency called, intensity of vibration, is increased, the heat transfer coefficient remains unchanged until a critical intensity of 0.52 ft/sec is reached. He found that coincident with the occurrence of a change in heat transfer coefficient there was an inception of waviness in the boundary layer. Also he found that this waviness was intensified by increases in vibration intensity. He pointed out that this waviness signifies a flow transition away from the laminar flow and presented this as a mechanism to explain the change in heat transfer rate. He presented some of his data as the ratio of the temperature differences between the plate and the ambient air for the vibrating conditions and a stationary plate condition. This is shown in Figure 4-33. In Figure 4-34 taken from Shine (A-35), are shown some typical photographs of waves in the fringes. The waviness was found to be increased regardless whether frequency or amplitude was increased as long as the intensity of vibration exceeded the critical point. The top two photographs have an intensity of 0 and .88 respectively. The remaining four interferograms have an intensity greater than critical and a waviness can easily be seen. Also the degree of waviness can be seen as the intensity is increased. In this way Shine predicted the critical intensity value. Shine did not take into account the conduction and radiation losses of the system. Also the test sections used were flat plates without restrictions to prevent three dimensional effects. This is different, of course, from the two dimensional case considered in the
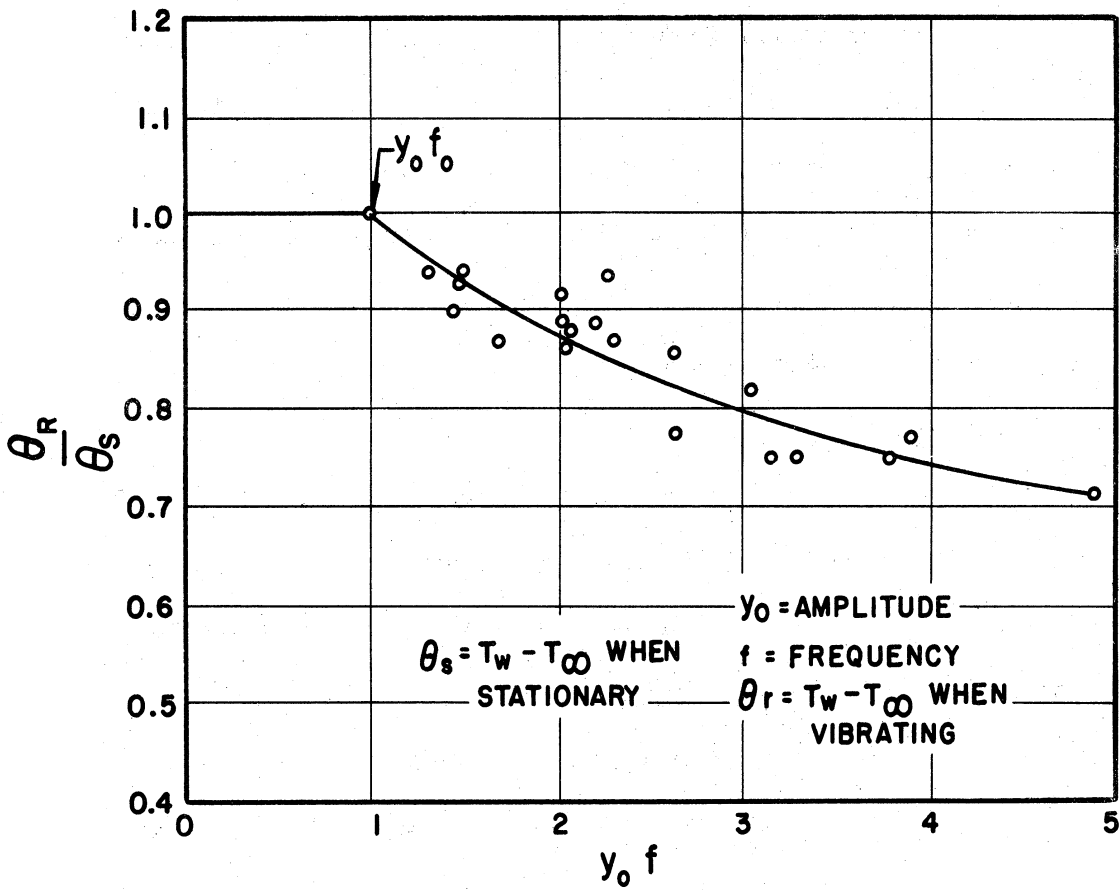
Figure 4-33. Experimental Heat Transfer Data Taken From
Shine (A-35)
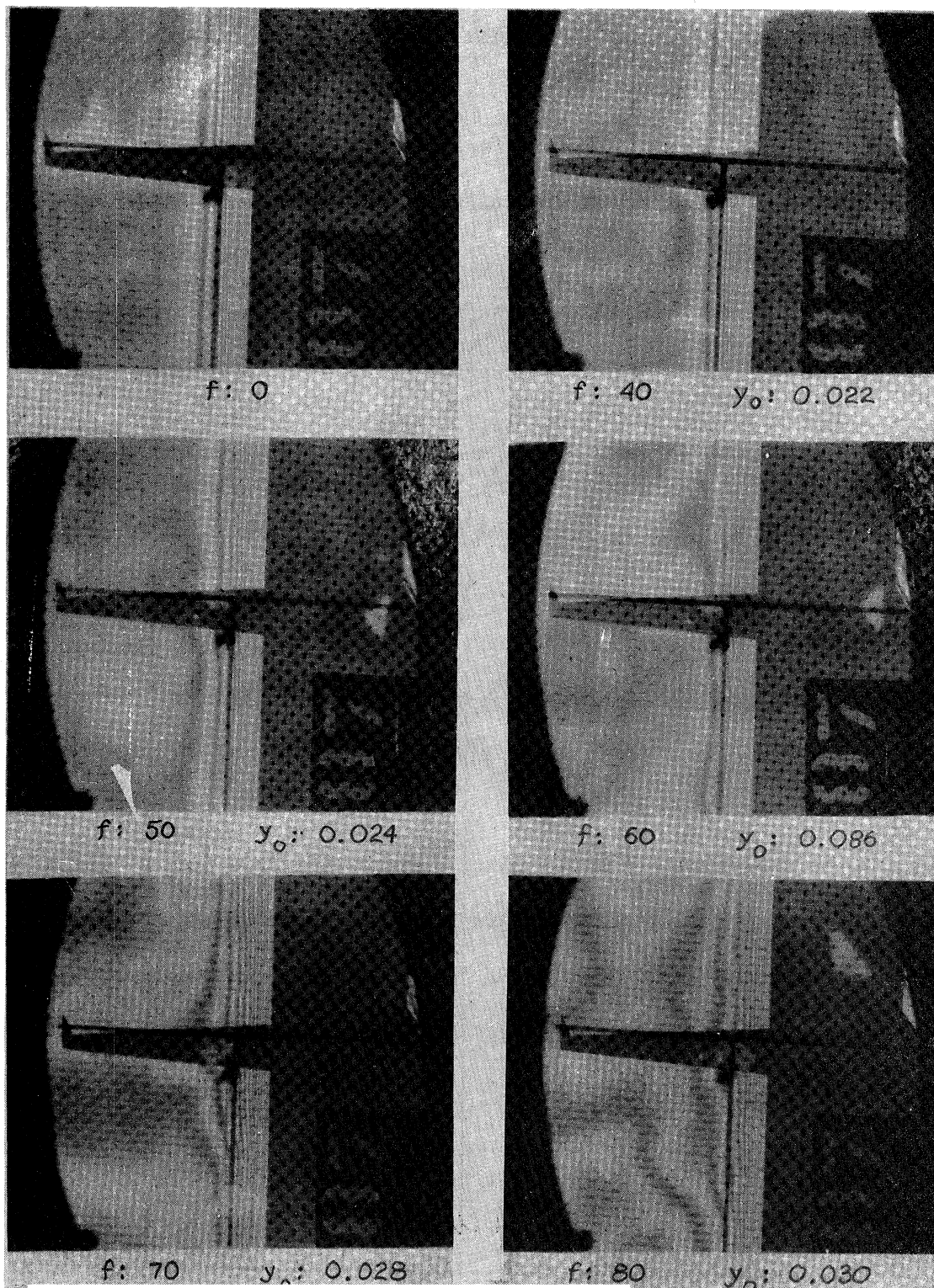
Figure 4-34. Photographs Showing Waves in the Fringes
Taken from Shine (A-35).

experiment. Another difference is that his plate was completely
heated while the test apparatus of this study was heated only in
the middle. Despite the differences these results support the
findings of the previous section in that a critical condition
occurs.

Some other pertinent experimental cases are those of
round cylinders undergoing both mechanical and acoustical vibration.
Both Westervelt (B-25) and Lighthill (A-20) pointed out that the
physical mechanism of interaction between free-convection from a
heated horizontal cylinder and horizontal vibration is essentially
the same, whether the vibrations are acoustically or mechanically
induced. This was demonstrated by Fand and Peebles (A-9). They
compared their findings, which treated horizontal vibration, to that
of Fand and Kaye (B-4) which treated the influence of sound. Their
results can be seen in Figure 4-35. They found a critical intensity
to be approximately 0.36 ft/sec, ascertained from the heat transfer
data. They tried smoke and photographic procedures, but found the
photographs not to be of publishable quality. As can be seen in
their results, Figure 4-35, at 0.7 ft/sec the data makes a bend.
Above this value Fand and Kaye have made the following empirical
correlation equation.

$$h_V = 0.722 \left[\Delta T (a w)^2 F \right]^{1/3} \tag{4-17}$$

The factor F is a geometrical weighing factor defined in reference (B-4).
They found that a flow visualization study indicated the observed increases
in the heat transfer coefficient to be that of vibrationally induced
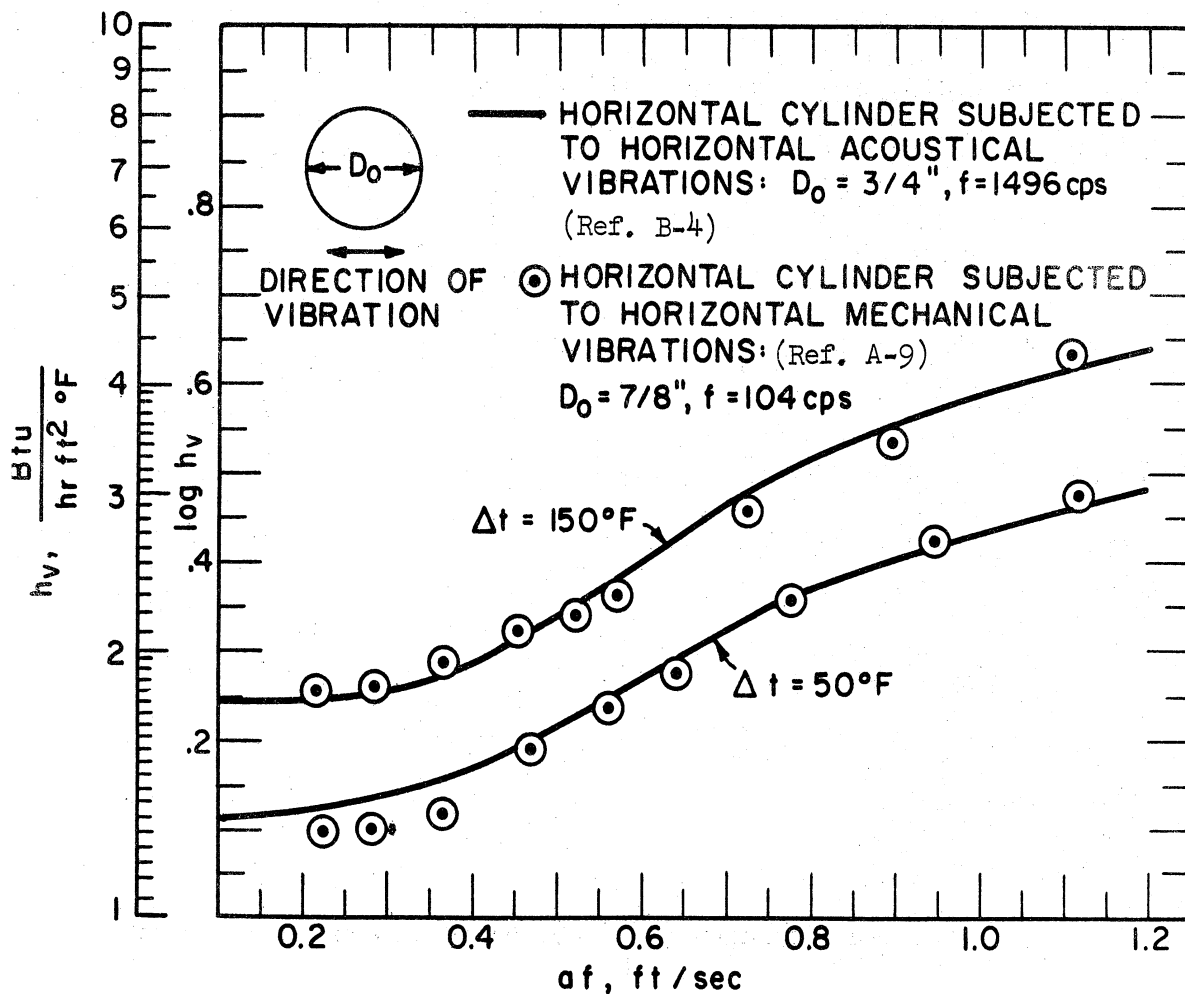
Figure 4-35. Comparison of Heat Transfer Data at Constant Difference in Temperature. For a Horizontal Heated Cylinder Subjected to Mechanical and Acoustical Vibrations in Air Taken from Fand and Peebles (A-9).

turbulence. They pointed out that this turbulent type of boundary-
layer flow differed radically from the vortex type of flow which
develops near a horizontal cylinder in the presence of acoustically
induced transverse vibrations. This vortex type of flow has been
called thermoacoustic streaming. Two photographs of the acoustic
streaming, from Fand and Kaye (B-4), are shown in Figures 4-36.
These photographs were taken by employing smoke as the indicating
medium. The smoke studies in this present work appear not to be that
of a vortex type of flow.

The results of Martinelli and Boelter (A-22) are shown in
Figure 4-37 for vertical vibrations of a horizontal cylinder in water.
As can be seen in their results, the heat transfer coefficient experi-
enced a critical condition. It should be noted however, that Boelter
reported that later measurements did not agree with the original
measurements.

It is appropriate at this point in the discussion to mention
briefly some work concerning boundary layer oscillations because of
their relevance to the problem of transition from laminar to turbulent
flow.

Eckert and Soehngen (A-7) conducted an experimental study of
the stability of laminar flow in free convection by using interference
photographs. They found that the instability region, the region where
small oscillations do not damp out, began at a Grashof number of 4×10^8.
Also they found that the velocity of the disturbance was approximately
73 per cent of the maximum flow velocity in the boundary layer at the
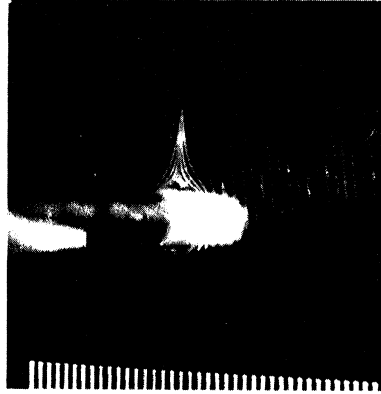
Free Convection: Δt = 200 $^{\circ}$F
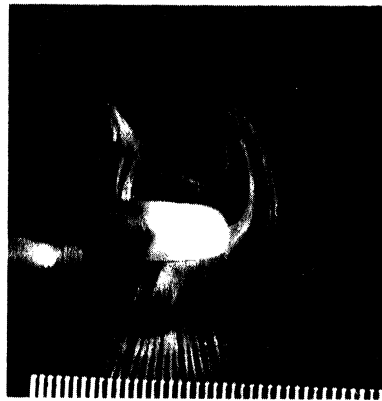
Thermoacoustic Streaming:
f = 1100 cps, SPL = 148 db, Δt = 200 $^{\circ}$F

Figure 4-36. Photograpsh Representing Acoustic Streaming Taken
from Fand and Kaye (B-4).

point of observation which was in the range of the value of the velocity at the point of inflection which is 0.683 U_{max}. They concluded that the boundary layer filtered out fluctuations of certain critical frequencies and amplified these until turbulent waves were produced.

Birch (A-2) studied critical boundary layer frequency in more detail by introducing controlled disturbances into the flow with an electrically pulsed wire. By utilizing an interferometer he determined wave lengths and amplitudes at the outer edges of the thermal boundary layer. He found that for certain disturbance frequencies higher amplitude oscillations were produced than for other disturbance frequencies. Because of this the conclusion was that the boundary layer absorbed energy more readily at these frequencies. Birch (A-2) made the following correlations

$$e^f = 1.65 \left(Gr_x \, Pr \right)^{0.08} \qquad (4\text{-}18)$$

and

$$e^\lambda = 18.2 \left(Gr_x \, Pr \right)^{0.091} \qquad (4\text{-}19)$$

where f is the disturbance frequency expressed in cycles per second and λ is the wave length expressed in inches. Since these frequencies and wave lengths represented some sort of resonance phenomena they were called "natural" values. It should be noted that f is not the frequency of the boundary layer oscillation but rather the pulse frequency. The boundary layer may vary well and does oscillate at a frequency different from that of the pulse frequency.

Holman, J. P., Gartrell, H. E., and Soehngen (B-7) investigated the physical processes involved in the propagation of oscillations in free convection boundary layers. A Zehnder Mach interferometer and motion picture camera were used to witness various boundary layer phenomena on a vertical flat isothermal plate. Disturbances were created in the boundary layer by introducing a fine wire into the boundary layer at various distances from the heated surface. The wire was pulsed with a square-wave electrical signal which heated it periodically and created pulses in the boundary layer. The pulse energy was, in general, of the order of one percent of the boundary layer energy. The pulse energy which is dissipated from the small heated wire creates a decrease in the air density of a small cylindrical volume around the wire so that through buoyancy forces an additional local velocity component is superimposed on the free convection profile. As this energy pulse moves up its energy is diffused throughout the boundary layer until it has finally imposed a velocity pulse on the whole field due to the transient heating process. This pulsing process is repeated periodically and waves advance up the plate in a complicated fashion. These waves become unstable and break up into more waves at higher frequencies. This instability occurs in a region of the plate which is characterized by a certain local Grashof number.

These authors also measured wave length, wave speed, and wave amplitude in plane free convection as functions of the distances from the leading edge and plate surface. Use was made of a wave energy parameter. The wave energy flux was written as

$$\text{Boundary layer wave energy} \sim \frac{1}{T} \lambda w_1^3 a^2 \tag{4-20}$$

where a is the amplitude of the wave and ω_1 is the boundary layer

frequency. They chose a wave energy parameter which

represents the wave energy flux to be

$$\lambda \omega^3 a^2 \tag{4-21}$$

since the absolute temperature varied only by eight percent. It was

found that wave energy was zero at the wall and increased towards the

outer layers of the boundary as the boundary layer became progressively

thicker. It was postulated that when the wave energy in the outer por-

tion of the boundary layer is large compared to that of the region near

the wall then transition turbulence begins. Experiments furnished some

confirmation of this postulate. It was also found that there is disturb-

ance frequency which will produce a maximum wave amplitude.

The above papers were investigated because of the existence of

a critical condition for laminar free convection flow. Since the Grashof

number is a type of Reynolds number and since the Prandtl number affects

the temperature field and thereby the Grashof number it was logical to

suspect that the critical condition was dependent in some way on both of

these numbers. Physically, the stability of a laminar free convection

flow decreases for increasing Grashof number. If the Grashof number is

large enough, of course, the flow is turbulent and small oscillations or

disturbances would immediately cause an increase in the heat transfer co-

efficient. Therefore it was postulated that for a constant Gr Pr product

the critical intensity is constant and for increasing values of Gr Pr

the critical intensity decreases and approaches zero when Gr Pr is

large enough for the flow to be turbulent to begin with without disturb-
ance or oscillations.   The data of Peebles and Fand (A-9) and Fand and
Kaye (A-8), in Figure 4-35, seem to show this effect.

CHAPTER V

SUMMARY OF RESULTS

In Chapter II the system of partial differential equations governing fluid motion and heat transfer were solved by a perturbation technique for the case of a finite vertical flat plate in free convection oscillating normal to its own plane. The behavior of the boundary layer due to oscillations of the finite plate were investigated. Two influences were found which alter the boundary layer flow. These influences are first, the potential flow outside the boundary layer and second, the existence of an inertial force within the boundary layer. The influence of the potential flow was found to predominate over the influence of the inertial force. The problem treated is for large Grashof numbers (boundary layer type of flow) subjected to the perturbing effect of potential flow for low vibrational amplitude and high frequency. The perturbation technique was used up to the second order solution in order to show time-independent effects. First order, periodic, and second order, time-independent, solutions were found for velocity, temperature, shear stress and Nusselt number. Calculated results are given for Prandtl numbers of 0.72 and 10. The Nusselt number was found to be decreased slightly for both Prandtl numbers. This theoretical result was confirmed in the experimental findings of Chapter IV.

The work of Reference (A-33) was extended in Chapter III to show time-independent effects resulting from transverse oscillations of an infinite, vertical plate in free convection. The alteration of the boundary layer is due to an oscillating pressure gradient which

arises from a coupling of the thermal variations of density with the acceleration (inertial force) of the oscillatory motion. A perturbation technique due to Reference (A-33) was used and extended by finding the second order solutions. A different method from that of Reference (A-33) was used in solving the first order solution in order to facilitate the second order solutions. Both first order solutions were found to agree within their range of applicability. First order and second order solution were found for velocity, temperature, shear stress and Nusselt number. Calculated results are given for Prandtl numbers of 0.72 and 10. The time-independent Nusselt number was found to decrease while the shear stress was found to increase under the influence of oscillation.

In both Chapters II and III it was shown that vibrations and flow oscillations are capable of causing permanent (time-independent) alterations in both the velocity and temperature profiles in the laminar boundary layer of systems having pressure gradients in the flow direction. This provides a secondary, time-independent flow, and permanently alters the wall shear stress and heat transfer rate. These changes are small and are detected from the analysis only when solutions are obtained to at least the second order approximation beyond the solution for the steady free convection problem. Furthermore, while the alteration in the wall shear stress is such as to increase its value, the opposite effect is both predicted and observed for the heat transfer rate under laminar flow conditions. This emphasizes an important character of this new class of phenomena, namely, that the traditional heat transfer - momentum transfer analogy is no longer a useful guide, at least for oscillating systems in laminar flow over flat surfaces. Similar phenomena associated

with curved surfaces, especially at stagnation points, may be quite different owing the necessity to consider a simultaneous influence of momentum effects in a direction normal to the surface. This is suggested by the experiments of Kestin, et al. (A-44).

Experimental findings are reported in Chapter IV. The heat transfer rate from a finite plate was found to decrease a small but definite amount due to being oscillated normal to its own plane for small values of a vibrational Reynolds number. This confirms the theoretical results of Chapter II. However, as the Reynolds number increased, sharp increases in the heat transfer rate were found. It would appear that a critical condition such as this represents transition from a laminar to a turbulent flow. Smoke studies indicate this transition is occurring. This critical condition was found for the transition of the free convection laminar boundary layer to a turbulent boundary layer and is described in terms of a critical vibratory Reynolds number dependent on the Grashof-Prandtl number of the laminar boundary layer.

A. UNSTEADY PAPERS

1. Anantanarayanan, R., Ramachandran, A., "Effect of Vibration on Heat Transfer from a Wire to Air in Parallel Flow," ASME Paper No. 57-A-100, July 1957.

2. Birch, W. D., "On the Stability of Free Convection Boundary Layers on a Vertical Flat Plate," M.S. Thesis, Air Force Institute of Technology, Wright-Patterson AFB, Ohio, 1957.

3. Carrier, G. F., DiPrima, R. C., "On the Unsteady Motion of a Viscous Fluid Past a Semi-Infinite Flat Plate," Journal of Mathematics and Physics, January 1957, pp. 359-383.

4. Cheng, S. I., Elliot, D., "The Unsteady Laminar Boundary Layer on a Flat Plate," Proc. Heat Transfer and Fluid Mechanics Institute (1956), Trans. ASME, Vol. 79, (1957), pp. 725-753.

5. Cheng, S. I., "Some Aspects of Unsteady Boundary Layer Flows," Quarterly of Applied Mathematics, (January 1957), pp. 359-383.

6. Chung, P. M., Anderson, A. O., "Unsteady Laminar Free Convection," Journal of Heat Transfer, Series C., No. 4, November 1961.

7. Eckert, E. R. G., and Soehengen, F., "Interferometric Studies on the Stability and Transition to Turbulence of a Free Convection Boundary Layer," Proc. General Discussion on Heat Transfer, Inst. of Mech. Engr., London, 1951.

8. Fand, R. M., Kaye, J., "The Influence of Vertical Vibrations on Heat Transfer by Free Convection from a Horizontal Cylinder," Second International Heat Transfer Conference, Boulder, Colorado, (1961) Paper A-17.

9. Fand, R. M., Peebles, F. M., "A Comparison of the Influence of Mechanical and Acoustical Vibrations on Free Convection from a Horizontal Cylinder," To be published.

10. Goldstein, R. J., Eckert, E. R. G., "The Steady and Transient Free Convection Boundary Layer on a Uniformly Heated Vertical Plate," Int. J. Heat Mass Transfer, Vol. 1, (1960), pp. 208-218.

11. Glauert, M. B., "The Laminar Boundary Layer on Oscillating Plates and Cylinders," Journal Fluid Mech., Vol. 1, (1956), pp. 97-110.

12. Harrje, D. T., Croke, E. J., "Heat Transfer in Oscillating Flow," Princeton Aero. Eng. Rept. #483, October 3, 1959.

13. Hassan, M. A., "On Unsteady Boundary Layers," Journal of Fluid Mechanics, Vol. 9, Part 2, October 1960.

14. Hellums, J. D., "Finite Difference Computation of Natural Convection Heat Transfer," Ph.D. Thesis, University of Michigan, September 1960.

15. Hill, P. G., Stenning, A. M., "Laminar Boundary Layers in Oscillatory Flow," (59-A-265) Journal of Basic Engineering, Vol. 82, Series D, No. 3, (1960), pp. 593.

16. Karlsson, S. K. F., "An Unsteady Turbulent Boundary Layer," Journal of Fluid Mechanics, Vol. 5, Part 4, (1951), pp. 622-636.

17. Kestin, J., Maeder, P. F., Wang, H. E., "On Boundary Layers Associated with Oscillating Streams," Appl. Sci. Res., Section A., Vol. 10, 1960.

18. Layton, J. P., "Heat Transfer in Oscillating Flow," Princeton Aero Engr. Rept. #266A, May 15, 1956.

19. Lemlich, R., "Effect of Vibration on Natural Convection Heat Transfer," Industrial and Eng. Chem 47, (1955), pp. 1175-1180.

20. Lighthill, M. J., "The Response of Laminar Skin Friction and Heat Transfer to Fluctuations in the Stream Velocity," Proc. Roy. Soc. Ser. A., Vol. 224, (1954), pp. 1-24.

21. Lin, C. C., "Motion in the Boundary Layer with Rapidly Oscillating External Flow," Proc. IX Int. Cong. Appl. Mech. (1956) Vol. 4, pp. 155.

22. Martinelli, R. C., Boelter, L. M. K., "The Effect of Vibration on Heat Transfer by Free Convection from a Horizontal Cylinder," Proc. 5th Int. Cong. of Appl. Mech., (1938), p. 578.

23. Martini, W. R., Carr, J. W., Churchill, S. W., "Machine Computation of Natural Convection Inside a Horizontal Cylinder," Mimeograph Sheets.

24. Mickelson, W. R., and Laurence, J. E., "Measurements and Analysis of Turbulent Flow Containing Periodic Flow Fluctuations," NACA RM E53 F19, 1953.

25. Moore, F. K., "Unsteady Laminar Boundary-Layer Flow," NACA, TN 2471, 1951.

26. Nickerson, R. J., "The Effect of Free-Stream Oscillations on the Laminar Boundary Layers on a Flat Plate," WADC Tr 57-481, ASTIA Doc. No. AD 210477, Wright Air Development Center, December 1958.

27. Ostrach, S., "Note on the Aerodynamic Heating of an Oscillating Surface," NACA Tn 3146, 1954.

28. Ostrach, S., "Compressible Laminar Boundary Layer and Heat Transfer for Unsteady Motions of a Flat Plate," NACA TN 3569, 1955.

29. Rosenblat, S., "Torsional Oscillations of a Plane in a Viscous Fluid," Journal of Fluid Mechanics, Vol. t, (1959) pp. 206-222.

30. Rott, N., "Unsteady Viscous Flow in the Vicinity of a Stagnation Point," Quarterly of Applied Math., Vol. 13, No. 4, 1956.

31. Rozin, L. A., "The Growth of a Laminar Boundary Layer on a Flat Plate Set Impulsively into Motion," Jour. of Applied Math. and Mechanics, Trans. of the Soviet Journal, Prilkaoniaia Matematika 1 Mekhanika, Pergamon Press, Vol. 22, (1958), pp. 568-575.

32. Schlichting, H., "Berechung ebener periodischer Grenzschicht Stroemungen," Phy. Zs. 33., (1932), p. 327.

33. Schoenhals, R. J., Clark, J. A., "The Response of Laminar Incompressible Fluid Flow and Heat Transfer to Transverse Wall Vibrations," ASME Paper No. 61-WA-174, 1961.

34. Schoenhals, R. J., "The Response of Laminar Incompressible Fluid Flow and Heat Transfer to Transverse Wall Vibrations," Ph.D. Thesis, University of Michigan, January 1961.

35. Shine, A. J., "The Effect of Transverse Vibrations on the Heat Transfer Rate from a Heated Vertical Plate," M.S. Thesis, Air Inst. of Tech., Wright-Patterson Air Force Base, Ohio, (1957), ASME Preprint 59-HT-27.

36. Siegel, R., "Transient Free Convection from a Vertical Flat Plate," ASME Paper No. 57-SA-8, 1957.

37. Stuart, J. T., "Solutions of the N. S. and Energy Equations Illustrating the Response of Skin Friction and Temperature of an Infinite Plate Thermometer to Fluctuations in the Stress Velocity," Proc. Royal Soc., Vol. 231, Series A, (1955), p. 116.

38. Teleki, C., "The Influence of Vertical Vibrations on the Rate of Heat Transfer from a Horizontal Cylinder in Air," WADC Technical Note 59-357, Aeronautical Research Lab., Oct. 1960.

39. Tennekes, H., "Another Unsteady Turbulent Boundary Layer," John Hopkins Univ. Contract AF 49(638) - 496, May 1959.

40. Tsui, Y. T., "The Effect of Vibrations on Heat Transfer Coefficients," Ph.D. Thesis, Ohio State University, 1952.

41. West, F. B., and Taylor, A. T., "The Effect of Pulsations on Heat Transfer," Chem. Eng. Progress, Vol. 48, 1953.

42. Wu, T. Y., "Small Perturbations in the Unsteady Flow of a Compressible Viscous and Heat-Conducting Fluid," Journ. of Math. and Physics, (January 1957), pp. 13-27.

43. Wang, K. T., "Unsteady Laminar Boundary Layers in an Incompressible Stagnation Flow," Jour. of Basic Engineering, Vol. 25, No. 4, (1958), p. 421.

44. Kestin, J., Maeder, P. F., Sogin, H. H., "The Influence of Turbulence on the Transfer of Heat to Cylinders Near the Stagnation Point," Jour. of Applied Math. and Physics (ZAMP) Vol. XII, Fasc. 2, (1961), pp. 115-132.

B. RELATED PAPERS FROM THE FIELD OF ACOUSTICS

1. Andres, J. M. and Ingard, U., "Acoustic Steaming at High Reynolds Numbers," Journal Acoust. Soc. Am. 25, 928, 1953.

2. Andres, J. M., and Ingard, U., "Acoustic Steaming at Low Reynolds Numbers," Journal Acoust. Soc. Am. 25, 032, 1953.

3. Eckert, C., "Vortices and Streams Caused by Sound Waves," Phys. Rev. 73, 68, 1958.

4. Fand, R. M., Kaye, J., "The Effect of High Intensity Stationary and Progressive Sound Fields on Free Convection from a Horizontal Cylinder," WADC Tech. Note 59-18, ASTIA Doc. No. AD 209532, March 1959.

5. Holman, J. P., "The Mechanism of Sound Field Effects on Heat Transfer," Jour. of Heat Transfer, Tech. Brief, Vol. 82, Series C., No. 4, (November 1960), p. 393.

6. Holman, J. P., Mott-Smith, T. P., "The Effect of High Constant Pressure Sound Fields on Free Convection Heat Transfer from a Horizontal Cylinder," WADC Technical Note 58-352, ASTIA Doc. No. AD 206906, Wright Air. Dev. Center, December 1958.

7. Holman, J. P., Gartrell, H. E., Soehngen, E. E., "A Study of Free Convection Boundary Layer Oscillations and Their Effects on Heat Transfer," WADD Tech. Rep. 59-3, Wright Air. Dev. Div., December 1959.

8. Holtsmark, J., Johnsen, I., Sekkelanc, T., and Skavlen, S., "Boundary Layer Flow Near a Cylindrical Obstacle in an Oscillating Incompressible Fluid," J. Acoustical Soc. Am. 26, 1954.

9. Hunt, F. V., "Notes on the Exact Equations Governing the Propagation of Sound in Fluids," J. Acoustic Soc. Am. 27, 1019, 1955.

10. Jackson, T. W., Harrison, W. B., and Boteler, W. C., "Free Convection, Forced Convection, and Acoustic Vibrations in a Constant Temperature Vertical Tube," ASME Paper No. 58-HT-6, September, 1958.

11. Lane, C. A., "Acoustical Streaming in the Vicinity of a Sphere," J. Acoust. Soc. Am. 27, 1082 (1955).

12. Mawardi, O. K., "On the Thermo-Acoustic Transduction in Potential Flow," J. Acoustic Soc. Am., 28, 239, 1956.

13. Mawardi, O. K., "On Acoustic Boundary Layer Heating," J. Acoustic Soc. Am. 26, 766, 1954.

14. Medwin, H., and Rudnick, I., "Surface and Volume Vorticity in Acoustic Fields," J. Acoustic Soc. Am. 25, 1953.

15. Nyborg, W. L., "Acoustic Streaming Due to Attenuated Plane Waves," Jour. Acoustic Soc. Am. 25, (1953), p. 68-75.

16. Nyborg, W. L., "Acoustic Streaming Near a Boundary," Jour. Acoustic Soc. Am. 30, (1958), p. 329-339.

17. Raney, W. P., Corelli, J. C., and Westervelt, F. J., "Acoustical Streaming in the Vicinity of a Cylinder," J. Acoustic Soc. Am. 26, 1007, 1954.

18. Soehngen, E. E., Holman, J. P., "Experimental Studies on the Interaction of Strong Sound Fields with Free Convection Boundary Layers," ARL Tech Rep. 60-232, October 1960.

19. Sprott, A. L., Holman, J. P., Durand, F. L., "An Experimental Study of the Interaction of Strong Sound Fields with Free Convection Boundary Layers," WADC Tech. Rep. 59-717, Wright Air Dev. Center, November, 1959.

20. Spurlock, J. M., Jackson, T. W., Purdy, K. R., Oliver, C. C., Johnson, H. L., "The Effects of Resonant Acoustic Vibrations on Heat Transfer to Air in Horizontal Tubes," WADC TN 59-330 Contract No. AF 33(616)-5742, Wright Air Dev. Center, June 1959.

21. Walker, C. T., Adams, C. E., "Thermal Effects of Acoustic Streaming Near a Cylindrical Boundary," Jour. Acoustic Soc. Am. 31, (1959) pp. 813-814.

22. Westervelt, F. J., "The Theory of Steady Rotational Flow Generated by a Sound Field," Jour. Acoustic Soc. Am. 25, 60, 1953.

23. Westervelt, F. J., "Hydrodynamic Flow and Oseen's Approximations," J. Acoustic Soc. Am. 25, 951, 1953.

24. Westervelt, F. J., "Acoustic Streaming near a Small Obstacle," Jour. Acoustic Soc. Am. 25, (1953), p. 1123.

25. Westervelt, F. J., "The Effects of Sound Waves on Heat Transfer," Jour. Acoustic Soc. Am., Vol. 32, No. 3, (March 1960), pp. 337-338.

26. Zartman, W. N., "Heat Transfer from Acoustically Resonating Gas Flames in a Cylindrical Burner," University of Michigan, Ph.D. Thesis, 1960.

C. RELATED PAPERS AND BOOKS

1. Eckert, E. R. G., Soehngen, E. E., "Studies on Heat Transfer in Laminar Free Convection with the Zehnder-Mach Interferometer," Tech. Rep. No. 5747, ATI No. 44580, Air Materiel Command (Dayton, Ohio) December 27, 1948.

2. Ku, Y. K., "Boundary Layer Problems Solved by the Method of Non-linear Mechanics," Proc. IX Int. Cong. Appl. Mech., Vol. 4, (1956), 132.

3. Levy, S., "Effect of Large Temperature Changes (Including Viscous Heating) Upon Laminar Boundary Layers with Variable Free-Stream Velocity," J. of the Aero. Sciences, Vol. 21, No. 7, (1954), pp. 459-474.

4. Martini, W. R., "Natural Convection Inside a Horizontal Cylinder," Ph.D. Thesis, University of Michigan, August 1956.

5. McAdams, W. H., Heat Transmission, Third Edition, McGraw-Hill Book Company, Inc., 1942.

6. Ostrach, S., "An Analysis of Laminar Free-Convection Flow and Heat Transfer About a Flat Plate Parallel to the Direction of the Generating Body Force," U.S. NACA TN2635, 1952.

7. Ostrach, S., "Laminar Natural Convection Flow and Heat Transfer of Fluids with and without Heat Sources in Channels with Constant Wall Temperatures," NACA TN 2863, December 1952.

8. Ostrach, S., "An Analysis of Laminar Free-Convection Flow and Heat Transfer About a Flat Plate Parallel to the Direction of the Direction of the Generating Body Force," NACA TR 1111, 1953.

9. Ostrach, S., Thornton, P. R., "On the Stagnation of Natural-Convection Flows in Closed-End Tubes," ASME Paper No. 57-SA-2, 1957.

10. Schecter, R. S., Isbin, H. S., "Natural Convection Heat Transfer in Regions of Maximum Fluid Density," AICHE Paper No. 570HT-25, 1957.

11. Schmidt, E., and Beckman, W., "Das Temperatures-und Geschwundegkeits-feld von einer Warme abgehenden senkrechter Platte bei naturlicher Konvektion," Tech. Mech. U. Thermodynamick, Bd. 1 Nr. 10, Oxt. 1930, pp. 341-349; cont. Bd. 1, Nr. 11, Nov. 1930, pp. 391-406.

12. Sparrow, W. M., Gregg, J. L., "Laminar Free Convection From a Vertical Plate with Uniform Surface Heat Flux," Trans. ASME, Vol. 78, (1956), pp. 435-440.

13. Sparrow, E. M., Gregg, J. L., "Similar Solutions for Free Convection from a Nonisothermal Vertical Plate," ASME, Paper No. 57-SA-3, 1957.

14. Sparrow, E. M., Gregg, J. L., "The Variable Fluid-Property Problem in Free Convection," ASME Paper No. 57-a-46, 1958.

15. Sparrow, E. M., Gregg, J. L., "Prandtl Number Effects on Unsteady Forced Convection Heat Transfer," NACA TN 4311, 1958.

16. Sparrow, E. M., Eichhorn, R., Gregg, J. L., "Combined Forced and Free Convection in a Boundary Layer Flow," The Physics of Fluids, Vol. 2, No. 3, May-June 1959.

17. Tomotika, S., Yosinobu, M., "The Flow of a Viscous Liquid Past a Flat Plate at Small Reynolds Numbers," Jour. of Math. and Physics, (January 1957), pp. 1-12.

APPENDIX I

COMPUTER EVALUATION METHOD

The method of two of the programs are presented herein by which solutions to the two analytical cases of Chapters II and III were numerically evaluated. This method was found to be lengthy due to the algebra involved but very advantageous from an accuracy of results standpoint. It should be noted that the similarity of this method for the analytical cases lies in the general flow of the programming and not in the detailed algebra of each specific case. The programs were written in MAD Language, Michigan Algorithm Development, for the IBM 709 digital computer at the University of Michigan Computing Center.

Each analytical case was divided into approximately five programs which were dependent, except for the first program, on the preceeding program. The punched output and printed results from each program were checked for errors and discrepancies. The punched output were then entered as data in the subsequent programs. To make these points clear two of the smaller programs are included in this section. They come from Chapter III. The following symbols were used.

$$A(0) = \zeta(0)$$
$$A(1) = K_1$$
$$A(2) = K_2$$
$$A(3) = H'(0)$$
$$A(4) = P_R$$
$$A(5) = \omega$$

$A(6) = X$

$B(I) = \eta$

$X(1) = \text{Real } V_1$

$X(2) = \text{Real } V_2$

$\circ$

$\circ$

$\circ$

$Z(1) = \text{Imag. } V_1$

$Z(2) = \text{Imag. } V_2$

$\circ$

$\circ$

$\circ$

$U(1) = \text{Real } \left(\dfrac{2V_1}{2X}\right)$

$U(2) = \text{Real } \left(\dfrac{2V_2}{2X}\right)$

$\circ$

$\circ$

$V(1) = \text{Imag. } \left(\dfrac{2V_1}{2X}\right)$

$V(2) = \text{Imag. } \left(\dfrac{2V_2}{2X}\right)$

For example the first order velocity is

$$ U_1 = V_1 e^{-K_1 \eta} - V_1 e^{-\sqrt{i\gamma}\,\eta} + V_2\, \eta\, e^{-K_1 \eta} $$

where

$$ V_1 = \frac{-\mathcal{Y}(0)}{(4X)^{1/4}\left[K_1{}^2 - i\omega\,(4X)^{1/2}\right]} - \frac{2\,\mathcal{Y}(0)\,K_1{}^2}{(4X)^{1/4}\left[K_1{}^2 - i\omega\,(4X)^{1/2}\right]^2} \;,\quad V_2 = \frac{-\mathcal{Y}(0)\,K_1}{(4X)^{1/4}\left[K_1{}^2 - i\omega\,(4X)^{1/2}\right]} \;, $$

The program called part 1 on page 217 is evaluated by the computer

first. The punched output of part 1 is then entered as data into prog-

ram ANA 1A. The printed results of ANA 1A are first order velocity

and temperature versus η for each specific value of Prandtl number, X

and frequency.

For higher values of V_n the derivative with respect to X became

very difficult because of the large amount of algebra involved. These

V_n were evaluated by taking finite difference derivatives in the program
by

$$U(m) = \frac{U(m)_{X_0 + \Delta X} - U(m)_{X_0}}{\Delta X}$$

To make certain that ΔX was small enough for each case, different values

of ΔX were evaluated and compared to the exact derivative. Four place

accuracy was the criteria.

```
VICTOR D. BLANKENSHIP          S141F              003   015   200    PART IA
VICTOR D. BLANKENSHIP          S141F              003   015   200    PART IA
$ PRINT OBJECT, PUNCH OBJE CT                                PART1000
$ COMPILE MAD, EXECUTE, DUMP                                             001
                DIMENSION A(100),X(100),Y(100),Z(100)
START           READ DATA
                Y(0)=4.*A(6)
                Y(1)=SQRT.(Y(0))                                        *07
                Y(2)=SQRT.(Y(1))                                        008
                Y(3)=A(1)*A(1)                                          009
                Y(4)=Y(3)*Y(3)                                          010
                Y(5)=Y(3)*Y(4)                                          011
                Y(6)=Y(4)+A(5)*A(5)*Y(0)                                012
                Y(7)=Y(6)*Y(6)                                          013
                X(1)=(-3.*A(0)*Y(5)+A(0)*Y(3)*A(5)*A(5)*Y(0))/(Y(2)*Y(6)*Y(6)  014
                1)                                                      015
                Z(1)=(-5.*A(0)*A(5)*Y(2)*Y(4)-A(0)*Y(2)*Y(1)*Y(1)*A(5)  016
                1*A(5)*A(5))/(Y(6)*Y(6))                                017
                X(2)=-A(0)*A(1)*Y(3)/(Y(2)*Y(6))                        018
                Z(2)=-A(0)*A(1)*Y(2)*A(5)/Y(6)                          019
                Y(8)=Y(5)-3.*Y(3)*A(5)*A(5)*Y(0)                        020
                Y(9)=-3.*Y(4)*A(5)*Y(1)+A(5)*A(5)*A(5)*Y(1)*Y(1)*Y(1)   021
                Y(10)=A(0)*(3.*Y(4)/(Y(2).P.5)-3.*A(5)*A(5)/Y(2))       022
                Y(11)=-14.*A(0)*Y(3)*A(5)/(Y(2).P.3.)
                Y(12)=Y(6)*Y(6)*Y(6)                                    024
                X(0)=(Y(10)*Y(8)+Y(11)*Y(9))/Y(12)                      025
                Z(0)=(Y(11)*Y(8)-Y(10)*Y(9))/Y(12)                      026
                Y(13)=Y(4)-A(5)*A(5)*Y(0)                               027
                Y(14)=-2.*Y(3)*A(5)*Y(1)                                028
                Y(15)=A(0)*A(1)*Y(3)/(Y(2).P.5)
                Y(16)=-A(0)*3.*A(5)*A(1)/(Y(2).P.3)
                X(24)=(Y(15)*Y(13)+Y(16)*Y(14))/Y(7)                    031
                Z(24)=(Y(16)*Y(13)-Y(15)*Y(14))/Y(7)                    032
                Y(17)=-A(3)*Y(2)*A(4)/(SQRT.(2.*A(5)))                  033
                X(5)=Y(17)*(X(0)+Z(0))                                  034
                Z(5)=Y(17)*(Z(0)-X(0))                                  035
                Y(18)=-A(2)*A(4)/Y(1)                                   036
                X(7)=Y(18)*X(1)                                         037
                Z(7)=Y(18)*Z(1)                                         038
                Y(19)=-A(3)/A(2)                                        039
                X(6)=Y(19)*X(7)+X(5)/Y(19)                              040
                Z(6)=Y(19)*Z(7)+Z(5)/Y(19)                              041
                Y(20)=Y(19)/A(1)                                        042
                Y(21)=A(3)*Y(1)*A(4)/A(1)                               043
                Y(22)=A(3)*A(4)/(Y(3)*Y(1))                             044
                X(3)=-X(5)-Y(20)*X(7)-Y(21)*(X(0)+X(24)/A(1))-Y(22)*X(2)  045
                Z(3)=-Z(5)-Y(20)*Z(7)-Y(21)*(Z(0)+Z(24)/A(1))-Y(22)*Z(2)  046
                X(4)=X(3)/Y(19)                                         047
                Z(4)=Z(3)/Y(19)                                         048
                Y(23)=2.*A(2)*A(4)/Y(1)                                 049
                X(13)=0.
                Z(13)=0.
                Y(24)=0.5+Y(19)                                        052
                Y(25)=A(2)*A(4)*Y(1)/A(1)                               053
                X(12)=-Y(25)*X(24)-Y(23)*X(2)/(2.*A(1))
                Z(12)=-Y(25)*Z(24)-Y(23)*Z(2)/(2.*A(1))
                X(8)=-X(3)-X(5)                                         056
                Z(8)=-Z(3)-Z(5)                                         057
                Y(26)=-2.*Y(19)                                         058
```

```
Y(27)=0.5*Y(20)                                                     059
X(11)=X(8)/Y(19)+Y(19)*X(12)
Z(11)=Z(8)/Y(19)+Y(19)*Z(12)
X(9)=SQRT.(A(5)*Y(1)/2.)                                            062
Z(9)=X(9)                                                          063
X(10)=A(1)+X(9)                                                    064
Z(10)=Z(9)                                                         065
Y(28)=X(10)*X(10)-Z(10)*Z(10)                                      066
Y(29)=A(5)*A(4)*Y(1)                                               067
Y(30)=2.*X(10)*Z(10)-Y(29)                                         068
Y(31)=Y(4)+Y(29)*Y(29)                                             069
X(16)=(Y(3)*X(4)-Y(29)*Z(4))/Y(31)                                 070
Z(16)=(Y(3)*Z(4)+Y(29)*X(4))/Y(31)                                 071
X(15)=(Y(3)*X(3)+2.*A(1)*Y(3)*X(16)-Y(29)*(Z(3)+2.*A(1)*Z(16)      072
1))/Y(31)                                                          073
Z(15)=(Y(3)*Z(3)+2.*A(1)*Y(3)*Z(16)+Y(29)*(X(3)+2.*A(1)*X(16)      074
1))/Y(31)                                                          075
Y(32)=Y(28)*Y(28)+Y(30)*Y(30)                                      076
X(19)=(X(7)*Y(28)+Z(7)*Y(30))/Y(32)                                077
Z(19)=(Z(7)*Y(28)-X(7)*Y(30))/Y(32)                                078
X(18)=(X(6)*Y(28)+Z(6)*Y(30)+4.*Y(28)*(X(10)*X(19)-Z(10)*Z(19      079
1))+4.*Y(30)*(X(19)*Z(10)+X(10)*Z(19)))/Y(32)                      080
Z(18)=(Z(6)*Y(28)-X(6)*Y(30)+4.*Y(28)*(X(19)*Z(10)+Z(19)*X(10      081
1))-4.*Y(30)*(X(10)*X(19)-Z(10)*Z(19)))/Y(32)                      082
X(17)=(X(5)*Y(28)+Z(5)*Y(30)-2.*X(19)*Y(28)-2.*Z(19)*Y(30)         083
1+2.*Y(28)*(X(10)*X(18)-Z(10)*Z(18))+2.*Y(30)*(Z(10)               084
2*X(18)+X(10)*Z(18)))/Y(32)                                        085
Z(17)=(Z(5)*Y(28)-X(5)*Y(30)-2.*Z(19)*Y(28)+2.*X(19)               086
1*Y(30)+2.*T(28)-(Z(10)-X(18)+X(10)*Z(18))-2.*Y(30)*(X(10)         087
2*X(18)-Z(10)*Z(18)))/Y(32)                                        088
Y(33)=16.*Y(4)+Y(29)*Y(29)                                         089
Y(34)=4.*Y(3)                                                      090
X(23)=(Y(34)*X(13)-Y(29)*Z(13))/Y(33)                              091
Z(23)=(Y(34)*Z(13)+Y(29)*X(13))/Y(33)                              092
X(22)=(Y(34)*X(12)+48.*A(1)*Y(3)*X(23)-Y(29)*(Z(12)+12.            093
1*A(1)*Z(23)))/Y(33)                                               094
Z(22)=(Y(34)*Z(12)+48.*A(1)*Y(3)*Z(23)+Y(29)                       095
1*(X(12)+12.*A(1)*X(23)))/Y(33)                                    096
X(21)=(Y(34)*(X(11)-6.*X(23)+8.*A(1)*X(22))-Y(29)*(Z(11)           097
1-6.*Z(23)+8.*A(1)*Z(22)))/Y(33)                                   098
Z(21)=(Y(34)*(Z(11)-6.*Z(23)+8.*A(1)*Z(22))+Y(29)                  099
1*(X(11)-6.*X(23)+8.*A(1)*X(22)))/Y(33)                            100
Y(35)=X(8)-2.*X(22)
Y(36)=Z(8)-2.*Z(22)***0
X(20)=(Y(34)*(Y(35)+4.*A(1)*X(21))-Y(29)*(Y(36)+4.*A(1)
1*Z(21)))/Y(33)                                                    102
Z(20)=(Y(34)*(Y(36)+4.*A(1)*Z(21))+Y(29)*(Y(35)+4.*A(1)
1*X(21)))/Y(33)                                                    104
X(14)=-X(15)-X(17)-X(20)                                           105
Z(14)=-Z(15)-Z(17)-Z(20)                                           106
PRINT FORMAT DATA,A(0)...A(6)                                      004
VECTOR VALUES DATA=$6E12.4*$                                       005
WHENEVER CHECK.NE.0.,PRINT RESULTS Y(0)...Y(34)
PRINT COMMENT $ X(0)...X(24)$
PRINT FORMAT RESULT,X(0)...X(24)
PUNCH FORMAT INPUT,X(0)...X(24)
PRINT COMMENT $ Z(0)...Z(24)$
PRINT FORMAT RESULT,Z(0)...Z(24)
```

```
          PUNCH FORMAT INPUT,Z(0)...Z(24)
          VECTOR VALUES INPUT=$6K12*$
          VECTOR VALUES RESULT=$1H0,5E15.5*$
          TRANSFER TO START                                          109
          VECTOR VALUES CHECK=0.
          END OF PROGRAM                                             110
$ DATA
 VICTOR D. BLANKENSHIP          S141F          005   010   090    ANA 1A
 VICTOR D. BLANKENSHIP          S141F          005   010   090    ANA 1A
$ COMPILE MAD, EXECUTE, PUNCH OBJECT, PRINT OBJECT, DUMP
          DIMENSION A(100),B(100),X(100),Z(100),
         1YC(70),YD(70),YE(70),YF(70),YG(70),
         2YH(70),YH(70),UR(70),UI(70),UT(70),
         3UA(70),YI(70),YJ(70),YK(70),YL(70),YM(70),
         4YN(70),YO(70),YP(70),YQ(70),YR(70),VR(70),VI(70),
         5VT(70),VA(70)
          INTEGER I
          PRINT COMMENT $1ANALYSIS$
START     READ DATA
          READ FORMAT INPUT,X(0)...X(24)
          READ FORMAT INPUT,Z(0)...Z(24)
          VECTOR VALUES INPUT=$6K12*$
          PRINT FORMAT DATA,A(0)...A(6),B(1)...B(45),X(0)...X(24),
         1Z(0)...Z(24)
          THROUGH BETA, FOR I=1,1,I.G.39
          BI=B(I)
          YC(I)=EXP.(-A(1)*B I )
          YD(I)=X(9)*B I
          YE(I)=Z(9)*BI
          YF(I)=EXP.(-YD(I))
          YG(I)=SIN.( YE(I))
          YH(I)=COS.( YE(I))
          UR(I)=(X(1)+X(2)*B I )*YC(I)-X(1)*YF(I)*YH(I)
         1    -Z(1)*YF(I)*YG(I)
          UI(I)=(Z(1)+Z(2)*B I )*YC(I)-Z(1)*YF(I)*YH(I)
         1    +X(1)*YF(I)*YG(I)
          UT(I)=SQRT.(UR(I).P.2+UI(I).P.2)*A(5)*A(5)
          UA(I)=ATAN.(UI(I)/UR(I))
          YI(I)=EXP.(-2.*A(1)*B I )
          YJ(I)=X(9)*B I *SQRT.(A(4))
          YK(I)=Z(9)*B I *SQRT.(A(4))
          YL(I)=EXP.(-YJ(I))
          YM(I)=SIN.(YK(I))
          YN(I)=COS.(YK(I))
          YO(I)=EXP.(-X(10)*B I )
          YP(I)=Z(10)*B I
          YQ(I)=SIN.(YP(I))
          YR(I)=COS.(YP(I))
          VR(I)=(X(15)+X(16)*B I )*YC(I)+(X(20)+X(21)*B I
         1    +X(22)*B I *B I +X(23)*B I *B I *B I )*YI(I)
         2    +X(14)*YL(I)*YN(I)+Z(14)*YL(I)*YM(I)
         3    +(X(17)+X(18)*B I +X(19)*B I *B I )*YO(I)
         4    *YR(I)+(Z(17)+Z(18)*B I +Z(19)*B I *B I )
         5    *YO(I)*YQ(I)
          VI(I)=(Z(15)+Z(16)*B I )*YC(I)+(Z(20)+Z(21)*B I
         1    +Z(22)*B I *B I +Z(23)*B I *B I *B I )*YI(I)
         2    +Z(14)*YL(I)*YN(I)-X(14)*YL(I)*YM(I)
         3    +(Z(17)+Z(18)*B I +Z(19)*B I *B I )*YO(I)
```

```
4      *YR(I)-(X(17)+X(18)*B I +X(19)*B I *B I )
5      *YO(I)*YQ(I)
       VT(I)=SQRT.(VR(I).P.2+VI(I).P.2)*A(5)*A(5)
       VA(I)=ATAN.(VI(I)/VR(I))
BETA   PRINT FORMAT RESULT,UR(I),UI(I),UT(I),UA(I),VR(I),VI(I),VT(
       1I),VA(I)
       VECTOR VALUES DATA=$6E12.4*$
       VECTOR VALUES RESULT=$1H0,8E14.4*$
       TRANSFER TO START
       END OF PROGRAM
$ DATA
```

EXPERIMENTAL DATA

Heat Transfer Data

a	ω	$a\omega$	T_f	T_{amb}	h	$G_{rL}P_r$	R_{eV}	Nu
in.	cycle / sec.		F	F	$\frac{BTU}{hrftF}$	10^{-6}	10^{-3}	
0.011	20.8	0.228	216.1	81.5	1.306	14.85	0.28	40.31
0.0105	41.5	0.435	216.1	80.9	1.298	14.9	0.536	40.06
0.025	20.8	0.52	216.3	80.6	1.292	14.9	0.662	39.87
0.0065	20.8	0.135	216.3	81.1	1.298	14.9	0.172	40.06
0.025	31.2	0.775	216.5	80.5	1.287	15	0.99	39.72
0.05	26	1.30	204.6	77.2	1.336	14.7	1.685	41.2
0.025	52	1.30	212	83.6	1.336	14.2	1.655	40.8
0.025	78	1.95	198.8	74.4	1.432	13.4	2.55	44.3
0.025	26	0.65	209.6	77.6	1.29	14.9	0.8375	39.6
0.05	52	2.6	187.6	76.6	1.554	13.6	3.47	48.6
0.025	104	2.6	187.4	78.7	1.57	13.2	3.45	48.9
0.043	78	3.74	210.4	89.2	2.02	13.43	4.775	61.8
0.05	26	1.3	204.6	77.2	1.33	14.62	1.69	41.05
0.01	20.8	0.208	187.6	79.4	1.228	11.9	0.275	38.38
0.0095	41.5	0.394	188.0	79.4	1.224	11.9	0.501	38.25
0.005	20.8	0.104	187.6	79.4	1.23	11.9	0.132	38.43
0.0275	20.8	0.57	188.4	79.2	1.215	12.0	0.726	37.97
0.025	31.2	0.779	187.8	79.0	1.223	12.0	1.029	38.22
0.058	41.6	2.42	176.7	81.6	1.415	11.45	3.27	44.1
0.055	52	2.75	108.7	81.5	1.05	4.53	4.06	34.3
0.055	72.8	3.85	105.2	83.2	1.32	3.67	5.7	43.3
0.075	52	3.9	189.2	91.4	1.808	11.8	5.08	55.8
0.048	78	3.75	187.7	91.6	1.812	11.2	4.89	54.9

APPENDIX IIA

Smoke Studies Data

a	ω	$a\omega$	$a\omega^2$	$\dfrac{a\omega^2}{g}$	ΔT	$G_R\,P_R$	T_p	$Re^2 v$
in.	$\dfrac{cycles}{sec.}$	$\dfrac{in\text{-}cycle}{sec.}$	$\dfrac{ft}{sec^2}$		°F	10^{-6}		$G_{RL}\left(\dfrac{a}{L}\right)$
0.012	50	0.6	98.75	3.06	133.8	14.45	217.6	56
0.01	50	0.5	82.25	2.55	133.8	14.45	2.7.6	11.6
0.02	50	1.0	164.5	5.11	84.4	11.15	163.8	140.8
0.023	50	1.15	189.5	5.875	84.4	11.15	163.8	162
0.018	50	0.9	148.5	4.59	110.4	13.2	190.6	99.2
0.018	50	0.9	148.5	4.59	108.4	12.95	188.6	101.2
0.008	70	0.56	129	4	110.4	13.2	190.6	86.4
0.009	70	0.63	145	4.5	110.4	13.2	190.6	97.2
0.017	50	0.85	140	4.34	114.6	13.7	193.2	90.4
0.016	50	0.8	132	4.083	114.6	13.7	193.2	84.8
0.008	70	0.56	129	4	118.2	13.95	196.8	81.6
0.007	70	0.49	113	3.5	118.2	13.95	196.8	71.4
0.054	25	1.35	111.5	3.45	118.2	13.95	196.8	70
0.0194	50	0.97	160	4.96	51.6	7.8	131.6	236
0.009	70	0.63	145	4.5	51	7.7	131.4	215.6
0.01	70	0.7	161.5	5.0	50.8	7.69	130.8	240
0.027	50	1.35	222	6.9	0	0	80	-----
0.03	50	1.5	247	7.65	0	0	80	-----
0.094	25	2.2	182	6.06	0	0	80	-----

APPENDIX III

TABULATED RESULTS

APPENDIX III

The tabulated results of Ostrach Reference C are found on the following pages.

APPENDIX IIIA

This section was taken from Schoenhals Reference A-34. The forcing function is defined as

$$\mathcal{Y}(\eta) = \int_{\infty}^{\eta} \eta H'(\eta) \, d\eta .$$

Schoenhals obtained tabulated results by integrating

$$\mathcal{Y}(\eta) = \int_{0}^{\infty} H(\eta) \, d\eta + \eta H(\eta) - \int_{0}^{\eta} H(\eta) \, d\eta .$$

The results are found on the following pages.

Prandtl number, 0.01

η	F	F'	F''	H	H'	η	F	F'	F''	H	H'
0	0.0000	0.0000	0.9862	1.0000	-0.0812	4.16	1.9319	0.4037	-0.0615	0.6741	-0.0723
.1	.0048	.0936	.8868	.9919	-.0812	4.18	1.9400	.4024	-.0614	.6726	-.0722
.2	.0184	.1774	.7891	.9838	-.0812	4.20	1.9480	.4012	-.0612	.6712	-.0721
.3	.0399	.2516	.6942	.9756	-.0812	4.24	1.9640	.3988	-.0609	.6683	-.0720
.4	.0684	.3164	.6030	.9675	-.0811	4.28	1.9799	.3964	-.0605	.6654	-.0718
.5	.1029	.3723	.5163	.9594	-.0811	4.32	1.9957	.3939	-.0602	.6626	-.0716
.6	.1426	.4198	.4349	.9513	-.0811	4.36	2.0114	.3915	-.0599	.6597	-.0714
.7	.1866	.4595	.3595	.9432	-.0811	4.40	2.0270	.3891	-.0595	.6568	-.0713
.8	.2342	.4919	.2906	.9351	-.0810	4.50	2.0657	.3832	-.0587	.6497	-.0708
.9	.2848	.5178	.2285	.9270	-.0809	4.60	2.1037	.3774	-.0579	.6427	-.0704
1.0	.3376	.5379	.1734	.9189	-.0809	4.70	2.1411	.3716	-.0572	.6357	-.0699
1.1	.3922	.5527	.1253	.9108	-.0808	4.80	2.1780	.3660	-.0564	.6287	-.0695
1.2	.4480	.5631	.0839	.9028	-.0807	4.90	2.2143	.3604	-.0556	.6218	-.0690
1.3	.5047	.5697	.0489	.8947	-.0806	5.00	2.2501	.3548	-.0549	.6149	-.0686
1.4	.5618	.5731	.0198	.8866	-.0804	5.10	2.2853	.3494	-.0541	.6081	-.0681
1.5	.6192	.5739	-.0039	.8786	-.0803	5.20	2.3200	.3440	-.0534	.6013	-.0676
1.6	.6765	.5725	-.0229	.8706	-.0801	5.40	2.3877	.3335	-.0520	.5878	-.0667
1.7	.7336	.5694	-.0379	.8626	-.0800	5.60	2.4534	.3232	-.0506	.5746	-.0657
1.8	.7904	.5650	-.0493	.8546	-.0798	5.80	2.5170	.3132	-.0493	.5615	-.0648
1.9	.8466	.5596	-.0579	.8466	-.0796	6.00	2.5787	.3035	-.0479	.5487	-.0638
2.0	.9023	.5535	-.0641	.8387	-.0794	6.20	2.6384	.2940	-.0467	.5360	-.0628
2.1	.9573	.5469	-.0685	.8307	-.0792	6.40	2.6963	.2849	-.0454	.5236	-.0618
2.2	1.0117	.5399	-.0714	.8228	-.0789	6.60	2.7524	.2759	-.0442	.5113	-.0608
2.3	1.0653	.5326	-.0732	.8150	-.0787	6.80	2.8067	.2671	-.0430	.4993	-.0598
2.4	1.1182	.5253	-.0742	.8071	-.0784	7.00	2.8593	.2586	-.0419	.4874	-.0588
2.5	1.1703	.5178	-.0746	.7993	-.0782	7.40	2.9594	.2423	-.0397	.4643	-.0568
2.6	1.2217	.5104	-.0745	.7915	-.0779	7.80	3.0532	.2269	-.0376	.4420	-.0547
2.7	1.2724	.5029	-.0741	.7837	-.0776	8.20	3.1411	.2123	-.0356	.4205	-.0527
2.8	1.3223	.4956	-.0735	.7760	-.0773	8.60	3.2232	.1984	-.0337	.3998	-.0508
2.9	1.3715	.4882	-.0728	.7682	-.0770	9.00	3.2999	.1853	-.0319	.3799	-.0489
3.0	1.4200	.4810	-.0719	.7606	-.0766	9.40	3.3715	.1729	-.0302	.3607	-.0470
3.1	1.4677	.4739	-.0711	.7529	-.0763	9.80	3.4383	.1612	-.0285	.3423	-.0451
3.2	1.5148	.4668	-.0701	.7453	-.0760	10.20	3.5005	.1501	-.0270	.3246	-.0432
3.3	1.5611	.4598	-.0692	.7377	-.0756	10.60	3.5584	.1396	-.0254	.3069	-.0413
3.4	1.6067	.4530	-.0683	.7302	-.0753	11.00	3.6123	.1297	-.0241	.2915	-.0397
3.45	1.6293	.4496	-.0678	.7264	-.0751	11.40	3.6622	.1203	-.0228	.2759	-.0380
3.5	1.6517	.4462	-.0674	.7227	-.0749	11.80	3.7086	.1114	-.0215	.2610	-.0364
3.55	1.6739	.4428	-.0669	.7189	-.0747	12.20	3.7514	.1031	-.0203	.2468	-.0348
3.6	1.6960	.4395	-.0664	.7152	-.0745	12.60	3.7911	.0952	-.0192	.2332	-.0332
3.65	1.7179	.4362	-.0660	.7115	-.0743	13.00	3.8276	.0877	-.0181	.2202	-.0317
3.7	1.7396	.4329	-.0655	.7078	-.0741	13.60	3.8771	.0773	-.0165	.2018	-.0296
3.75	1.7611	.4296	-.0651	.7041	-.0739	14.20	3.9206	.0679	-.0151	.1847	-.0276
3.8	1.7825	.4264	-.0646	.7004	-.0738	14.80	3.9587	.0592	-.0138	.1687	-.0257
3.85	1.8308	.4232	-.0642	.6967	-.0736	15.40	3.9918	.0513	-.0126	.1538	-.0239
3.9	1.8249	.4200	-.0638	.6930	-.0734	16.00	4.0204	.0441	-.0114	.1399	-.0223
3.95	1.8458	.4168	-.0633	.6893	-.0732	17.00	4.0591	.0335	-.0097	.1189	-.0197
4.00	1.8665	.4136	-.0629	.6857	-.0729	18.00	4.0880	.0246	-.0082	.1003	-.0175
4.05	1.8871	.4105	-.0625	.6821	-.0727	19.00	4.1088	.0171	-.0069	.0839	-.0154
4.10	1.9076	.4074	-.0620	.6784	-.0725	20.00	4.1226	.0108	-.0057	.0694	-.0137
4.12	1.9157	.4061	-.0619	.6770	-.0725	21.00	4.1308	.0057	-.0046	.0565	-.0121
4.14	1.9238	.4049	-.0617	.6755	-.0724	22.00	4.1343	.0015	-.0037	.0452	-.0107

Prandtl number, 0.72

η	F	F'	F''	H	H'
0	0.0000	0.0000	0.6760	1.0000	-0.5046
.1	.0032	.0627	.5785	.9495	-.5045
.2	.0122	.1159	.4866	.8991	-.5037
.3	.0261	.1602	.4007	.8488	-.5016
.4	.0440	.1962	.3210	.7989	-.4979
.5	.0651	.2246	.2479	.7493	-.4921
.6	.0887	.2460	.1817	.7005	-.4840
.7	.1141	.2612	.1224	.6526	-.4735
.8	.1407	.2708	.0700	.6059	-.4607
.9	.1681	.2754	.0246	.5606	-.4456
1.0	.1957	.2759	-.0143	.5168	-.4284
1.1	.2231	.2728	-.0468	.4749	-.4095
1.2	.2501	.2667	-.0734	.4350	-.3891
1.3	.2764	.2583	-.0945	.3972	-.3676
1.4	.3017	.2480	-.1106	.3615	-.3453
1.5	.3260	.2363	-.1224	.3281	-.3227
1.6	.3490	.2236	-.1302	.2970	-.3000
1.7	.3707	.2104	-.1347	.2681	-.2775
1.8	.3910	.1968	-.1363	.2415	-.2556
1.9	.4100	.1832	-.1356	.2170	-.2344
2.0	.4277	.1697	-.1331	.1945	-.2141
2.1	.4440	.1566	-.1290	.1741	-.1949
2.2	.4590	.1440	-.1238	.1555	-.1768
2.3	.4728	.1319	-.1178	.1387	-.1598
2.4	.4854	.1204	-.1113	.1235	-.1441
2.5	.4969	.1097	-.1044	.1098	-.1296
2.6	.5074	.0996	-.0973	.0976	-.1163
2.7	.5168	.0902	-.0903	.0865	-.1041
2.8	.5254	.0815	-.0834	.0767	-.0930
2.9	.5332	.0735	-.0767	.0679	-.0830
3.0	.5401	.0661	-.0703	.0601	-.0739
3.1	.5464	.0594	-.0642	.0531	-.0657
3.2	.5520	.0533	-.0585	.0469	-.0584
3.3	.5571	.0477	-.0531	.0414	-.0518
3.4	.5616	.0427	-.0481	.0365	-.0459
3.6	.5692	.0339	-.0392	.0284	-.0359
3.8	.5735	.0269	-.0317	.0220	-.0281
4.0	.5801	.0212	-.0255	.0170	-.0219
4.2	.5838	.0166	-.0204	.0132	-.0170
4.4	.5868	.0130	-.0162	.0102	-.0132
4.6	.5891	.0101	-.0128	.0078	-.0102
4.8	.5908	.0078	-.0102	.0060	-.0080
5.0	.5922	.0060	-.0079	.0046	-.0061
5.2	.5933	.0046	-.0063	.0035	-.0048
5.4	.5941	.0034	-.0048	.0027	-.0037
5.6	.5951	.0019	-.0029	.0015	-.0022
6.2	.5957	.0010	-.0018	.0009	-.0013
6.8	.5960	.0003	-.0008	.0003	-.0006
7.3	.5961	.0000	-.0004	.0001	-.0003

Prandtl number, 0.733

η	F	F'	F''	H	H'
0	0.0000	0.0000	0.6741	1.0000	-0.5080
.1	.0032	.0625	.5767	.9492	-.5079
.2	.0122	.1155	.4849	.8984	-.5071
.3	.0260	.1597	.3990	.8478	-.5050
.4	.0438	.1955	.3194	.7975	-.5012
.5	.0649	.2238	.2465	.7477	-.4953
.6	.0884	.2451	.1804	.6985	-.4870
.7	.1137	.2601	.1212	.6503	-.4763
.8	.1402	.2695	.0691	.6033	-.4632
.9	.1674	.2741	.0237	.5578	-.4478
1.0	.1949	.2745	-.0149	.5139	-.4303
1.1	.2222	.2713	-.0473	.4718	-.4110
1.2	.2490	.2652	-.0737	.4317	-.3902
1.3	.2752	.2568	-.0946	.3938	-.3684
1.4	.3003	.2465	-.1106	.3581	-.3458
1.5	.3244	.2348	-.1222	.3246	-.3228
1.6	.3473	.2222	-.1299	.2935	-.2998
1.7	.3688	.2090	-.1342	.2647	-.2771
1.8	.3891	.1954	-.1358	.2381	-.2549
1.9	.4079	.1819	-.1350	.2136	-.2335
2.0	.4254	.1685	-.1324	.1913	-.2130
2.1	.4416	.1554	-.1283	.1710	-.1937
2.2	.4565	.1429	-.1230	.1526	-.1754
2.3	.4702	.1309	-.1170	.1359	-.1584
2.4	.4827	.1195	-.1104	.1208	-.1427
2.5	.4941	.1088	-.1035	.1073	-.1281
2.6	.5045	.0988	-.0965	.0952	-.1148
2.7	.5139	.0895	-.0895	.0843	-.1026
2.8	.5224	.0809	-.0826	.0746	-.0916
2.9	.5301	.0729	-.0759	.0660	-.0816
3.0	.5370	.0657	-.0695	.0583	-.0725
3.1	.5433	.0590	-.0635	.0514	-.0644
3.2	.5489	.0530	-.0578	.0454	-.0571
3.3	.5539	.0475	-.0524	.0400	-.0506
3.4	.5584	.0425	-.0474	.0352	-.0448
3.6	.5660	.0339	-.0386	.0273	-.0350
3.8	.5720	.0269	-.0312	.0211	-.0272
4.0	.5769	.0213	-.0250	.0163	-.0211
4.2	.5807	.0169	-.0200	.0126	-.0164
4.4	.5837	.0133	-.0159	.0097	-.0127
4.6	.5860	.0105	-.0125	.0074	-.0098
4.8	.5879	.0082	-.0099	.0057	-.0076
5.0	.5893	.0065	-.0077	.0044	-.0058
5.2	.5905	.0051	-.0061	.0033	-.0045
5.4	.5914	.0040	-.0047	.0025	-.0035
5.6	.5921	.0032	-.0036	.0019	-.0027
5.8	.5927	.0025	-.0028	.0015	-.0021
6.0	.5932	.0021	-.0022	.0011	-.0016
6.4	.5938	.0014	-.0013	.0006	-.0009
6.8	.5943	.0010	-.0006	.0003	-.0006
7.2	.5946	.0007	-.0004	.0001	-.0003
7.6	.5949	.0006	-.0002	.0000	-.0002
8.0	.5951	.0005	-.0001	.0000	-.0001

Prandtl number, 1

η	F	F'	F''	H	H'
0	0.0000	0.0000	0.6421	1.0000	−0.5671
.1	.0030	.0593	.5450	.9433	−.5669
.2	.0115	.1092	.4540	.8867	−.5657
.3	.0246	.1503	.3694	.8302	−.5627
.4	.0413	.1833	.2916	.7742	−.5572
.5	.0610	.2089	.2208	.7189	−.5488
.6	.0829	.2277	.1572	.6645	−.5371
.7	.1064	.2406	.1008	.6116	−.5221
.8	.1308	.2481	.0516	.5602	−.5038
.9	.1558	.2511	.0093	.5109	−.4826
1.0	.1809	.2502	−.0263	.4638	−.4589
1.1	.2058	.2461	−.0557	.4192	−.4330
1.2	.2300	.2393	−.0793	.3772	−.4056
1.3	.2535	.2304	−.0975	.3381	−.3772
1.4	.2761	.2199	−.1110	.3018	−.3484
1.5	.2975	.2083	−.1203	.2684	−.3197
1.6	.3177	.1960	−.1260	.2379	−.2915
1.7	.3367	.1832	−.1287	.2101	−.2642
1.8	.3543	.1708	−.1288	.1850	−.2382
1.9	.3707	.1575	−.1268	.1624	−.2136
2.0	.3859	.1450	−.1233	.1422	−.1907
2.1	.3997	.1339	−.1185	.1242	−.1695
2.2	.4125	.1213	−.1127	.1082	−.1501
2.3	.4240	.1104	−.1064	.0941	−.1324
2.4	.4346	.1001	−.0997	.0817	−.1164
2.5	.4441	.0904	−.0928	.0708	−.1020
2.6	.4527	.0815	−.0859	.0613	−.0892
2.7	.4604	.0733	−.0791	.0529	−.0777
2.8	.4673	.0657	−.0725	.0457	−.0676
2.9	.4736	.0588	−.0662	.0392	−.0587
3.0	.4791	.0524	−.0602	.0339	−.0509
3.1	.4841	.0467	−.0546	.0291	−.0441
3.2	.4885	.0415	−.0493	.0250	−.0381
3.3	.4924	.0368	−.0444	.0215	−.0329
3.4	.4959	.0326	−.0399	.0185	−.0283
3.6	.5016	.0254	−.0321	.0136	−.0210
3.8	.5061	.0197	−.0255	.0099	−.0155
4.0	.5096	.0151	−.0202	.0072	−.0115
4.2	.5122	.0116	−.0158	.0053	−.0084
4.4	.5143	.0087	−.0124	.0038	−.0062
4.6	.5158	.0066	−.0096	.0027	−.0045
4.8	.5169	.0049	−.0075	.0020	−.0034
5.0	.5177	.0035	−.0057	.0014	−.0024
5.2	.5183	.0025	−.0044	.0010	−.0018
5.5	.5189	.0014	−.0029	.0006	−.0011
6.0	.5194	.0004	−.0014	.0002	−.0005
6.25	.5194	.0000	−.0010	.0000	−.0004

Prandtl number, 2

η	F	F'	F''	H	H'
0	0.0000	0.0000	0.5713	1.0000	−0.7165
.1	.0027	.0523	.4749	.9284	−.7161
.2	.0101	.0952	.3861	.8569	−.7135
.3	.0215	.1297	.3049	.7858	−.7069
.4	.0358	.1565	.2318	.7157	−.6949
.5	.0525	.1763	.1666	.6470	−.6768
.6	.0709	.1901	.1095	.5805	−.6523
.7	.0904	.1985	.0602	.5168	−.6215
.8	.1104	.2024	.0185	.4564	−.5852
.9	.1307	.2024	−.0161	.3999	−.5443
1.0	.1508	.1994	−.0440	.3476	−.5002
1.1	.1705	.1938	−*0659	.2999	−.4543
1.2	.1895	.1864	−.0824	.2568	−.4077
1.3	.2077	.1775	−.0942	.2183	−.3619
1.4	.2250	.1677	−.1020	.1844	−.3178
1.5	.2412	.1572	−.1063	.1547	−.2763
1.6	.2564	.1465	−.1078	.1290	−.2380
1.7	.2706	.1357	−.1071	.1069	−.2032
1.8	.2836	.1252	−.1046	.0882	−.1721
1.9	.2956	.1149	−.1008	.0724	−.1446
2.0	.3066	.1050	−.0960	.0592	−.1207
2.1	.3166	.0957	−.0906	.0482	−.1001
2.2	.3257	.0869	−.0849	.0391	−.0826
2.3	.3340	.0787	−.0789	.0316	−.0677
2.4	.3415	.0711	−.0729	.0254	−.0553
2.5	.3483	.0641	−.0671	.0204	−.0450
2.6	.3543	.0577	−.0614	.0164	−.0364
2.7	.3598	.0518	−.0560	.0131	−.0294
2.8	.3647	.0465	−.0509	.0105	−.0237
2.9	.3691	.0417	−.0461	.0083	−.0190
3.0	.3731	.0373	−.0416	.0066	−.0152
3.1	.3766	.0333	−.0375	.0053	−.0121
3.2	.3798	.0298	−.0338	.0042	−.0097
3.3	.3826	.0266	−.0303	.0033	−.0077
3.4	.3851	.0237	−.0272	.0026	−.0061
3.6	.3893	.0188	−.0218	.0017	−.0038
3.8	.3927	.0149	−.0174	.0010	−.0024
4.0	.3953	.0118	−.0138	.0007	−.0015
4.2	.3974	.0094	−.0109	.0004	−.0009
4.4	.3991	.0074	−.0086	.0003	−.0006
4.6	.4004	.0059	−.0068	.0002	−.0004
4.8	.4015	.0047	−.0054	.0001	−.0002
5.0	.4023	.0037	−.0042	.0001	−.0001
5.4	.4035	.0024	−.0026	.0001	−.0001
5.8	.4043	.0015	−.0016	.0000	.0000
6.4	.4049	.0008	−.0008	.0000	.0000
7.0	.4053	.0005	−.0004	.0000	.0000
8.0	.4056	.0002	−.0001	.0000	.0000
9.0	.4058	.0001	.0000	.0000	.0000
10.0	.4059	.0001	.0000	.0000	.0000
11.0	.4059	.0001	.0000	.0000	.0000

Prandtl number, 10

η	F	F'	F''	H	H'
0	0.0000	0.0000	0.4192	1.0000	−1.1694
.1	.0019	.0371	.3251	.8832	−1.1671
.2	.0071	.0654	.2428	.7670	−1.1521
.3	.0147	.0861	.1723	.6534	−1.1155
.4	.0241	.1003	.1134	.5448	−1.0526
.5	.0346	.1091	.0655	.4437	−.9640
.6	.0458	.1137	.0279	.3527	−.8545
.7	.0573	.1150	−.0011	.2733	−.7322
.8	.0687	.1137	−.0221	.2064	−.6061
.9	.0800	.1107	−.0367	.1519	−.4849
1.0	.0908	.1066	−.0462	.1090	−.3753
1.1	.1012	.1016	−.0518	.0763	−.2813
1.2	.1111	.0963	−.0545	.0522	−.2045
1.3	.1205	.0908	−.0552	.0349	−.1445
1.4	.1293	.0853	−.0544	.0228	−.0993
1.5	.1376	.0799	−.0527	.0146	−.0665
1.6	.1453	.0748	−.0505	.0092	−.0435
1.7	.1525	.0699	−.0480	.0056	−.0278
1.8	.1593	.0652	−.0453	.0034	−.0174
1.9	.1656	.0608	−.0427	.0020	−.0107
2.0	.1714	.0567	−.0400	.0012	−.0065
2.1	.1769	.0528	−.0375	.0007	−.0038
2.2	.1820	.0491	−.0351	.0004	−.0022
2.3	.1868	.0458	−.0328	.0002	−.0013
2.4	.1912	.0426	−.0306	.0001	−.0007
2.5	.1953	.0396	−.0286	.0001	−.0004
2.6	.1991	.0369	−.0267	.0000	−.0002
2.7	.2027	.0343	−.0249	.0000	−.0001
2.8	.2060	.0319	−.0232	.0000	−.0001
2.9	.2090	.0297	−.0216	.0000	.0000
3.0	.2119	.0276	−.0201	.0000	.0000
3.1	.2146	.0256	−.0187	.0000	.0000
3.2	.2170	.0238	−.0174	.0000	.0000
3.3	.2193	.0221	−.0162	.0000	.0000
3.4	.2215	.0206	−.0151	.0000	.0000
3.6	.2253	.0178	−.0131	.0000	.0000
3.8	.2286	.0153	−.0113	.0000	.0000
4.0	.2314	.0132	−.0098	.0000	.0000
4.2	.2339	.0114	−.0084	.0000	.0000
4.4	.2360	.0098	−.0073	.0000	.0000
4.6	.2379	.0085	−.0063	.0000	.0000
4.8	.2394	.0073	−.0054	.0000	.0000
5.0	.2408	.0063	−.0047	.0000	.0000
5.4	.2430	.0047	−.0035	.0000	.0000
5.8	.2446	.0035	−.0026	.0000	.0000
6.2	.2458	.0026	−.0019	.0000	.0000
7.0	.2474	.0014	−.0011	.0000	.0000
8.0	.2484	.0007	−.0005	.0000	.0000
9.0	.2489	.0003	−.0002	.0000	.0000
10.0	.2491	.0002	−.0001	.0000	.0000

Prandtl number, 100

η	F	F'	F''	H	H'
0.000	0.0000	0.0000	0.2517	1.0000	−2.191
.025	.0001	.0060	.2274	.9452	−2.191
.050	.0003	.0114	.2044	.8905	−2.188
.075	.0006	.0162	.1828	.8359	−2.180
.100	.0011	.0205	.1626	.7815	−2.166
.125	.0017	.0244	.1438	.7276	−2.144
.150	.0023	.0277	.1263	.6744	−2.113
.175	.0031	.0307	.1101	.6221	−2.071
.200	.0039	.0332	.0952	.5709	−2.018
.225	.0047	.0355	.0816	.5213	−1.954
.250	.0056	.0373	.0692	.4733	−1.880
.275	.0066	.0389	.0580	.4273	−1.786
.300	.0076	.0402	.0479	.3836	−1.704
.325	.0086	.0413	.0389	.3422	−1.604
.350	.0096	.0422	.0309	.3034	−1.498
.375	.0107	.0429	.0238	.2674	−1.388
.400	.0118	.0434	.0176	.2341	−1.276
.425	.0129	.0438	.0128	.2036	−1.163
.450	.0140	.0440	.0076	.1759	−1.052
.475	.0151	.0442	.0036	.1510	−.9430
.500	.0162	.0442	.0002	.1287	−.8393
.525	.0173	.0442	−.0026	.1089	−.7404
.550	.0184	.0441	−.0050	.0916	−.6478
.575	.0195	.0439	−.0070	.0765	−.5621
.600	.0206	.0437	−.0087	.0634	−.4837
.65	.0227	.0432	−.0111	.0427	−.3496
.70	.0249	.0426	−.0126	.0280	−.2440
.75	.0270	.0420	−.0135	.0178	−.1657
.80	.0291	.0413	−.0140	.0111	−.1088
.85	.0311	.0406	−.0142	.0067	−.0693
.90	.0331	.0399	−.0142	.0039	−.0428
.95	.0351	.0392	−.0141	.0022	−.0256
1.00	.0371	.0385	−.0140	.0012	−.0149
1.10	.0408	.0371	−.0136	.0004	−.0046
1.20	.0445	.0357	−.0132	.0001	−.0013
1.30	.0480	.0344	−.0128	.0000	−.0003
1.40	.0514	.0332	−.0124	.0000	−.0001
1.50	.0546	.0320	−.0119	.0000	.0000
1.60	.0578	.0308	−.0116	.0000	.0000
1.70	.0608	.0297	−.0112	.0000	.0000
1.80	.0637	.0286	−.0108	.0000	.0000
1.90	.0665	.0275	−.0104	.0000	.0000
2.0	.0692	.0265	−.0101	.0000	.0000
2.1	.0718	.0255	−.0097	.0000	.0000
2.2	.0743	.0245	−.0094	.0000	.0000
2.3	.0767	.0236	−.0091	.0000	.0000
2.4	.0790	.0227	−.0088	.0000	.0000
2.6	.0834	.0210	−.0082	.0000	.0000
2.8	.0874	.0195	−.0076	.0000	.0000
3.0	.0912	.0180	−.0071	.0000	.0000

Prandtl number, 100—Concluded

η	F	F'	F''	H	H'
3.2	0.0917	0.0166	−0.0066	0.0000	0.0000
3.4	.0979	.0154	−.0061	.0000	.0000
3.6	.1008	.0142	−.0056	.0000	.0000
3.8	.1035	.0131	−.0052	.0000	.0000
4.0	.1061	.0121	−.0049	.0000	.0000
4.4	.1105	.0103	−.0042	.0000	.0000
4.8	.1143	.0088	−.0036	.0000	.0000
5.2	.1176	.0074	−.0031	.0000	.0000
5.6	.1203	.0063	−.0026	.0000	.0000
6.0	.1226	.0053	−.0022	.0000	.0000
6.6	.1254	.0041	−.0018	.0000	.0000
7.2	.1276	.0032	−.0014	.0000	.0000
8.0	.1297	.0022	−.0010	.0000	.0000
9.0	.1315	.0014	−.0007	.0000	.0000
10.0	.1326	.0008	−.0005	.0000	.0000
11.0	.1332	.0004	−.0003	.0000	.0000
12.0	.1335	.0002	−.0002	.0000	.0000
13.0	.1336	.0000	−.0001	.0000	.0000

Prandtl number, 1000

η	F	F'	F''	H	H'
0.	0.0000	0.0000	0.1450	1.0000	−3.966
.025	.0000	.0033	.1212	.9009	−3.962
.050	.0002	.0061	.0999	.8021	−3.933
.075	.0003	.0083	.0811	.7046	−3.861
.100	.0006	.0102	.0647	.6096	−3.731
.125	.0008	.0116	.0506	.5186	−3.538
.150	.0012	.0127	.0387	.4332	−3.283
.175	.0015	.0135	.0289	.3549	−2.975
.200	.0018	.0142	.0209	.2847	−2.628
.225	.0022	.0146	.0146	.2236	−2.261
.250	.0026	.0149	.0096	.1717	−1.893
.275	.0029	.0151	.0059	.1288	−1.541
.300	.0033	.0152	.0032	.0944	−1.220
.325	.0037	.0153	.0012	.0675	−.9381
.350	.0041	.0153	−.0003	.0471	−.7012
.375	.0045	.0152	−.0012	.0321	−.5093
.400	.0048	.0152	−.0019	.0213	−.3596
.425	.0052	.0152	−.0023	.0138	−.2467
.450	.0056	.0151	−.0026	.0087	−.1645
.475	.0060	.0150	−.0027	.0053	−.1066
.500	.0063	.0150	−.0028	.0032	−.0672
.525	.0067	.0149	−.0029	.0019	−.0412
.550	.0071	.0148	−.0029	.0011	−.0245
.575	.0075	.0147	−.0029	.0006	−.0142
.600	.0078	.0147	−.0029	.0003	−.0080
.625	.0082	.0146	−.0029	.0002	−.0044
.800	.0107	.0141	−.0028	.0000	.0000
1.000	.0135	.0136	−.0027	.0000	.0000
1.40	.0187	.0125	−.0025	.0000	.0000
1.80	.0235	.0115	−.0023	.0000	.0000
2.20	.0279	.0106	−.0022	.0000	.0000
2.60	.0320	.0098	−.0020	.0000	.0000
3.0	.0358	.0090	−.0019	.0000	.0000
3.6	.0409	.0080	−.0017	.0000	.0000
4.2	.0454	.0070	−.0015	.0000	.0000
5.0	.0505	.0060	−.0012	.0000	.0000
5.8	.0549	.0050	−.0011	.0000	.0000
7.0	.0603	.0039	−.0008	.0000	.0000
8.0	.0638	.0032	−.0007	.0000	.0000
10.0	.0691	.0022	−.0004	.0000	.0000
12.0	.0727	.0015	−.0003	.0000	.0000
14.0	.0752	.0011	−.0002	.0000	.0000
16.0	.0771	.0008	−.0001	.0000	.0000
18.0	.0786	.0007	.0000	.0000	.0000
20.0	.0798	.0006	.0000	.0000	.0000
22.0	.0809	.0005	.0000	.0000	.0000
23.6	.0816	.0005	.0000	.0000	.0000

Prandtl Number = .01

η	$\zeta(\eta)$	$\int_0^\eta \zeta(\eta)d\eta$	η	$\zeta(\eta)$	$\int_0^\eta \zeta(\eta)d\eta$
0	8.25	0	4.2	7.57	33.68
.2	8.25	1.65	4.4	7.51	35.18
.4	8.24	3.30	4.6	7.45	36.68
.6	8.23	4.95	4.8	7.38	38.16
.8	8.22	6.59	5.0	7.31	39.63
1.0	8.21	8.24	5.8	7.03	45.37
1.2	8.19	9.88	6.6	6.71	50.87
1.4	8.17	11.51	7.4	6.39	56.11
1.6	8.15	13.14	8.2	6.04	61.08
1.8	8.12	14.77	9.0	5.70	65.77
2.0	8.09	16.39	9.8	5.34	70.19
2.2	8.06	18.00	10.6	4.98	74.32
2.4	8.02	19.61	11.4	4.64	78.17
2.6	7.98	21.21	12.2	4.30	81.74
2.8	7.94	22.80	13.0	3.96	85.04
3.0	7.89	24.39	14.2	3.48	89.51
3.2	7.85	25.96	15.4	3.02	93.40
3.4	7.80	27.53	16.0	2.80	95.15
3.6	7.74	29.08	18.0	2.13	100.1
3.8	7.69	30.62	20.0	1.55	103.7
4.0	7.63	32.15	22.0	1.03	100.3
			24.0		107.5

Prandtl Number = .72

η	$\zeta(\eta)$	$\int_0^\eta \zeta(\eta)d\eta$	η	$\zeta(\eta)$	$\int_0^\eta \zeta(\eta)d\eta$
0	1.252	0	2.4	.396	2.144
.1	1.250	.125	2.5	.363	2.181
.2	1.242	.250	2.6	.332	2.216
.3	1.230	.373	2.7	.302	2.248
.4	1.212	.496	2.8	.275	2.277
.5	1.190	.616	2.9	.250	2.303
.6	1.163	.733	3.0	.227	2.327
.7	1.132	.848	3.1	.206	2.349
.8	1.097	.960	3.2	.187	2.368
.9	1.059	1.067	3.3	.167	2.386
1.0	1.017	1.171	3.4	.152	2.402
1.1	.973	1.271	3.6	.124	2.430
1.2	.927	1.366	3.8	.100	2.452
1.3	.880	1.456	4.0	.081	2.470
1.4	.832	1.542	4.2	.065	2.484
1.5	.783	1.622	4.4	.052	2.496
1.6	.735	1.698	4.6	.042	2.505
1.7	.687	1.769	4.8	.033	2.513
1.8	.641	1.836	5.0	.025	2.519
1.9	.596	1.898	5.2	.021	2.523
2.0	.552	1.955	5.4	.016	2.527
2.1	.510	2.008	5.8	.010	2.532
2.2	.470	2.057	6.2	.006	2.535
2.3	.432	2.102	6.8	.002	2.538
			7.3	.001	2.538

Prandtl Number = 10

η	$\zeta(\eta)$	$\int_0^\eta \zeta(\eta)d\eta$	η	$\zeta(\eta)$	$\int_0^\eta \zeta(\eta)d\eta$
0	.510	0	1.2	.075	.378
.1	.504	.051	1.3	.053	.384
.2	.487	.100	1.4	.037	.388
.3	.458	.148	1.5	.025	.391
.4	.420	.192	1.6	.017	.394
.5	.375	.232	1.7	.011	.395
.6	.325	.267	1.8	.007	.396
.7	.273	.296	1.9	.004	.396
.8	.223	.321	2.0	.003	.397
.9	.177	.341	2.1	.002	.397
1.0	.137	.357	2.2	.001	.397
1.1	.102	.369			

Prandtl Number = 1000

η	$\zeta(\eta)$	$\int_0^\eta \zeta(\eta)d\eta$
0	.148	0
.025	.147	.0037
.050	.143	.0073
.075	.137	.0108
.100	.129	.0141
.125	.118	.0172
.150	.107	.0201
.175	.094	.0226
.200	.081	.0247
.225	.068	.0266
.250	.056	.0281
.275	.044	.0294
.300	.034	.0304
.325	.026	.0311
.350	.019	.0317
.375	.014	.0321
.400	.010	.0324
.425	.007	.0326
.450	.004	.0327
.475	.003	.0328
.500	.002	.0329
.525	.001	.0329